NEW EXTENDED METHINE DYES FOR APPLICATION IN LASER TECHNOLOGY

by

Valerie Millar

Submitted in accordance with the

requirements for the degree of

Doctor of Philosophy

Department of Colour Chemistry and Dyeing

University of Leeds

January 1993

To Laurie

ACKNOWLEDGEMENTS

SYNOPSIS

Based on the known reverse saturable absorption properties of certain coumarin and long chain polymethine dyes, the synthesis of new related structures was undertaken in order to examine the relationships between structure and RSA activity. It was hoped that in this way, more effective RSA chromophores could be synthesised. In addition to RSA activity (at 532nm) the general light absorption and fluorescence characteristics of the new dye materials were examined.

In the first series of dyes, the 7-diethylaminocoumarin system with extensively conjugated acceptor groups in the 3-position were examined. Several dyes with absorption maxima in the range 500-700nm were prepared, but none showed RSA properties at 532nm. The poor photostability properties of these dyes prompted the synthesis of related fused ring systems derived from 4-chloro-7-diethylamino--3-formyl-coumarin and in at least one example a marked improvement in photostability was achieved.

In an attempt to move the absorption maxima of the coumarin dyes into the near-infrared, chromophores with extended chains containing an isophorone bridge were introduced into the 3-position of the coumarin system. Although this gave greater conjugation and an increase in structural rigidity, λ_{max} values could not be obtained at wavelengths greater than about 570nm, and photostability properties of the dyes were poor.

Condensation of active methylene compounds with 2-chloro-1-formyl-3-hydroxymethylenecyclohexene led to the synthesis of a series of extended donor-acceptor chromophores containing a chlorocyclohexene bridge, where the donor was the 1,3,3-trimethylindoline ring system. Absorption maxima of the dyes ranged from 620-860nm. However, none showed RSA properties and their photostability in cellulose acetate film was generally poor. In an attempt to improve photostability the intermediate formed from 2-methylene-1,3,3-trimethylindoline (Fischer's base) and 2-chloro-1-formyl-3-hydromethylenecyclohexene was condensed with active methylene compounds

containing groups capable of intramolecular nucleophilic displacement of the chlorine atom. Thus under suitably forcing reaction conditions intramolecular cyclisation occurred, giving a series of extended donor-acceptor chromophores containing fused heterocyclic residues, the absorption maxima of these new chromophores ranging from 540-730nm. However, resultant increase in molecular rigidity did not give the expected improvement in photostability.

In a further attempt to prepare RSA active chromophores, selected symmetrical polymethine dyes were synthesised and evaluated. All showed a measurable RSA effect at 532nm but in particular, near-infrared absorbing squarylium dye containing 2,3-dihydroperimidine end groups exhibited the greatest degree of RSA thus far observed.

SCF-CI PPP-MO theory was applied to the theoretical qualitative prediction of the RSA properties of dye chromophores. Theoretical predictions were in good agreement with experimental observations, enabling a distinction to be made between dyes with high or zero RSA activity.

CONTENTS

LIST OF TABLES

LIST OF FIGURES

1. INTRODUCTION

INFRARED DYES AND THEIR APPLICATIONS IN LASER TECHNOLOGY

Before discussing the chemistry of extended methine infrared dyes and their applications in laser technology of relevance to this project, it is useful first to summarise the general principles of dye laser operation.

1.1 THE DYE LASER

Light can act as a wave or a particle. In the wave description it is defined by a wavelength which determines colour and oscillator frequency. As a particle it is termed a photon and carries a discrete amount of energy, E. Quantum mechanical restrictions limit molecules to certain discrete electronic states of energy, the lowest energy state being the ground state E_0. Transitions from the ground state to the electronically excited state E_1, requires absorption of a photon whose energy is given by;

$$\Delta E = E_1 - E_0 = h\upsilon = hc/\lambda$$

where   h = Planck's constant

            υ = frequency

            c = velocity of light

            λ = wavelength of absorbed radiation

For a molecule to be coloured it must contain mobile electrons, and electronic excitation of the molecule from E_0 to E_1 must be associated with a ΔE value between 297 kJ/mole (400nm) and 148.4 kJ/mole (800nm) [1][2].

The energy of an excited molecule can be dissipated via several pathways [3];

E_1 -> Radiationless processes -> E_0 + heat

-> Radiative processes -> E_0 + Emission (fluorescence, phosphorescence)

-> Loss of energy by intermolecular energy transfer -> E_0 + molecule BE_1

-> Chemical reaction -> products.

The dye laser is dependent upon the radiative deactivation process of fluorescence. LASER is the acronym for Light Amplification by the Stimulated Emission of Radiation.

Tunable dye lasers can cover the ultra-violet, visible and near infrared regions of the electromagnetic spectrum. Thermal and photochemical stability of the laser dye limits the short - wavelength and the long - wavelength emission maxima of the dye laser. The shortest dye laser wavelength quoted by Maeda (1984)[4] is at 308.5nm (2,2'-dimethyl-p-terphenyl) [5] whereas the longest dye laser wavelength is at 1285nm ie. 3,3'-diethyl-9,11,15,17-dineopentylene-5,6,5',6'-tetramethoxy-thiapentacarbocyanine perchlorate [6].

Fluorescence emission can be explained using a Jablonski diagram, (Figure 1) [7].
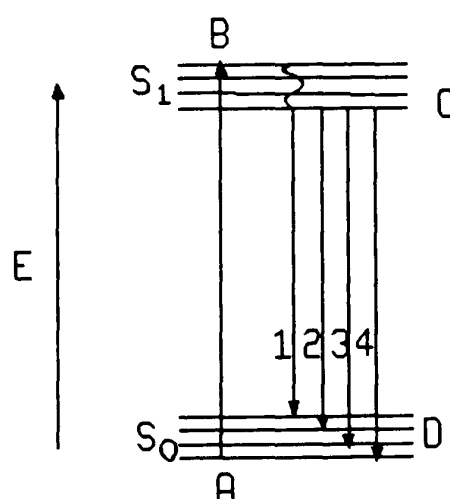
Figure 1. The origin of fluoresence

After excitation of the molecule from the lowest vibrational level of the singlet ground state, S_0, to a higher vibrational level of the first excited singlet state, S_1 (i.e. A -> B) rapid vibrational relaxation brings the dye molecule down to point C, the lowest vibrational level of S_1. Fluorescence emission can then occur from point C to D_{1-4}, etc., leading to the fluorescence emission band.

Fluorescence emission can be of two types, namely spontaneous or stimulated, (Figure 2).

(a) Absorption   (b) Spontaneous   (c) Stimulated
                      emission   emission
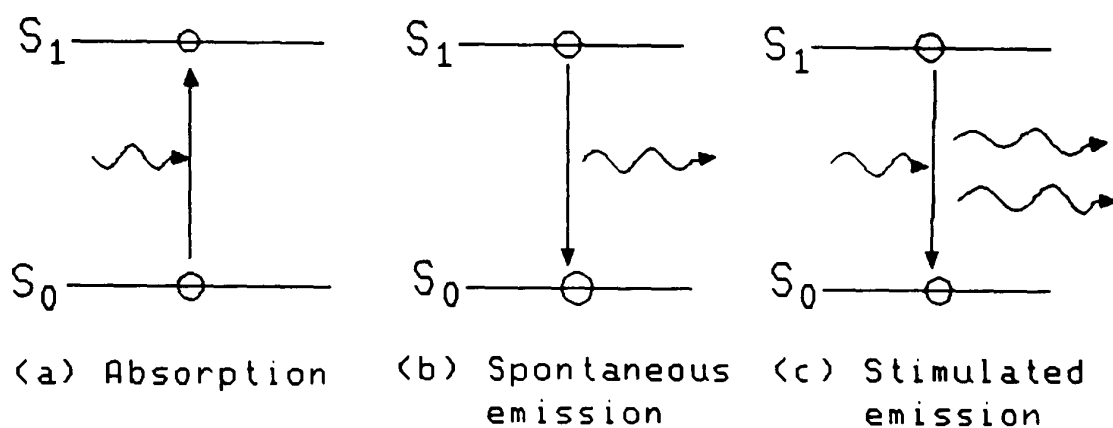
Figure 2. Spontaneous and Stimulated emission

Absorption (Fig 2(a)) as already mentioned requires the absorption of a photon raising the energy level of the dye molecule from S_0 to S_1. Spontaneous emission (Fig 2(b)) occurs on spontaneous decay of the dye molecule from S_1 -> S_0, simultaneously emitting a photon.

Stimulated emission (Fig 2(c)) occurs when the molecule is 'triggered' or stimulated to release energy when 'hit' by another photon. Thus two photons are emitted by this process, one corresponding to the original photon and one the fluorescence photon. It is important from the point of view of laser action, to note that the two photons have exactly the same energy (wavelength), the same direction of propagation and are exactly in phase. Such radiation is said to be coherent.

The principle of the operation of a laser is shown diagrammatically in Figure 3 [8][9].

(a) Spontaneous emission

Optically flat and
parallel ends

Excited state
molecules

50% Reflecting
surface

100% Reflecting surface
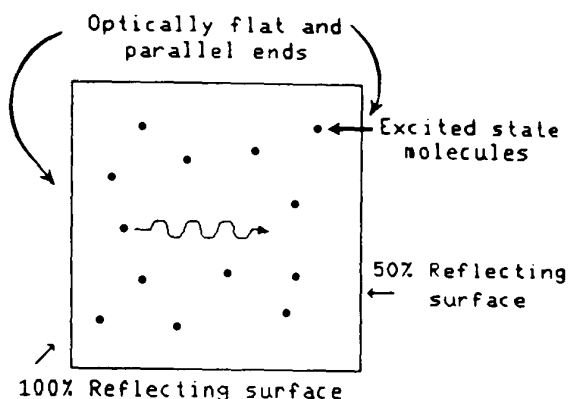
(b) Photon collison leading to

stimulated emission

Only the spontaneously emitted

photon travelling exactly along the

cell axis can trigger other dye

molecules in their excited state

to release photons. Off-axis photons

leave the cell sides.
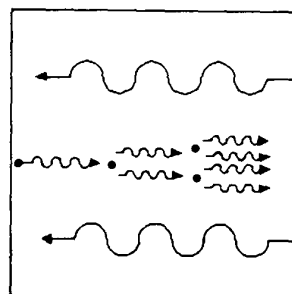
(c) After several reflections the pulse

of stimulated emission leaves the

50% transmitting cell face in

perfect coherence.

COHERENT
LASER
PULSE
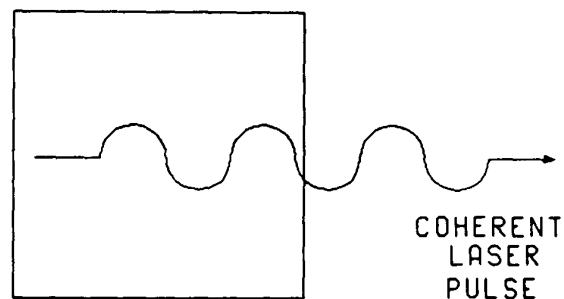
Figure 3. The principle of dye laser
operation

Light amplification or fluorescence gain requires a certain magnitude of light intensity incident upon the laser dye solution. When light of wavelength, λ, is incident on an assembly of molecules in their ground state, a net decrease of light intensity occurs due to absorption. If the light intensity is increased until the rate of excitation S_0-S_1 equals the rate at which S_1 reverts to S_0, a steady state situation is achieved, when the number molecules in S_0 equals the number in S_1. Thus as much

light is absorbed as is emitted by stimulated emission and the light wave intensity is neither increased or decreased on passing through the solution. If the number of molecules in S_1 is greater than the number of molecules in S_0 then the emergent wave will be more intense than the incident wave, due to stimulated emission. This situation is termed <u>population inversion</u> and requires a 'pump' source, for example another laser, to promote a high percentage of the molecules into the excited state. Population inversion is an essential requirement for light amplification.

In theory the phosphorescence band of a dye solution could also be used as the source of laser emission. Figure 4, depicts the origin of phosphorescence.
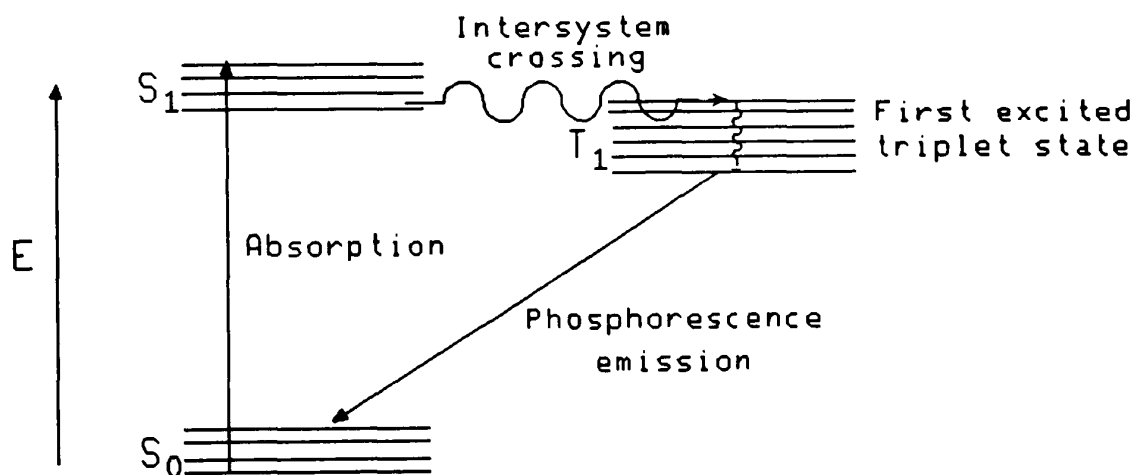
Figure 4. The origin of phosphorescence

However, the intersystem crossing process $S_1 \rightarrow T_1$ is usually a strongly forbidden process, and thus extremely high concentrations of phosphorescent material would be required to obtain amplification large enough to overcome cavity losses [10]. Schafer also reports losses due to triplet - triplet absorption. Triplet - triplet absorption bands are broad and diffuse, increasing the probability of overlap with the phosphorescent band. Thus it can be concluded that the utility of the phosphorescence band in dye lasers is unfavourable.

1.1.1 Dye laser construction [10]

The simplest dye laser can be constructed using an optical pump, a cuvette with parallel end windows coated with a reflective layer, and a fluorescent dye solution. Practically there are two types of pumping arrangement; (a) transverse pumping and (b) longitudinal pumping.

(a) Transverse pumping arrangement
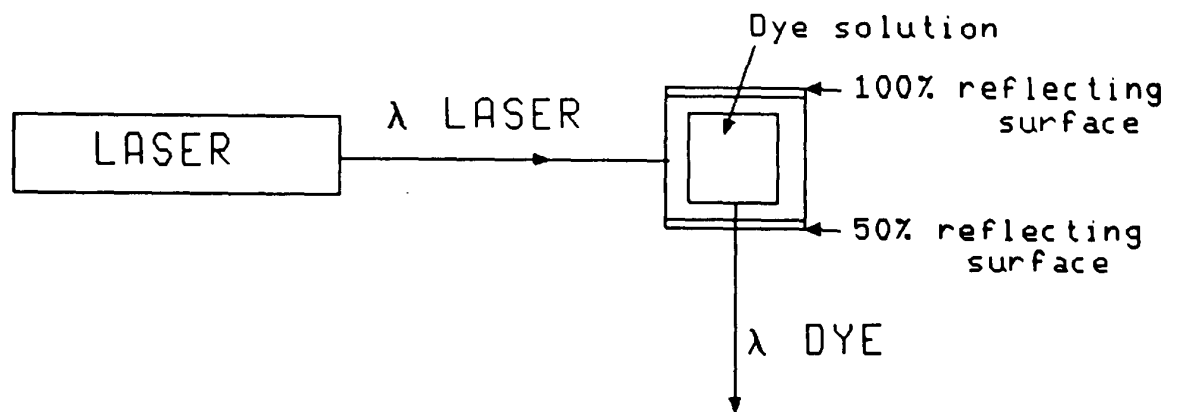
Figure 5. Transverse pumping arrangement

Figure 5 shows a simple lay out of a transversely pumped dye solution laser. The dye solution is contained within a spectrophotometer cuvette. Excitation of the dye molecules is achieved using a laser beam. The resonator is formed by the two glass-air interfaces of the polished sides of the cuvette. The exciting laser and dye laser beams are at right angles to each other. If one incorporates into the system a diffraction grating as in figure 6, it is possible to tune the laser. By varying the angle of the diffraction grating only a specific λ eg C -> D_2 (Fig. 1) will be reflected back into the cell, thus the laser is then tuned to this wavelength and only this wavelength will be emitted by the laser cell.
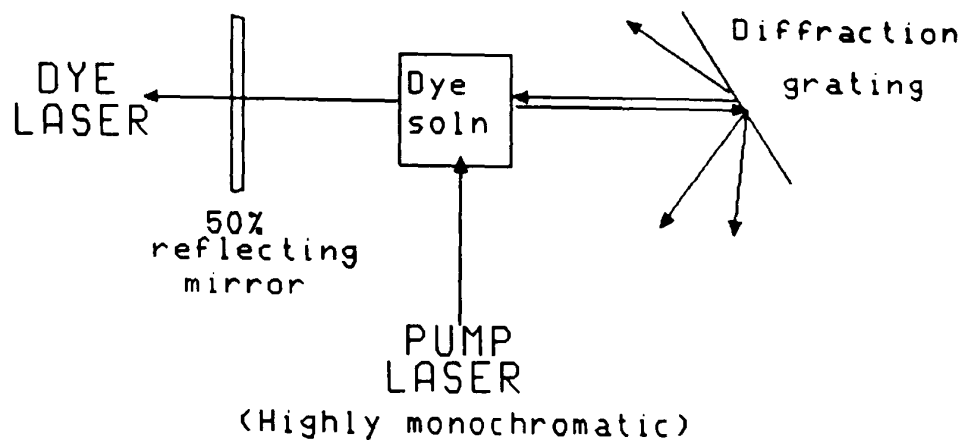
Figure 6. The tunable dye laser

(b) Longitudinal pumping arrangements,

$R(\lambda_L) = 0\%$ $R(\lambda_L) = 100\%$

$R(\lambda_D) = 100\%$ $R(\lambda_D) = 0\%$

AR = Antiflection coating
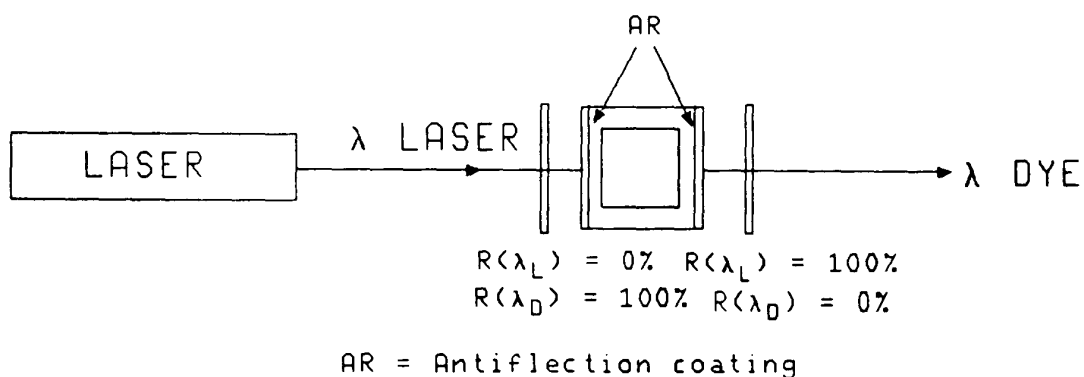
Figure 7. Longitudinal pumping arrangement

Figure 7, represents the configuration of a longitudinal pumped dye solution laser. The exciting laser beam passes through a mirror coated with a dielectric multilayer having a low reflection coefficient at this exciting laser wavelength. The emerging dye laser is differentially allowed to pass through a 100% reflecting exciting laser mirror. A more practical arrangement is shown in figure 8.

Orientation of the laser beam a few degrees to the normal of the mirror, separates the exciting laser and the dye laser beams.
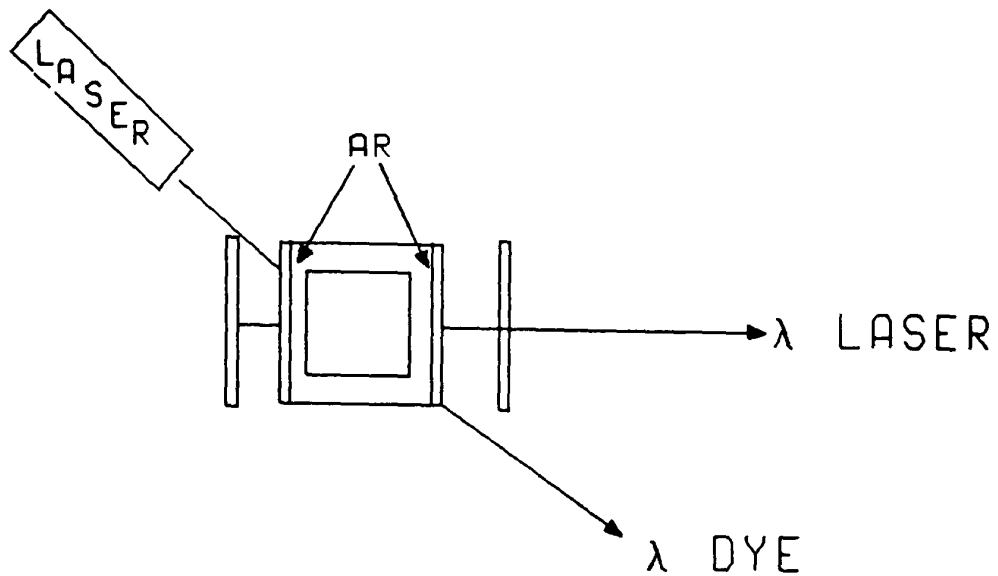
Figure 8. A more practical longitudinal pumping arrangement

It must be noted that the pumping arrangements shown are in their simplest form, the reader is directed to the text "Principles of Dye Laser Operation" by F. P. Schafer [10] for a detailed description.

1.1.2 Excitation sources [10]

The excitation source is dependent on the laser system in operation, i.e., flashlamp-pumped-dye laser, laser-pumped-dye laser, or continuous wave dye laser.

Flashlamps permit the pumping of dye solutions with an incoherent light source, eg. xenon flashlamp. Laser-pumped-dye lasers require a monochromic light source such as the ruby laser (694nm), nitrogen laser (337nm), He/Ne laser (632.8nm), Nd:YAG frequency doubled laser (532nm) and other dye lasers amongst many others. Continuous wave (CW) operation of dye lasers can be achieved using high powered gas lasers and the Argon ion laser as excitation sources. Dye solutions, for example rhodamine 6G, in CW operation must contain a triplet state quencher. The laser dye in use should have an absorption spectrum which matches the emission spectrum of the excitation source. For example, flashlamps have substantial emission in the ultra-violet, thus the laser dye must have strong absorption in the ultra-violet to take full advantage of the excitation source.

1.2 **LASER DYES** [11]

Historically Sorokin and Lankard (1966) were the first to obtain stimulated emission from an organic compound, namely chloro-aluminium-phthalocyanine [12]. Using a giant pulse ruby laser and a resonator they produced a powerful laser beam at 755.5nm.

Today laser dyes are available which cover the electromagnetic spectrum from the ultra-violet to the infrared, Gordon and Gregory [13] have listed typical examples which cover this region, (Table 1).
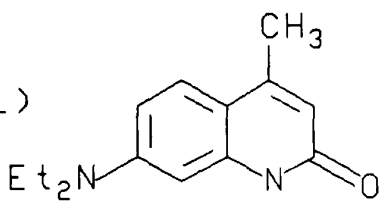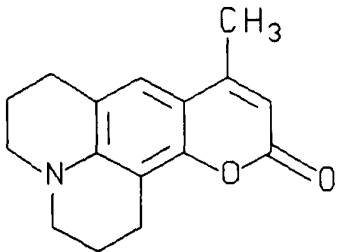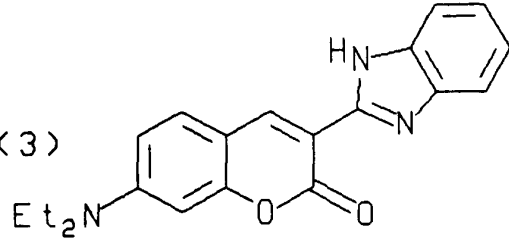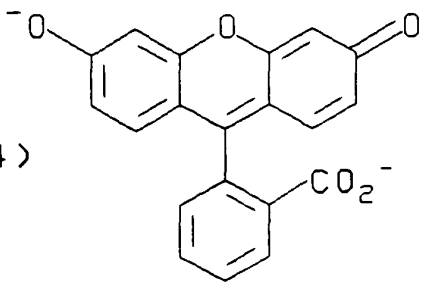
	Absorption λ_{max}/nm	Lasing λ_{max}/nm	Name/Acronym
(1)	360	425	Carbostyril 165
(2)	389	480	Coumarin 102
(3)	436	573	Coumarin 7
(4)	501	560	Fluorescein

Table 1. Some typical laser dyes
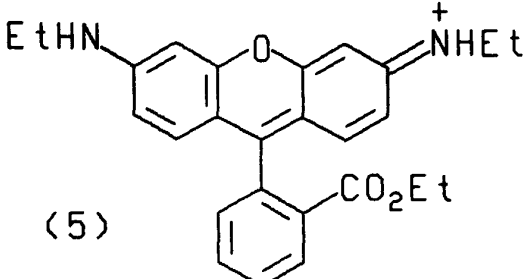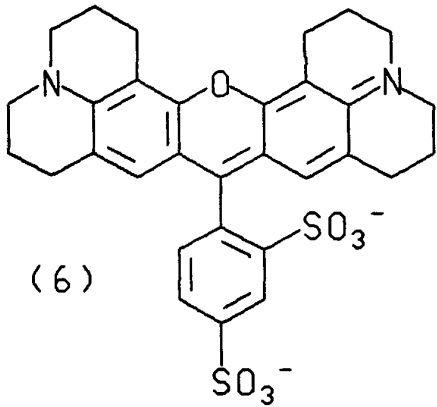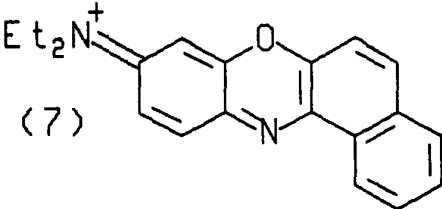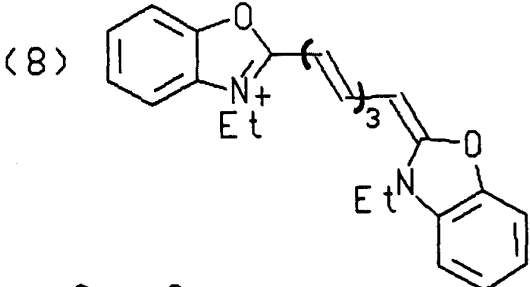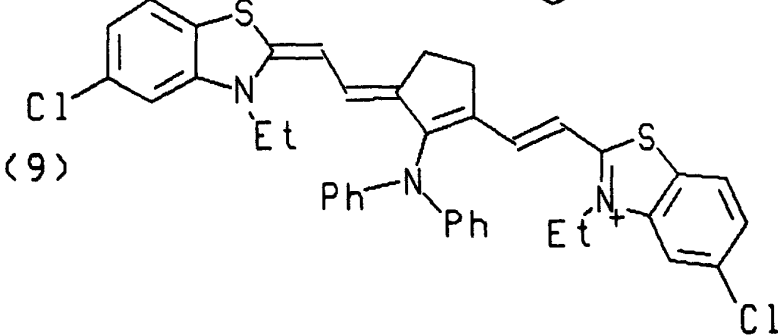
530	590	Rhodamine 6GP
576	648	Rhodamine 101
628	690	Nile blue
687	780	DEOTC
823	950	IR140

Table 1. continued

The ideal laser dye has a quantum yield of fluorescence equal to unity. This is never the case, however, there are many factors which reduce optimum laser gain [11].

(a) Nonradiative processes

The nonradiative processes $S_1 \leadsto S_0$ and $S_1 \leadsto T_1 \leadsto S_0$ effectively compete with light emission, so reducing laser gain.

(b) Purity of dye

Laser dyes should be extremely pure, as impurities can quench the laser output.

(c) Thermal effects

Intense radiation causes rapid overheating of the dye solution leading to fluorescence losses. Use of water as a solvent and circulation of the dye solution with cooling overcomes this problem. This brings in the need for water soluble laser dyes.

(d) Photostability

Photodegradation of the laser dye during operation obviously leads to a loss in laser gain. With dye solutions this is not such a problem because the dye can be circulated. Photodegradation is a serious problem when the dye is incorporated into solid matrix and cannot be circulated.

(e) Structural properties affecting fluorescence efficiency

In general a rigid, planar molecular structure attributes to a high quantum yield of fluorescence. For example phenolphthalein (10) is non-fluorescent whereas its oxygen -bridged relative, fluorescein (4) has a fluorescence quantum yield of 90% [14].

(10)

(4)
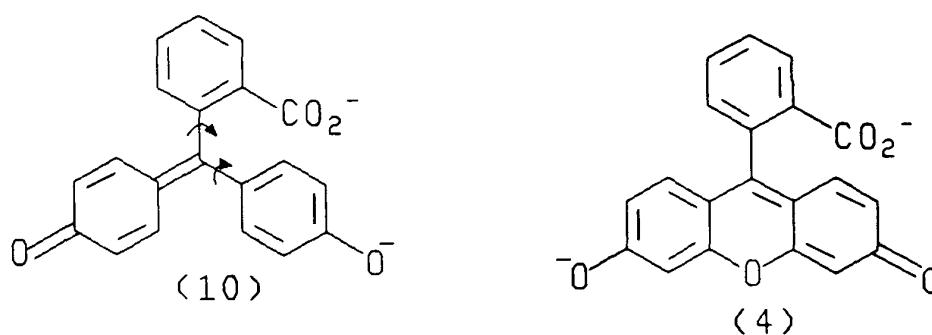
The oxygen bridge prevents free rotation of the phenol groups. Restriction of the mobility of the diethylamino groups in rhodamine 101 (12) increases the quantum yield to 100% compared to rhodamine B (11) , which has freely mobile diethylamino groups and a quantum yield in ethanol of 40% at 25°C [15][16].

(11)

(12)
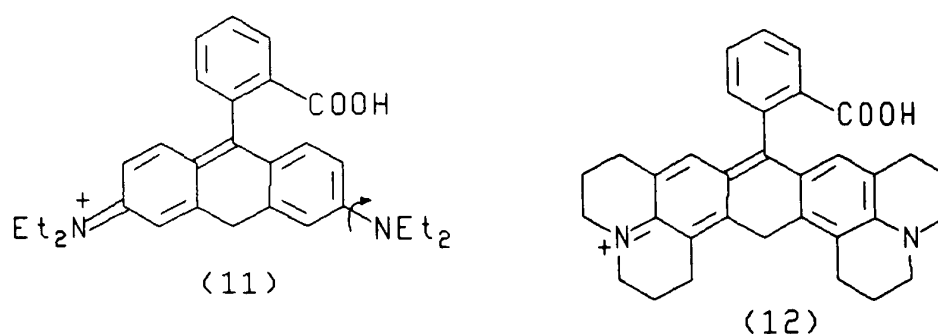
For the application purposes of this project it was necessary to synthesize infrared absorbing dyes showing excited state absorption properties at high pump intensity. The following section deals with chromophores which exhibit loss of gain at high pump intensity. The mechanism of this loss and the applications of the dyes are also discussed.

1.3 THE LOSS OF GAIN AT HIGH PUMP INTENSITY

In order to maximise the optical gain from a dye laser system it is necessary to optimise experimental conditions, such as the pump configuration. During the course of such optimisation procedures, Wieder [17] found that at high pump intensities, when using a nitrogen-laser-pumped tunable dye laser, the fluorescence quantum efficiency of 7-diethylamino-4-methyl-coumarin (13) and 4-methyl-umbelliforone (14) was reduced.
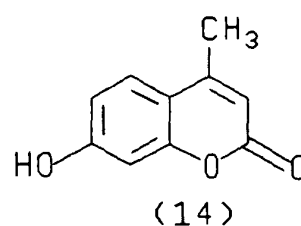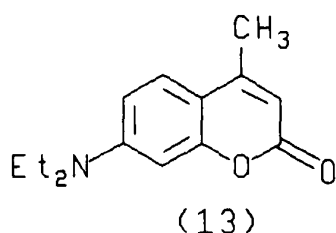
At the highest incident intensity, 200×10^6 watt/cm^2, the relative quantum yield is reduced to 10% of its original value.

Decker [18] has also observed this phenomenon when optically pumping infrared emitting polymethine dyes with a frequency doubled Nd:YAG laser (pumping wavelength = 532nm). Decker optically pumped five infrared dyes, namely HITC iodide, IR-144, IR-132, IR-140, and IR-125 at 532nm (all are polymethine cyanine in structure) and assessed the pump energy to dye energy conversion efficiency. As the pumping radiation was more strongly focused in order to increase the pump power density incident on the dye solution, it was observed in the case of IR-140 that the transmission of 532nm radiation decreased. This is summarised in Figure 9.

IR-140 curve is for a 5×10^{-4}mol solution in DMSO

CVP curve is for a 2×10^{-4}mol solution in methanol
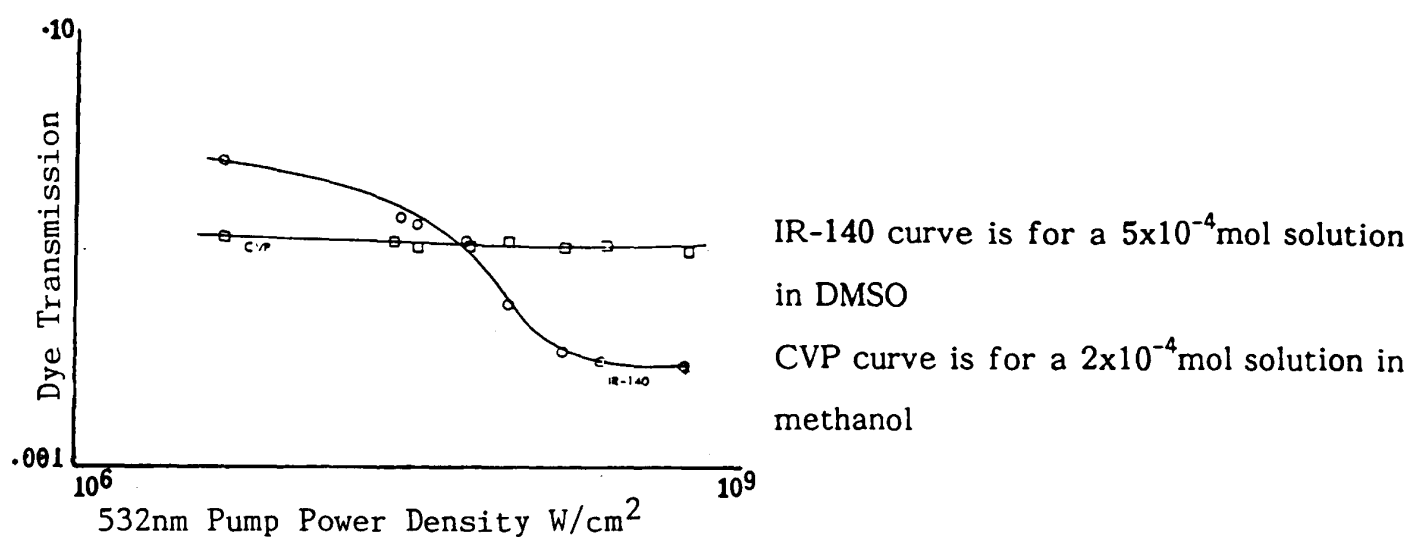
Figure 9. 532nm transmission as a function of pump power density [18]

This non-linear absorption at high pump intensity was not seen at 532nm with IR-144. Experiments to establish non-linear absorption were only carried out on the two most efficient laser dyes, IR-140 and IR-144. This non-linear relationship between dye absorption and light intensity is referred to as reverse saturable absorption (RSA).

Many workers in this field have observed reduction in transmission when operating laser systems at high intensity levels. Table 2, lists other materials which show this phenonemon.
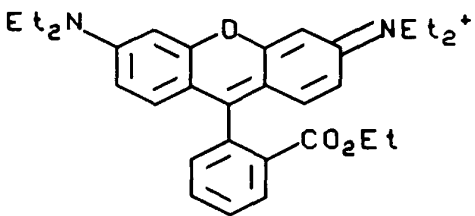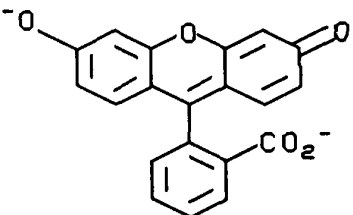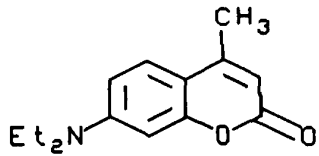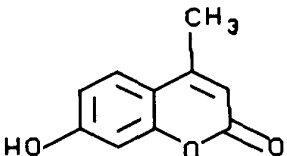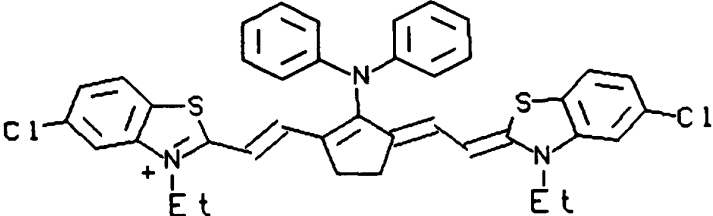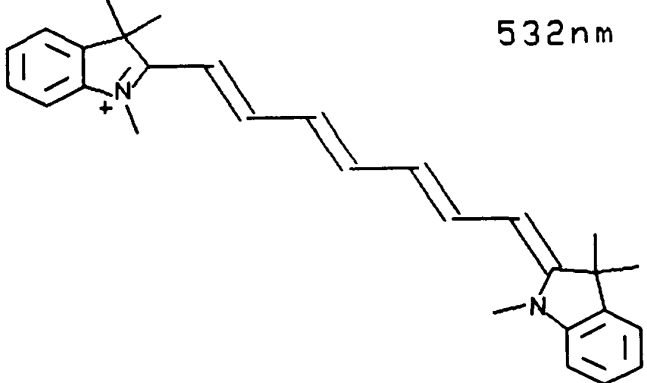
Name	Structure	Wavelength of RSA	Ref
Alexandrite (15)	$BeAl_2O_4{:}Cr^{3+}$	488nm	[19][20][21]
Rhodamine 6G (5)		337.1nm and 435nm	[20][22][23] [24][25]
Fluorescein (4)		337.1nm	[25]
7-Diethyl amino-4-methyl-coumarin (13)		337nm	[25][17]
4-Methyl-umbelliferone (14)		337nm	[17]
IR140 (9)		532nm	[18]
HITC iodide (16)		532nm	[22]

Table 2. Dyes which show RSA
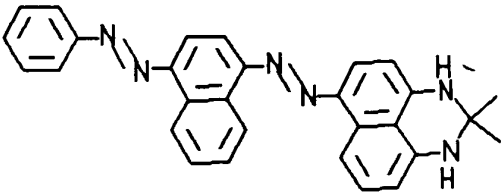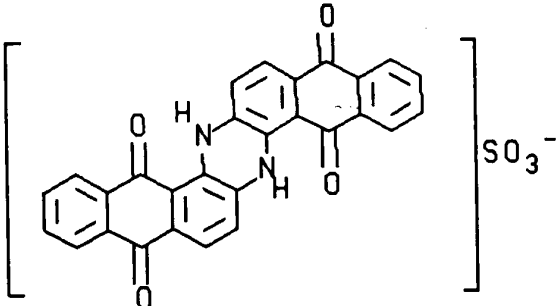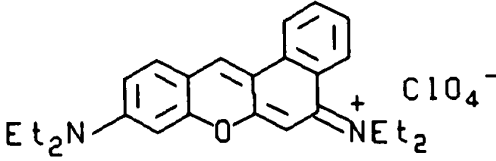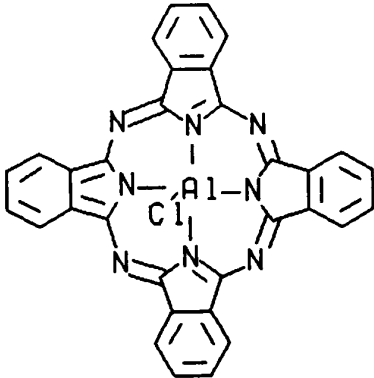
Name	Structure	Wavelength of RSA	Ref
Sudan black B (17)		694.3nm	[26]
Sulphonated indanthrone (18)		694.3nm	[26]
Cresyl violet perchlorate (19)		514.5nm	[27][28]
Chloro-aluminium-phthalo-cyanine (20)		694.3nm	[29][30]
Acridine red (21)		20,000-25,000 cm^{-1}	[21]

Table 2. continued

The decrease in transmission with increase in incident intensity can be due to a number of physical phenomena, such as excited state absorption, two photon absorption, free carrier absorption, stimulated Raman scattering, and parametric

oscillation [20].

Various literature sources conclude that the loss of laser gain in dye laser systems at high input power is due largely to excited state absorption [18][20][30].

1.3.1 Excited state absorption

Harter et al [20] have explained the process of excited state absorption using a diagram of electronic potential energy levels versus nuclear configuration coordinate, as shown in Figure 10.
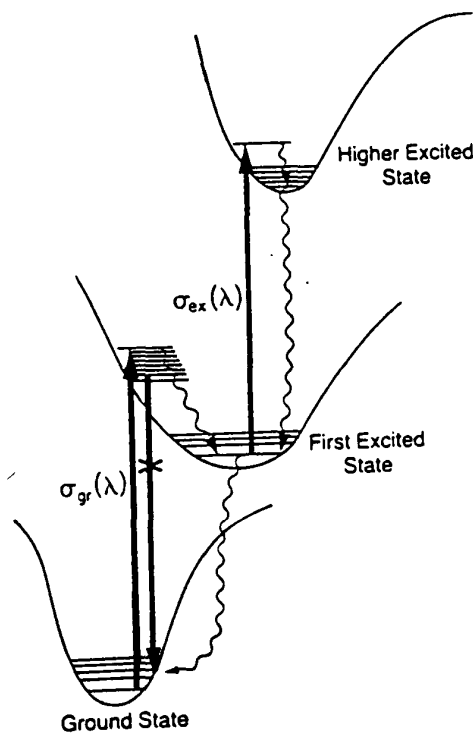
Figure 10. The process of excited state absorption

Absorption of laser radiation from the lowest level of the first excited state to higher lying electronic excited states is the process of excited state absorption.

Band and Scharf [31] suggest that for excited state absorption to occur the excited

state absorption cross section Θ_{ex} at a wavelength λ, must be larger than the ground state absorption cross section Θ_{gr}. Band and Scharf also report three other criteria for a molecule to be a successful excited state absorber;

1. The $\Theta_{gr}(\lambda)$ must be sufficiently large such that the incident pulse saturates the first excited state.

2. The first excited state or higher - lying excited state should not decay to other levels which trap excitation.

3. The emission cross section should be small.

It is important to consider the nature of this excited state absorption, i.e., is it singlet -> singlet or triplet -> triplet in mechanism. Because of short pulse excitation times in all the experiments, a population in the triplet state should not build up. Thus the mechanism of excited state absorption cannot be triplet to triplet in nature [25][27][29].

Excited state absorption is wavelength dependent, and for example, Shah and Lehery [27] have shown that a 5×10^{-6} mol/l solution of cresyl violet perchlorate in methanol, pumped with a nitrogen laser-pumped dye laser at high intensity can behave as either an excited state absorber or saturable absorber, (Figure 11).
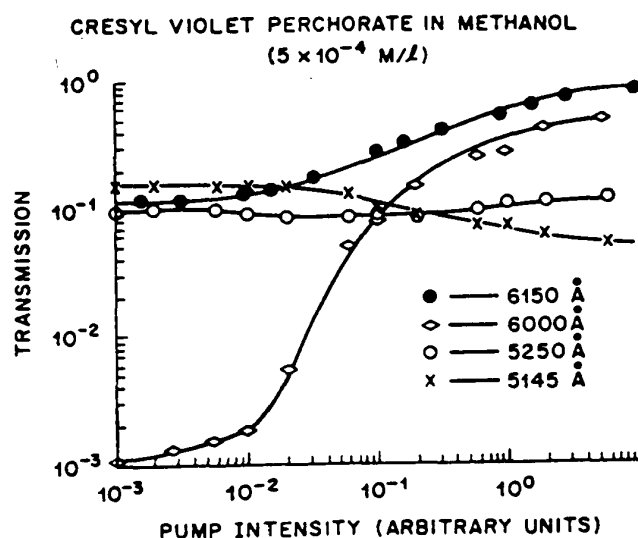
Figure 11. Absorption properties of CVP at high pump intensity [27]

Curves at 600nm and 615nm show saturable absorption with transmission increasing

at high input flux. There is no change in transmission at 525nm but at 514.5nm there is excited state absorption leading to a decrease in transmission.

Saturable absorption can be explained via two mechanisms;

1. If the intensity is high enough to saturate the transition and the absorption rate equals the rate of stimulated emission then the solution will be bleached.
2. All molecules are removed from the ground state to metastable excited states, if these states have a small absorption cross section at the exciting frequency then the solution is effectively bleached.

1.3.2 Measurement of the absorption cross section of the first excited state

The effect of excited state absorption can be detrimental to high power dye laser systems, resulting in fluorescence quenching. Wieder and Sahar [32] describe a procedure to measure the excited state absorption cross section, and Figure 12 shows the apparatus system employed.

A nitrogen laser delivers pulses of 100kW, of 8ns duration. A beam splitter reflects a portion of the light into the sample, and this is the pump source which promotes the dye molecules to their excited state. The other part of the nitrogen laser beam is directed via mirrors M_1 and M_2 onto the sample, this is the probe pulse and is delayed with respect to the pump pulse typically by 1-2ns.

The energy of the probe pulse transmitted through the sample is measured once with the pump beam blocked before it reaches the sample and then with the pump beam present. With no pump source, all the absorption is due to ground state absorption. With the pump beam present the probe beam encounters a large excited state population, and thus suffers from ground and excited state absorption. The difference between transmission in the two cases gives a measure of excited state absorption at the probe wavelength.
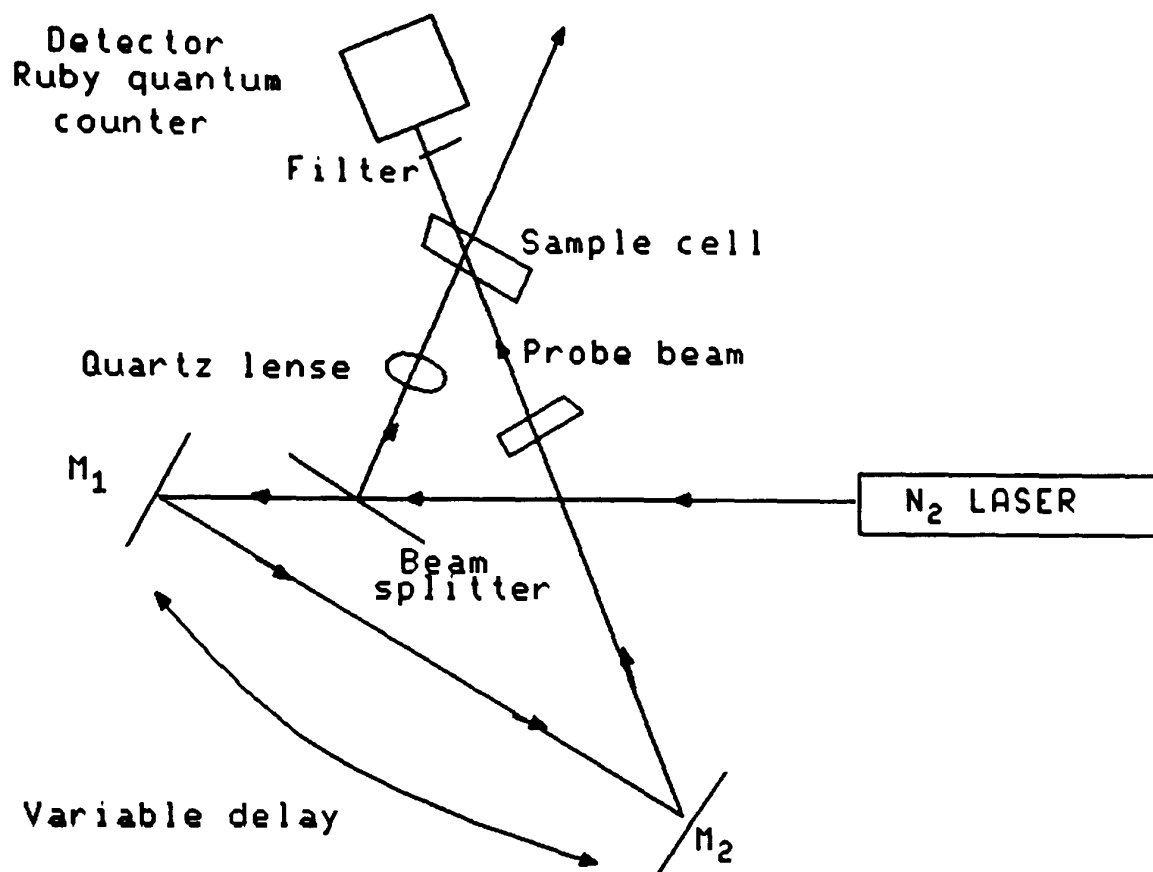
Figure 12. Measurement of excited state absorption cross section

Absolute measurement of absorption cross section requires the pump source to completely bleach the dye solution before probing. Dolan and Goldschmidt [33] have measured the absolute excited singlet-singlet absorption of rhodamine 6G using the high intensity of the second generation harmonic of a neodymium laser in a flash photolysis system. Wieder and Sahar [25] have modified their system with the incorporation of a tunable dye laser as the probe beam, (Figure 13). Using several dyes probe beams can be obtained over the range 350-740nm.

1.3.3 The application of excited state absorbers

Measurement of fast molecular processes such as rotational diffusion of molecules, relaxation and isomerisation of large molecules and the rapid initiation of photochemical processes introduces the necessity for ultra short intense light pulses [9][34]. The excited state absorber in conjunction with a saturable absorber functions
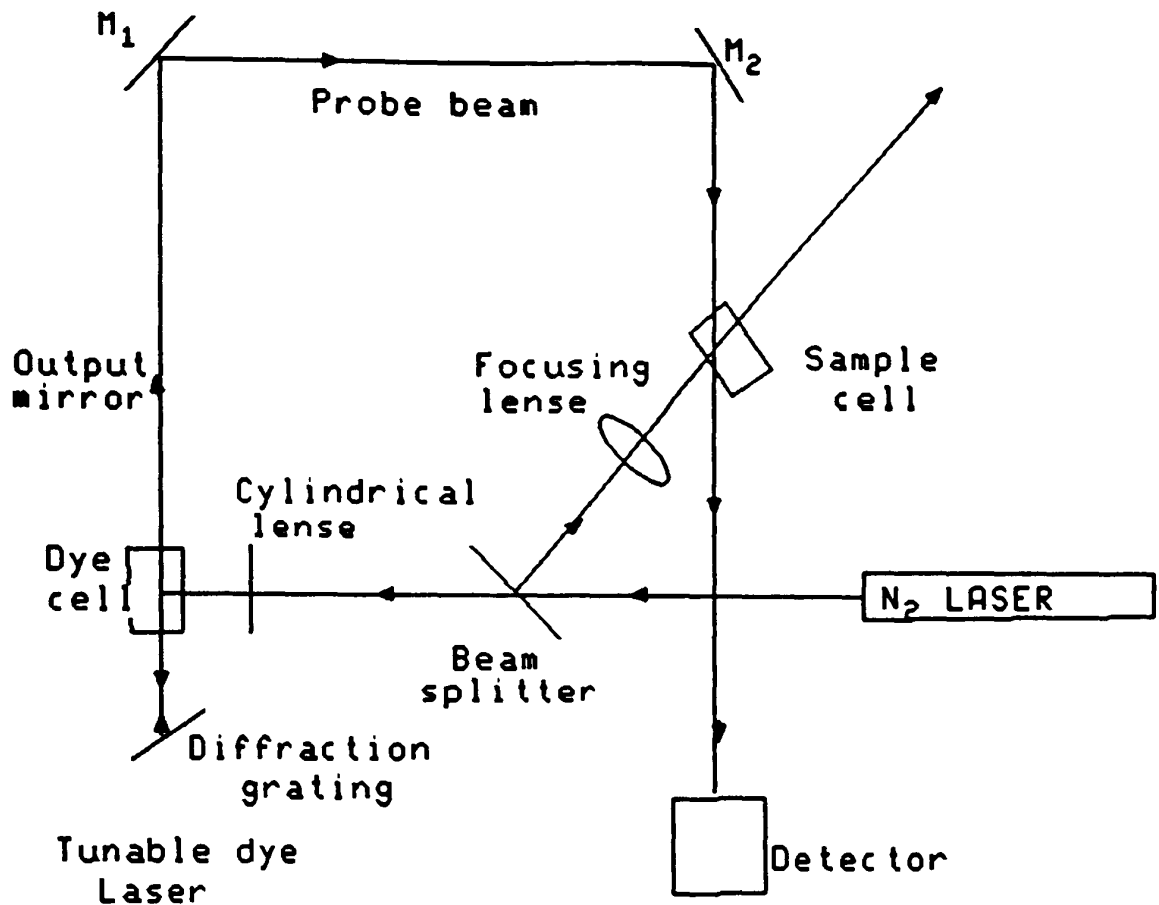
Figure 13. Modified measurement of excited state absorption cross section

as a pulse compressor for the typical short optical pulse, (Figure 14(a)) [17][33]. The excited state absorber reduces the tailing edge of the pulse, whereas the saturable absorber reduces the leading edge of the pulse, (Figure 14(b)).
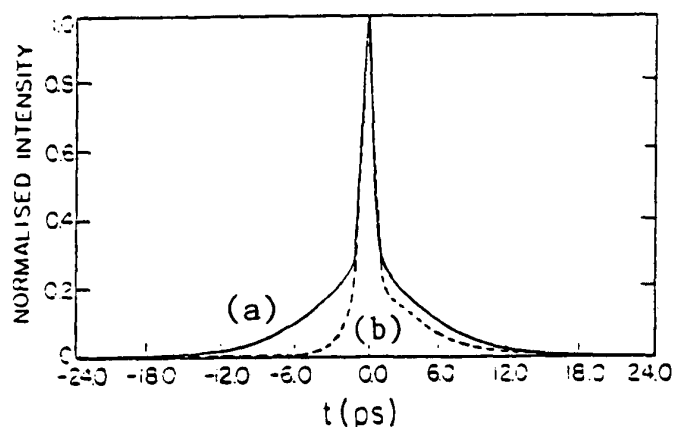
Figure 14. Incident pulse shape vs. time (solid line) and exit pulse shape after passage through the medium (dashed line)

Mechanistically, absorption of the leading edge of the pulse saturates the ground state transition of the saturable absorber. As the saturable absorber by definition has no excited state absorption, the intensity of the central portion of the pulse is not reduced. However the leading edge and the central portions of the pulse are reduced by the ground state absorption of the excited state absorber. In the time taken for the trailing edge of the pulse to pass through the excited state absorber, the excited state has been sufficiently populated so ensuring increased absorption due to excited state absorption.

Excited state absorbers in conjunction with saturable absorbers are also used as pulse shorteners in mode locked laser systems [24][36].

1.4 LONG-WAVELENGTH CHROMOPHORES AND NEAR-INFRARED DYES

1.4.1 The Chemistry of Polymethine dyes

The majority of long wavelength chromophores used in laser technology are of the polymethine type. Many infrared dyes also fall into this category. Before reviewing infrared dyes, it is useful to consider the chemistry of polymethine dyes. Characteristically a 'polymethine dye' contains a chain of methine groups. In general polymethine dyes can be sub-divided into three categories [37];

1. Amidinium cationic systems (cyanine dyes)

(a)   (22)   (b)
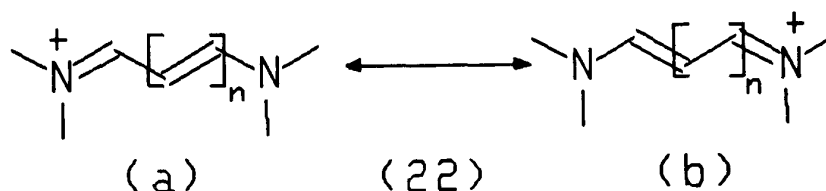
2. Carboxylate anionic systems (oxonol dyes)

(a)   (23)   (b)
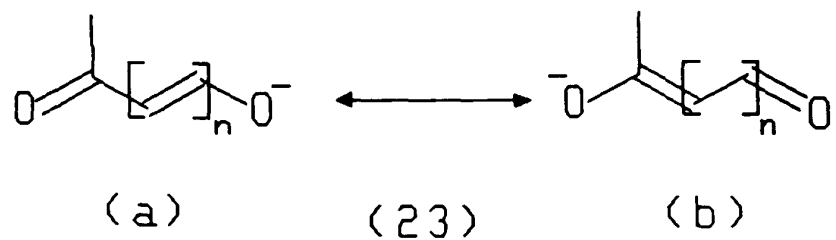
3. Dipolar-amidic neutral systems (merocyanine dyes)

(a)   (24)   (b)
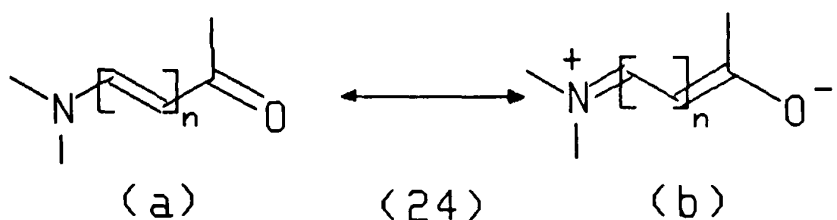
Examples from each class include the cyanine dye (25), oxonol dye (26) and the merocyanine dye (27) [38].

(25)

(26)

(27)
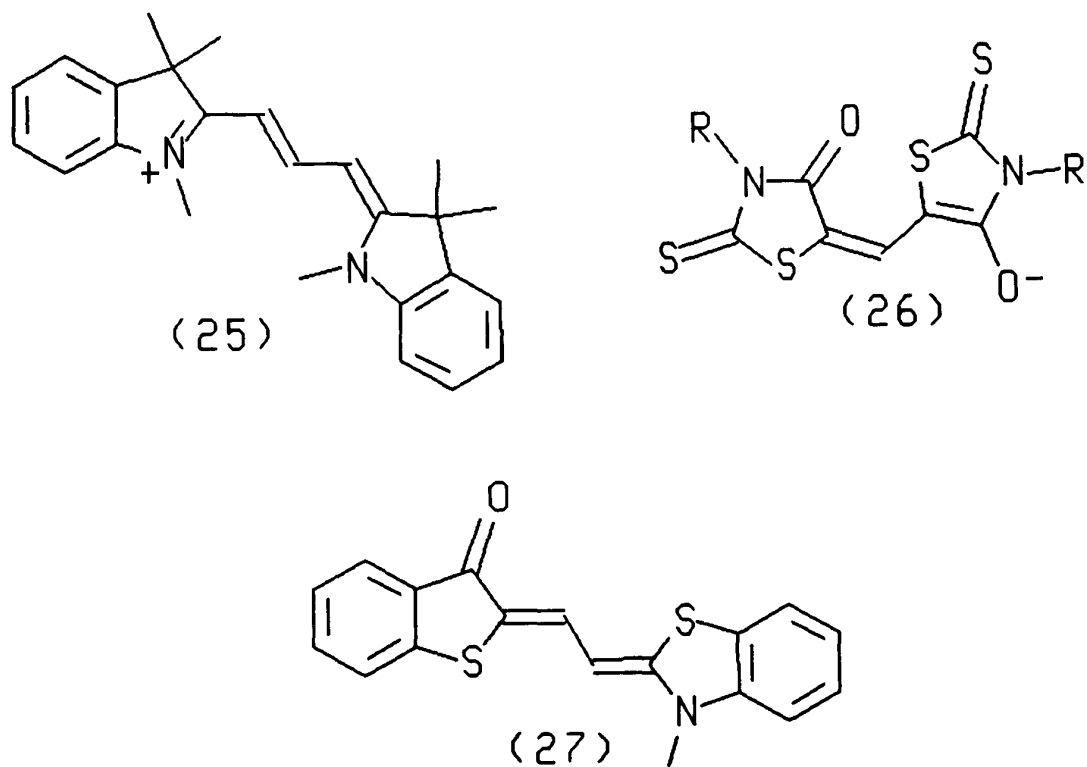
There are of course miscellaneous polymethine dyes which do not fit into these

categories. An example is the donor-acceptor chromogen (28) [39].
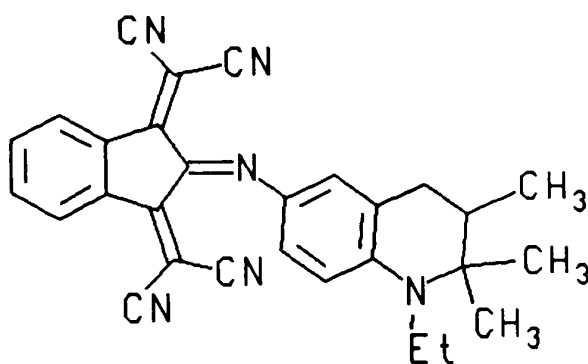
(28)

This dye has been classified as a "meropolymethine" dye. Historically the first polymethine dye to be discovered was 'cyanine' (29), synthesised by Greville Williams in 1856 [40]. However the chemistry of cyanine dyes only developed significantly after the discovery by Vogel in 1873 of the ability of cyanine to sensitise silver halide emulsions in the green region of the visible spectrum. Before this discovery silver halide emulsions were only sensitive to violet and blue light of short wavelength. Throughout the following century conjugation in the cyanine polymethine chain was progressively extended, giving ultimately near-infrared absorbing cyanine dyes (Figure 14) [41], some of which were near-infrared sensitisers. A recent example of a 'supersensitiser' is given by dye (42) [42].
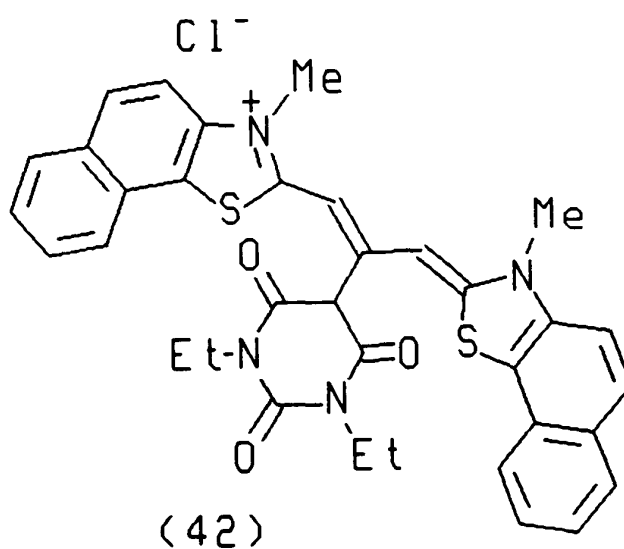
(42)
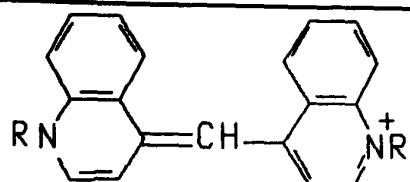
Williams Cyanine
1856
(29)
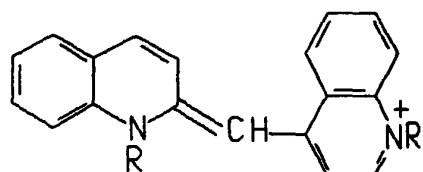
Early 1880's
(30)
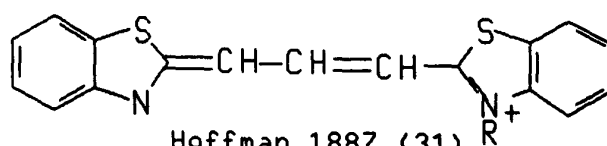
Hoffman 1887 (31)
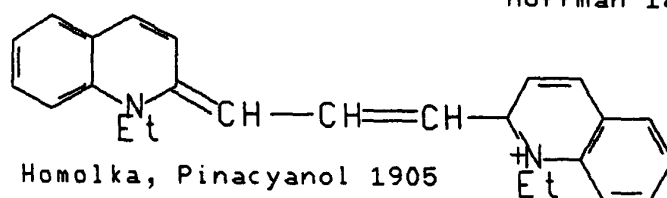
Homolka, Pinacyanol 1905
(32)
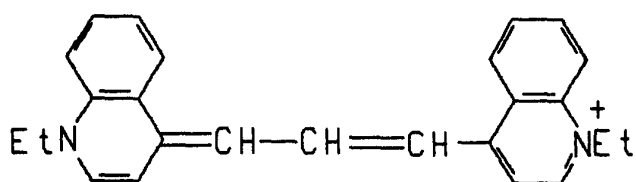
Adams and Haller, Kryptocyanine
1920 (33)
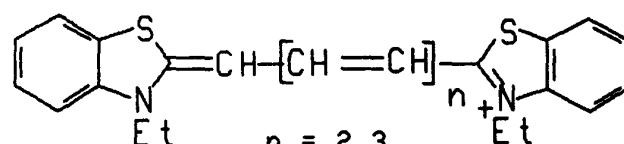
n = 2,3
1920's (34)
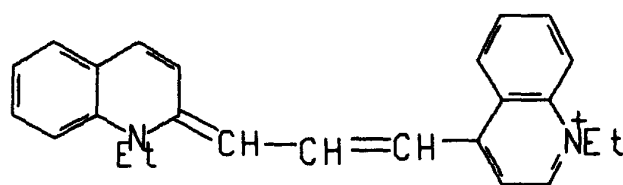
Piggotts and Rodd 1930
(35)
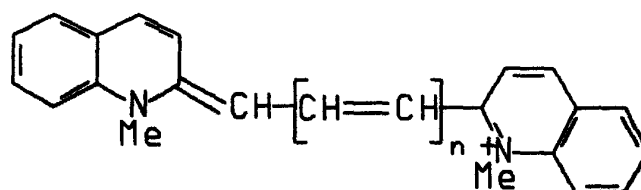
n = 2,3 (1930)
(36)

Figure 15. Chronological development of extended conjugation in cyanine dyes
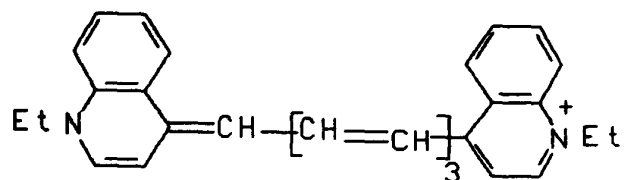
Brooker, Zenocyanine 1933
(37)
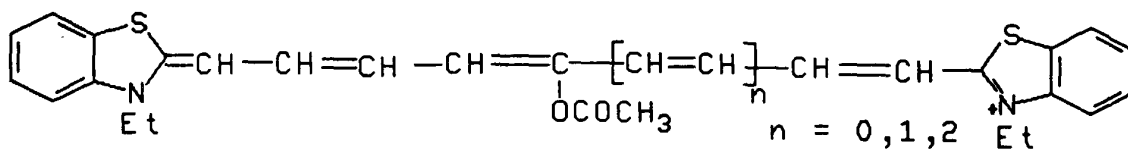
Konig 1934 Brooker 1935
(38)

$n = 0,1,2$

(39) $n = 5,6$
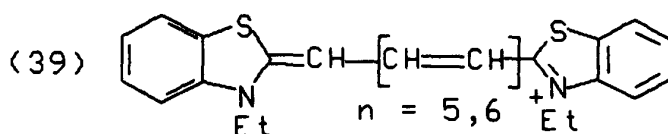
Dieterle and Riester 1937
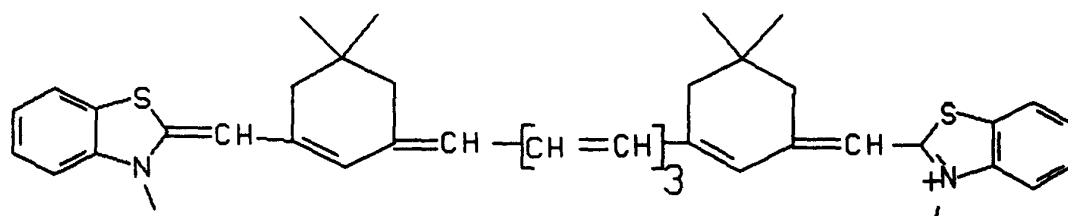
Hesiltine 1953 (40)

Kodak (41)

Figure 15. continued
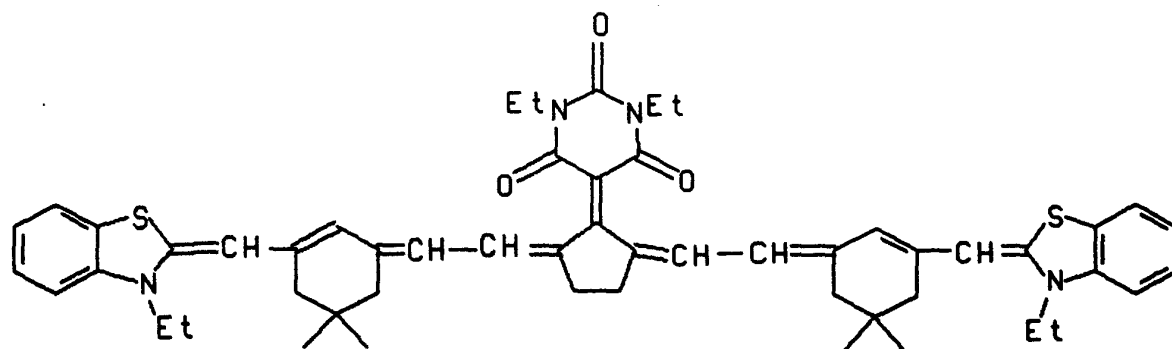
1.4.1.1 Synthetic routes to polymethine dyes

The simple methine dye (44) can be prepared via a Knoevenagel-type condensation between a formylated aromatic amine (43) and an active methylene compound (Scheme 1).
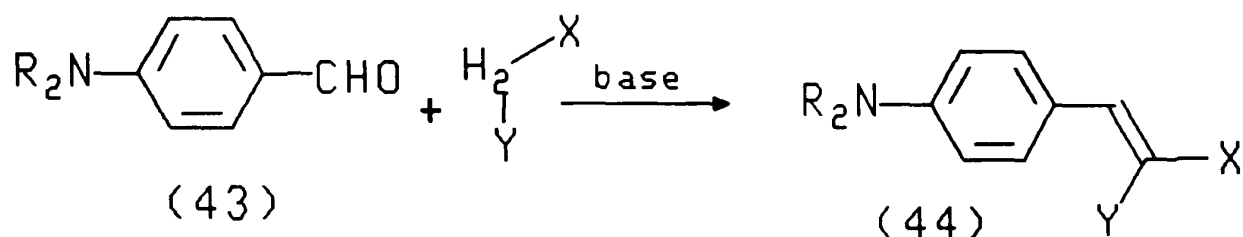
Scheme 1. Knoevenagel condensation

For the reaction to proceed efficiently, X and Y have to be electron withdrawing groups, so making the CH_2 acidic, i.e. an "active methylene" group. This procedure is also used in the preparation of the cationic polymethine styryl dyes (45) and (46), as in Scheme 2 [43].
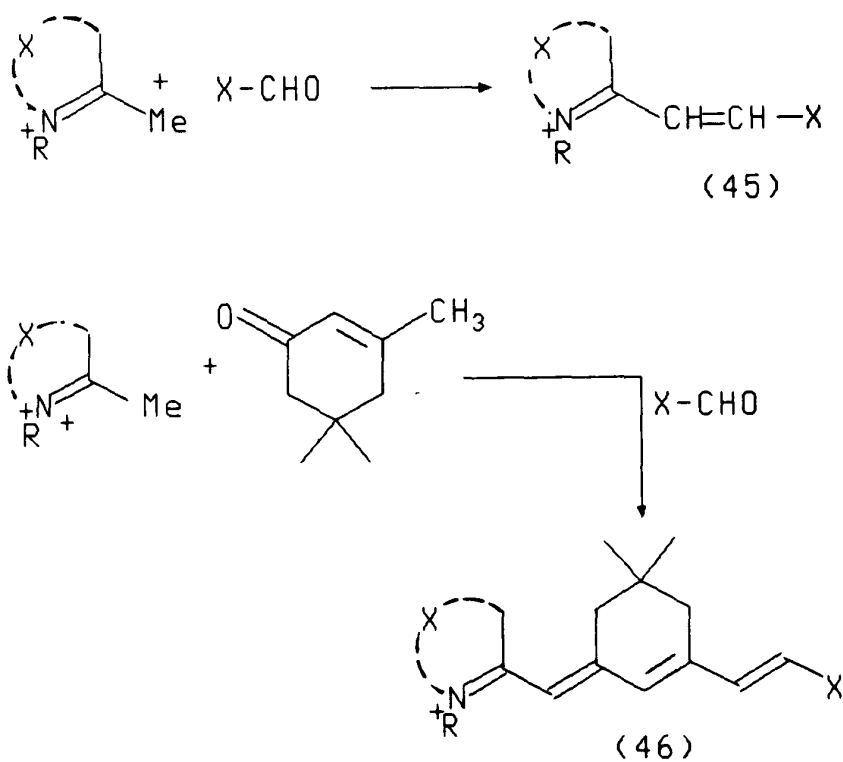
Scheme 2. Synthetic route to polymethine styryl dyes

In these instances the acidity of the -CH$_3$ group is caused by the adjacent quaternised nitrogen atom. Synthetic routes to cyanine dyes are well documented, and variation of the terminal heterocyclic moieties enables the preparation of a vast range of oxonol and merocyanine dyes [37][42][44].

In general cyanines are prepared via condensation type reactions. The general routes can be classified as either oxidative or nonoxidative. Scheme 3, shows examples of the oxidative route.
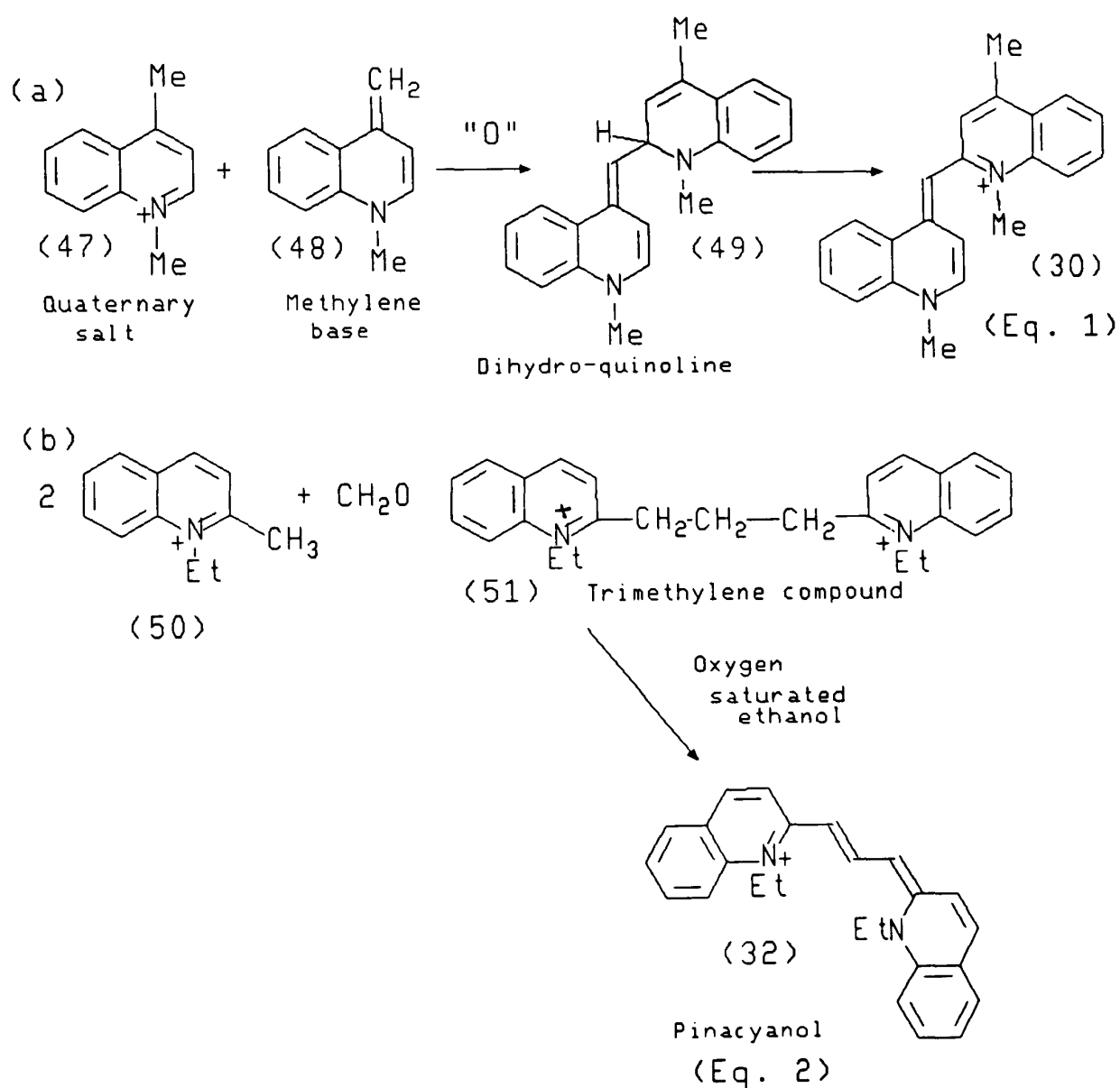
Scheme 3. Oxidative routes to cyanine dyes

Direct condensation of a quaternary salt (47) with a methylene base (48) gives the dihydro-quinoline (49), and oxidation of this gives the corresponding cyanine (30) (Eq.1). In the case of pinacyanol (32) the dye is formed from the condensation of two mole equivalents of quinaldium salt (50) with formaldehyde. The trimethylene compound (51) is then oxidised to give the cyanine dye (Eq.2). Formaldehyde supplies the central -CH= group of the three carbon bridge.

Of more importance are the non-oxidative condensation routes, and the main nonoxidative pathways to polymethine dyes are summarised in Scheme 4.

Direct condensation of the heterocyclic active methylene (51) with the thioalkyl compound (52) yields the monomethine dye (53) (Eq.3). Condensation of two mole equivalents of active methylene (51) with triethylorthoformate yields the trimethine cyanine dye (54) (Eq.4). This is also formed from the anilino intermediate (55). This type of intermediate was first made by Piggott and Rodd of I.C.I (1930), by the reaction of diphenylformamidine PhN=CH-NHPh with the active methylene (51). Shown is the acetanilido derivative (Eq.5). Use of the amine (56) affords a cyanine system incorporating a central bridging unit (Eq.6). Condensation of the active methylene (51) with β-anilinoacrolein anil (58), n=1, yields a pentamethine cyanine dye (59) (n=2) (Eq.7). Alkynes (60) (Eq.8), and compounds containing labile halogen atoms (61) (Eq.9), are also of use in the preparation of cyanine dyes (62)(63).

(Eq. 3)

(Eq. 4)

(Eq. 5)

(Eq. 6)

(Eq. 7)

(Eq. 8)

(Eq. 9)
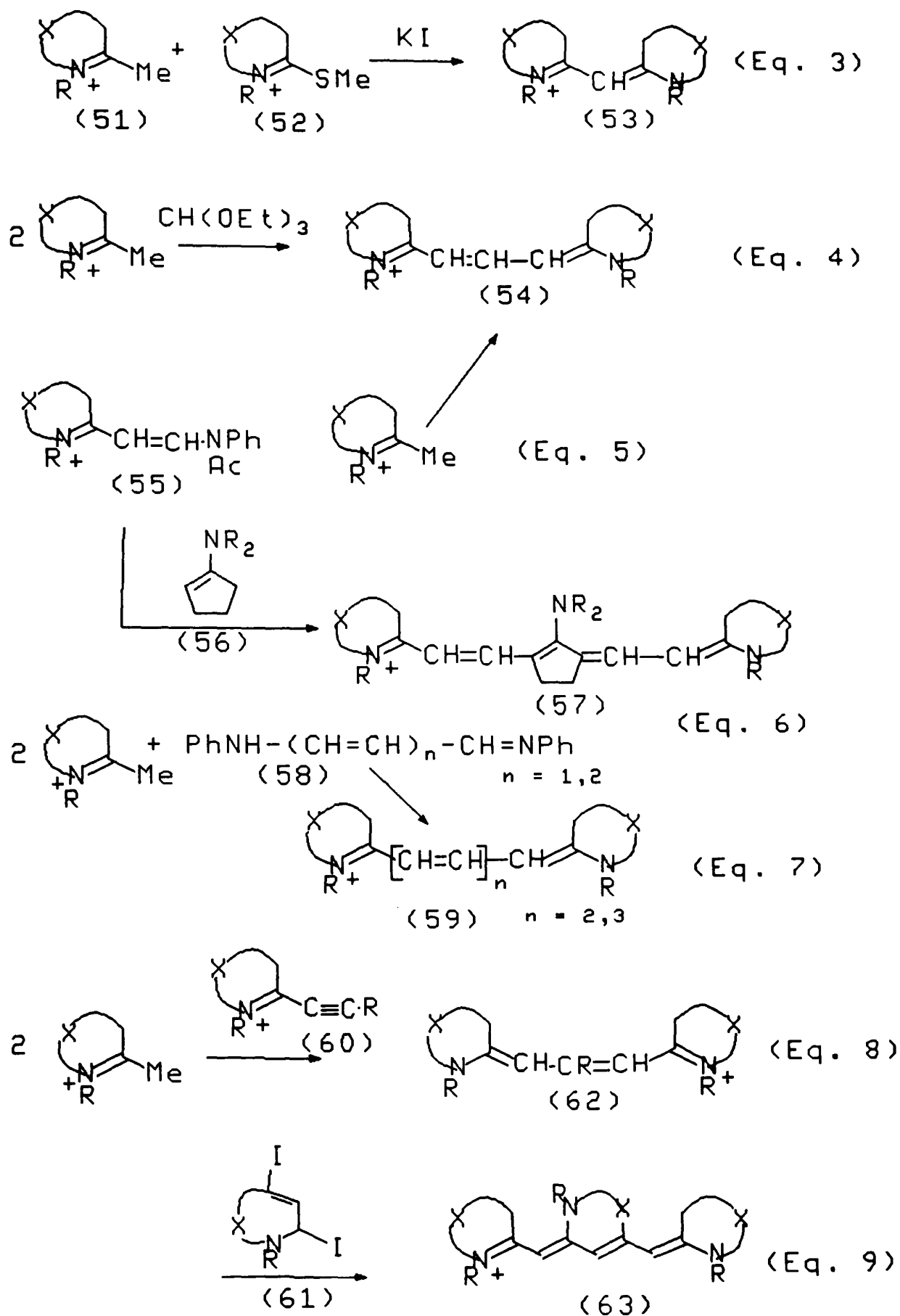
Scheme 4. Non-oxidative routes to cyanine dyes

Common heterocycles encountered as terminal groups in cyanine dyes have been listed by Griffiths (Table 3) [1].

Table 3. Common heterocyclic end groups
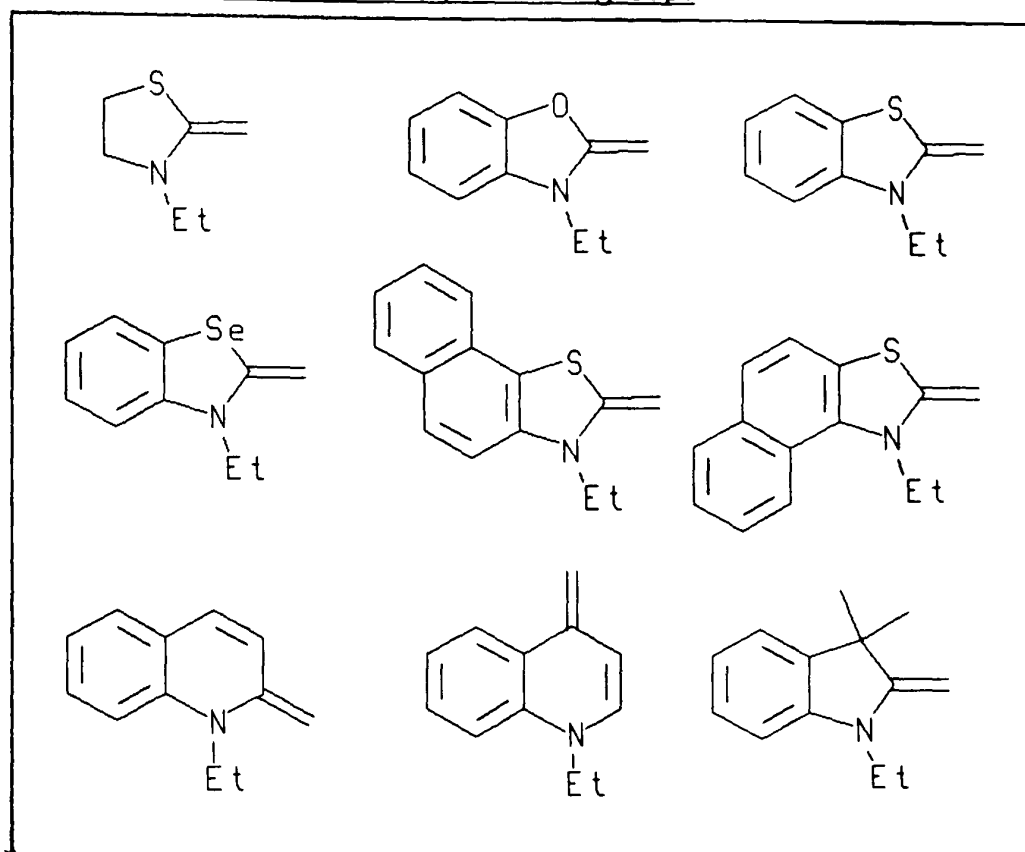
A few examples of more recently developed end groups are summarised in Table 4 [44].

Table 4. New heterocyclic end groups
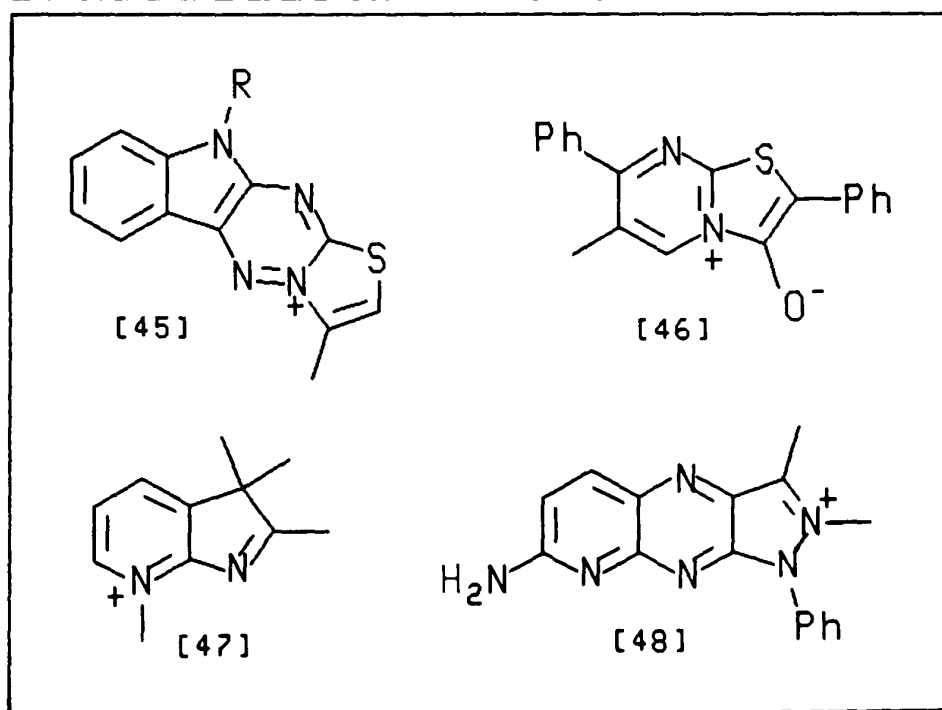
Polymethine dyes characteristically have poor stability properties. Inclusion of ring systems into the polymethine backbone restricts movement of the long conjugated chains, improving thermal and photochemical stability properties. Matsuoka has summarised the various types of bridging units used to improve structural stability (Table 5) [49].

Table 5. Bridging units in cyanine dyes

$(CR_2)_n$
R = H, Me   X = CH_2, NR   X = Cl, NR_2
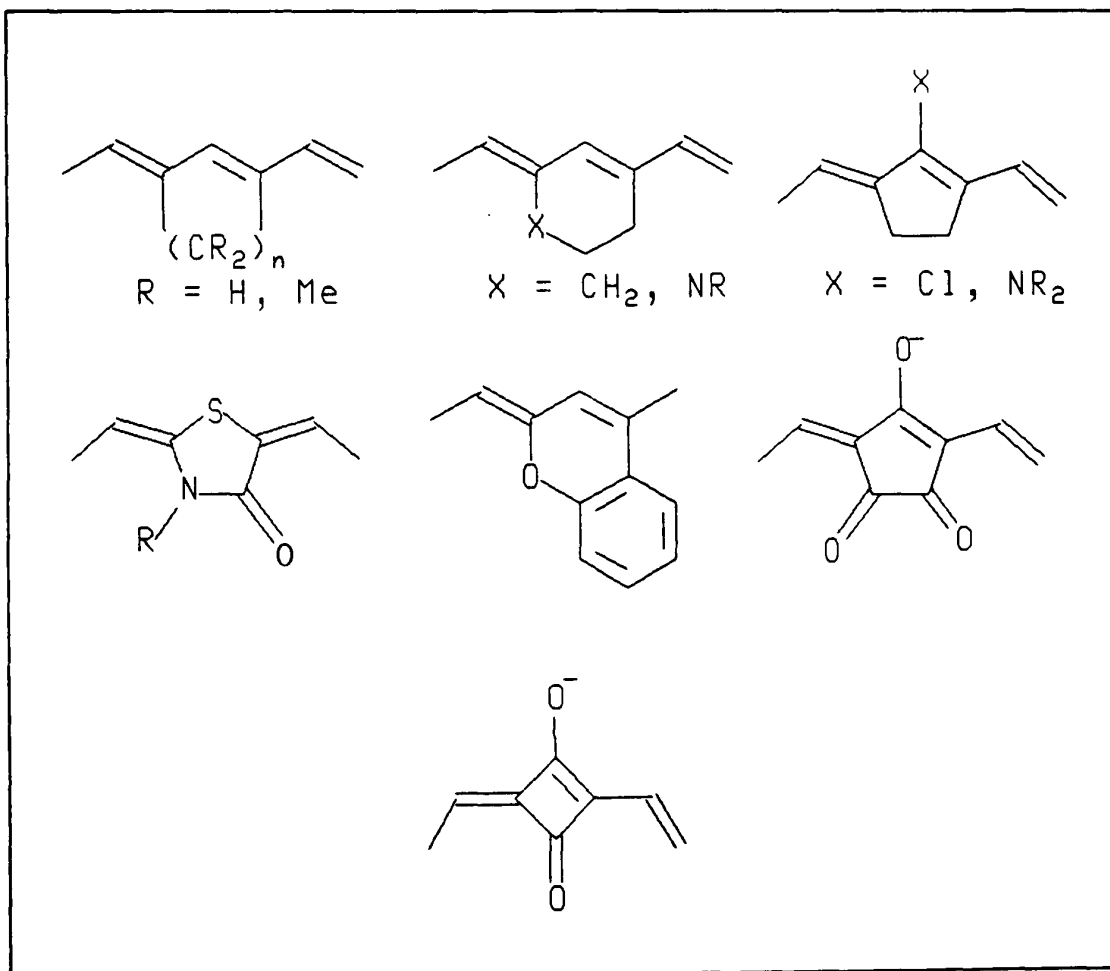
Using this technique Reynolds and Drexhage (1976) [50] prepared stable near-infrared absorbing heptamethine pyrylium dyes, some examples of which are shown in table 6.
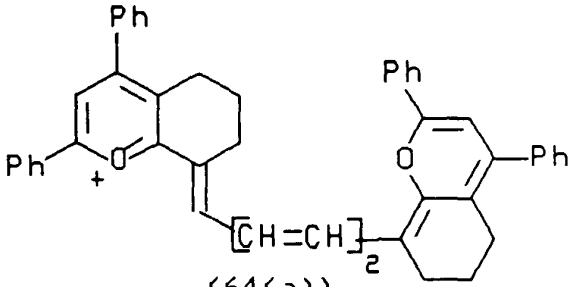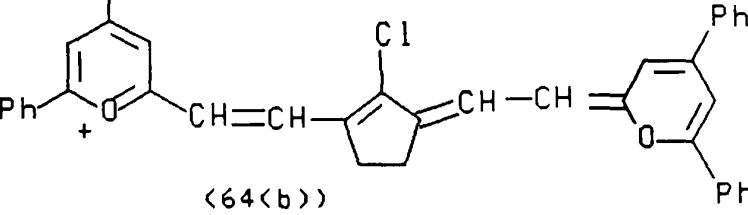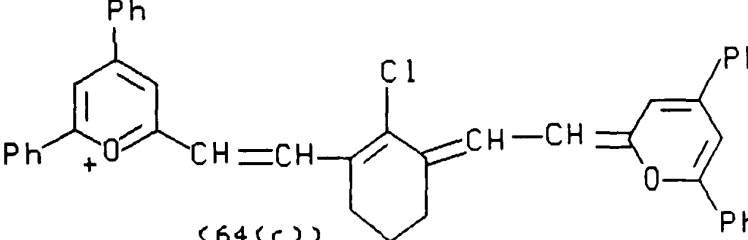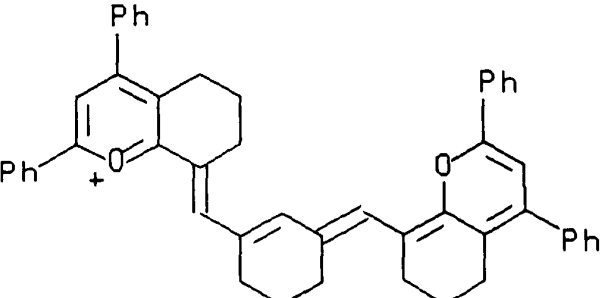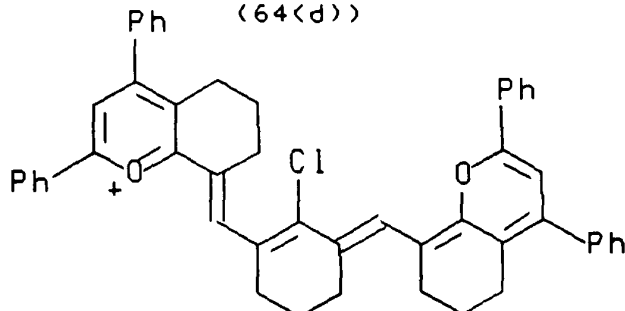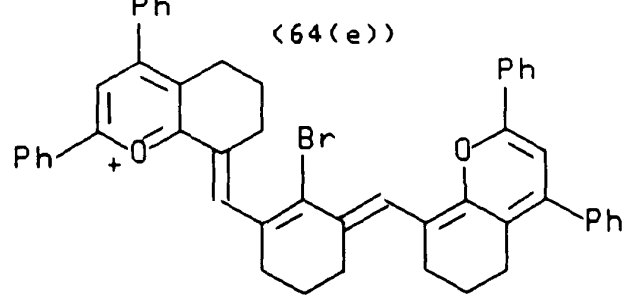
	Relative stability
(64(a))	1
(64(b))	35
(64(c))	78
(64(d))	76
(64(e))	128
(64(f))	201

Table 6. Relative stability of heptamethine pyrylium dyes

It can be seen that a central cyclohexane bridge (64(c)) imparts greater stability relative to a central cyclopentane bridge (64(b)). It is also apparent that a central halogen substituent improves stability, this is especially noticeable in the bromine derivative (64(f)).

There are also examples of cyanine dyes which have been completely rigidised, for example dyes (65) [51] and (66) [52].

(65)   (66)
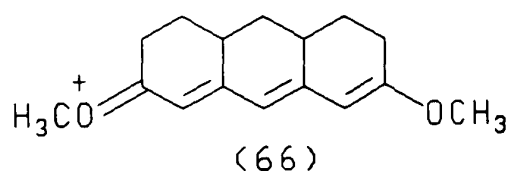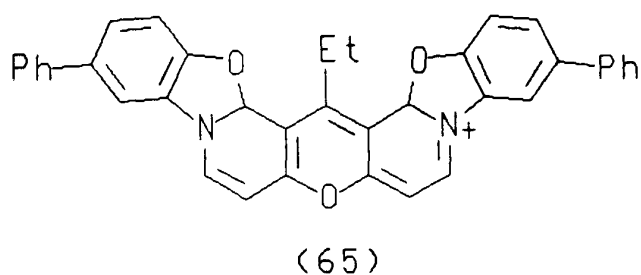
Structural rigidity not only improves stability properties but it increases the fluorescence efficiency of the dyes. Dye (65) has a fluorescence quantum yield Φ f of 0.77 compared to 0.04 for the oxacarbocyanine analogue (67) [51].

(67)
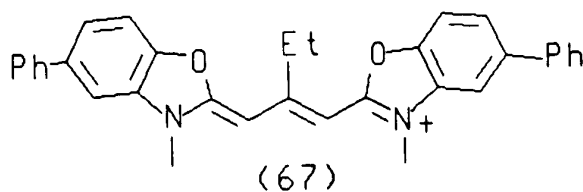
The high photostability properties of the rigidised near-infrared cyanine dye (68) [53] allows it to be used as a laser dye, delivering pulses between 1400 and 1600nm.

(68)
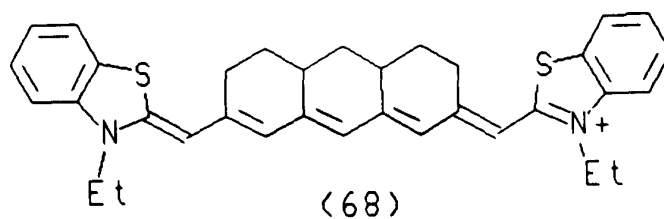
Stability to attack by nucleophiles is also an important consideration. For example, yellow methine dyes of the type (69) are hydrolysed in hot water, due to reversion of the condensation process (Scheme 5).
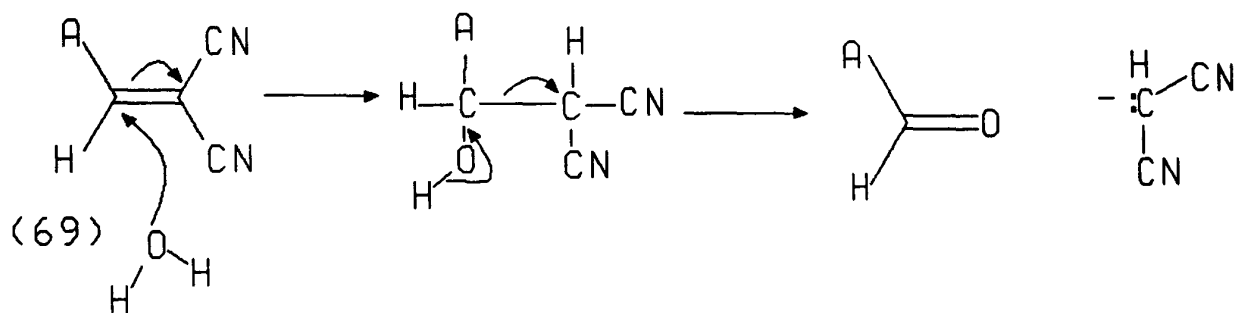
Scheme 5. Hydrolysis of a methine dye

Hydrolysis is minimised by introducing steric crowding into the molecule, for example as in (70).

Retards hydrolysis
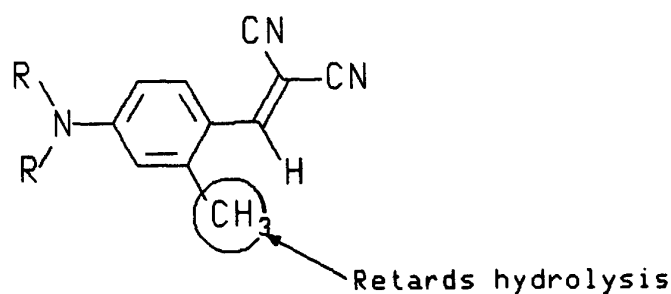
(70)

1.4.1.2 Colour and constitution of cyanine dyes

In practice the absorption maximum of a cyanine dye is dependent on two factors: (a) the nature of the heterocyclic end groups, and (b) the length of the chain –

(CH=CH)$_n$, between the two end groups. Dyes (71) and (72) show the powerful effect of different heterocyclic end groups, and (71) is yellow whereas (72) is blue [54].
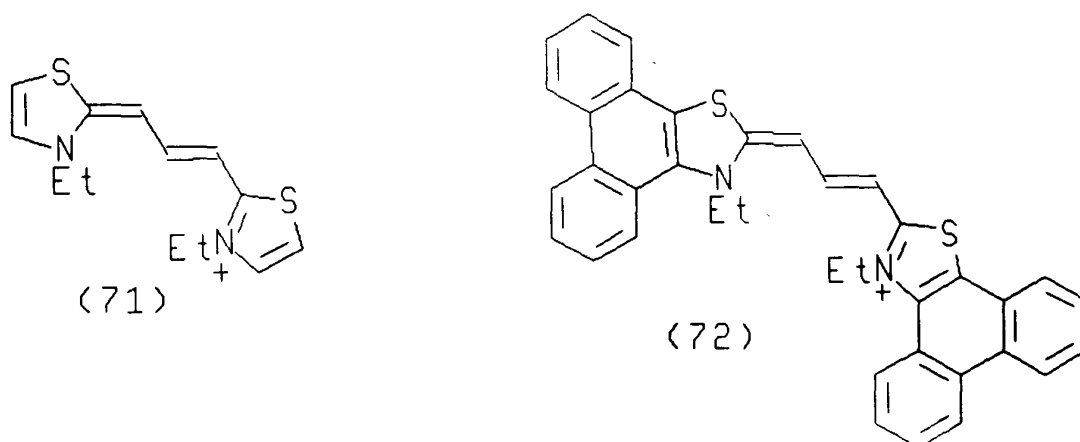
The heteroatom 'X' in dyes of general structure (34) can also have a dramatic effect on colour. It can be seen from Table 7 that there is a 95nm shift when the heteroatom is changed from 'O' to 'Se' [55].

X	λ_{max}/nm
Se	790
S	763
CMe$_2$	741
O	695

Table 7. Effect of heteroatom on the colour of dye (34), n=3

The effect of increasing the chain length on the λ_{max} of cyanine dyes of type (34) is shown in Figure 16 [38].
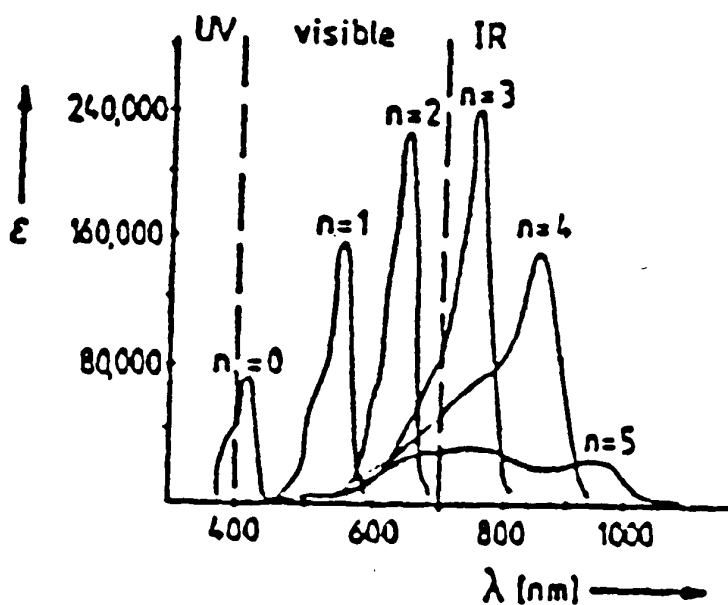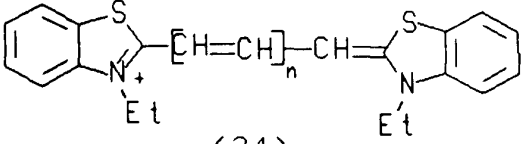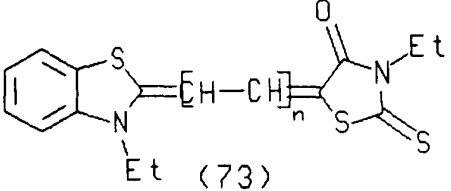
Figure 16. The effect of chain length on λ_{max} in cyanine dyes

The increase in chain length causes a progressive shift of λ_{max} to longer wavelengths. It is important to remember that the λ_{max} of symmetrical cyanine dyes shifts ~100nm per additional vinylene group (non converging series). Unsymmetrical cyanines however show reduced red shifts as additional vinyl groups are added, and the λ_{max} values converge at long chain lengths, cf. Table 8.

Table 8. Vinylene shifts in symmetrical and unsymmetrical cyanine dyes

	Non converging series [56]			
	n	0	1	2	3
	λmax/nm	423	557	650	758
	(ethanol)			

	Converging series [57]			
	n	0	1	2	3
	λmax/nm	432	528	605	635
	(pyridine)			

The colour of a dye can be predicted theoretically using the Pariser-Parr-Pople self-consistent field molecular orbital method [1][58]. This technique, accompanied by a knowledge of the general structural features that lead to long wavelength absorption (covered in the next section), enables the design and synthesis of near-infrared absorbing dyes to be undertaken efficiently.

1.4.2 Classes of Near-infrared absorbing dyes

Ideally an infrared absorbing dye has a narrow, intense absorption band beyond 700nm, with minimal absorption in the visible region of the electromagnetic spectrum (400-700nm). Infrared absorption corresponds to an electronic excitation energy ΔE of 150kJ/mole or less [59].

Near-infrared absorbing dyes can be divided into two specific groups: organic dyes, and metal complex dyes. Within each group, classification can be made according to chemical structure. Table 9, summarises the major classes of organic infrared absorbing dyes, and Table 10, some common metal complex infrared dyes.
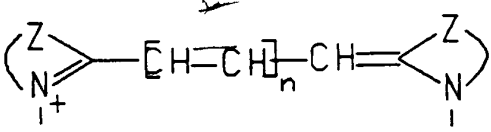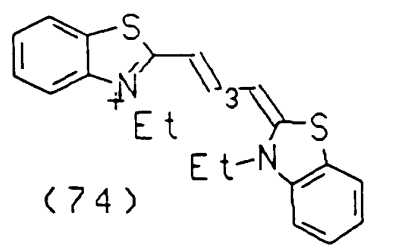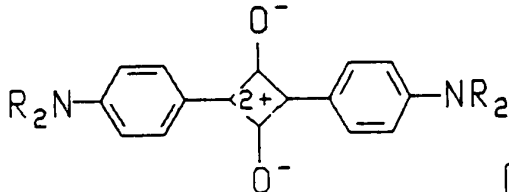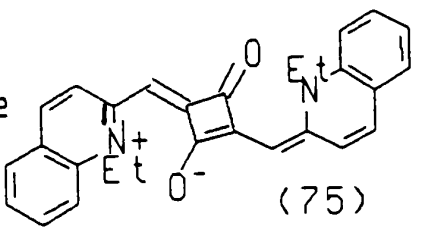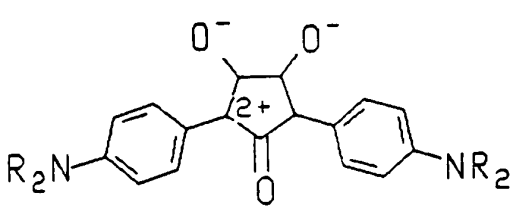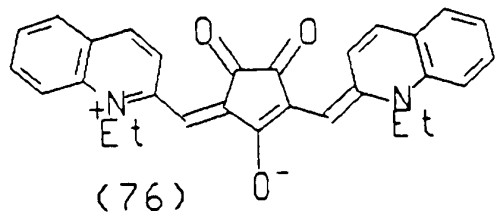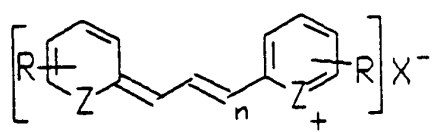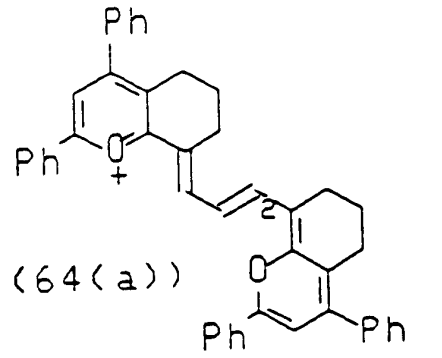
Class	Basic chemical structure	Example
Polymethine cyanine		 (74) $\lambda max = 757nm$ (MeOH) [56][57]
Squarylium		 (75) $\lambda max = 708nm$ (methanol) [60]
Croconium		 (76) $\lambda max = 807nm$ (methanol) [60]
Pyrylium and related dyes		 (64(a)) $\lambda max = 1040nm$ (CH_2Cl_2) [50]

Table 9.   Infrared absorbing organic dyes
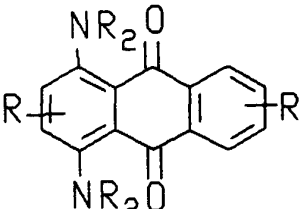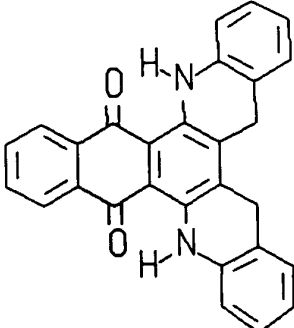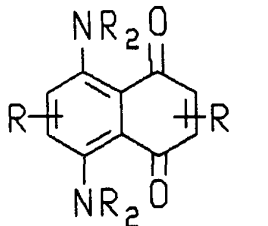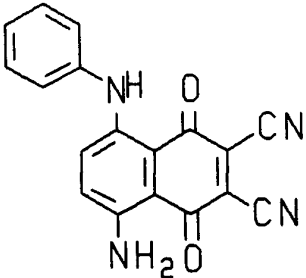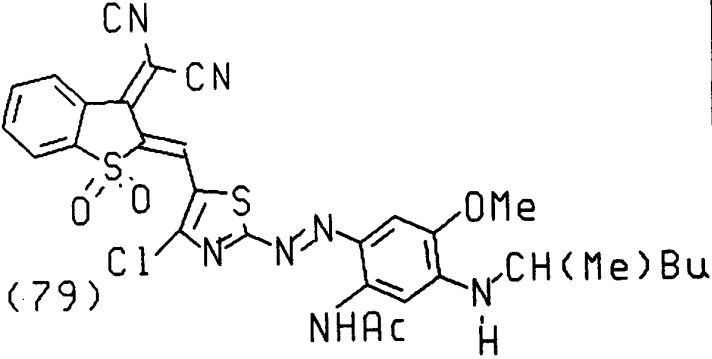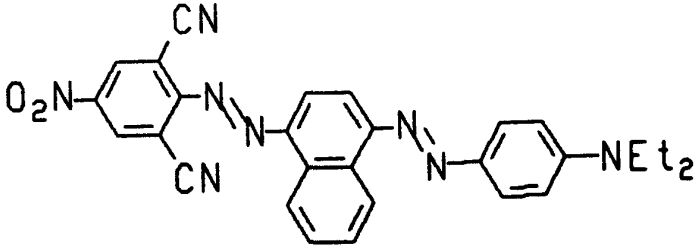
Class	Basic chemical structure	Example
Quinone dyes	Anthraquinone	λmax = 725nm (chloroform) (77) [61]
	Naphthoquinone	λmax = 759nm (acetone) (78) [62]
Azo dyes	Monoazo	(79) λmax = 778nm (CH_2Cl_2) [63]
	Disazo	λmax = 710nm (80) [49]

Table 9. Infrared absorbing organic dyes cont.
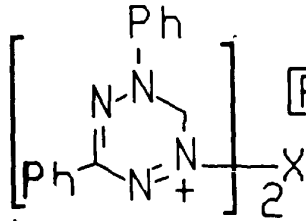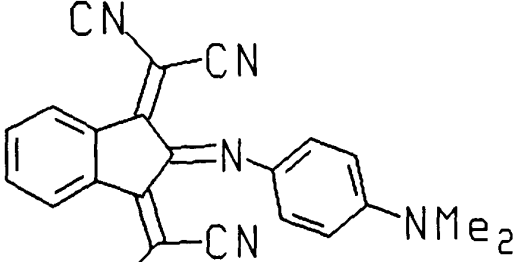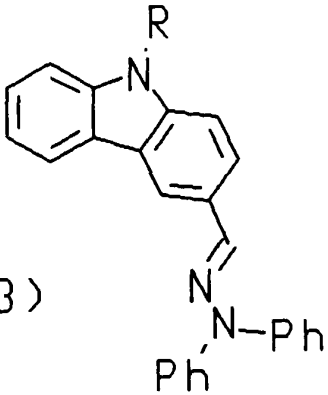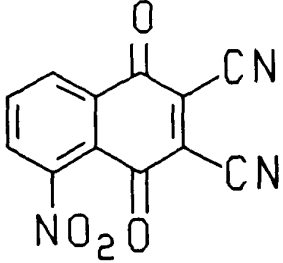
Class	Basic chemical structure	Example
Aminium radical salts	$[Ar_3N^{.+}]X^-$	(81) X = p/ phenylene λmax =885nm [64]
Methine and related dyes	(82) λmax = 755nm	[65]
Charge transfer complexes	(83) Donor + Acceptor λmax_1 = 1100nm (CH_2Cl_2) λmax_2 = 604nm	[66]

Table 9. Infrared absorbing organic dyes cont.
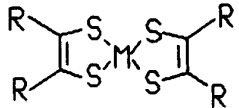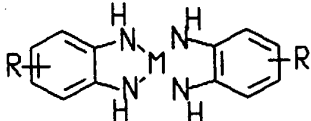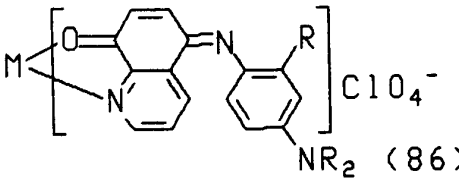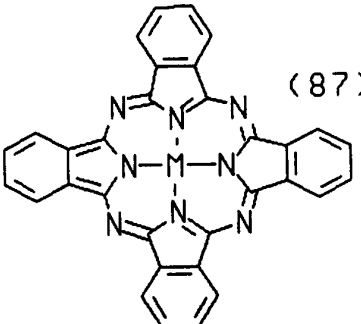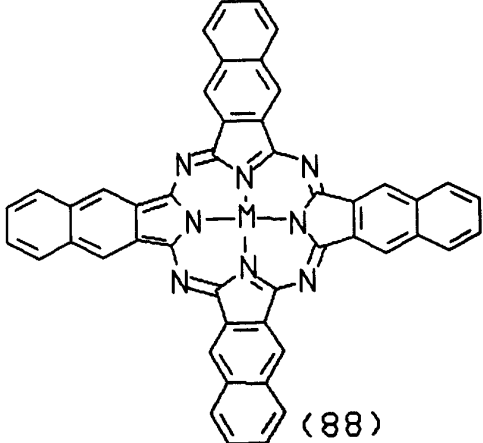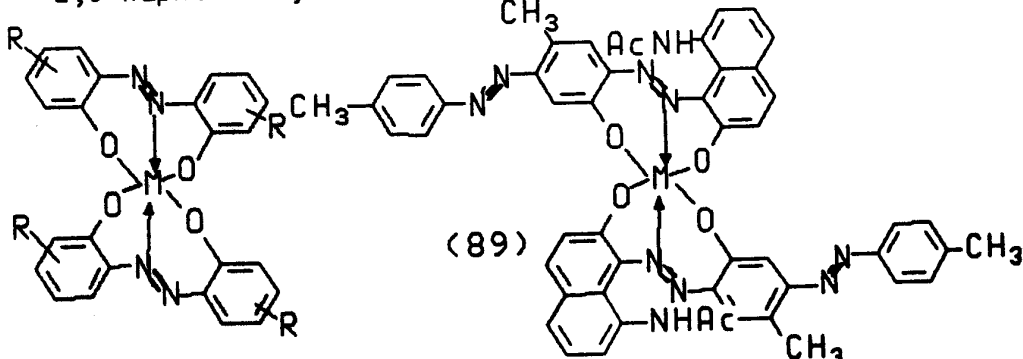
Class	Basic chemical structure	Example
Dithiolene	(84)	(a) R = Ph, M = Pb, λmax = 885nm (CHCl₃) [67] (b) R = Ph, M = Ni, λmax = 855nm (CH₂Cl₂) [68]
Phenylene-diamine	(85)	R = 4-Bu, λmax = 795nm (DMF) [69]
Indoaniline	(86)	M = Ni, R = Me, R' = Et [70], λmax = 775nm (EtOH)
Phthalo-cyanine	(87)	(a) no M, λmax = 698nm [71][35] (b) M = Cu, λmax = 678nm [72] (c) M = Pb, λmax = 790nm [59]
Naphthalo-cyanine	(88) 2,3 naphthalocyanine	M = Zn, λmax = 760nm [73]
Azo dyes	(89)	λmax = 730nm (DMF) [74]

Table 10. Infrared absorbing metal complex dyes

Infrared dyes have many uses in high-technology fields, such as optical data storage, thermal imaging processes and security printing. The oldest and best known infrared dyes are the long chain cyanines, developed for the photographic area. Typically the cyanine dyes (74) possess high extinction coefficients that initially increase with chain length, and several are useful as laser materials because of their high fluorescence quantum yield. However, for many applications they suffer from the disadvantages of poor chemical and light stability.

Squarylium (75) and croconium (76) dyes although non-ionic resemble the cyanines in many ways, and exhibit narrow, very intense absorption bands. These are valuable features for many applications, but although these dyes generally exhibit better stability than cyanine analogues, their photostability is still not as high as is desirable.

Near-infrared absorbing quinone dyes eg (77) (78), show good stability properties and have been used in optical recording materials. Their main disadvantages are low solubility and low molar extinction coefficients.

Metal complex dyes (Table 10) can be particularly stable and find use in optical recording materials, as Q-switch dyes, and as IR absorbers in sunglasses and goggles. Phthalocyanines (87) and naphthalocyanines (88) are particularly noted for their excellent stability to light and heat, and the former types heavily substituted with thioether groups, have been marketed by ICI for use in security printing inks. Other specialised applications of phthalocyanine and naphthalocyanine i.r. dyes include photoconductors for electrophotography and laser printer systems, sensitizers for photodynamic therapy, and fluorescent labels for plastics and for biological materials (cells, antibodies, proteins).

It is clear that infrared dyes have a very important role to play in high technology areas, and this is particularly the case where the relatively inexpensive near-infrared diode lasers (ca. 750-850nm) are employed. Thus such lasers can be used for

information recording, reading, for detection in analysis, and for photosensitisation, and an infrared absorbing dye can facilitate the application of the laser in each particular case. There is a move towards low cost diode lasers emitting in the visible region, in which case normal dyes may fulfil most of the requirements as the absorbing material. However, there are still many applications where a colourless i.r. dye can offer distinct advantages. These include 'invisible' dyes for security printing and marking, and RSA dyes with maximum transmission in the visible range. Thus research into new near-infrared absorbing chromophores is likely to continue for some time to come.

2. RESULTS AND DISCUSSION

2.1 INTRODUCTION

One of the main objectives of this project was the development of new, improved dyes which can act as 'shutters' for laser radiation by the phenomenon known as "reverse saturable absorption", (RSA). Certain dyes, such as IR140 (9) (Eastman Kodak) will absorb an intense laser pulse at a wavelength well away from the absorption maximum to give an excited state which itself has a high absorption cross section (high extinction coefficient) for the radiation. This excited state can then absorb the incident radiation very effectively and so the dye solution acts as a 'shutter' or filter. For maximum effect, the excited state should have a relatively long lifetime, which suggests that the dye should have a normally low fluorescence efficiency contrary to the high efficiency required for laser dyes. The excited state should also have as high an absorption cross section as possible at the wavelength concerned, but the dye itself should be virtually transparent at that wavelength. From an applications viewpoint, it was desirable to design near-infrared absorbing chromophores which exhibit a large degree of excited state absorption (ESA) when irradiated with a relatively low energy laser (~1-20 mJ, λ= 532nm). Decker has already shown that IR140 exhibits ESA when irradiated at high pump intensity at 532nm (Nd:YAG laser) (c.f. Fig. 9, page 14) [18]. Work at D.R.A. has also shown IR140 to have ESA when pumped at 532nm with an excimer pumped dye laser (coumarin 307 (90)), but to a lower degree (Figure 17).

(90)
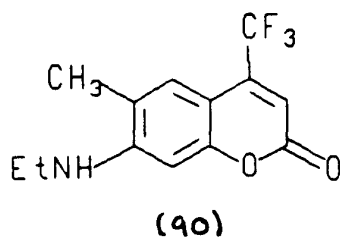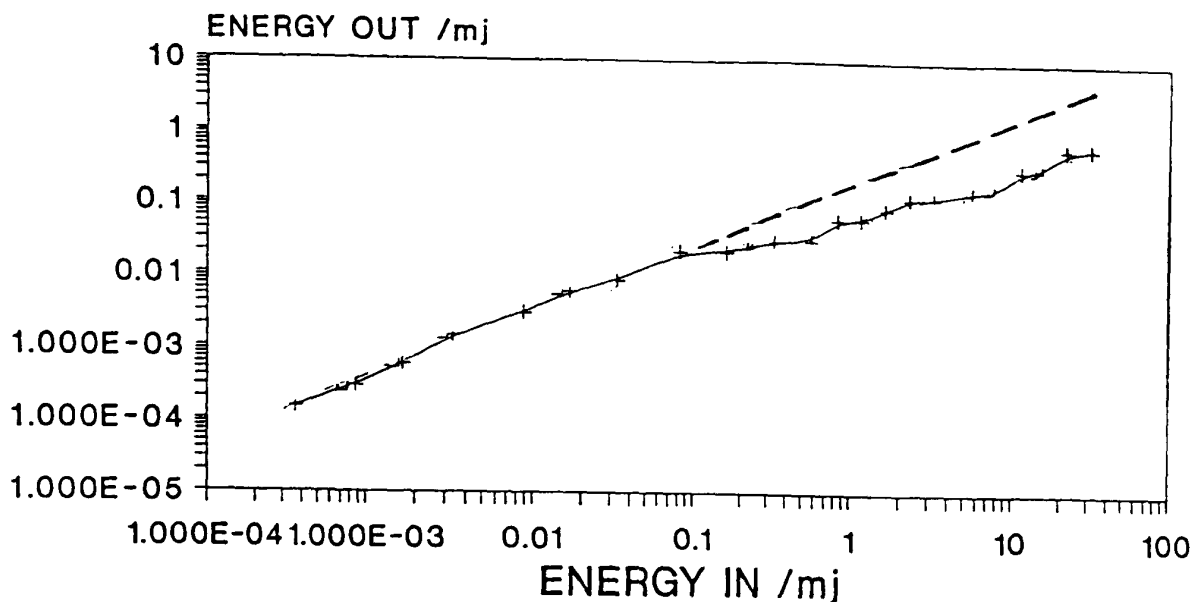
Figure 17. ESA of IR140 at 532nm (sample OD = 0.47)

The considerable difference in degree of non-linearity can possibly be attributed to two factors: (a) the difference in laser power (D.R.A. : max energy 9×10^6 W/cm^2, Decker: max energy 10^9W, and (b) the optical density of the test solutions (D.R.A. OD = 0.47, Decker OD < 0.10).

For the purposes of this project the testing of all dyes was carried out using a 532nm pulsed radiation from an excimer pumped dye laser employing coumarin 307 dye. The experimental arrangement is shown by Figure 18.

The sample is contained in a 1 cm path length spectrometer cell. The radiation incident upon the sample was focused down to a 300 micron diameter spot using a 30 cm focal length lens. Energy falling onto the sample was adjusted by changing the neutral density filters situated in front of the sample. An S20 **** detector was used to measure the transmitted energy.

The degree of ESA shown by IR140, under D.R.A. experimental conditions was concluded to be inadequate. In addition the dye has poor stability properties, degrading easily, and thus more efficient materials were required. At the present time
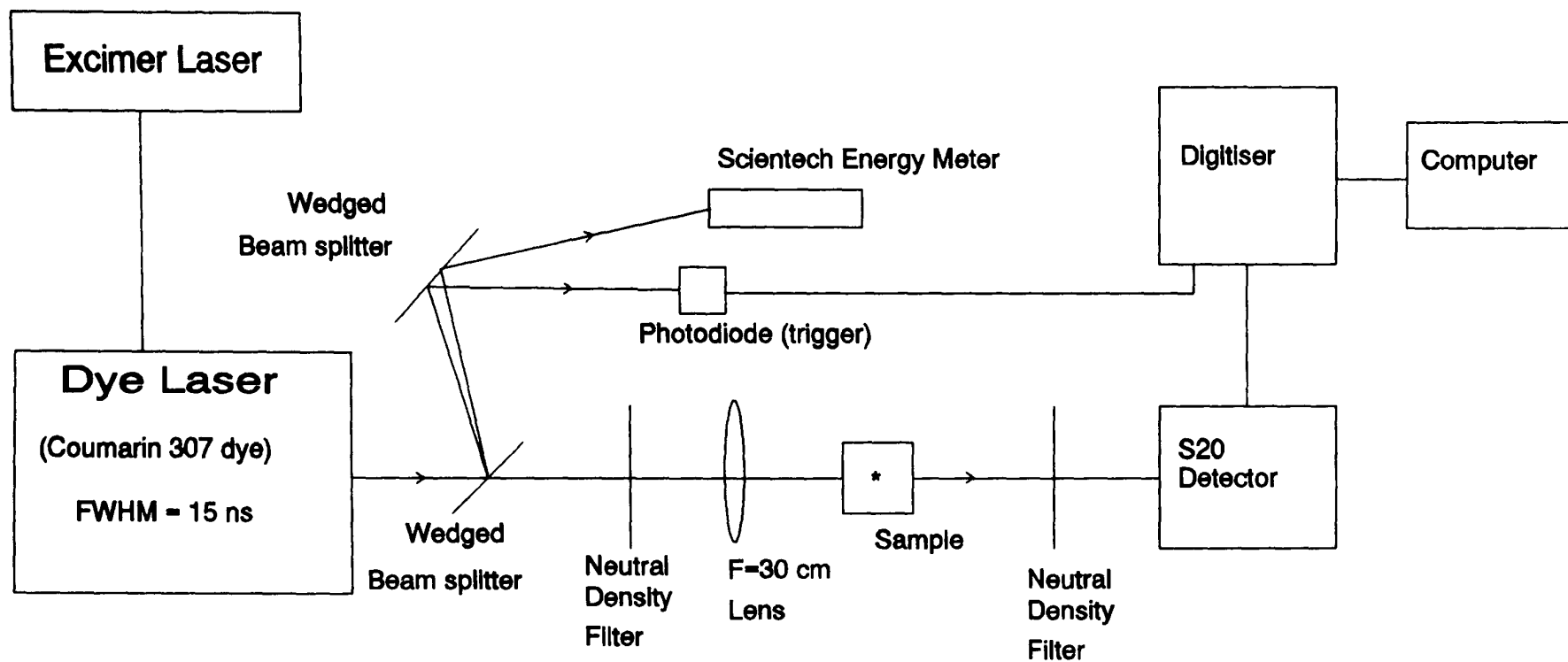
* Spot diameter at the middle of the sample = 300 microns

Figure 18. Schematic arrangement of apparatus for testing RSA properties of dye solutions

The degree of ESA shown by IR140, under D.R.A. experimental conditions was concluded to be inadequate. In addition the dye has poor stability properties, degrading easily, and thus more efficient materials were required. At the present time little is known about the relationships between dye structure and the excited state requirements for efficient ESA, and so synthesis of chromophores analogous to IR140 with well defined structural variation was undertaken. Thus empirical relationships between structure and ESA were sought. In this approach it was important to take into consideration the photochemical stability of the modified chromophores.

Prompted by the large degree of ESA shown by 7-diethylamino-4-methyl-coumarin in the experiments of Wieder [17], and also considering the superior photostability of the coumarin system, we were attracted to the synthesis of new coumarin dyes with extended chain length, in order to obtain longer wavelength materials with absorption properties approaching those of IR140.

2.2 SYNTHESIS AND EVALUATION OF NEW COUMARIN-BASED EXTENDED CHROMOPHORES

2.2.1 Synthesis of dyes

The synthetic route to coumarin systems is well established and one approach of particular interest leads to the intermediate 7-diethylamino-3-formylcoumarin (91).

(91)
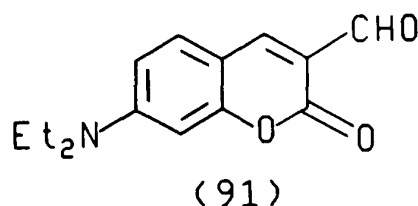
Knoevenagel type condensation of this aldehyde with active methylene compounds can then lead to a coumarin systems with extended conjugation. Monomethine and dimethine dyestuffs of this type have already been synthesised and patented by Harnisch [75][76]. For example dyes (92) and (93), give clear luminous red dyeings on polyester with high brilliancy and good fastness properties. Their use as laser dyes, energy converters in light collecting systems and as colourants for plastics was also noted.

(92)   (93)
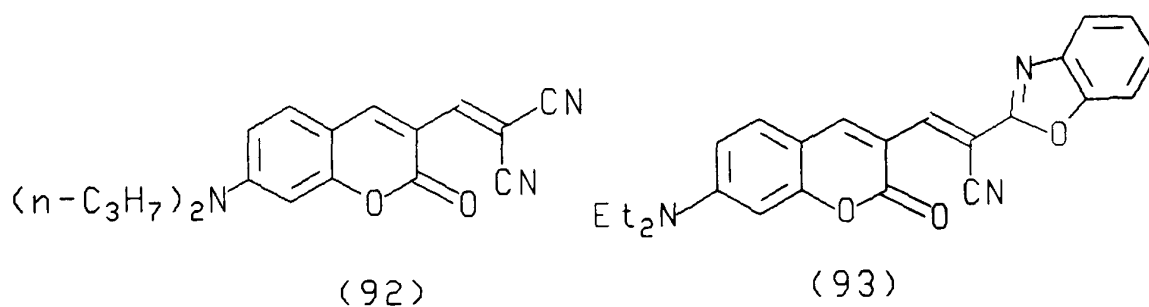
A combination of the N,N-diethylamino-coumarin donor with a wide range of acceptor groups of varying electron withdrawing strength should permit the synthesis of a series of extended coumarin dyes with absorption maxima ranging from 500 to 700nm, or even beyond. This possibility was thus explored in detail.

The general approach to aldehyde (91) and the derived dyes is summarised in Scheme 6 [77][78].
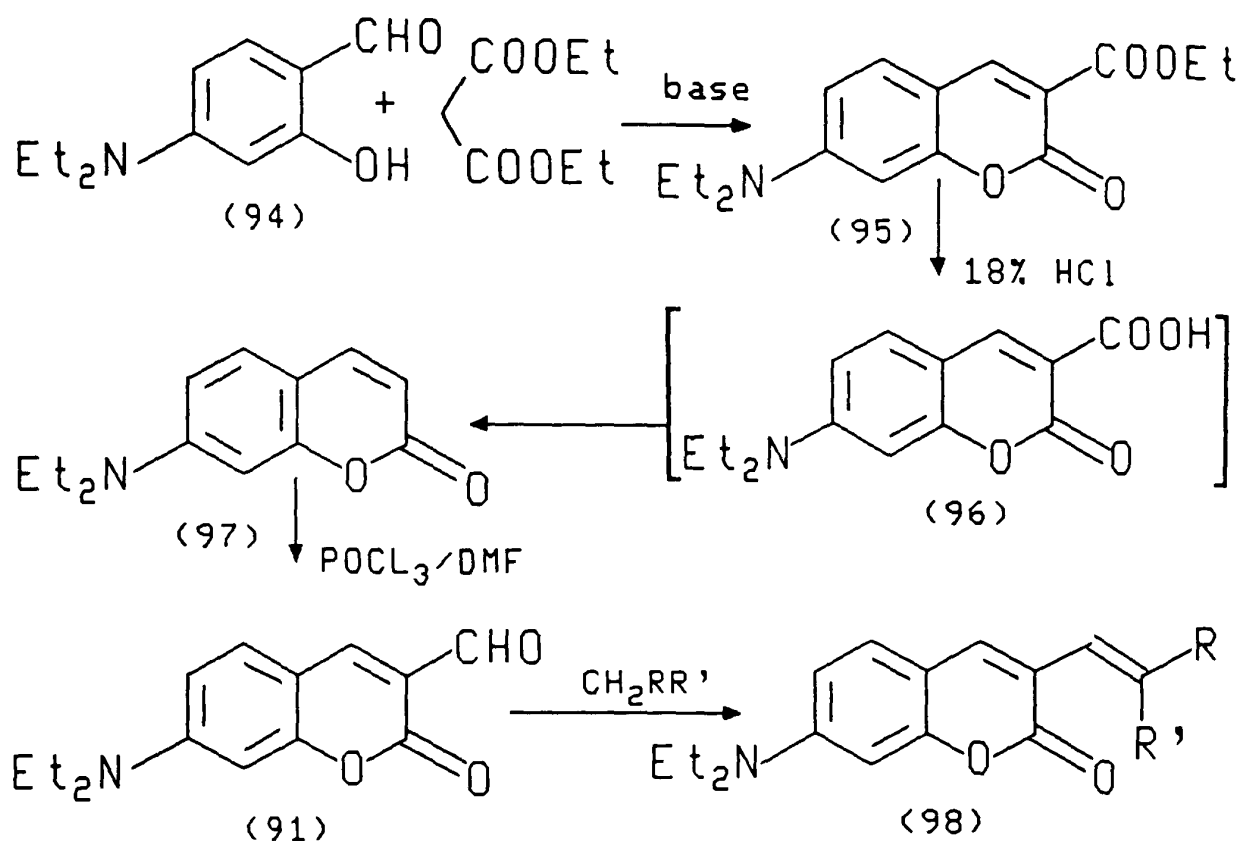
Scheme 6. Synthetic route to etended coumarin dyes

Reaction of 4-diethylaminosalicylaldehyde (94) with diethylmalonate, under base catalysed conditions with piperidine gave 7-diethylaminocoumarin-3-carboxylic acid ethyl ester (95). The carboxylic ester could then be converted to 7-diethylamino-coumarin (97) by refluxing in 18% HCl, the reaction proceeding via decarboxylation of carboxylic acid intermediate (96). Vilsmeier formylation of (97) then gave 7-diethylamino-3-formylcoumarin (91). By condensing the coumarin aldehyde with a suitable active methylene compound $RR'CH_2$ dyes of general formula (98) could be formed. The new extended coumarin dyes prepared by this general method are listed in Table 11. The structures were confirmed by elemental analysis or mass spectrometry.

Table 11. New coumarin based dyes prepared according to Scheme 6

Et$_2$N, coumarin core structure with R substituent at the 3-position (99)

R

99(a)

99(b)

99(c)

99(d)

99(e)

99(f)

99(g)

99(h)

99(i)

99(j)

99(k)

99(l)
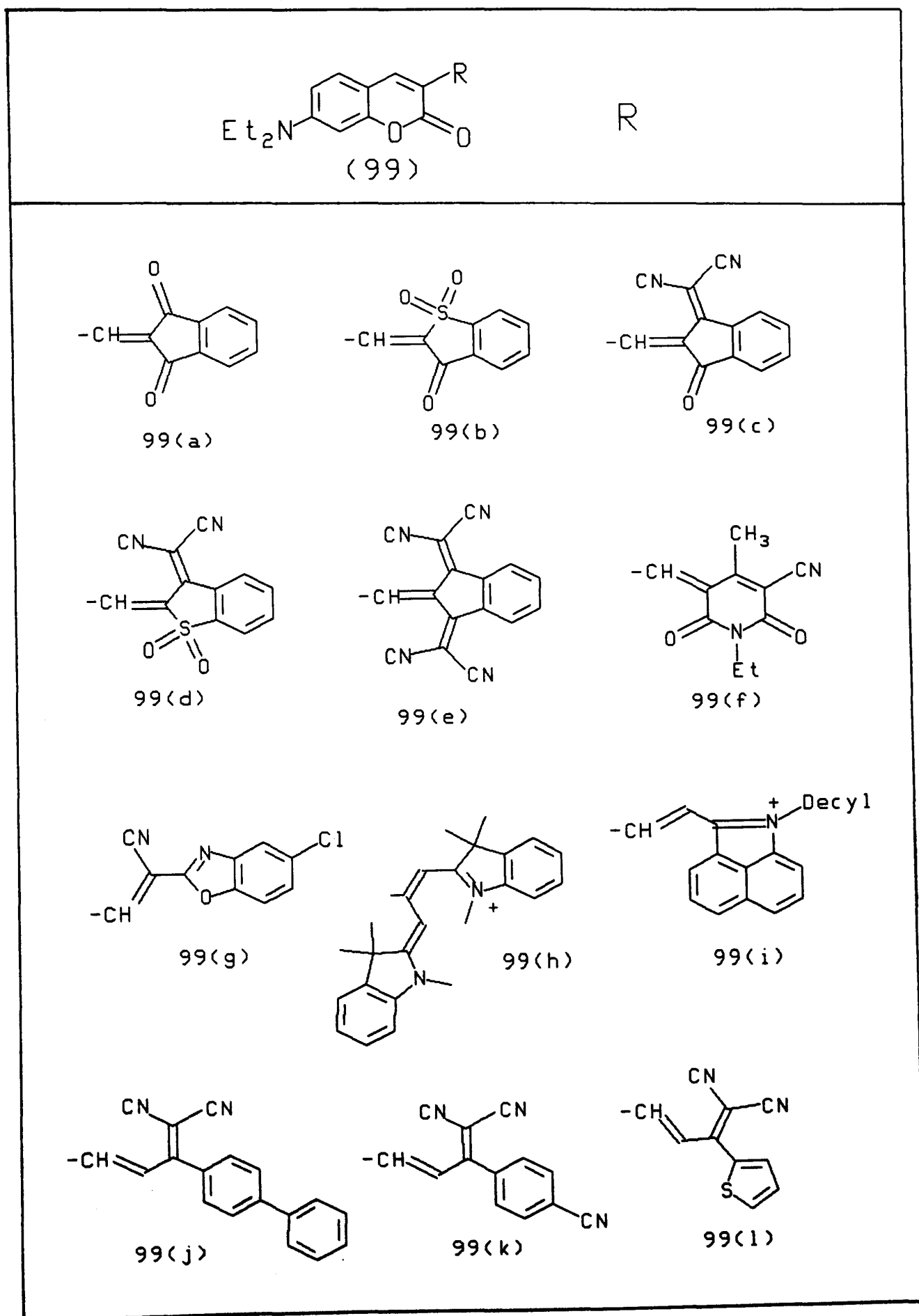
Table 11. continued

99(m)   99(n)   99(o)

99(p)   99(q)   99(r)
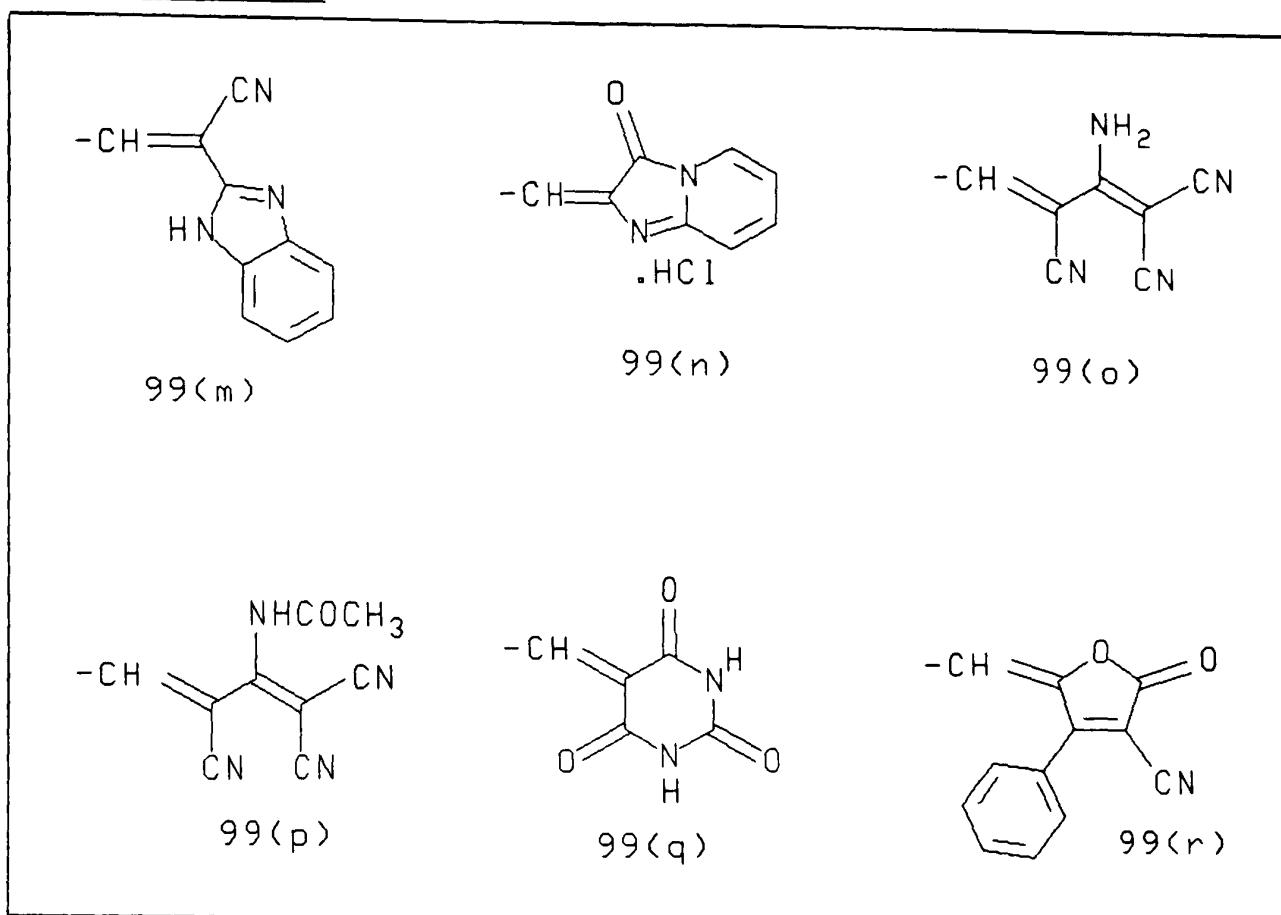
A complication was encountered in the reaction of (91) with Fischer's base, which gave dye (99h). The reaction of equimolar quantities of the two species gave a yellow product which slowly turned green with intense red fluorescence in dichloromethane. The absorption maximum of the green solution was at 600nm with a secondary absorption band at 400nm. If acid was added to a solution of the yellow product, a weakly fluorescent deep blue solution formed, the absorption band at **400nm** disappearing. Mass spectrometry (M+1 = 573) and microanalysis of the yellow species [Found: C,79.55; H,7.55; N,7.25%, $C_{38}H_{43}N_3O_2$ requires C,79.4; H,7.7; N,7.3%] suggested that a double condensation with Fischer's base had occurred, as shown in Scheme 7.
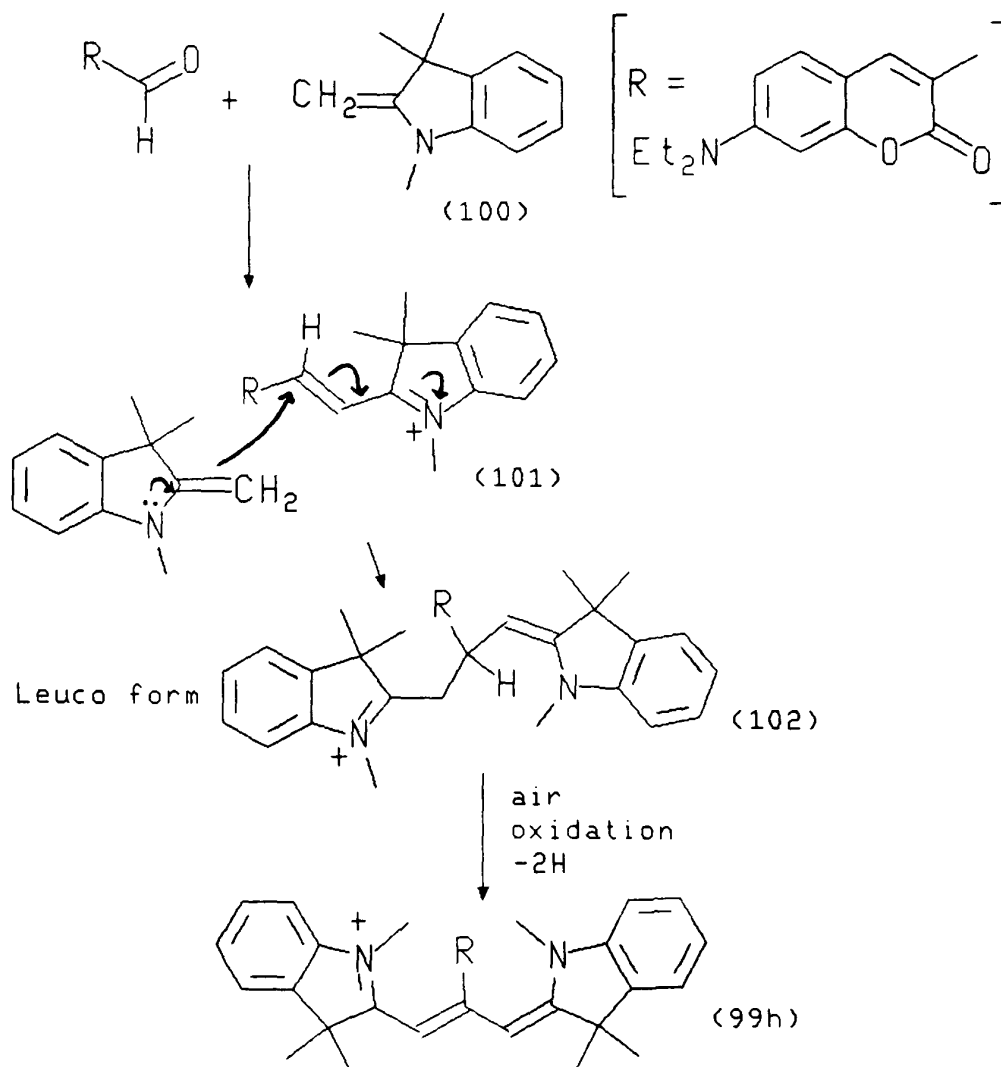
Scheme 7. Double condensation of Fischer's base with coumarin aldehyde (91)

The yellow product is probably the leuco compound (102) (Scheme 7) which has little conjugation and so absorbs at shorter wavelengths. Air oxidation of this (which is known to occur readily in analogous leuco triarylmethane dyes) would give (99h). This is an analogue of Malachite Green and so would be expected to show two absorption bands at ca. 600nm (x band) and 400nm (y band). Addition of acid to this would protonate the coumarin amino group and so convert (99h) to an analogue of Michler's Hydrol blue, with a single peak at ca. 600nm.

Another anomaly occurred in the preparation of dye (99o). Although this was shown to be pure by thin layer chromatography the microanalysis data did not fit for the

proposed structure. As the reaction between (91) and malononitrile dimer was carried out in acetic anhydride it was thought that acetylation of the NH_2 group had occurred, and this was in agreement with the found microanalysis figures. Thus the product was in fact (99p). The dye (99o) was eventually made by carrying out the condensation reaction between coumarin aldehyde (91) and malononitrile dimer in ethanol.

2.2.2 Light absorption properties of the coumarin dyes (99)

The visible absorption spectra of the coumarin dyes were measured in methylene chloride and toluene, so giving an indication of solvatochromic behaviour. Molar extinction coefficients of pure compounds were measured in methylene chloride. The results of the spectral evaluations are summarised in Table 12.

Table 12. Light absorption properties of dyes (99)

Dye	$\lambda_{max}^{CH_2Cl_2}$ /nm	λ_{max}^{Tol} /nm	Half band width $\Delta\lambda_{1/2}$/nm	ε_{max}/lmol^{-1}cm^{-1} (CH$_2$Cl$_2$)	$\Delta\lambda$max/nm (CH$_2$Cl$_2$-Tol)
99(a)	545	535	64	83,100	+10
99(b)	546	536	62	80,500	+10
99(c)	602	583	90	58,200	+19
99(d)	624	604	102	57,100	+20
99(e)	601	588	102	50,700	+13
99(f)	582	563	85	74,000	+19
99(g)	532	506	92	49,700	+26
99(h)	600	insol.	102		
99(i)	696	698	78	75,100	-2
99(j)	526	512	69	38,200	+14

Table 12. continued

99(k)	539	527	92	43,800	+12
99(l)	529	514	94	35,700	+15
99(m)	542	522	85	68,700	+20
99(n)*	522	517	109	38,200	+5
99(o)	531	513	104	42,800	+18
99(p)	502	489	100	45,000	+13
99(q)	544	insol.	56	76,400	-
99(r)	574	564	97	43,800	+10

* measured on neutral dye solutions

It is a general feature that when the electron acceptor strength is increased within a donor-acceptor system a bathochromic shift is observed. This is exemplified within the series of dyes 99(a)-(e) (Table 12). Interestingly progressive substitution of the carbonyl groups of dye 99(a) with dicyanovinyl and/or sulphone groups does not yield the magnitude of bathochromic shift that would be expected from simpler methine dye analogues. It is noticable that within this series there is a progressive reduction in extinction coefficient and increase in the half band width as further groups are added. This is indicative of steric hindrance, leading to decreased molecular planarity and thus reduced π, π overlap. Thus bathochromic shifts in the series 99(a) - (e) are smaller than expected.

The most bathochromic dye in the series (99) is the cationic system (99i), but even this does not absorb beyond 700nm.

Positive solvatochromism (ie a bathochromic shift on going from a non-polar to polar solvent) is typical of most donor-acceptor chromophores, and indicates that the excited state is more polar than the ground state. In the series of dyes (99), bathochromic shifts vary from 10 - 26nm between toluene and methylene chloride as solvents except in the case of cationic dye 99(i). The cationic nature of this dye

leads to a more uniform π-electronic structure and the system is not strictly donor-acceptor, but is cyanine type. Thus only a small negative solvent shift is observed. The dyes 99(m) and 99(n) have additional interesting halochromic properties, and show significant spectral shifts on addition of acid or alkali. Thus addition of base to a solution of the hydrochloride salt 99(n) gives the neutral donor-acceptor dye (103), λmax 518nm. The λmax of 585nm is restored on addition of acid (Scheme 8).
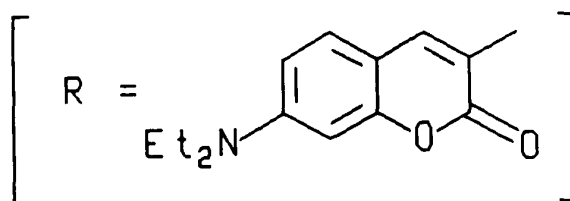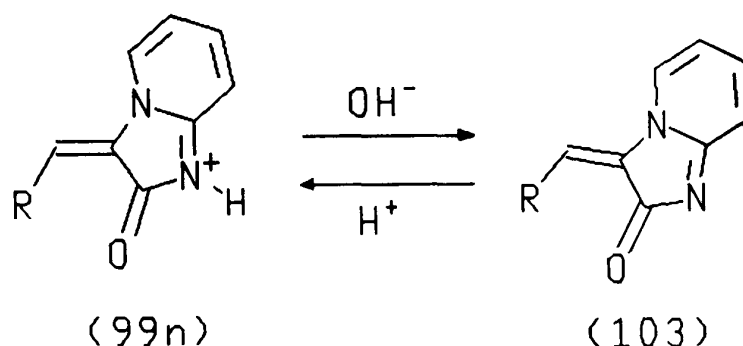
Scheme 8. Halochromism of dye 99(n)

The bathochromic shift accompanying protonation can be explained in terms of the increased electron accepting strength of the protonated azaindole residue in (99n).

Similarly dye 99(m) shows a bathochromic shift on protonation, from 497nm to 560nm, with a visual colour change from red to violet. Protonation of the benzimidazole ring to give species (104) is presumably occurring:

(104)
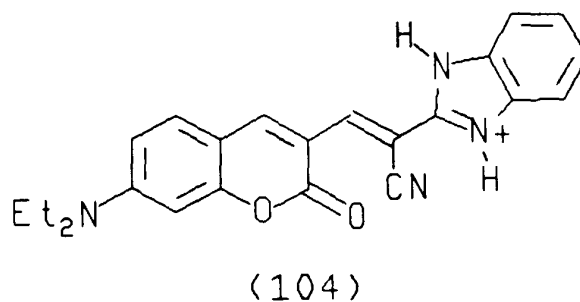
These halochromic effects are summarised in **Table** 13.

Table 13. Halochromic properties of dyes 99(m) and 99(n)

	λ_{max} (acetone)		Halochromic shift
	/nm		/nm
Dye	neutral	+HCl	(acidic-neutral)
(99m)	497	560	63
(99n)	518	585	67

2.2.3 Fluorescence properties of coumarin dyes (99)

It was of interest to examine the fluorescence properties of the new coumarin dyes synthesised, as they could have technical value as long wavelength fluorophores. Thus fluorescence spectra (uncorrected) were measured in dichloromethane. To obtain an **approximate** indication of the relative fluorescence efficiency of each dye

the auto concentration factor (A/C) was used. The A/C factor can have a value ranging from 0.0001 to 9999.9 and is an instrumental multiplicative factor which is required to result in a fluorescence reading of ~90 units. The value of 9999.9 corresponds to a solution with zero fluorescence. The lower the A/C value the greater is the fluorescence. In order to standardise this method, the A/C of the fluorescence standard 9,10-diphenylanthracene (quantum yield = 1) at a concentration of 5×10^{-6} mol l^{-1} was obtained in methylene chloride. This gave a value of 0.027. As a cross-check, the A/C factor was determined for a fluorescent dye at different concentrations, and a good linear correlation between A/C and concentration was

found.

The fluorescence data for dyes (99) are summarised in Table 14.

Table 14. Fluorescence excitation and emission data for coumarin dyes (99)

Dye	Excitation λmax/nm	Emission λmax/nm	Stoke's shift/nm	A/C at 5×10^{-6} mol l^{-1}
99(a)	548	587	39	58
99(b)	541	589	48	2
99(c)	556	631	75	3700
99(d)	620	652	32	9999
99(e)	601	642	41	300
99(f)	544	632	88	9999
99(g)	514	576	62	77
99(j)	514	578	64	25
99(k)	532	602	70	22
99(l)	529	616	87	17
99(m)	584	627	43	910
99(o)	513	546	33	2
99(p)	468	501	33	64
99(r)	555	625	70	41

It can be seen that the dyes are all less fluoresent than 9,10-diphenylanthracene, the most efficient dyes being 99(b) and 99(o). These were bright red dyes. However, their application as disperse dyes on polyester was unsuccessful, both dyes decomposing under hot aqueous dye bath conditions. Using thermal pad-bake methods the dyes decomposed on drying. Decomposition can be attributed to a reverse condensation

reaction (cf pg 35). The dyes are, however, stable in cellulose acetate film, as will be discussed in the next section, suggesting that their decomposition is hydrolytic in nature.

Coumarin dyes 99(a)-(i) were tested for RSA efficiency, but none exhibited this property. In some cases saturable absorption (bleaching) was observed. For example dye 99(g) at high intensity 532nm irradiation shows an increase in transmission (energy out) (Figure 19).
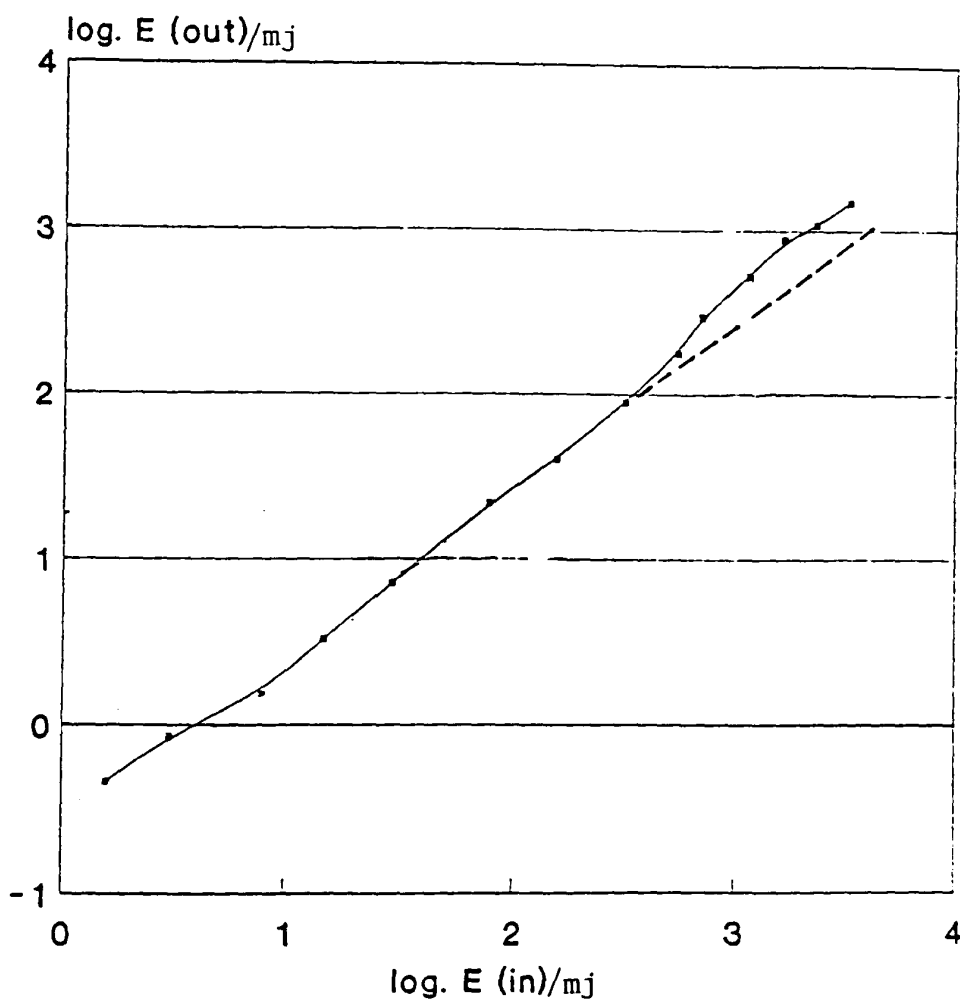
Figure 19. Bleaching phenomena observed in dye 99(g)

The low fluorescence efficiency of the majority of the dyes (99) is in contrast to the

normally high fluorescence yield of simpler coumarin derivatives. One explanation for this may be the extended chain length of chromophores (99), which leads to greater flexibility of the molecule. Molecular rigidity is an important factor in fluorescence efficiency, as this minimises internal conversion from the first excited singlet state to the ground state.

Stoke's shifts of the dyes (99) range from 32nm to 88nm (uncorrected), and it is interesting that the most fluorescent dyes, 99(b) and 99(o) have particularly low values (Table 14).

2.2.4 Stability properties of new coumarin dyes (99)

Although these dyes were found to be unstable under aqueous dyeing conditions, of equal technical importance is their general photostability in non-aqueous media. Tests were carried out with the dyes in cellulose acetate films. Transparent films containing dissolved dye were prepared and subjected to 72hr exposure in a photofadometer, and photostability was assessed by measuring the optical density of the films before and after exposure. In each instance the fading of an azo dye standard, dye (105) dissolved in the same medium, was measured in parallel. The results of the photostability evaluation experiments are summarised in Table 15.
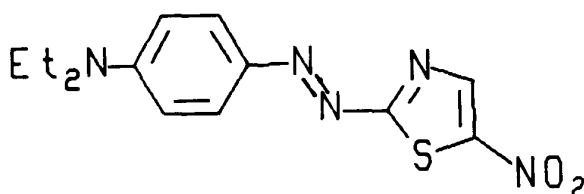
(105)

Table 15. Relative photostability properties of coumarin dyes (99)

Dye	Absorbance at λmax		% Degradation
	Start	Finish (72hr)	
Standard dye (105)	0.82	0.77	6
99(a)	1.95	0.30	84
99(b)	1.68	1.06	37
99(c)	1.03	0.40	62
99(d)	decomposed on film storage		
99(e)	" "	" "	
99(f)	" "	" "	
99(g)	1.05	0.94	11
99(h)	-		
99(i)	1.11	0.69	38
99(j)	1.70	1.03	40
99(k)	2.31	1.44	38
99(l)	1.59	1.12	47
99(m)[1]	-	-	-
99(n)	0.82	-	100
99(o)	0.91	0.80	12
99(p)	2.05	1.41	31
99(q)	0.73	0.55	25
99(r)	1.21	0.53	56

1 Because of the facile protonation of dye 99(m), films prepared containing this dye rapidly turned blue in colour. Thus it was not possible to carry out photostability properties of the neutral dye 99(m).

In general the photostability properties of the coumarin dyes are poor relative to the azo dye standard. However, dye 99(g), containing a benzoxazole ring, has comparable

light fastness properties to the azo dye standard. This ring system is used commercially in simpler fluorescent coumarin dyes, and thus has special advantages for lightfastness.

An increase in molecular rigidity is one route to improving the stability properties of dyes with extended chromophores. This approach was demonstrated by Drexhage and Reynolds [50] for several long chain cyanine dyes. Thus this principle was extended to the coumarin donor-acceptor chromophoric system, in an attempt to obtain long wavelength coumarin chromophores with good stability properties.

2.3 SYNTHESIS AND EVALUATION OF COUMARIN DYES WITH FUSED RING SYSTEMS

2.3.1 Introduction

There is some documented work on the synthesis of fused heterocyclic systems with structural similarity to the coumarin system. For example, the red dye (107) synthesised by Mach and co-workers is obtained from the condensation and simultaneous ring closure reaction of malononitrile and the iminocoumarin (106) [79]. This bright red fluorescent dye has good photostability and is used as a textile dye commercially.
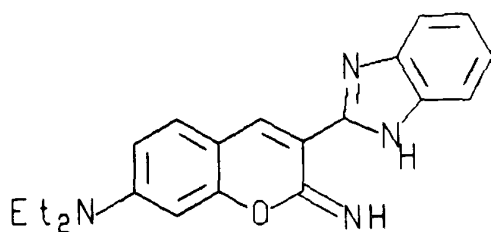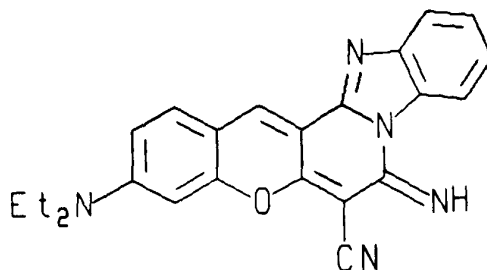
(106)   (107)

Also of interest is the work of Shenoy and Seshadri [80][81]. They have demonstrated the condensation and subsequent cyclisation reaction of 4-diethylamino-2-methoxybenzaldehyde with 2-cyanomethylbenzimidazole to obtain 7-

diethylaminobenzimidazo-(1,2a)-quinoline-3-carbonitrile (108) (see Scheme 9). Reduction of the cyano group leads to the functional formyl group. Further condensation reactions with active methylene compounds can lead to extension of the chromophoric system.
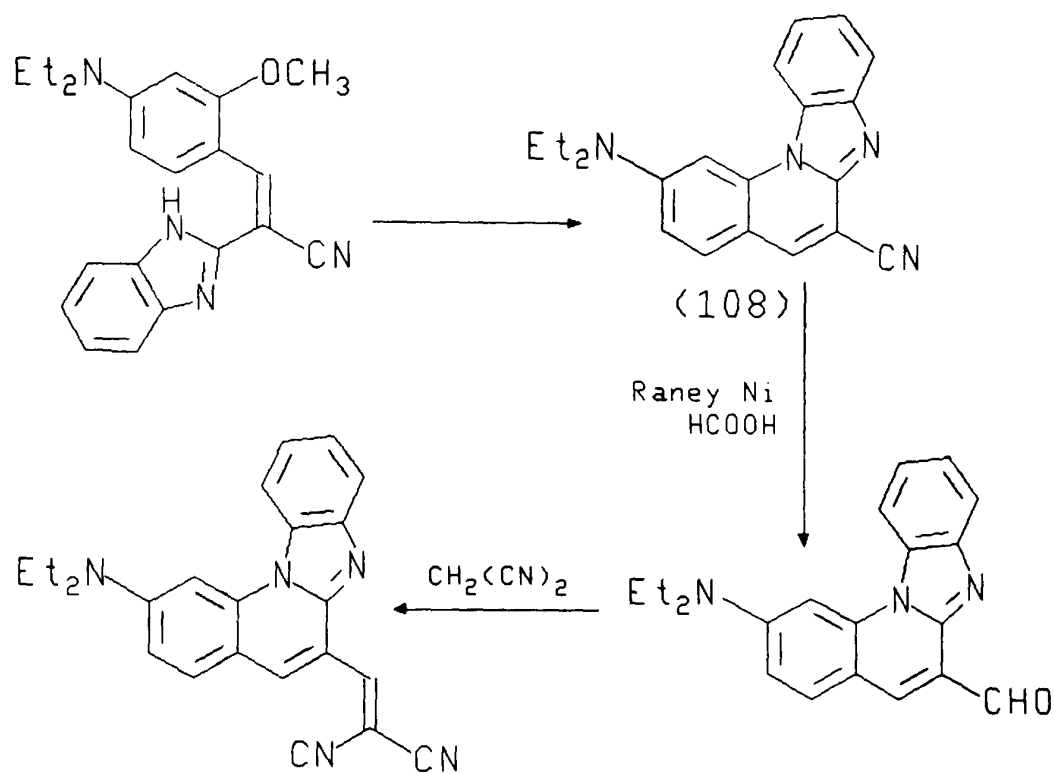
Scheme 9. Work of Shenoy and co-workers

Knierzinger and Wolfbeis [82] and Huadong and co-workers [83] have also demonstrated the synthesis of pyrones (111) from the condensation and ring closure reactions of 7-substituted-4-hydroxycoumarin (109) (Scheme 10).
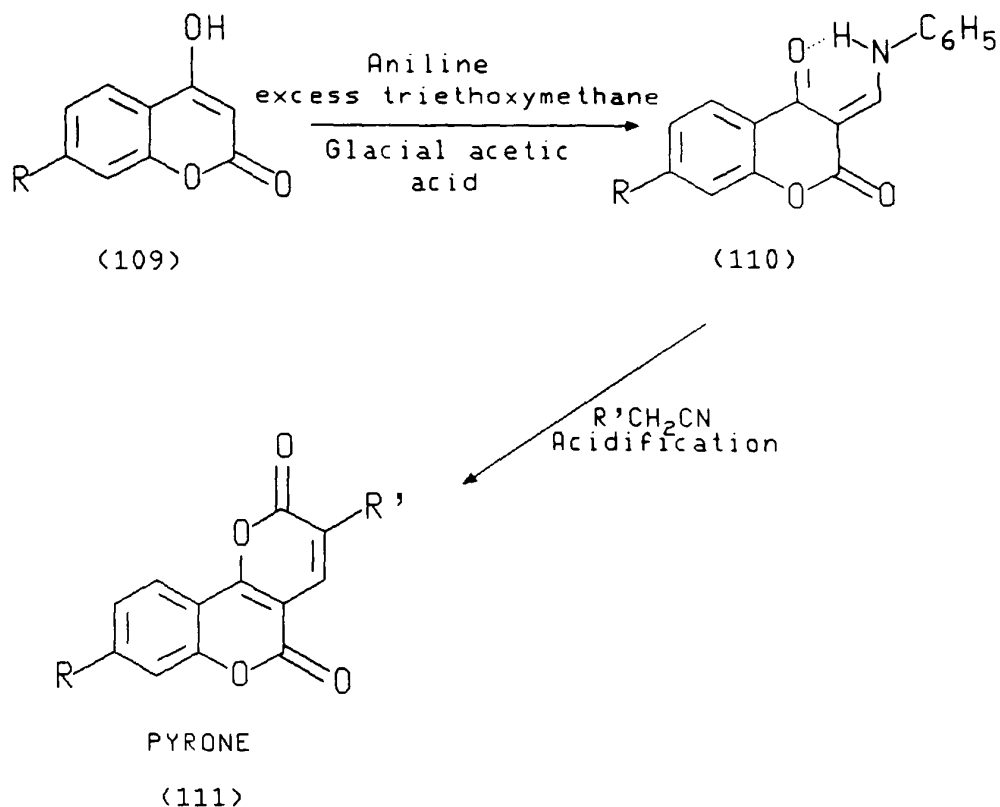
Scheme 10. The synthesis of pyrones [82]

The intermediate 2-aminomethylene-1,3-dione (110), is synthetically equivalent to the less stable 2-formylated 1,3 dicarbonyl. Reaction of the enamine with the nitrile compound in the presence of strong base results in the replacement of aniline by the nitrile carbanion species.

Of particular interest though is the use of ortho-chloroaldehydes in the synthesis of fused coumarin systems. Wiessenfels and co-workers [84] have demonstrated this type of reaction with the preparation of compound (113) from a 7-substituted-3-formyl-4-chloro-coumarin (112) and thioglycolic acid (Scheme 11).
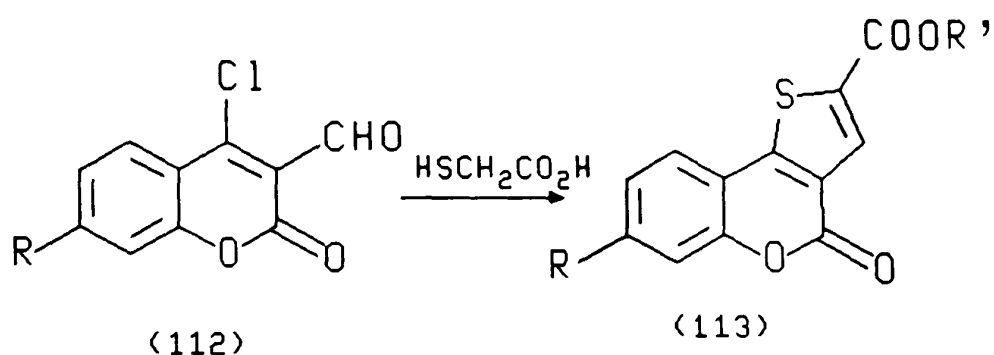
Scheme 11. Synthesis of fused coumarin systems

Intermediate (112) has great potential in the synthesis of fluorescent dyes, and thus it was decided to use this in an attempt to prepare longer wavelength absorbing fused ring analogues of the coumarin dyes.

2.3.2 Synthesis of dyes

7-Diethylamino-3-chloro-4-formylcoumarin (112) is obtained from the formylation of 7-diethylamino-3-hydroxycoumarin (115). The synthesis of this was initially attempted using the route described by Wolfbeis [85] (Scheme 12).
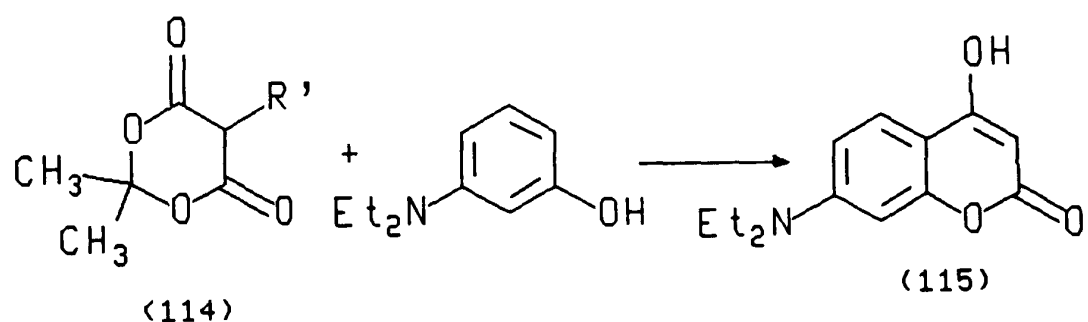
Scheme 12. Synthesis of 7-diethylamino-3-hydroxycoumarin

3-Diethylaminophenol was fused with Meldrum's acid (114) at 130°C, and the 7-diethylamino-3-hydroxycoumarin (115) was isolated from the dark brown reaction product by column chromatography (silica, eluent; toluene), in low yield. A

combination of pathways described by various other workers gave improved yields of this intermediate.

Wolfbeis and Knierzinger [82] have shown that malonic acid bis (2,4,6-trichlorophenyl) ester (116), originally synthesised by Ziegler and Maier [86], can be condensed with 3-diethylaminophenol to give 7-diethylamino-4-hydroxycoumarin in good yield (Scheme 13). The product was obtained satsifactorily by this method. Vilsmeier formylation of this compound by the method of Moorty and co-workers [87] then gave 7-diethylamino-4-chloro-3-formylcoumarin in 26% yield.
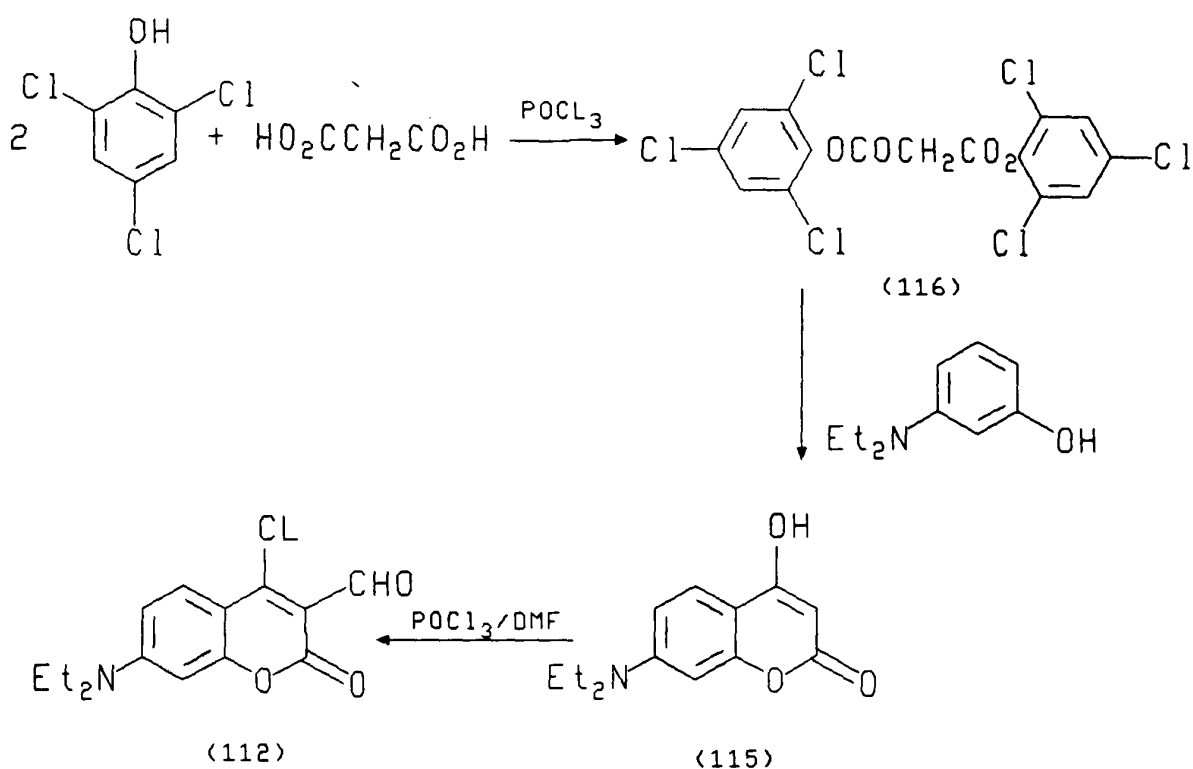
Scheme 13. Complete synthesis of 7-diethylamino-4-chloro-3-formylcoumarin

Condensation of 7-diethylamino-3-formyl-4-chlorocoumarin with 2-cyanomethylbenzimidazole was then attempted at 100°C in acetic anhydride, and this gave the ring closed dye (117) in good yield (Scheme 14). The structure was confirmed by microanalysis.
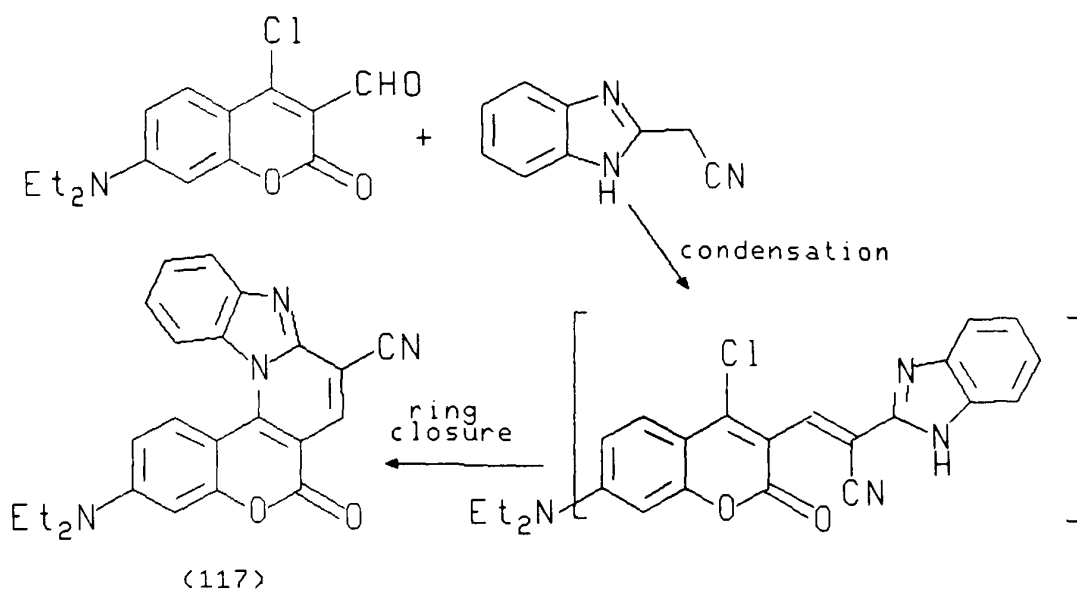
Scheme 14. Synthetic route to dye (117)

Thus the initial condensation reaction is followed by a particularly facile ring closure, in which the imidazole 1-nitrogen atom displaces chlorine from the coumarin ring.

Replacement of m-diethylaminophenol by 8-hydroxyjulolidine in this overal reaction scheme gave the aldehyde intermediate (118). Condensation of this with 2-cyanomethylbenzimidazole in acetic anhydride gave the analogous polycyclic dye (119), and the mass spectrum was consistent with the assigned structure.

(118)

(119)
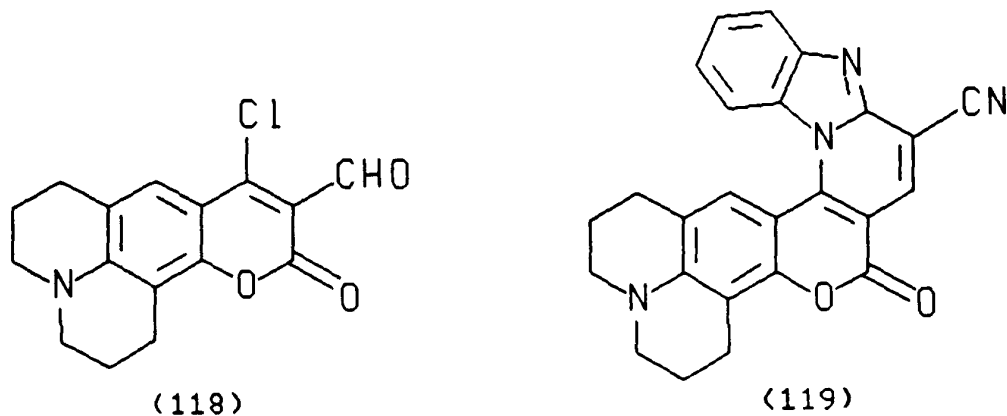
To take advantage of this reactivity of the _ortho_ chlorine atom in (112), other active methylene compounds with the capability of cyclisation were considered. In particular, malononitrile dimer (120) was considered. Due to the free amino group in the postulated initial condensation product (121) (Scheme 15) it is theoretically possible via cyclisation to produce the interesting extended chromophore (122) (Scheme 15).
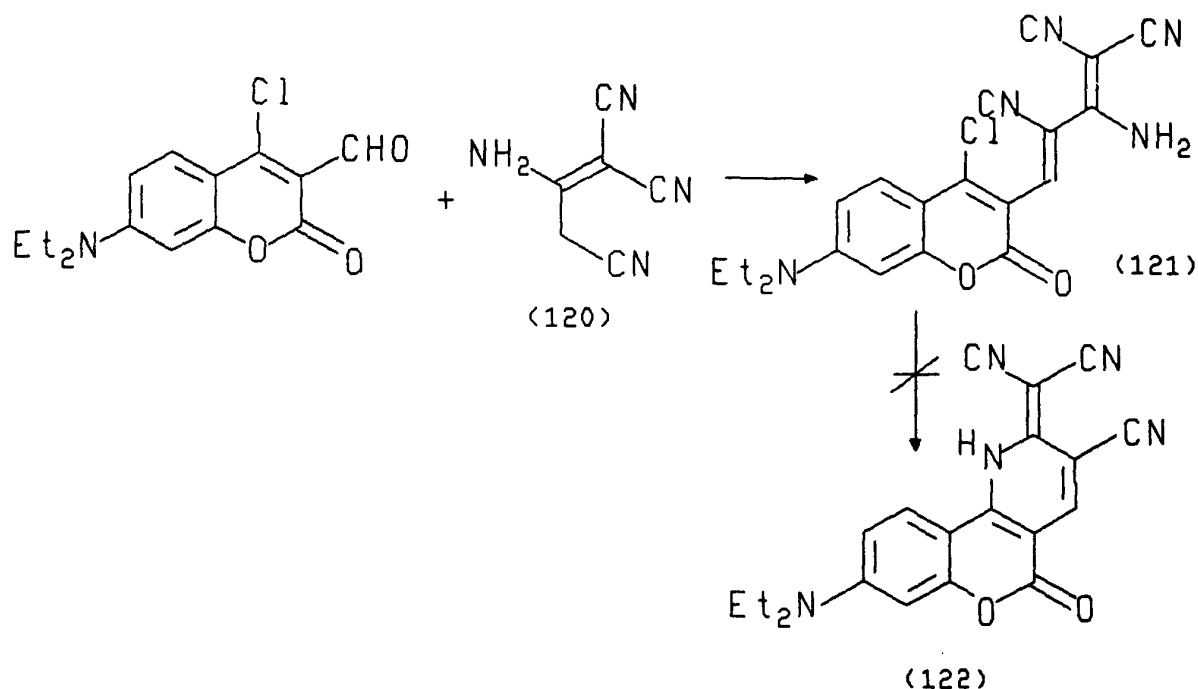
Scheme 15. Synthetic route to dye (122)

A structure such as (122) would be expected to exhibit strong fluorescent properties because of its highly rigidised structure. However, attempts to prepare (122) involving high temperatures in various solvents and with various bases, failed to give any identifiable products. The uncyclised dye (121) could be isolated when the condensation reaction between 7-diethylamino-4-chloro-3-formylcoumarin and malononitrile dimer was carried out in ethanol under reflux. The structure (121) was confirmed by microanalysis.

2.3.3 Light absorption and emission properties of fused coumarin dyes (117) and (119)

It is interesting to examine the effect of intramolecular cyclisation on the light absorption and emission properties of the dyes (99m) and (117). A comparison between the open-chain and cyclised chromophores (99m) and (117) is made in Figure 20.

(99m)   (117)
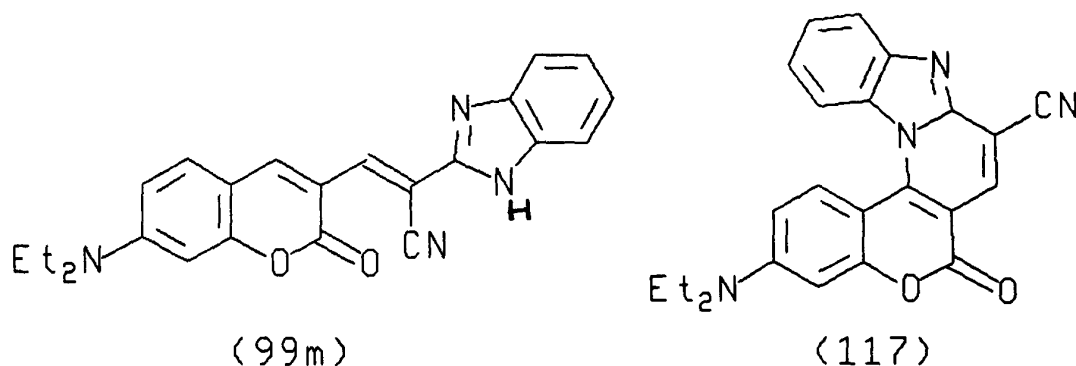
λ_{max} = 542nm	λ_{max} = 493nm
ε_{max} = 68,700 l mol^{-1}cm^{-1}	ε_{max} = 30,000 l mol^{-1}cm^{-1}
$\Delta\lambda_{1/2}$ = 85nm	$\Delta\lambda_{1/2}$ = 71nm
Fluorescence max. = 627nm	Fluorescence max. = 528nm
Intensity: low	Intensity : high
Stoke's shift: 43nm	Stoke's shift: 36nm

Figure 20.   Comparison of the light absorption and emission properties of dyes (99m) and (117)

The most notable differences between the two dyes are (a) the hypsochromic colour of (117) relative to (99m), and (b) the greater intensity of fluorescence from dye (117). The greater fluorescence from (117) can be explained in terms of the rigidity of the molecule, where bond rotation is restricted to the diethylamino group only. In the uncyclised chromophore (99m) bond rotation can occur at several sites in the

molecule.

The hypsochromic shift accompanying cyclisation of structure (99m) to structure (117) can be predicted using the classical perturbational MO theory of Dewar [88]. Thus Dewar's rules predict that if an electron donating group is attached to an unstarred position in the chromophore as is the case with dye (117), then a hypsochromic shift should result. It can be seen from Figure 21, that dye (117) has effectively an amino group attached to the unstarred 4-position of the coumarin ring.
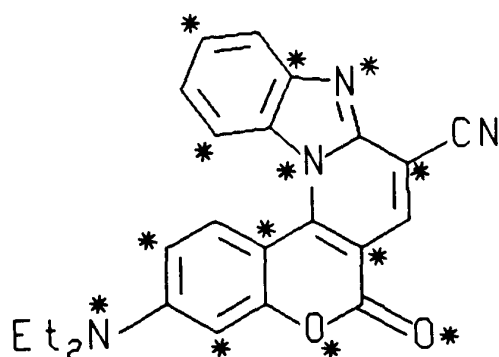
Figure 21. Starred and unstarred positions in dye 117

The effects of intramolecular cyclisation were also well predicted by the PPP SCF-CI MO method (Table 16).

Table 16. Calc. λ_{max} and observed λ_{max} for dyes (99m) and (117)

Dye	λ_{max} /nm	Calc. λ_{max} /nm	Calc. oscillator strength
(99m)	517	522	6.90
(117)	489	498	1.77

Complete rigidisation as in dye (119) by the incorporation of the 7-amino nitrogen atom in a julolidine residue leads to a dye which absorbs at slightly longer wavelengths (λ_{max} = 508nm, $\Delta\lambda_{1/2}$ = 60nm) than the diethylamino analogue (117)

$(\lambda_{max} = 493nm, \Delta\lambda_{1/2} = 71nm)$. The smaller half band width also reflects the increased molecular rigidity and explains why dye (119) has a greater fluorescence efficiency than (117).

2.3.4 Photostability properties of dye (117)

Irradiation of the dye (117) dissolved in cellulose acetate film, for 72 hours in the Microscal fadometer under standard conditions, gave 7.1% dye degradation. This is comparable to that of the standard azo dye (105) and is a great improvement relative to the uncyclised extended chain coumarin analogues (99).

The excellent stability and high fluorescence of this dye prompted its investigation for commercial application. After testing, dye (117) will now be introduced by Nippon Kayaku as a speciality green fluorescent disperse dye for polyester.

2.4 EXTENDED CHROMOPHORES CONTAINING AN ISOPHORONE BRIDGE

2.4.1 Introduction

Although RSA or 'shutter' dyes may be effective even if they do not have a strong absorption band in the near infrared, it is highly desirable to have such absorption. In this way colourless dyes may be obtained. Methods were therefore considered for displacing the absorption band of the coumarin and other donor-acceptor systems into the near infrared (ie. $\lambda > 700nm$). One approach is to extend the length of the conjugated system by introduction of additional vinyl groups, but unless some form of molecular rigidity is also enforced, this can lead to highly unstable systems.

One attractive way of achieving both effects makes use of the readily available ketone, isophorone, (3,5,5-trimethyl-2-cyclohexen-1-one) (123) a bifunctional molecule having the ability to undergo Knoevenagel type condensation reactions at both the ketone and active methylene positions (3/ position), thus leading to substituted triene chromophores.

(123)
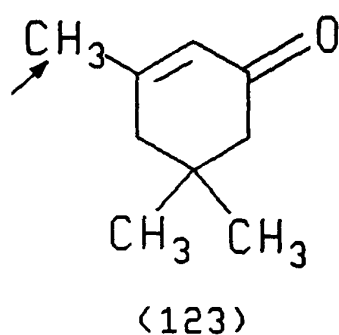
This type of reaction has been demonstrated by Lemke with the reaction shown in Scheme 16 [89].
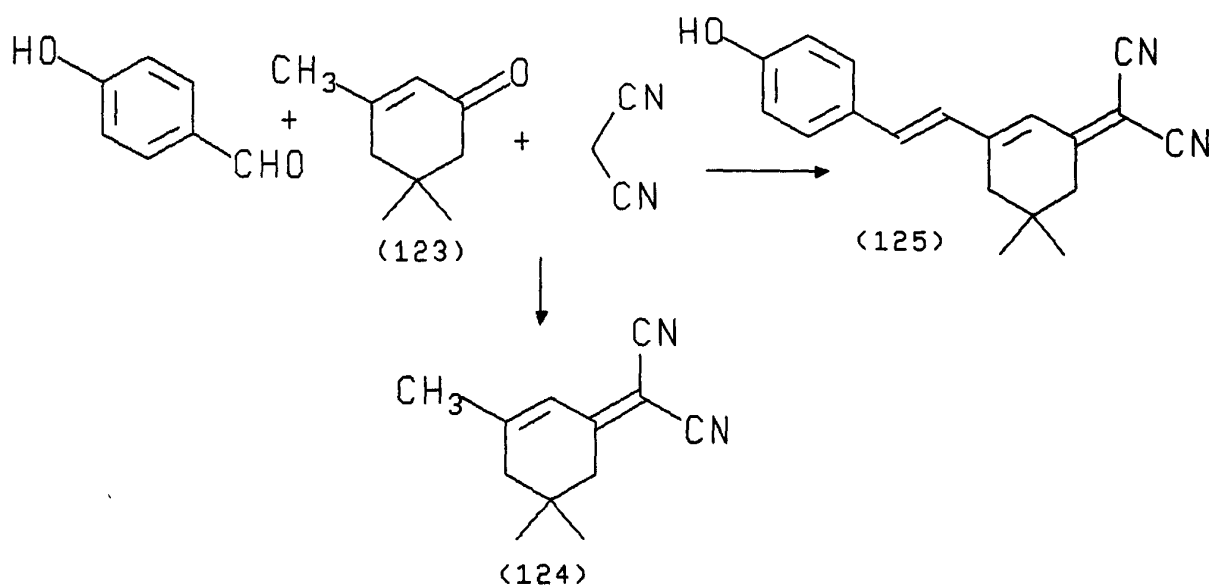
Scheme 16. Condensation of isophorone with p-hydroxybenzaldehyde and malononitrile

Lemke found that isophorone could be reacted with malononitrile first to give (124), which then has a highly active methylene group.

Thus if (124) is used to react with, for example, the coumarin aldehyde (91) then an analogue of dye (126) will be produced, i.e. structure (127), with two additional double bonds. Such a structure in theory should absorb ca 70-150nm to longer

wavelengths than (126), and the fact that one of the additional double bonds is included in a six membered ring should enhance the shift, the absorption intensity, and the photostability.

(126)   (127)
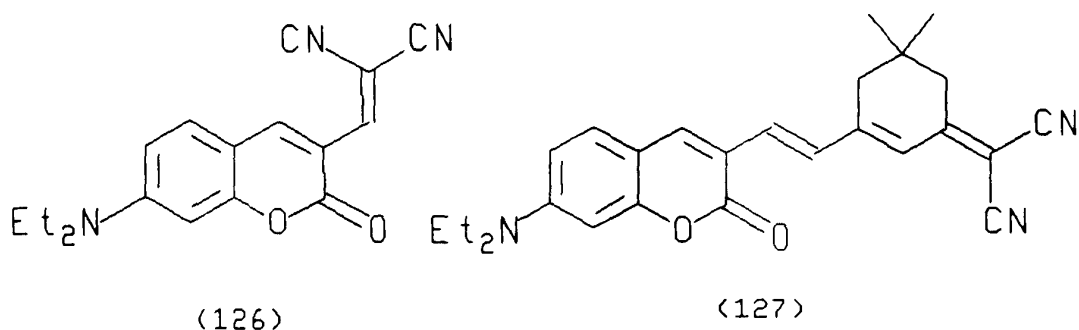
2.4.2 Synthesis of Dyes

Isophorone was condensed with malononitrile following the procedure of Lemke [89], and the product was obtained as a white solid in 30% yield. The condensation reactions between this and various aldehydes and nitroso compounds were then carried out and the resultant dyes (128) (see Table 17) isolated and characterised. In general the reactions were carried out in methanol containing a small amount of piperidine/acetic acid catalyst under reflux for a minimum time of 7 hours. Purification of the dyes was effected by column chromatography and/or recrystallisation, and the structures were confirmed by elemental analysis or mass spectrometry

(128) R structure

128(a)
Me₂N— phenyl —CH

128(e)
Et₂N— coumarin —CH

128(b)
Me₂N— phenyl —CH=CH

128(f)
indoline —CH

128(c)
Me₂N— phenyl —N

128(g)
pyrene —CH

128(d)
Me₂N— (OH-phenyl) —CH
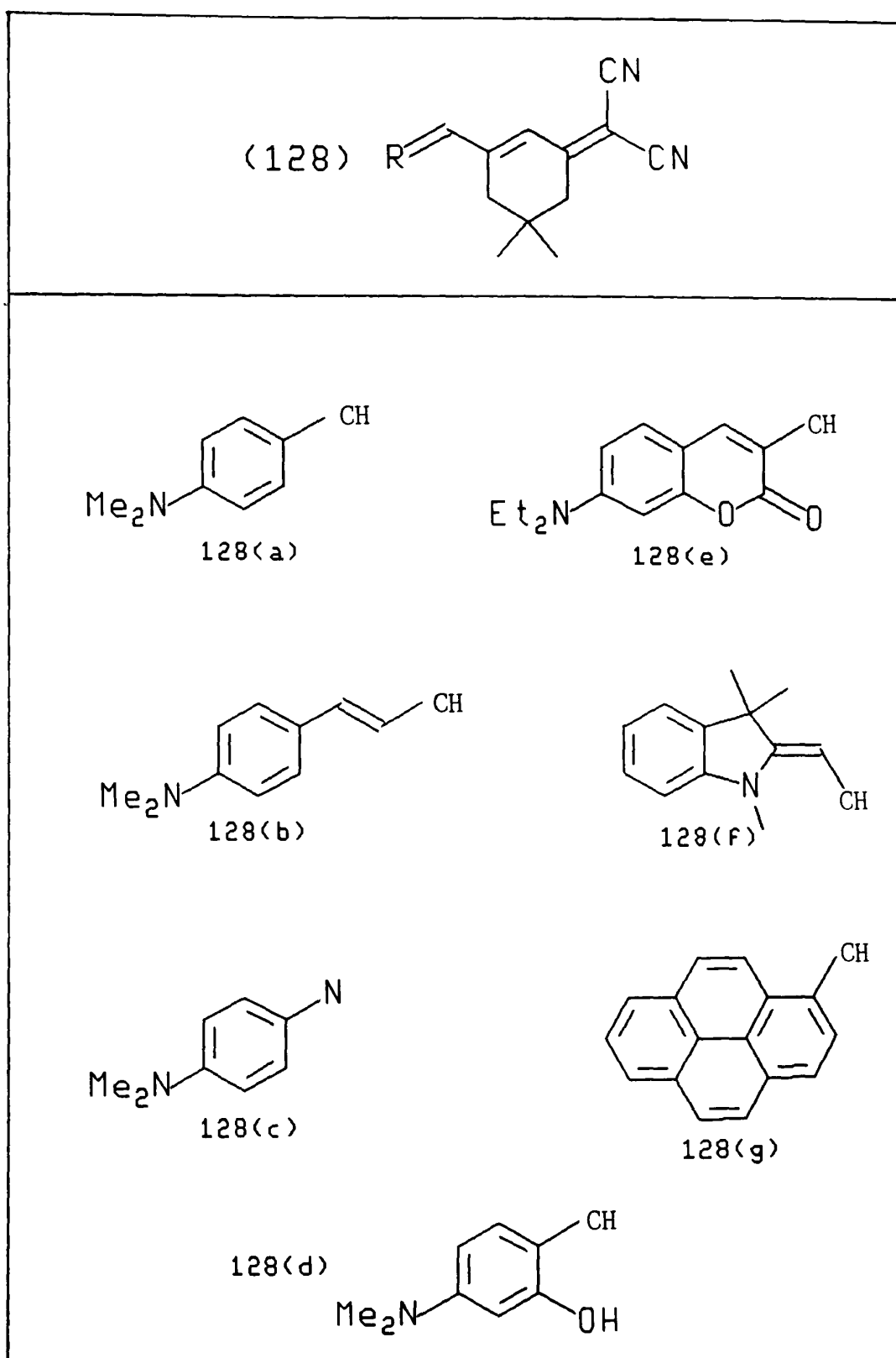
Table 17. Isophorone bridged dyes

2.4.3 Light absorption and emission properties of isophorone bridged dyes

Visible absorption spectra of the dyes (128) were recorded in dichloromethane and toluene, and the results are summarised in Table 18.

Table 18. Spectral properties of isophorone bridged dyes (128)

Dye	$\lambda_{max}^{CH_2Cl_2}$	λ_{max}^{Tol}	$\Delta\lambda_{1/2}$ (CH_2Cl_2)/nm	ε_{max} /lmol^{-1}cm^{-1}	$\Delta\lambda$/nm CH_2Cl_2-Tol
128(a)	500	490	64	27,200	+10
128(b)	513	512	124	-	+1
128(c)	525	520	124	26,500	+5
128(d)	525	512	109	37,400	+13
127	515	509	112	34,400	+6
128(e)	566	544	111	42,200	+22
128(f)	463	459	120	-	+4

It is evident that none of the isophorone bridged dyes are particularly bathochromic, and all are orange to purple in colour. A further increase in the extent of conjugation would in theory produce more bathochromic dyes, but considering the relative absorption maxima of the dye series shown in Figure 22 , a further increase in conjugation would probably have only a small bathochromic effect.

-
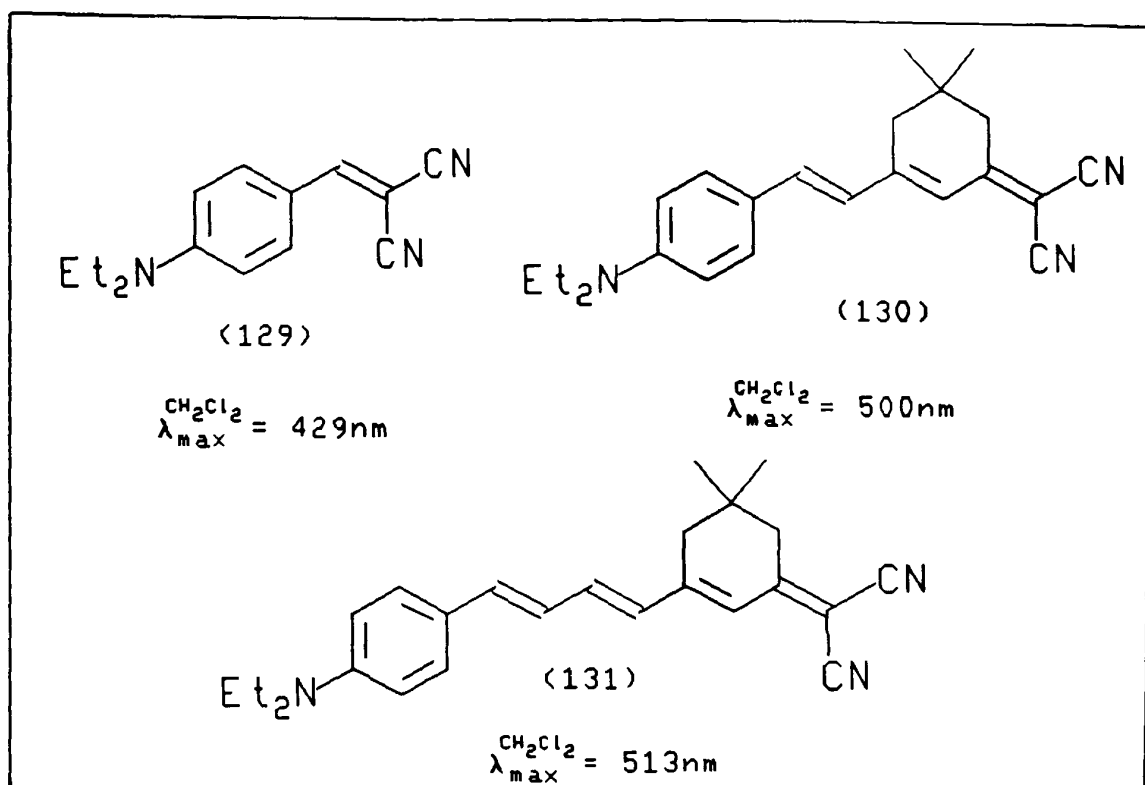
Figure 22. Dyes with extended conjugation

Figure 23, shows this effect graphically by plotting the length of the conjugated chain against λ_{max}/nm for dyes (129)-(131).
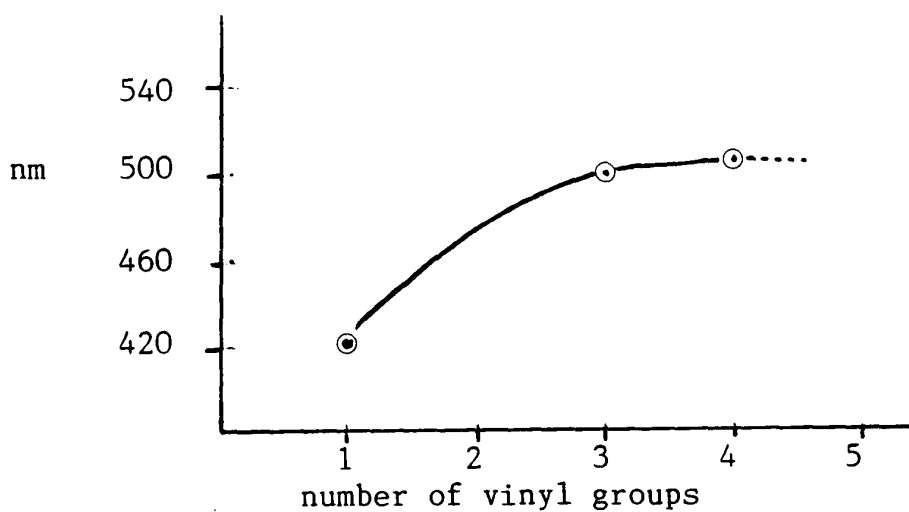
Figure 23. Variation of λ_{max} with chain length for dyes (129)-(131)

It is apparent that the convergent limit for this system is reached when there are

four vinyl groups, and thus increasing the linear conjugation still further will not produce a significant bathochromic shift.

It was surprising to note that a hypsochromic shift occurred when the isophorone bridge was introduced into the chromophore of dye (126). Dye (127), was expected to absorb 70-150nm to longer wavelengths than dye (126), but in fact a hypsochromic shift of 12nm was observed in dichloromethane.

(126)

(127)

λ_{max} = 527nm

$\Delta\lambda_{1/2}$ = 58nm

λ_{max} = 515nm

$\Delta\lambda_{1/2}$ = 112nm
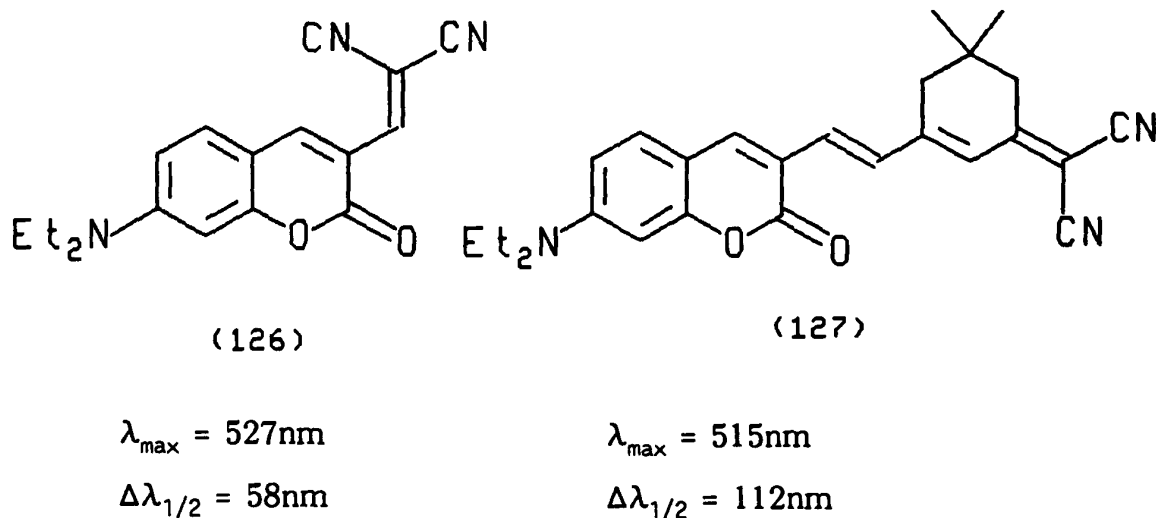
This is probably due to two factors:

1. The system (127) has already reached its convergent limit.
2. System (127) is less planar than (126). This is confirmed by the reduction in extinction coefficient and broadening of the absorption band of dye (127) relative to dye (126), which are good indications of reduced planarity and poor orbital overlap.

The isophorone bridged coumarin (127) ε_{max} 34,400 l mol^{-1}cm^{-1} shows a dramatic decrease in ε_{max} relative to the unbridged coumarin (126), ε_{max} 73,300 l mol^{-1}cm^{-1}.

The fluorescence excitation and emission data for the isophorone bridged dyes are summarised in Table 19.

Table 19. Fluorescence data for isophorone bridged dyes (128)

Dye	Excitation λ_{max} /nm	Emission λ_{max} /nm	Stoke's shift /nm	A/C at 5×10^{-6} mol l^{-1}
128(a)	508	546	38	1.5
128(c)	513	539	26	28
128(d)	507	546	39	5
127	497	614	117	88
128(e)	513	545	32	6

It is notable that all the bridged dyes have a greater fluorescence efficiency than dye (127) containing the coumarin moiety, which is surprising at first, but is consistent with the marked loss of planarity noted for this dye.

2.4.4 Photostability properties of isophorone-bridged dyes

Dye-containing cellulose acetate films were prepared in the usual way and were subjected to 72 hours exposure in a Microscal photofadometer. The optical density decrease was measured and the results are summarised in Table 20.

Table 20. Lightfastness properties of some isophorone-bridged dyes

Dye	% Degradation
Azo standard (105)	6
128(a)	74
128(c)	30
128(d)	100
127	100
128(e)	100

It was evident that all the isophorone bridged dyes, with the exception of dye (128c) had extremely poor photostability properties. The exceptional behaviour of 128(c) is unexpected, as in general imino bridged dyes are less stable than the vinyl bridged dyes.

None of the dyes were sufficiently bathochromic to be sent for testing as reverse saturable absorbers.

2.4.5 Conclusions

As a means of displacing the absorption maxima of donor-acceptor chromophores into the near-infrared, whilst simultaneously enhancing photostability by including a bridging ring system, the use of the active methylene intermediate (124) is distinctly unsuccessful. Thus wavelength shifts were much smaller than expected and the convergence limit for dye (127) had been reached. In addition, photostability was very poor. Thus other approaches to suitable long wavelength chromophores were sought.

2.5 EXTENDED DONOR-ACCEPTOR CHROMOPHORES CONTAINING A CHLOROCYCLOHEXANE BRIDGE

2.5.1 Introduction

A more effective way of moving the wavelength maxima of the chromophores to longer wavelengths is to increase the donor-acceptor interaction within the chromophoric system to such an extent that electronic symmetry is achieved, and the chromophore becomes cyanine-type. This gives the optimum bathochromic shift, and is exemplified by the cyanine dye IR-140.
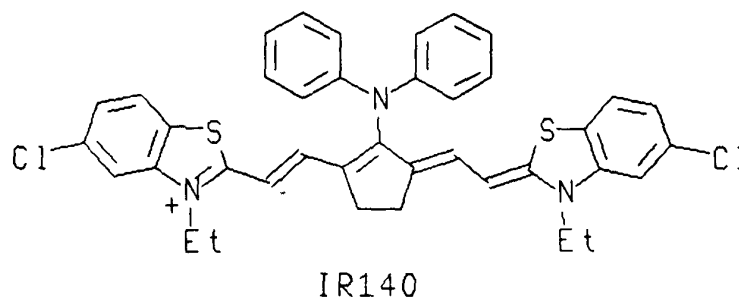
IR140

The terminal thiazole rings share the positive charge of the chromophore equally. Such dyes show a non-convergent behaviour with increasing chain length, and so large red shifts are easily achieved. IR-140 for example has λ_{max} = 823nm in DMSO [90]. We therefore examined chromophores related to IR-140, making use of a central chlorocyclohexane bridging unit to provide enhanced shift and good stability. IR-140 is prepared from 2-chloro-1-formyl-3-hydroxymethylene-cyclopentene (132), and by analogy we utilised 2-Chloro-1-formyl-3-hydroxymethylene-cyclohexene (133) the six membered ring analogue. This intermediate could be prepared from readily available materials and proved to be a valuable intermediate in the preparation of various highly conjugated, structurally stabilised, infrared absorbing dyes.

(132)

(133)
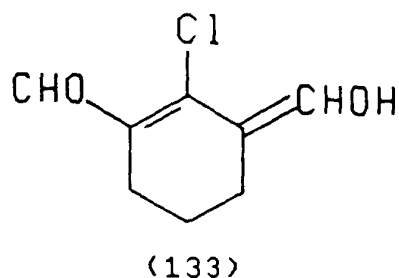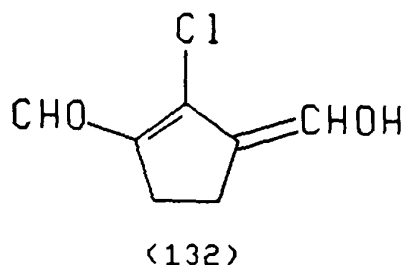
2.5.2 Synthesis of intermediates and dyes

The synthesis of 2-chloro-1-formyl-3-hydroxymethylene-cyclohexene is shown in Scheme 17, and routes to dyes derived from this are summarised in Scheme 18.
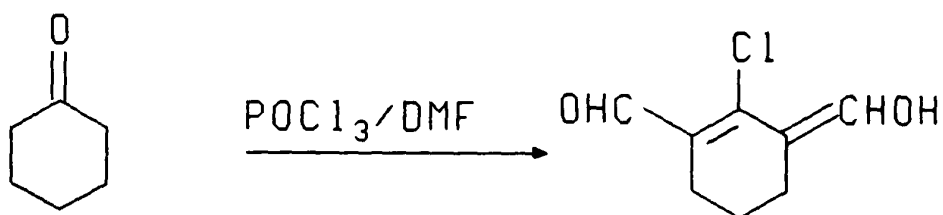
Scheme 17. Synthesis of 2-chloro-1-formyl-3-hydroxymethylene-cyclohexene

As shown in Scheme 18, there are two possible synthetic route to the donor-acceptor dyes (135), namely a) condensation of (133) with an electron withdrawing type active methylene compound (eg malononitrile) and then condensation of this with an electron donating type active methylene compound (eg Fischer's base); and b) the reverse situation, whereby (133) is first condensed with an electron-donating type active methylene and the intermediate (136) then condensed with an electron-accepting type active methylene compound.
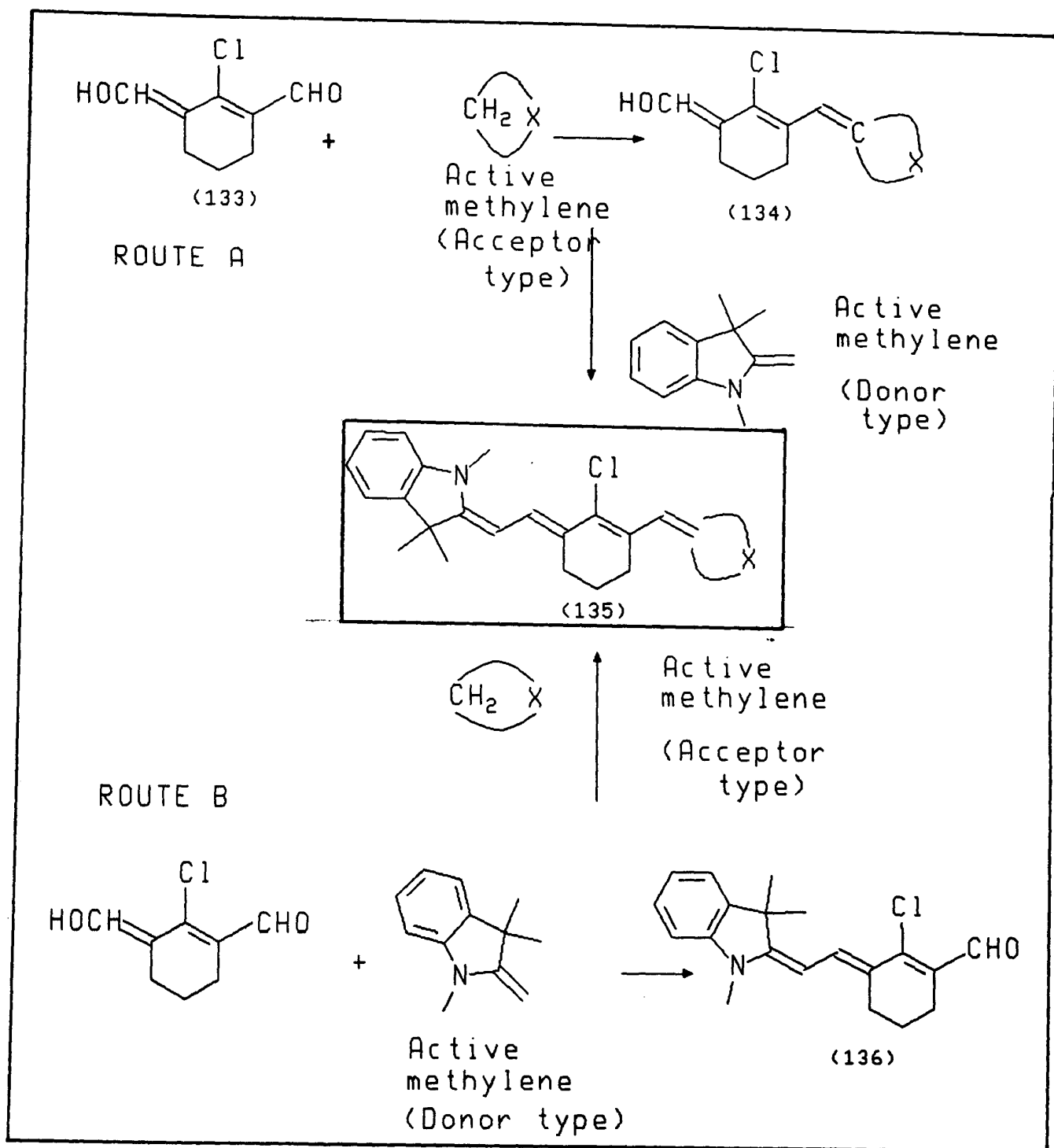
Scheme 18. Synthetic route to dyes derived from 2-chloro-1-formyl-3-hydroxymethylene-cyclohexene

The synthesis of a series of donor-acceptor methine dyes of general formula (135) was intially attempted via route (a), because of the excellent result obtained in the synthesis of dye (137a) by this method (Table 21). Thus reaction of (133) and malononitrile in ethanol gave an intense yellow reaction mixture due to the

formation of (138), which was not isolated.

(138)
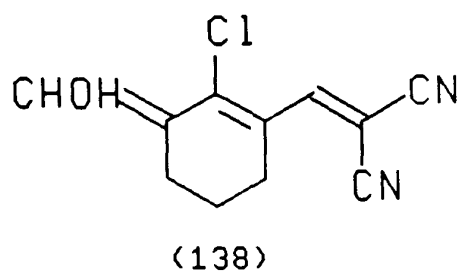
Upon addition of Fischer's base to the solution followed by gentle warming an intense cyan colour developed rapidly, and crystals of the dye (137a) deposited on cooling, in good yield. It was anticipated that other dyes could be synthesised by this simple method. However, in several other attempted syntheses, the reactions gave complex reaction mixtures, and in some cases thin layer chromatography showed that as many as twenty different coloured substances were present. In view of the general inefficiency of this approach, the alternative route (b) was examined. It was found that reaction of (133) and Fischer's base in ethanol at room temperature proceeded smoothly to give the red coloured intermediate 2-chloro-3-formyl-1-[[cyclohexene-2-yl]ethenyl]-1,3,3-trimethyl-3H-indolin (136) in excellent yield. The product crystallised out of solution and could be purified by column chromatography (silica gel, toluene). The principal impurity, the positively charged double Fischer's base condensate adhered strongly to the top of the column, and so could be removed readily and efficiently.

(136)
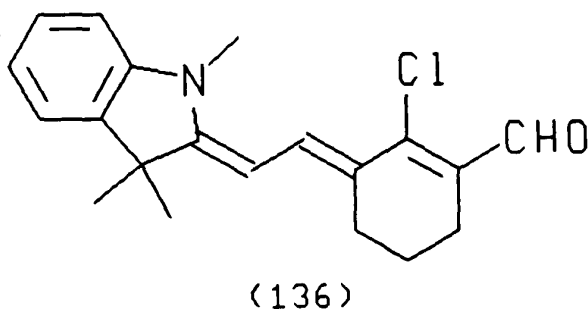
Condensation of the Fisher's base adduct (136) with a range of active methylene compounds, was then examined, and it was found that acetic anhydride was the most effective solvent in most cases. Several blue dyes were thus prepared and the structures of these are summarised in Table 21. The dye (137e) was exceptional, in that synthesis was best effected in boiling ethanol. The dyes were characterised by microanalysis.

Table 21. New extended methine dyes (137)
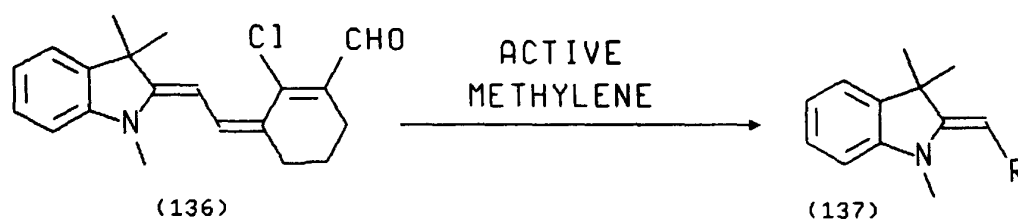
Dye	Active methylene	Dye structure (137) R
137(a)	$CH_2(CN)_2$	
137(b)		
137(c)		
137(d)		
137(e)		

Other dyes synthesised but which could not be purified satisfactorily for microanalytical characterisation due to poor stability properties were (137f) and (137g).

(137f)

(137g)
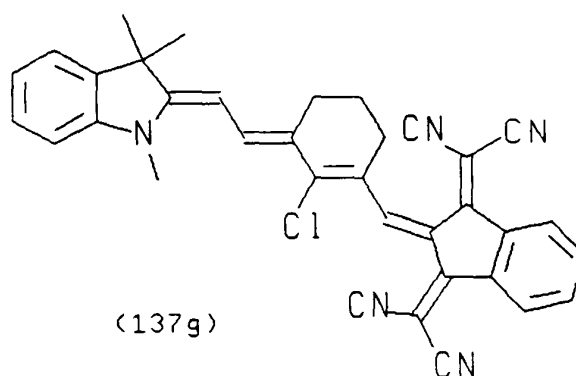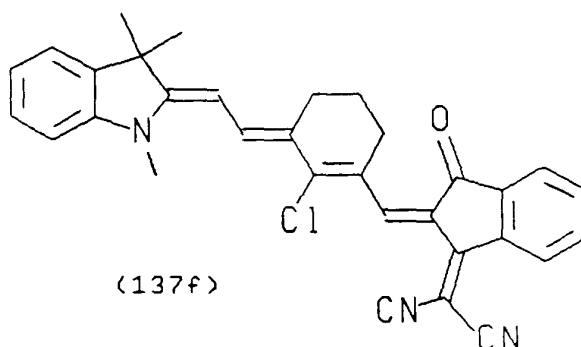
2.5.3 Light absorption properties of the extended Donor-acceptor Dyes

Visible absorption spectra of the dyes (137) were recorded in dichloromethane and toluene, and the results are summarised in Table 22.

Table 22. Spectral properties of extended donor-acceptor dyes (137)

Dye	λ_{max}^{Tol} /nm	$\lambda_{max}^{CH_2Cl_2}$ /nm	$\Delta\lambda_{1/2}$ /nm	ε_{max} l mol^{-1}cm^{-1}	$\Delta\lambda$ nm CH$_2$Cl$_2$-Tol
137(a)	584	623	108	91,200	+39
137(b)	744	861	71	167,900	+117
137(c)	599	623	127	66,000	+24
137(d)	567	586	117	52,200	+19
137(e)	632	697	139	41,100	+65

In methylene chloride dye (137f) had λ_{max}= 632nm and dye (137g) had λ_{max}= 718nm. The colour of the dyes in solution ranged from dark blue to cyan. The dye (137b) showed exceptional properties, absorbing in the near-infrared at 861nm in methylene chloride even though it is an non-cyanine, unsymmetrical donor-acceptor system. It was very solvatochromic, and in toluene the band shifted to 744nm. Although the visible absorption spectrum of this dye is broad, (Figure 24) its calculated half band width is small and its extinction coefficient very large (167,900 l mol^{-1}cm^{-1}).
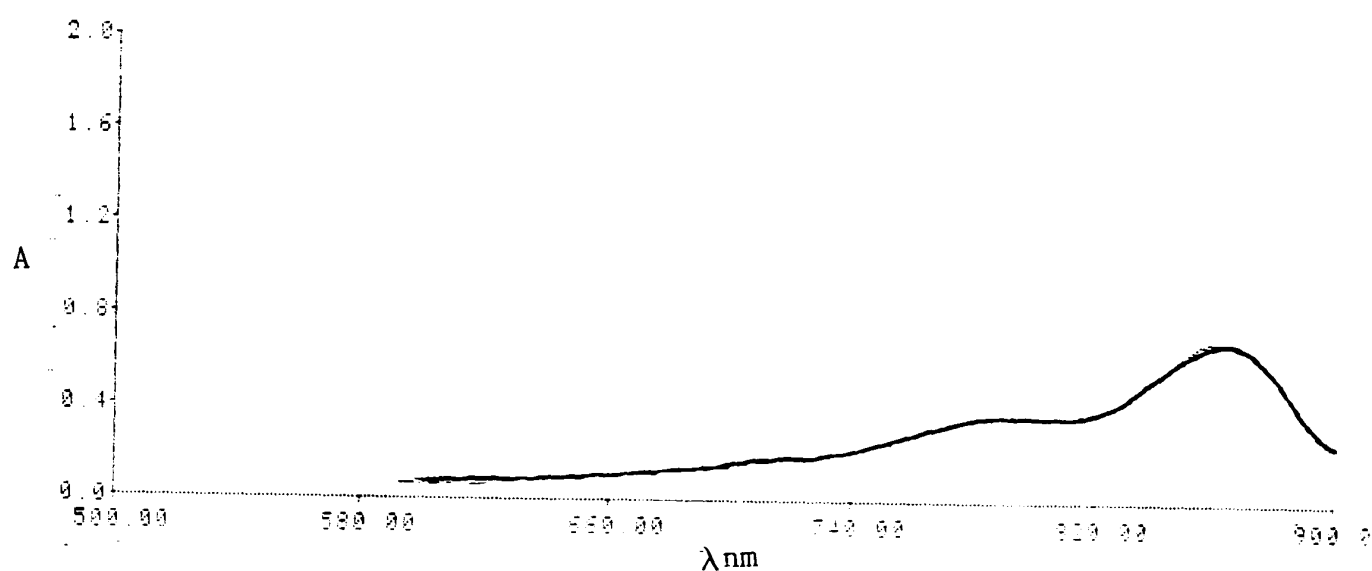
Figure 24. Visible absorption spectrum of dye (137b)

Dye (137d) containing a benzimidazole residue showed interesting halochromic properties. On addition of HCl to a solution of the dye in acetone, a 166nm bathochromic shift was recorded, and the dye absorbed at 752nm. This is probably the first example of a pH indicator dye which shows a coloured to near colourless shift on protonation, the colour loss being due to the large red shift of the band. The effect is presumably due to the process shown in Scheme 19, where the electron accepting properties of the benzimidazole ring are greatly enhanced by protonation.

$\lambda_{max} = 586nm$

$\lambda_{max} = 752nm$
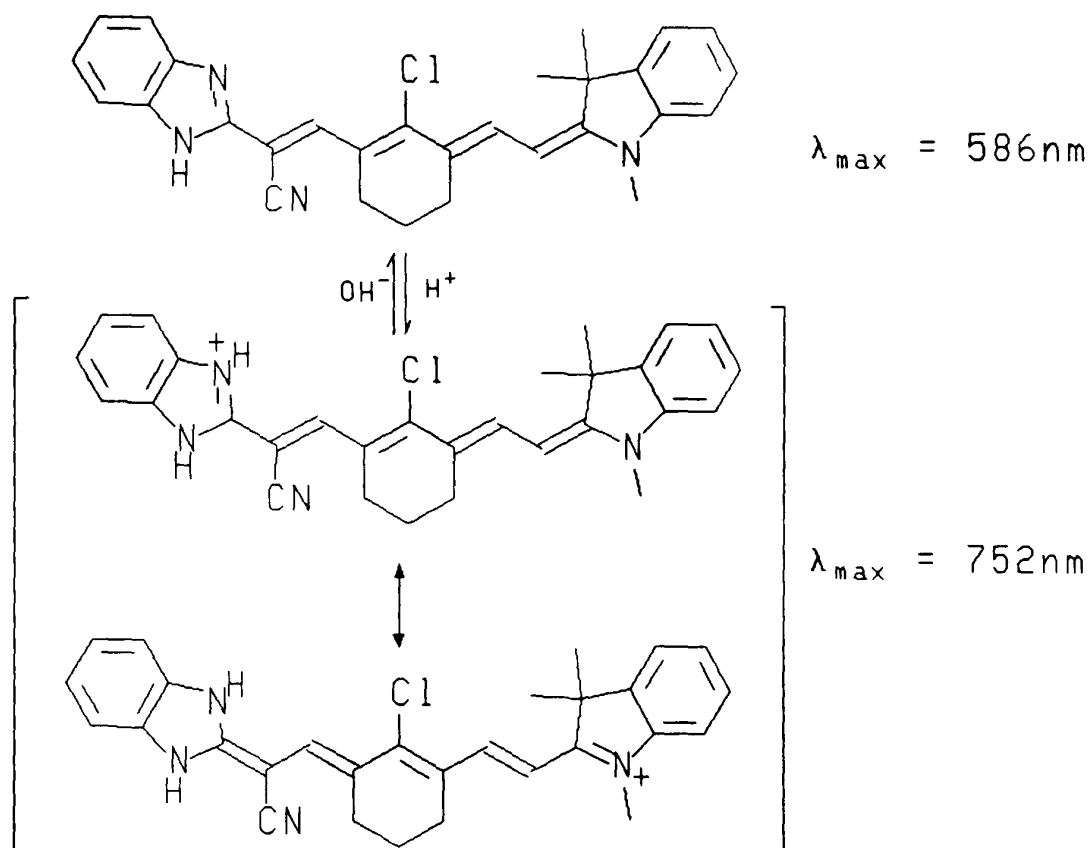
Scheme 19. Halochromic properties of dyes (137d)

2.5.4 Photostability properties of extended donor-acceptor dyes (137)

Dye-containing cellulose acetate films were prepared in the usual way and were subjected to 72 hours exposure in a Microscal photofadometer. All samples apart from the azo dye standard (105) had completely faded after this time period. The experiment was repeated with new films but exposing for only 1 hour. The optical density decrease was then measured, and the results are summarised in Table 23.

Table 23. Relative light fastness properties of extended donor-acceptor dyes (137)

Dye	% Degradation
Azo dye standard (105)	0
137(a)	53
137(b)	34
137(c)	50
137(d)	43
137(e)	65

As can be seen, the light fastness properties of dyes (137) are very poor and this is frequently the case with extended polymethine systems of this type.

2.6   EXTENDED DONOR-ACCEPTOR CHROMOPHORES CONTAINING FUSED HETEROCYCLIC RESIDUES

2.6.1   Introduction

Deligeorgiev and Gadjev [91][92] demonstrated recently the synthesis of novel near-infrared absorbing unsymmetrical trimethine pyrylium cyanine dyes (139) using 2-chloro-1-formyl-3-hydroxymethylene cyclohexane as an intermediate. The synthetic route is shown in Scheme 20.

It is notable that in this reaction sequence as well as the usual condensation reaction between the aldehyde group and an active methylene group, there is also a subsequent nucleophillic replacement of the central chlorine atom of (133).
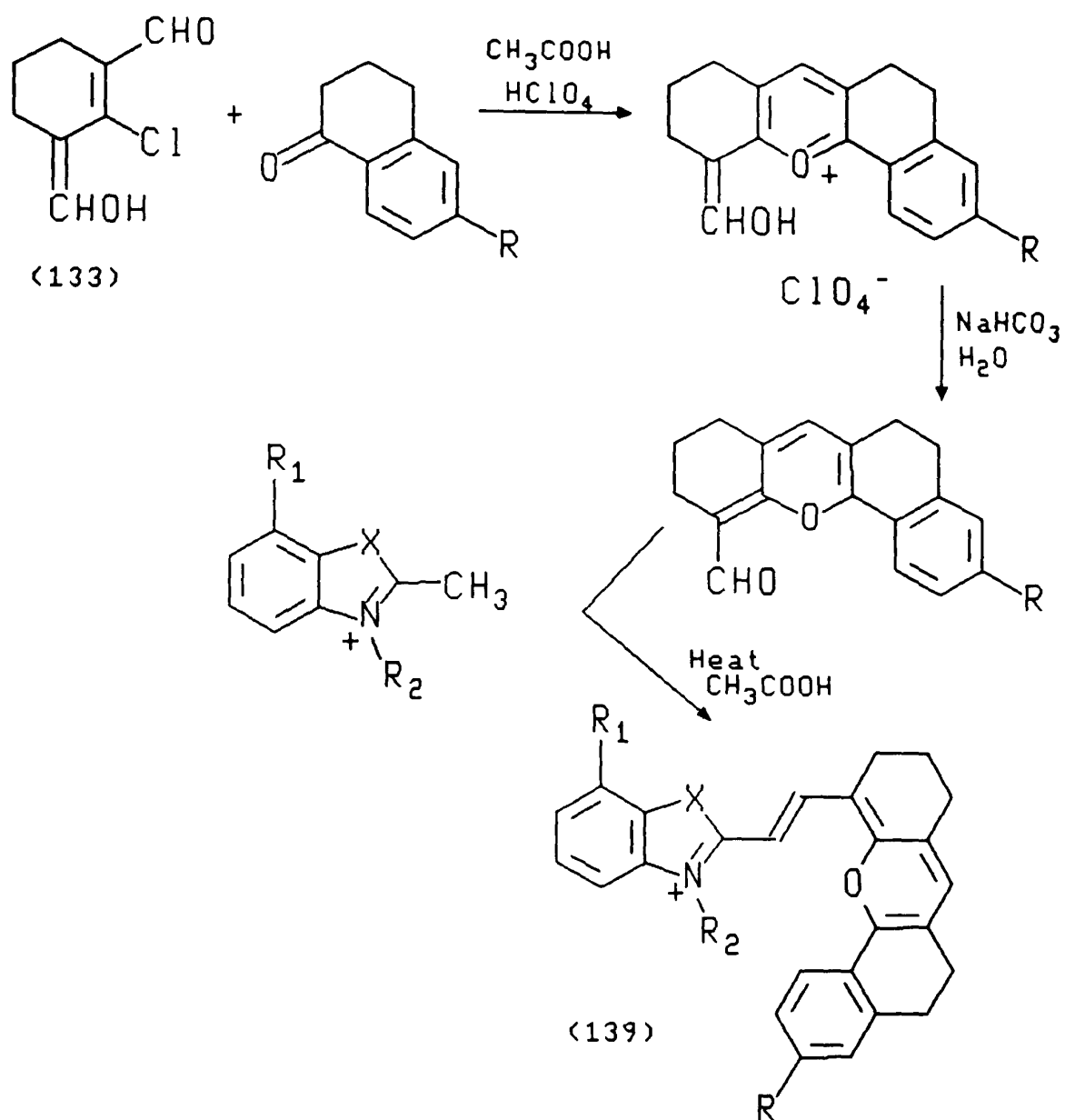
Scheme 20. Novel asymmetrical trimethine cyanine dyes

The lability of the central chlorine atom in (133) and derived dyes has also been demonstrated by Strekowski and co-workers [93][94]. These workers replaced the central atom of heptamethine cyanine dyes with various nucleophiles (Scheme 21(a)). Of particular practical value was the synthesis of the isothiocyanate derivative (140) which could then be used for labelling proteins (Scheme 21(b)).
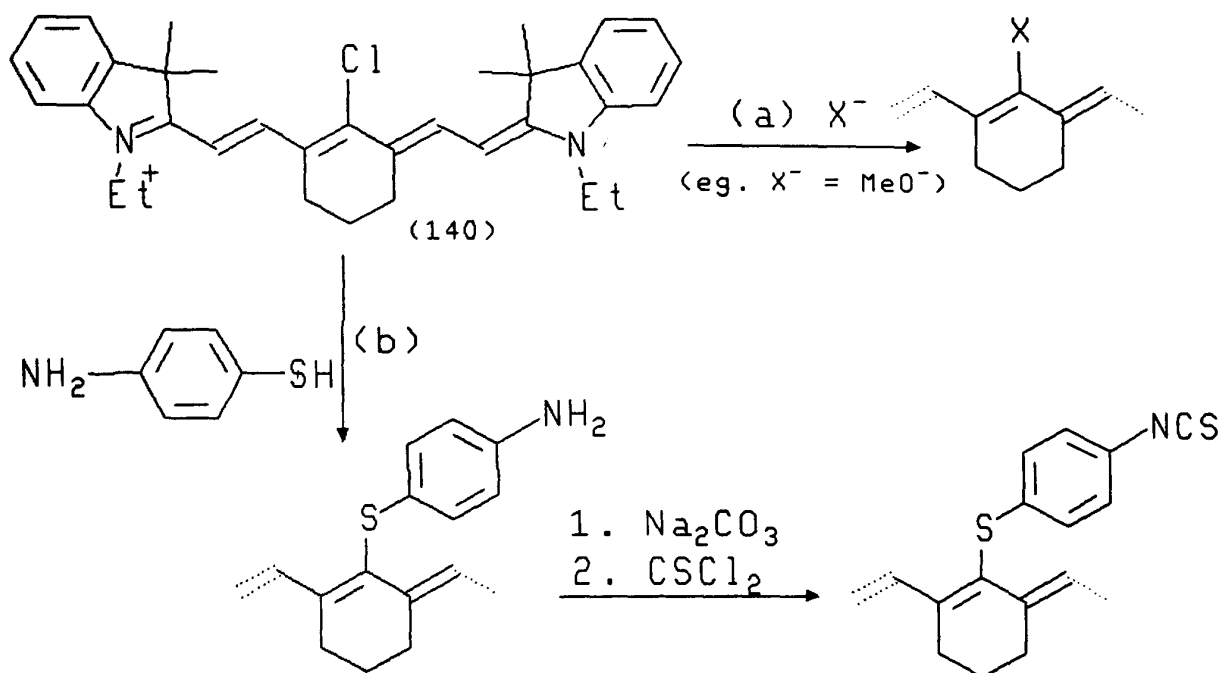
Scheme 21. Nucleophilic substitution reaction of heptamethine cyanine dye (140) [93][94]

Theoretically it should be possible to apply these principles to the cyclisation of certain of the open chain dyes prepared by us, provided suitable nucleophillic sites are present in the terminal component of the dye. This principle is shown in Scheme 22.
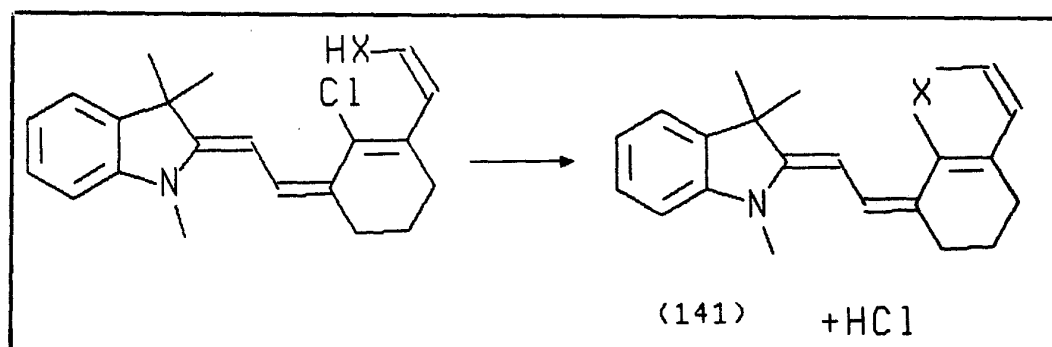
·Scheme 22. Intramolecular cyclisation

Dyes of the general type (141) are of potential interest for several reasons. Thus a new chromophoric system is generated, which may absorb with a significantly different λ_{max} or ε_{max} compared to the uncyclised dye. In addition, the increased structural rigidity in (141) could lead to better stability properties and/or

fluorescence efficiency.

2.6.2 Synthesis of dyes

The NH- group of the benzimidazole residue of dye (137d) provides a suitable nucleophilic site for cyclisation of the type shown in Scheme 23. When dye (137d) was heated in N-methylpyrrolidine at 200°C a colour change from purple to magneta was observed. The evolution of HCl fumes from the reaction vessel during the cyclisation reaction (Scheme 23), could be detected with moist litmus paper.
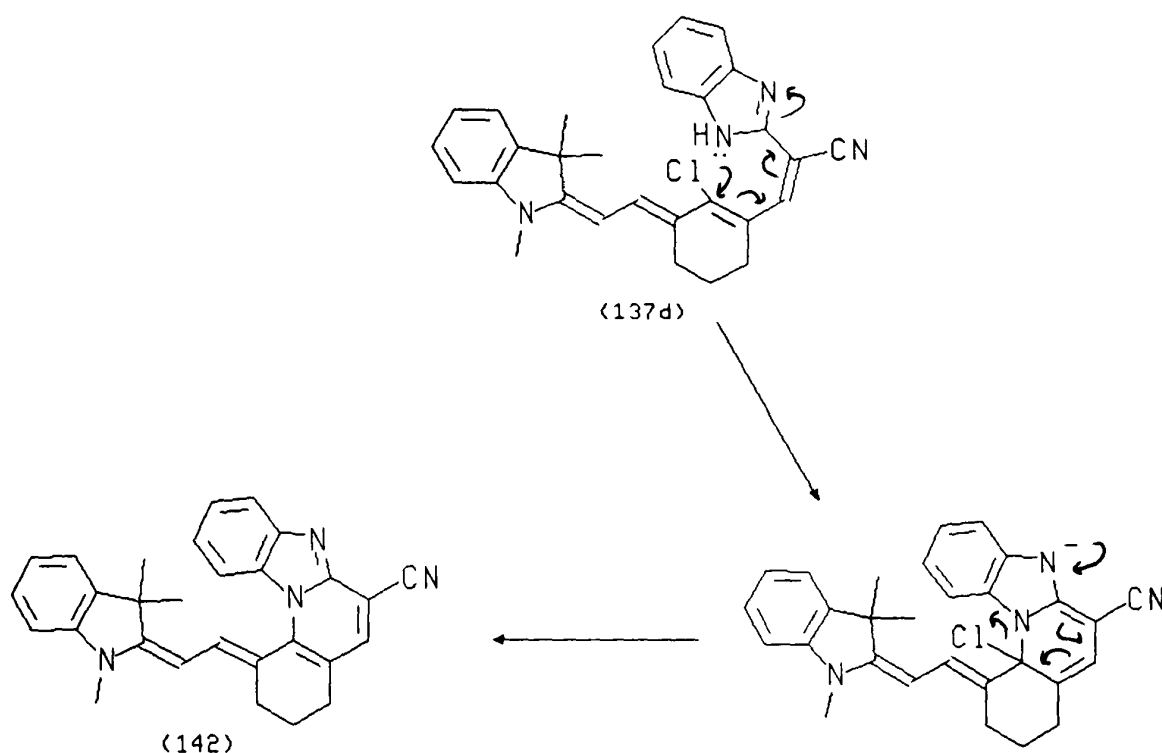
Scheme 23. Intramolecular cyclisation of dye (137d)

After isolation of the product and recrystallisation from ethyl acetate, the structure of dye (142) was confirmed by microanalysis, which showed loss of one molecule of HCl from the parent dye structure.

In view of the success of the cyclisation process, other ring systems were considered. To obtain suitably nucleophil ic end groups new dyes were prepared. Reaction of the Fischer's base adduct (136) with a range of active methylene compounds as shown in Table 24, in acetic anhydride or NMP at elevated temperatures gave dyes (143a)-(143e).

Table 24. Extended donor-acceptor dyes containing fused heterocyclic residues (143)

R =
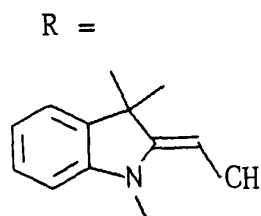
Dye	Active methylene	Dye structure
143(a)		
143(b)		
143(c)		
143(d)		
143(e)		

The active methylenes all contained carbonyl groups adjacent to the active methylene groups so that cyclisation could occur via enolate oxygen of the first formed open chain dye. This can be summarised as in Scheme 24. It was originally thought that from a mechanistic point of view it was essential for a NH group to be adjacent to the 'O' atom participating in the cyclisation reaction (Scheme 24), so enabling enolisation to occur prior to cyclisation.
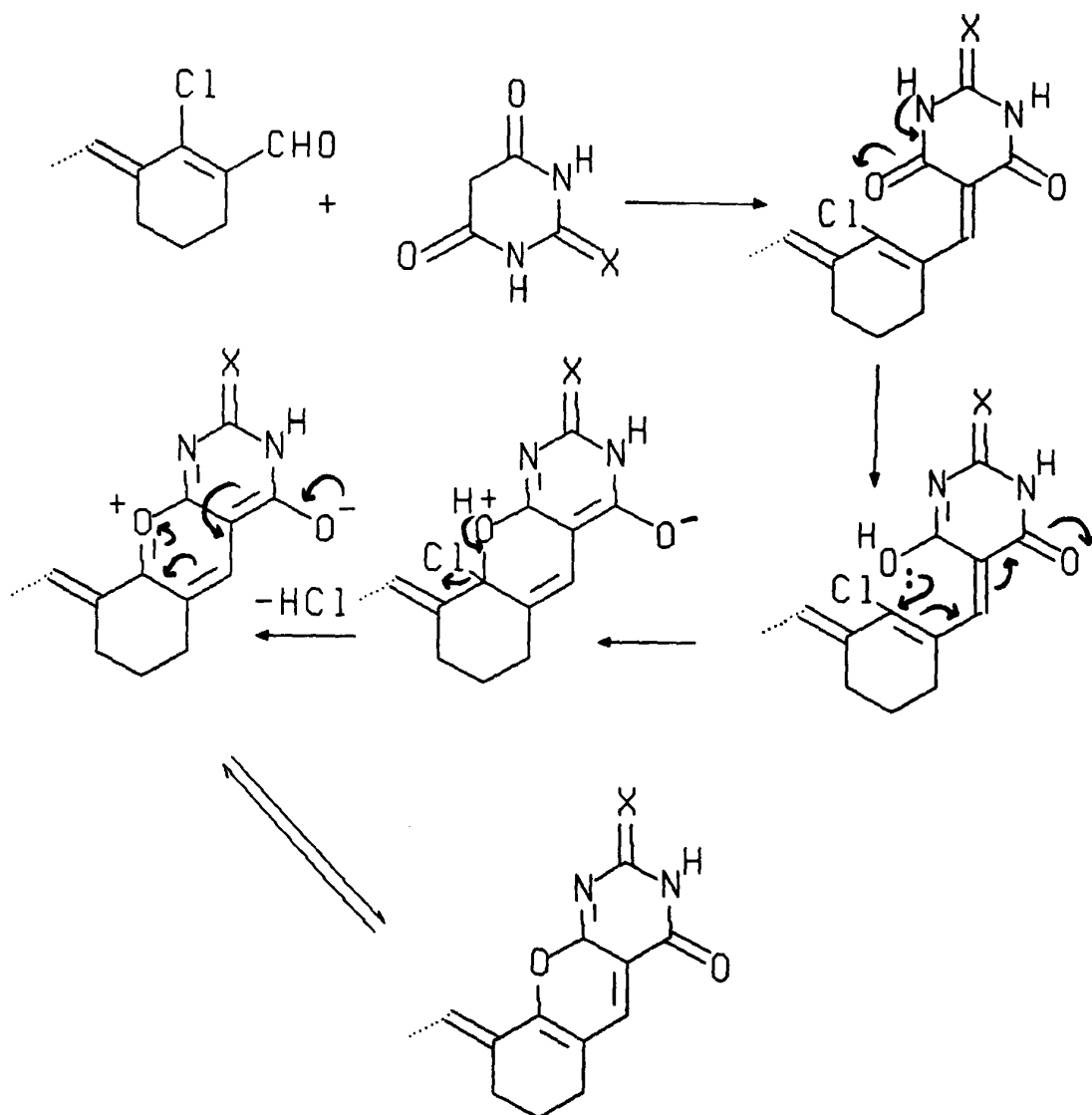
Scheme 24. Proposed mechanism of cyclisation

If enolisation is important, then the synthesis of cyclised dyes from intermediates such as N,N-dimethylbarbituric acid and N,N-diethylthiobarbituric acid would not be possible. However, when reactions with these compounds were examined, water soluble blue products were obtained which readily salted out with perchloric acid. This suggested that the chromogens were of a cationic nature. Reconsideration of

94

the mechanism leads to the conclusion that the +M effect of the alkylamino group is sufficient to bring about cyclisation of carbonyl oxygen (Scheme 25).
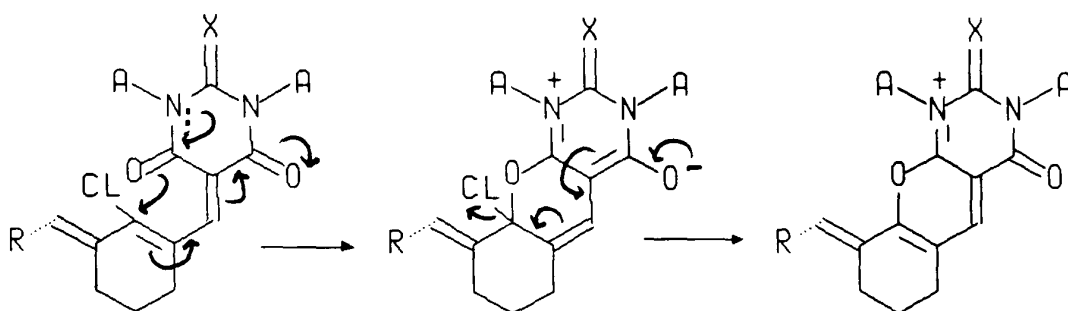
Scheme 25.

Thus the cationic dye (143c) was prepared from N,N-diethylaminothiobarbituric acid, as the perchlorate salt. Microanalysis figures were correct for the proposed structure. The proposed mechanism is more logical than that put forward by Andrieux and co-workers [95] in a similar type of ring closure reaction (Scheme 26), who assumed that the reaction proceeded via a carbocation intermediate.
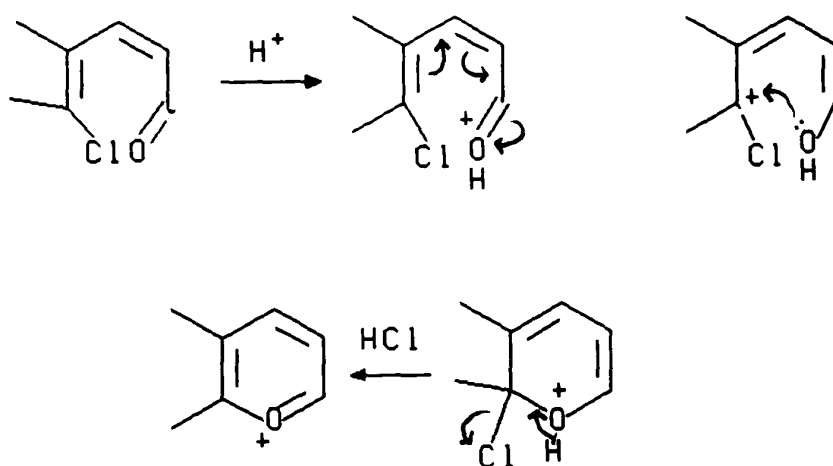
Scheme 26.

Other cationic dyes synthesised but not fully characterised in this series were (143f) and (143g).
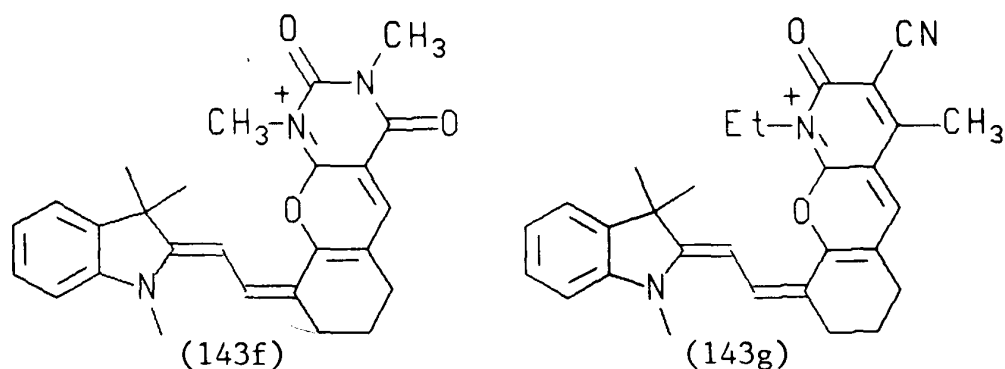
In theory it should also be possible to tie up the donor end of the donor-acceptor dye in a rigidised structure, as suggested in Scheme 27. The proposed reaction involves the condensation and subsequent ring closure reaction of 2,3,3-trimethyl-indolenine (144) with the chlorodialdehyde (133) to give intermediate (145).
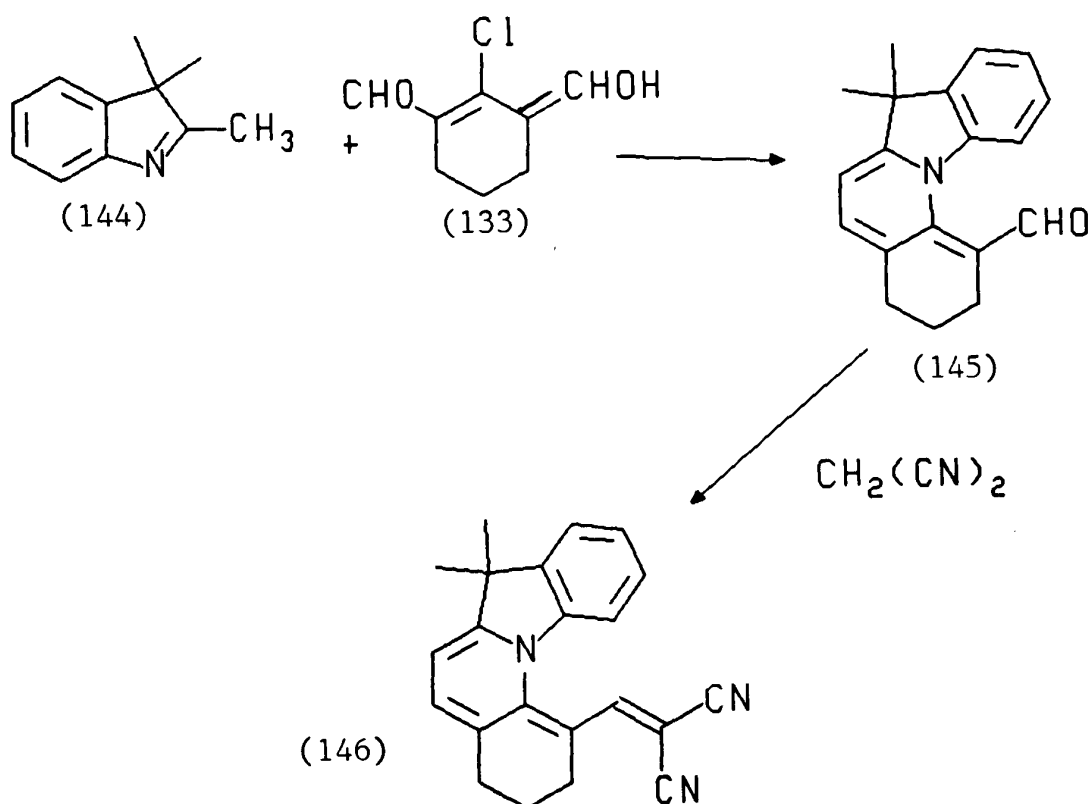
Scheme 27. Suggested route to extended methine dyes with intramolecularly cyclised donor groups

The resultant polycyclic aldehyde (145) could then undergo a Knoevenagel-type condensation reaction leading to donor-cyclised extended methine dyes. For example reaction of (145) with malononitrile would give dye (146).

Several methods were examined to bring about this reaction. Firstly 2,3,4-trimethyl-indolenine (144) and the dialdehyde (133) were stirred together for 3 hours under various conditions, and the selected solvent, catalyst and conditions are summarised in Table 25. Malononitrile was then added and the reaction mixture stirred for a further hour.

Table 25. Experimental conditions

Experiment	Solvent, catalyst, conditions	Observations
1	Ethanol, HCl at reflux	Unsuccessful (no colour)
2	Acetic anhydride, TEA, 100°C	" "
3	Acetic anhydride, p-tol-sulphonic acid, 100°C	Small amounts of blue and magenta products
4	Methanol, sodium methoxide, reflux	" " " " "

A larger scale attempt of experiment 3 gave a crude product, and column chromatography (silica, CH_2Cl_2) enabled isolation of the two most interesting components of the reaction mixture, in small quantity only. Component 1, was cyan in colour and mass spectrometry gave a molecular weight of 362 units, the spectrum also indicated the presence of a chlorine atom. This showed that the dye was uncyclised, and presumably had structure (147) and not the hoped-for cyclised dye (146).

(147)
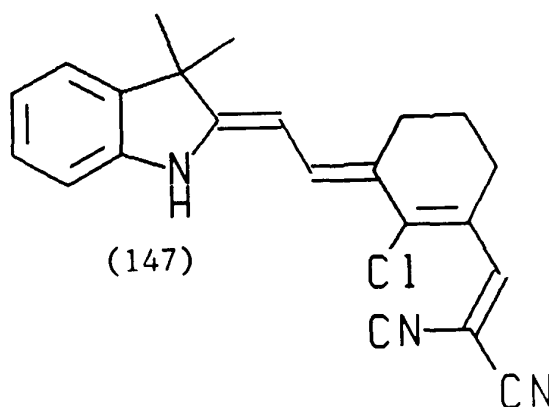
Component 2, was magenta in colour and had a molecular weight of 364, the spectrum also showing the presence of chlorine. This implies that structure (147) must in some way have reduced donor-acceptor character causing the hypsochromic shift in hue from cyan to magenta. This could have arisen by acetylation of the indolenine nitrogen. Such a structure might readily lose the CH_3CO group in the mass spectrometer, leading to m/e 364 (after picking up H atoms).

2.6.3 Light absorption and emission properties of dyes (143)

Visible absorption spectra of the dyes (143) were recorded in dichloromethane only as most dyes were insoluble in toluene, and the results are summarised in Table 26.

Table 26. Light absorption properties of dyes (143)

Dye	$\lambda_{max}^{CH_2Cl_2}$ /nm	$\Delta\lambda_{1/2}$ /nm	ε_{max} /l mol^{-1}cm^{-1}
142	544	109	30,800
143(a)	662	53	118,600
143(b)	703	38	119,100
143(d)	703	40	124,200
143(e)	731	85.5	117,500
143(c)	630,685	132(1)	64,900
143(f)	616,668	120(1)	-
143(g)	627,678	129(1)	-

Although one would expect the increased molecular rigidity in dye (142) relative to its open chain analogue dye (137d), to sharpen the absorption band and thus lead to a high absorption coefficint, in fact the cyclised dye (142) had a broader absorption band (Figure 25).
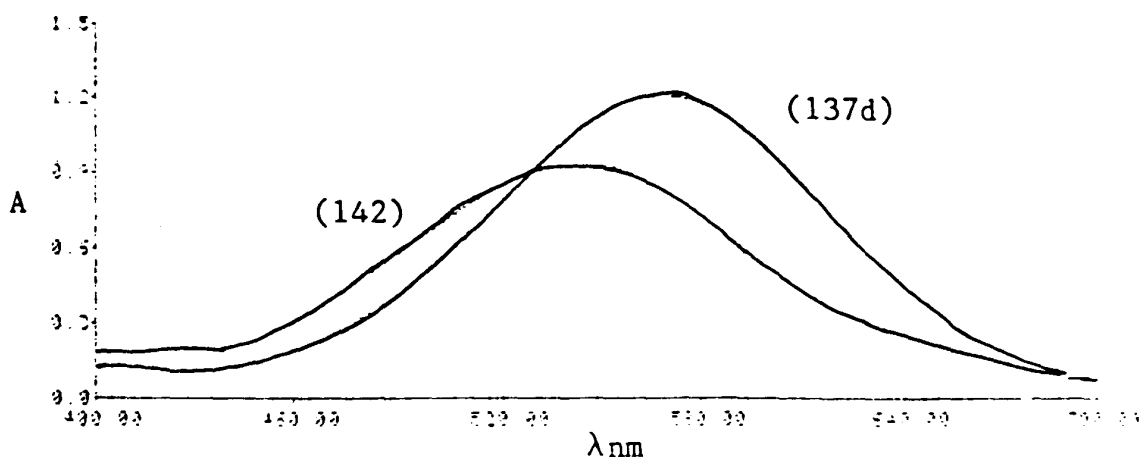
Figure 25. Comparison of the visible absorption spectra of dyes (137d) and (142)

As with the rigidised coumarin dye (117), the extinction coefficient of dye (142) has been reduced. A similar hypsochromic shift is observed on moving from the uncyclised to cyclised dye. Halochromic properties of dye (142) are less dramatic compared to its uncyclised analogue (137d), and on addition of acid to a solution of dye (142) in acetone a bathochromic shift of ~80nm is observed (λ_{max} 544nm -> λ_{max} 624nm). It is notable that dyes (143a), (143b), (143d), and (143e) have small half-bandwidths and high extinction coefficients (cf Figure 26(a)). On addition of acid to solutions of (143a), (143b), and (143d), the absorption spectra are observed to shift hypsochromically leading to broad absorption bands with two shoulders (Figure 26(b)). (The shape and intensity of the spectrum of protonated (143b) is remarkably similar to its close relative, cationic dye (143c), (Figure 26(c)).)
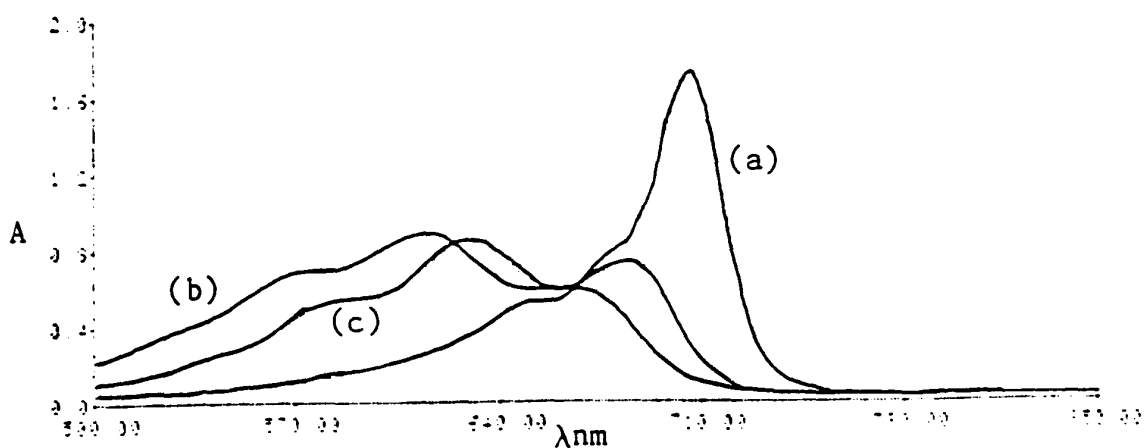
Figure 26. Visible absorption spectra of dyes (143b) and (143c)

The protonation process is fully reversible, and the original spectrum is formed on neutralisation. In contrast addition of sodium carbonate to solutions of cationic dyes (143c), (143f), and (143g) in methylene chloride does not alter their spectra, confirming the N-alkylated cationic nature of these dyes. The absorption bands of cationic dyes (143c), (143f), and (143g) are similar in shape to those of the unsymmetrical cyanine dyes described by Koraiem and co-workers [96] (Figure 27).
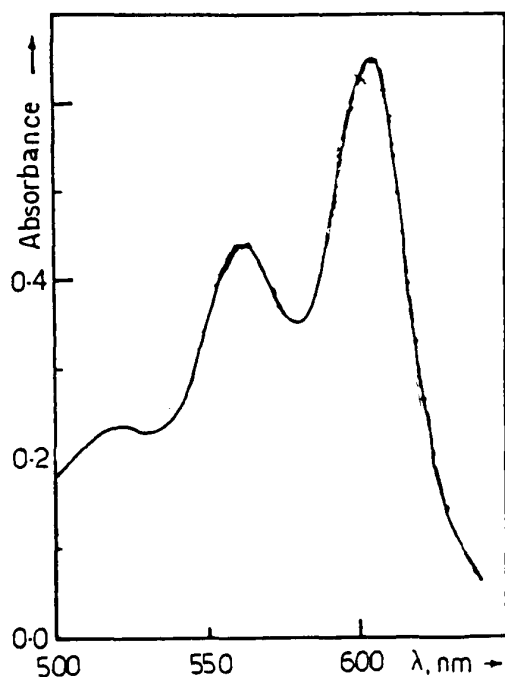
Figure 27. Visible absorption spectrum of unsymmetrical dye (148)
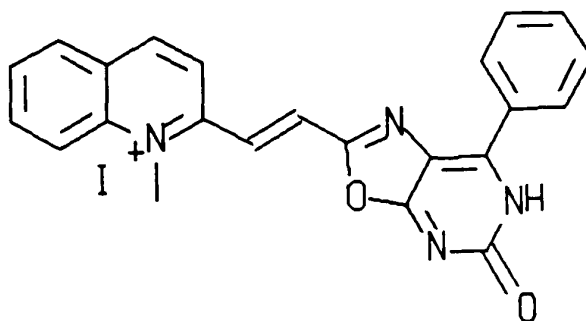
(148)

Comparison of the fluorescence properties of neutral dyes (143a), (143b), and (143d), and cationic dyes (143c), (143(f) and (143g) (Table 27), reveals that the neutral dyes are significantly more fluorescent than the cationic dyes.

Table 27. Fluorescence properties of dyes (143)

Dye	Excitation λ_{max}/nm	Emission λ_{max}/nm	Stoke's shift/nm	A/C at 5×10^{-6} mol l^{-1}
143(a)	660	690	30	0.4
143(b)	709	739	30	0.5
143(c)	715	774	59	76
143(d)	705	732	28	3
143(f)	715	779	64	148

It is notable that the Stoke's shift in neutral dyes (143a), (143b), and (143d) is typically only 30nm, where as cationic dyes (143c) and (143f) exhibit a Stoke's shift of ~60nm. This is consistent with Pestemer's rule, which relates Stoke's shift to band width.

2.6.4 Photostability properties of dyes (143)

Dye-containing cellulose acetate films were prepared in the usual way and then subjected to 1 hour exposure in a Microscal photofadometer. The optical density decrease was measured and the results are summarised in Table 28.

Table 28.   Lightfastness properties of dyes (142) and (143)

Dye	% Degradation
azo standard (105)	0
142	44
143(a)	51
143(c)	52
143(d)	41
143(e)	57
IR140	100
HITCI	82

Again it is notable that the lightfastness properties of dyes (142) and (143) are extremely poor. Comparison with the results obtained for uncyclised analogues (137), shows that rather suprisingly the greater rigidity in the present series offers no improvement in lightfastness properties. Although photostability properties are poor, nevertheless the chromophores show an improvement over commercial infrared dyes used as laser dyes or for RSA studies. Thus IR140 and HITCI degrade at almost twice the rate of the cyclised dyes (Table 28).

2.7   SYNTHESIS AND EVALUATION OF SELECTED CHROMOPHORES FOR RSA APPLICATION

2.7.1   Introduction

Because of our lack of success in attempting to synthesise an unsymmetrical donor-acceptor polymethine dye exhibiting RSA properties, at 532nm, the light absorption properties of a series of symmetrical polymethine dyes, selected from the cyanine, squarylium and holopolar dye classes, were examined. It was felt that these more

closely resembled IR140 structurally than the donor-acceptor systems, and might therefore exhibit similar RSA properties to IR140.

2.7.2 Synthesis of dyes

2.7.2.1 Synthesis of cyanine dyes

Dye (149) was selected for synthesis, as this most closely resembles IR140. Synthesis involved the condensation of 2-chloro-1-formyl-3-hydroxymethylene-cyclohexene (133) with two equivalents of Fischer's base, using acetic anhydride as solvent [97].

(149)

The dye was isolated by dissolving in water and then salting out with perchloric acid. It formed metallic green crystals, and showed λ_{max} 782nm in dichloromethane. Another symmetrical cationic dye related to (149) is (151), which involved the condensation of 2-chloro-1-formyl-3-hydroxymethylene-cyclohexene (133) with 3,7a-diazaindan-2-one hydrochloride (150) in N-methylpyrrolidone.

(150)

(151)

The dye was isolated by dissolving in water and then salting out with perchloric acid. Problems were encountered in the microanalytical characterisation of dye (151). After repeated recrystallisation from ethanol, C, H, and N values were consistantly high. One recalls that previous syntheses using 3,7a-diazaindan-2-one hydrochloride resulted in the formation of the cyclic structure (143e) by facile intramolecular cyclisation. In theory a similar intramolecular cyclisation reaction involving the nucleophilic displacement of the central chlorine atom in dye (151) could result, leading to the polycyclic dye structure (152).

(152)
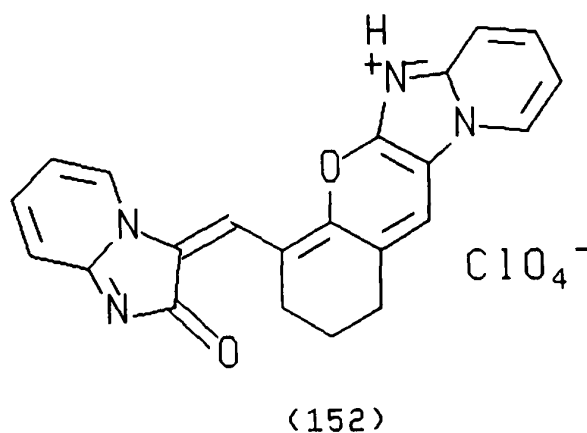
$$\lambda_{max}^{H_2O} = 657nm$$

The microanalysis figures were in fact correct for this structure, as the perchlorate salt. The shorter wavelength of absorption compared to (149) also suggests cyclisation has occurred.

2.7.2.2 Synthesis of Holopolar dyes [98][99]

Holopolar chromophores characteristically exist in a charge-separated zwitterionic form. Holopolar dyes (153) and (154) contain the same polymethine chains as (149)

and (151) respectively, but differ in that they have a central barbiturate anion group, which gives the dyes overal electrical neutrality.

(153)

$$\lambda_{max}^{EtOH} = 774nm$$

(154)
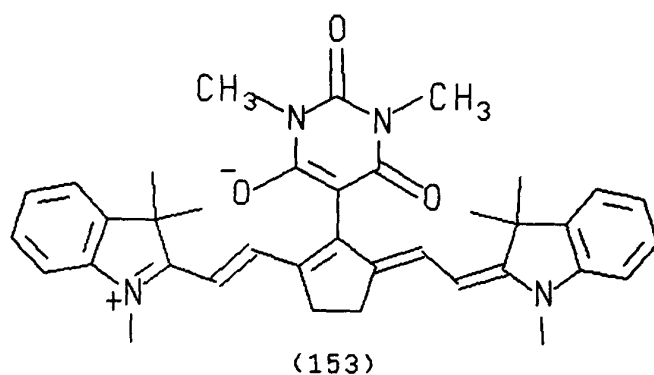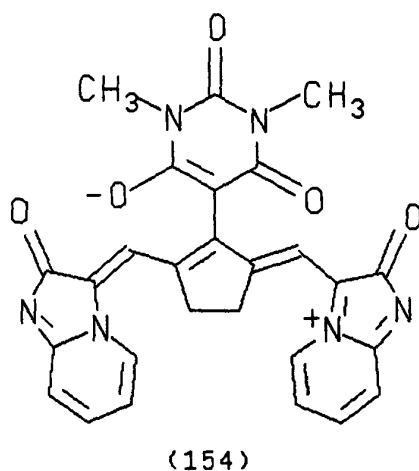
$$\lambda_{max}^{H_2O} = 760nm$$

The dyes were synthesised by the route shown in Scheme 28.

The condensation of cyclopentanone and dimethylbarbituric acid gave the N,N-dimethylcyclopentylidenylbarbituric acid (155). Reaction of this with two mole equivalents of N-ethylphenylformimidate gave the bis-anil (156). This could then be condensed with two mole equivalents of a suitable active methylene compound in DMF at 100°C with the loss of aniline to give the holopolar dye. In this way dyes (153) and (154) were prepared in yields of 40% and 76% respectively.
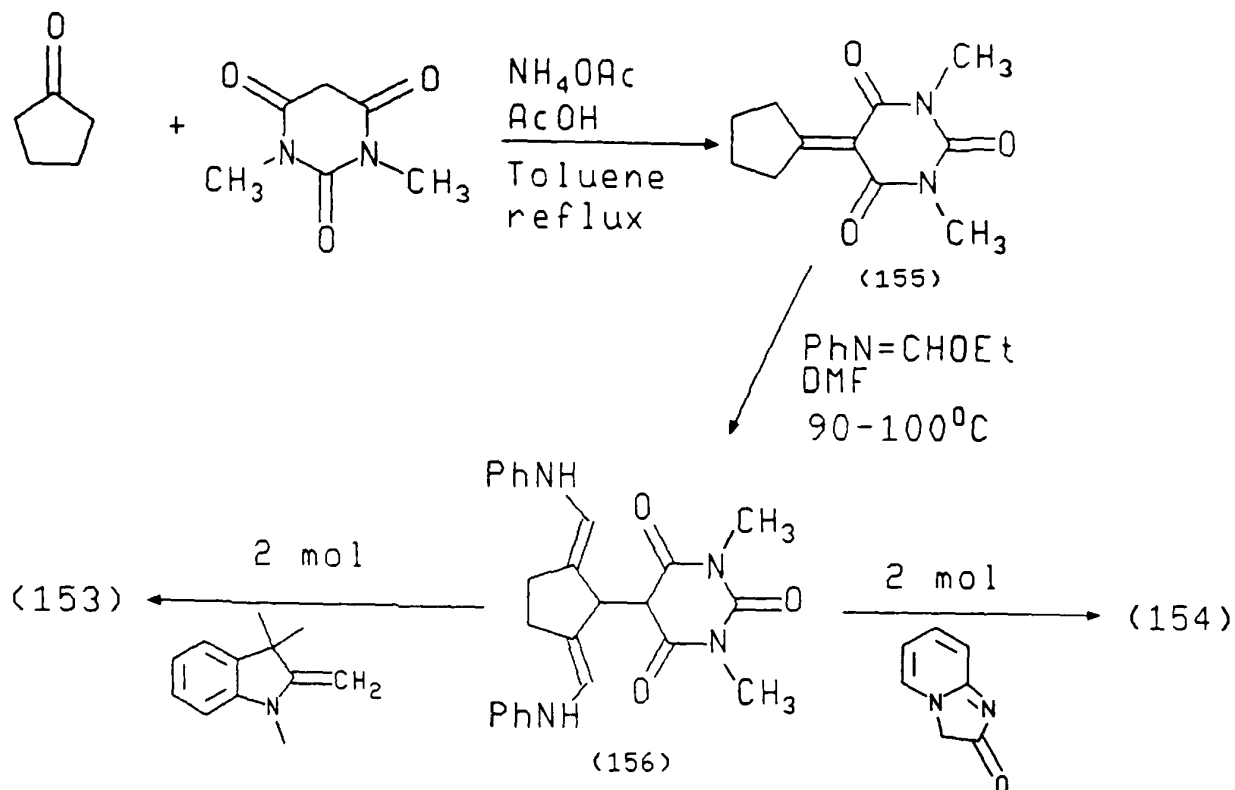
Scheme 28. Synthetic route to holopolar dyes (153) and (154)

2.7.2.3 Synthesis of near-infrared squarylium dyes [59][100]

Squarylium dyes with the desired absorption maxima near 800nm have been described by Bello and Griffiths [100] and have the general formula (160). Unfortunately they tend to have low solubility in organic solvents and in polymeric media. This was a major problem for RSA testing, as the measurements are carried out in polymeric film or in methanol solution. Thus it was necessary to synthesise a squarylium dye of this type with improved solubility properties. Dye (160) was selected for study as it has been reported by Corns [59] to have excellent solubility properties in non-polar solvents. The dye (160) was synthesised by the route shown in Scheme 29.

Purified 1,8-diaminonaphthalene (157), 4-acetylbiphenyl (158) and p toluene sulphonic acid were stirred in ethanol at 55°C for 4 hours. On cooling to room temperature the beige coloured dihydroperimidine (159) separated out. This was filtered off, washed
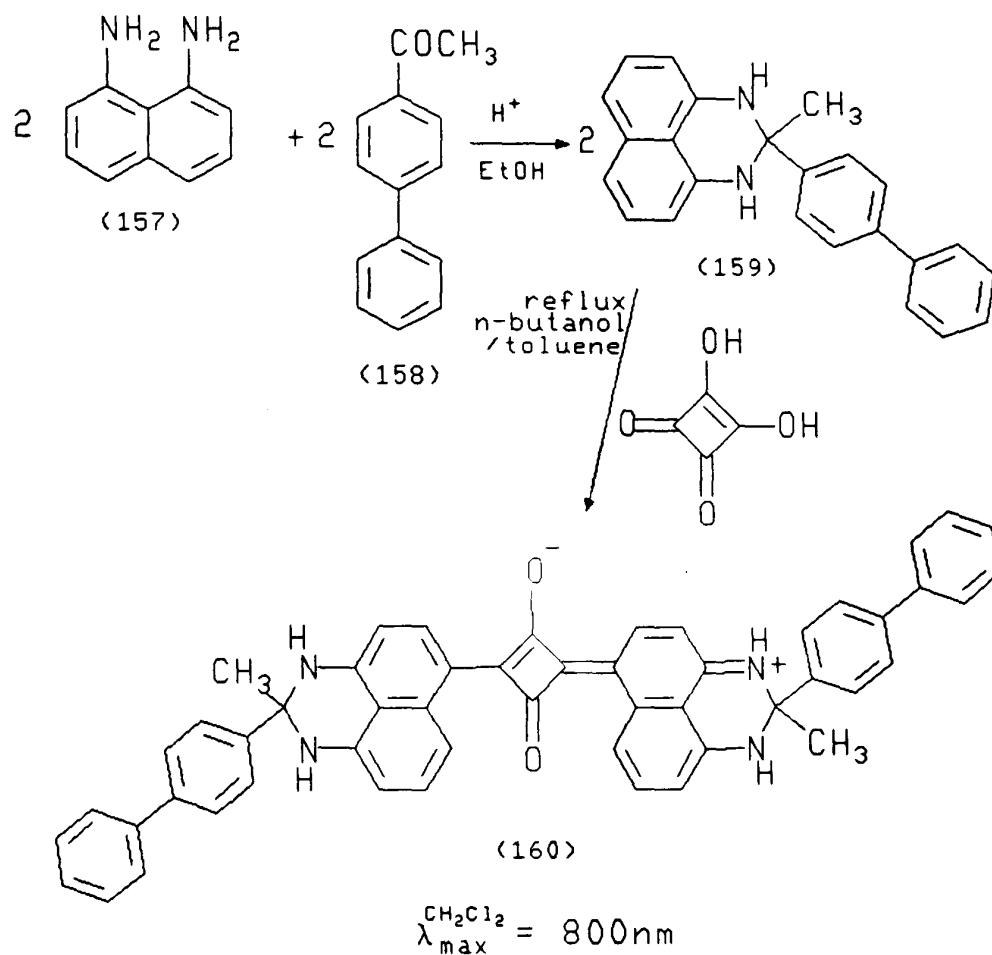
Scheme 29. Synthetic route to squarylium dye (160)

with water and dried. Two mole equivalents of the dihydroperimidine and one mole equivalent of squaric acid were stirred in a butanol/toluene mixture at reflux, for 4 hours using a Dean and Stark trap to remove water from the condensation reaction. The toluene was then removed and the alcoholic mixture was left stirring at 40°C overnight. On cooling in ice the product separated out as a dark green solid. This was filtered off, washed with ethanol and dried.

Suprisingly the synthesised dye (160) showed sparing solubility in most organic solvents in contrast to the observations of Corns [59] but did dissolve in dimethylformamide. This low solubility was believed to be due to the formation of the dye in a highly crystalline form, induced by stirring the dye solution with heating overnight.

Electron micrographs (Figure 28) of the insoluble squarylium dye reveal that the dye is indeed in a highly crystalline form.

Figure 28. Electron micrographs of insoluble squarylium dye (160)
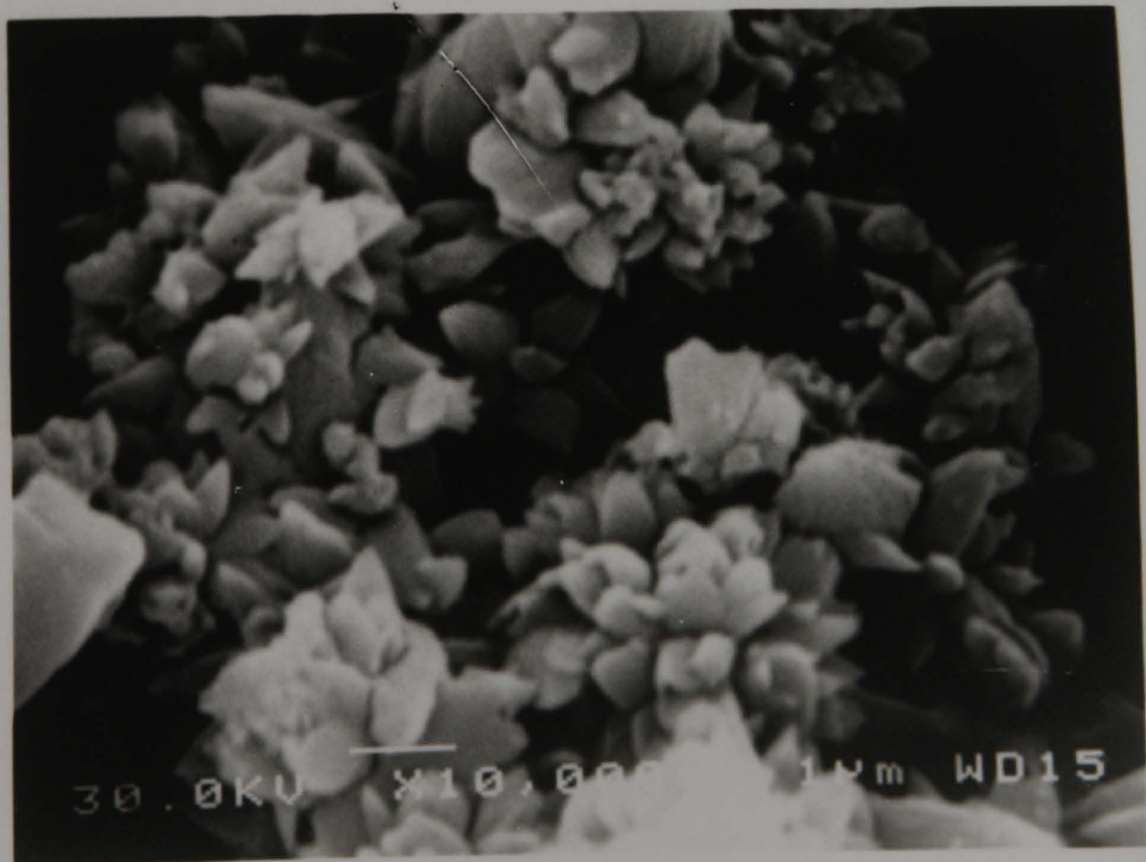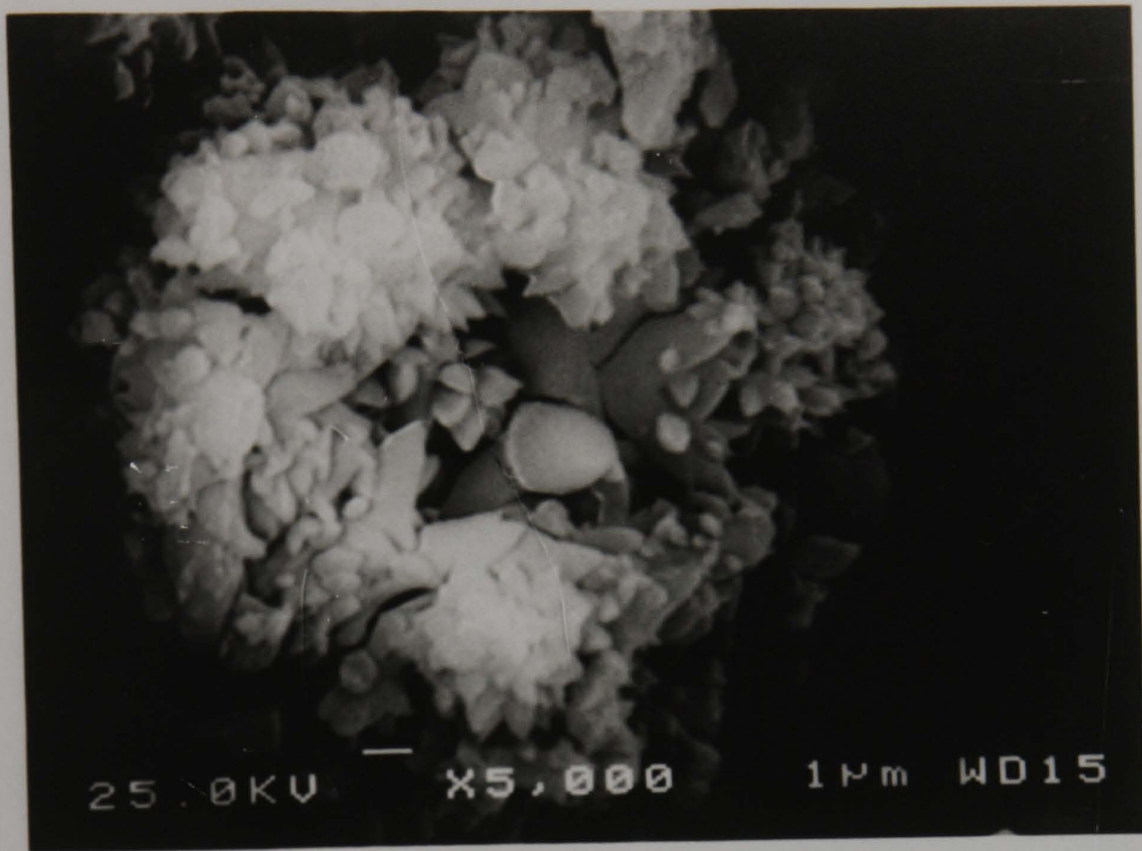
The experiment was repeated by refluxing for one hour only in butanol/toluene and then working up. However, this too gave a sample of the infrared dye in a highly insoluble crystalline form.

The decreased solubility of the dye with prolonged reaction times was noted with other squarylium dyes of this type. It seems likely that the initially formed dye is a mixture of the cis and trans forms (a) and (b).

CIS
(a)

TRANS
(b)
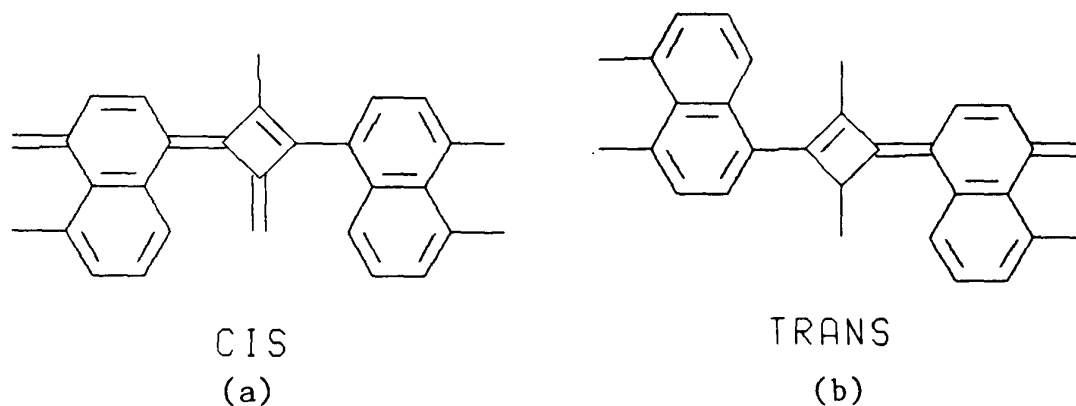
(This is further complicated if the two substituents in the 2-position of the dihydroperimidine ring system are different, as like groups can lie on the same side of the molecular plane or on opposite sides.) The mixture will remain in solution, and if isolated by chromatography and evaporated, will give a soluble amorphous product. However, if the reaction solution is heated for a sufficient length of time, conversion to one isomer (probably (b)) will occur, favoured by good crystal packing and deposition of crystals even from the hot solution. The resultant highly crystalline dye will then show poor solubility in organic solvents.

It was anticipated that the introduction of a butyl ester group into the dihydroperimidine residue would produce a squarylium dye with improved solubility properties. Thus the synthesis of dye (162) was examined (Scheme 30).
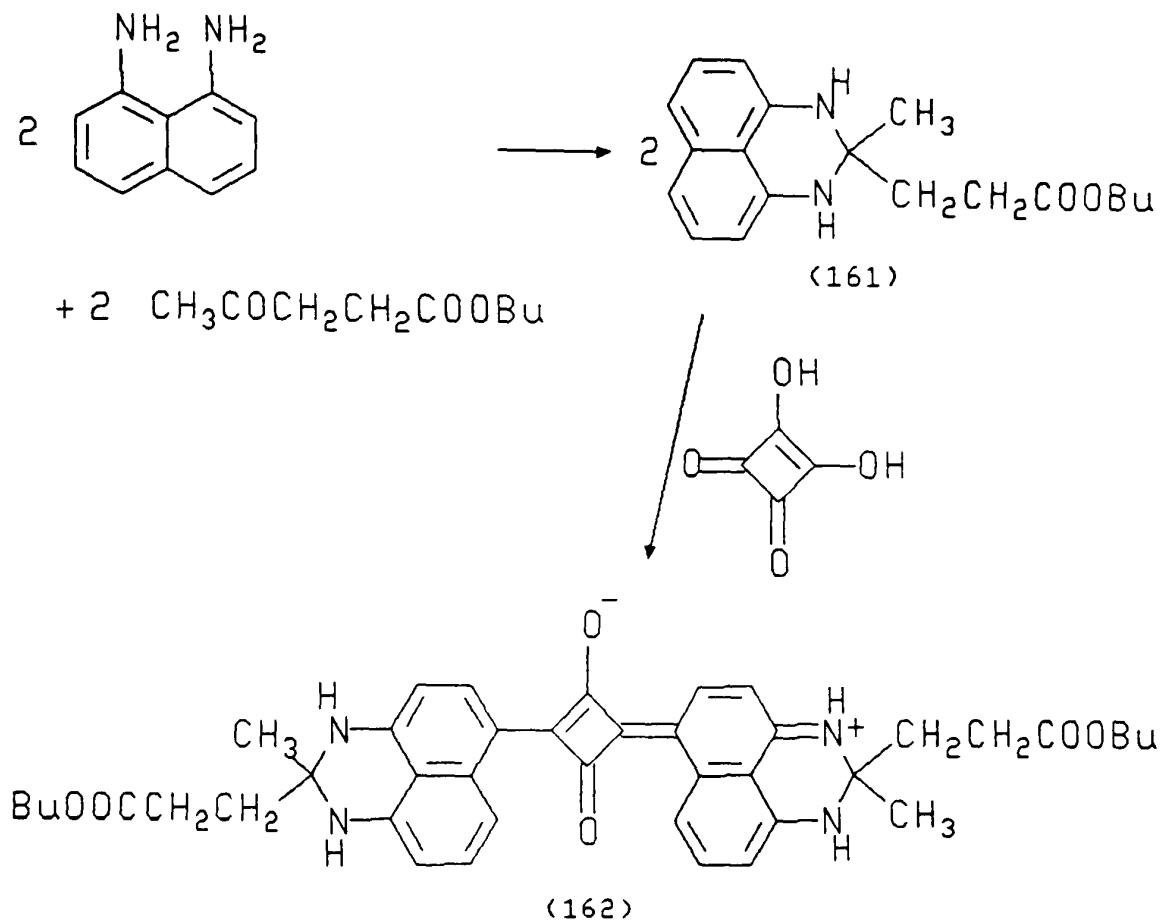
Scheme 30. Synthesis of squarylium dye (162)

In this preparation 1,8-diaminonaphthalene was condensed with butyl levulinate and the resultant dihydroperimidine (161) was condensed with squaric acid to form squarylium dye (162). The electronic spectrum of the product in acetone showed three absorption peaks in the range 700-800nm, rather than the expected single peak at 800nm. Thin layer chromatography (eluent 25% acetone in ethyl acetate) showed the product to be very impure, consisting of seven major bands (Figure 29(a)). Column chromatography was carried out in order to isolate the squarylium dye. Initially an eluent of ethyl acetate was used, and the polarity gradually increased from 5 to 50% acetone to remove the strongly absorbed bands (Figure 29(b)).
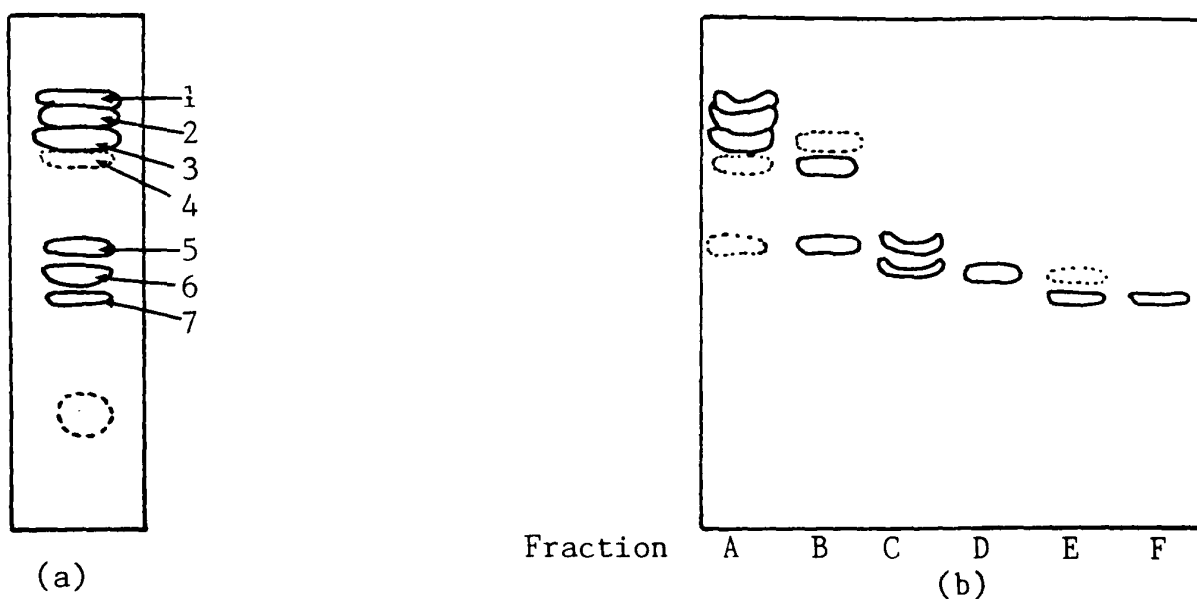
Figure 29. T.l.c results for the reaction mixture from the attempted preparation of squarylium dye (162). Silica gel, (a) 25% acetone, 75% ethyl acetate, (b) fractions from column chromatographic separation.

Conditions of elution, colour and wavelength of the components isolated are summarised in Table 29.

Table 29. Spectral properties of isolated fractions from the reaction mixture from the attempted preparation of squarylium dye (162)

Fraction	Eluent	Components	Colour/λ_{max}	
A	Ethyl acetate	1	Yellow/orange	790nm
		2	Pale blue	
		3	Lime green	
		4	Pale green/brown	
		5	Blue	
B	Ethyl acetate	3		790nm
		4		
		5		
C	5% acetone	5		790nm
	in ethyl acetate	6	Cyan/green	754nm
D	15% acetone	6		754nm
	in ethyl acetate			
E	25% acetone	6		754nm
	in ethyl acetate	7	Bright cyan	710nm
F	50% acetone	7		710nm
	in ethyl acetate			

From this analysis it can be seen that the required squarylium dye has a λ_{max} = 790nm in ethyl acetate and is contained largely in fractions A & B.

The formation of dyes whose λ_{max} is shorter than 800nm can be attributed to the cyclisation reaction of the ester group. This phenomena has been described by Corns (Scheme 31).
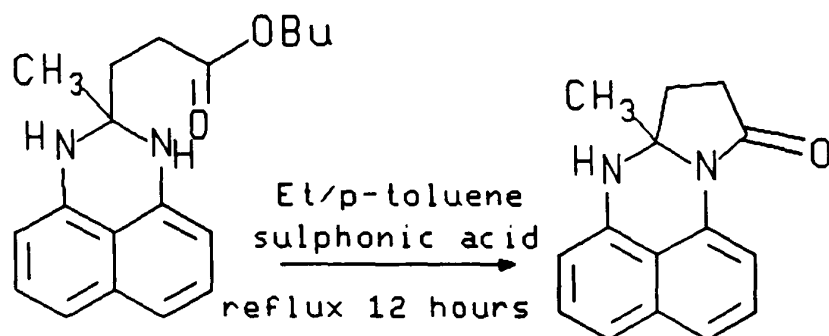
Scheme 31. Cyclisation of the terminal ester group [59]

He has shown that the azo dye (164) absorbs about 60nm to shorter wavelengths than the uncyclised analogue (163). He attributes this observation to the -M effect of the carbonyl group bonded to the dihydroperimidine nitrogen significantly reducing the electron donating capacity of the dihydroperimidine residue, which in turn shifts the lambda max to shorter wavelengths.

(163)

(164)
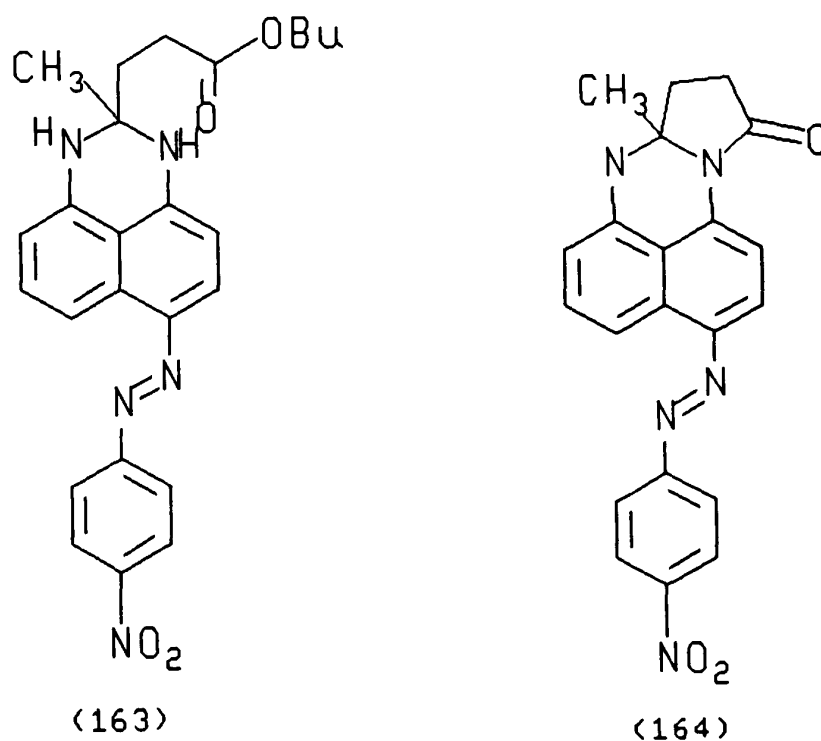
Because of the possibility of cyclisation at both sides of the squarylium dye two additional dyes could in theory be formed, one with a lactone type group on one side only and the other with lactone groups on both sides of the molecule and thus absorbing to even shorter wavelengths than the former dye. This could explain the triple peaked absorption spectrum initially reported.

Due to the inefficient formation of the desired dye (162) in this reaction an alternative route to a suitable soluble squarylium dye was sought.

As noted previously insolubility is believed to be due to efficient packing of the squarylium dye leading to a high degree of crystallinity, caused by formation formation of one particular regioisomer of the dye. Prevention of crystallisation could possibly be achieved by making several structurally modified squarylium dyes in a "one pot" reaction so preventing efficient crystal packing To test this a mixture of dihydroperimidines (165a-d) was reacted with squaric acid to form a mixed squarylium dye system.

(165a)

(165b)

(165c)

(165d)
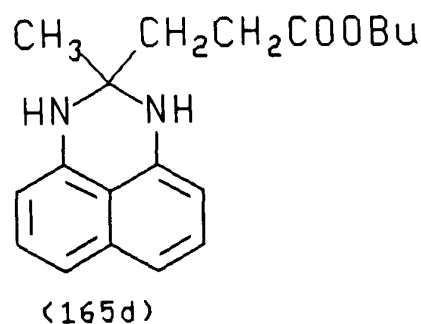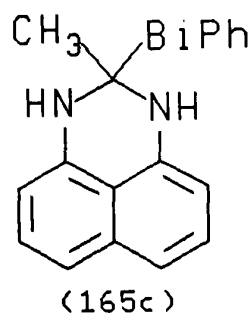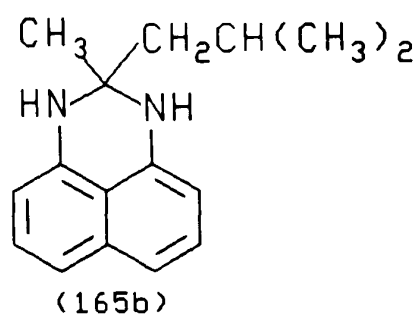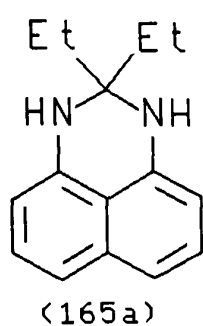
Isolation of the composite infrared dye was affected by column chromatography (stationary phase; silica, eluent; methylene chloride). The fast moving band containing the infrared dye-mixture was collected and concentrated, but was not evaporated to dryness. As expected, this gave a highly soluble mixed dye system with an absorption peak at 800nm. The squarylium dye solution was used directly to colour the polymer films.

2.7.3 Evaluation of RSA effect

Various dyes synthesised in this program were evaluated for RSA properties in the laboratories of the Defence Research Agency, D.R.A., Fort Halstead. Testing was carried out with methanolic solutions of the dyes, or in some cases with clear cellulose acetate films containing the dissolved dye, using 532nm pulsed laser radiation.

Unsymmetrical extended donor-acceptor chromophores (137) and (143) typically showed no RSA effect at 532nm, and in Figure 30, the results obtained for the RSA-inactive neutral dye (137a) and the RSA-active symmetrical cyanine dye (149) are compared.
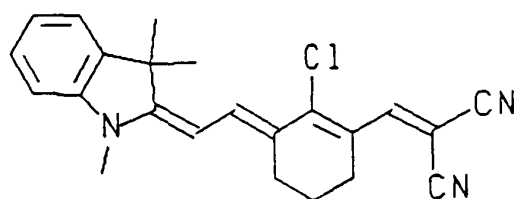
neutral dye (137a)

$\lambda_{max}^{CH_2Cl_2} = 623nm$
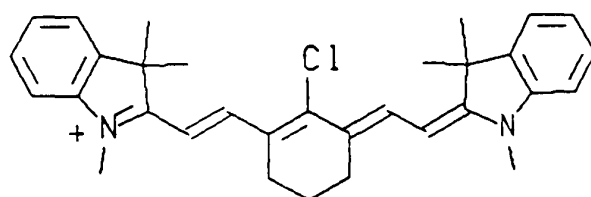
cationic dye (149)

$\lambda_{max}^{CH_2Cl_2} = 782nm$
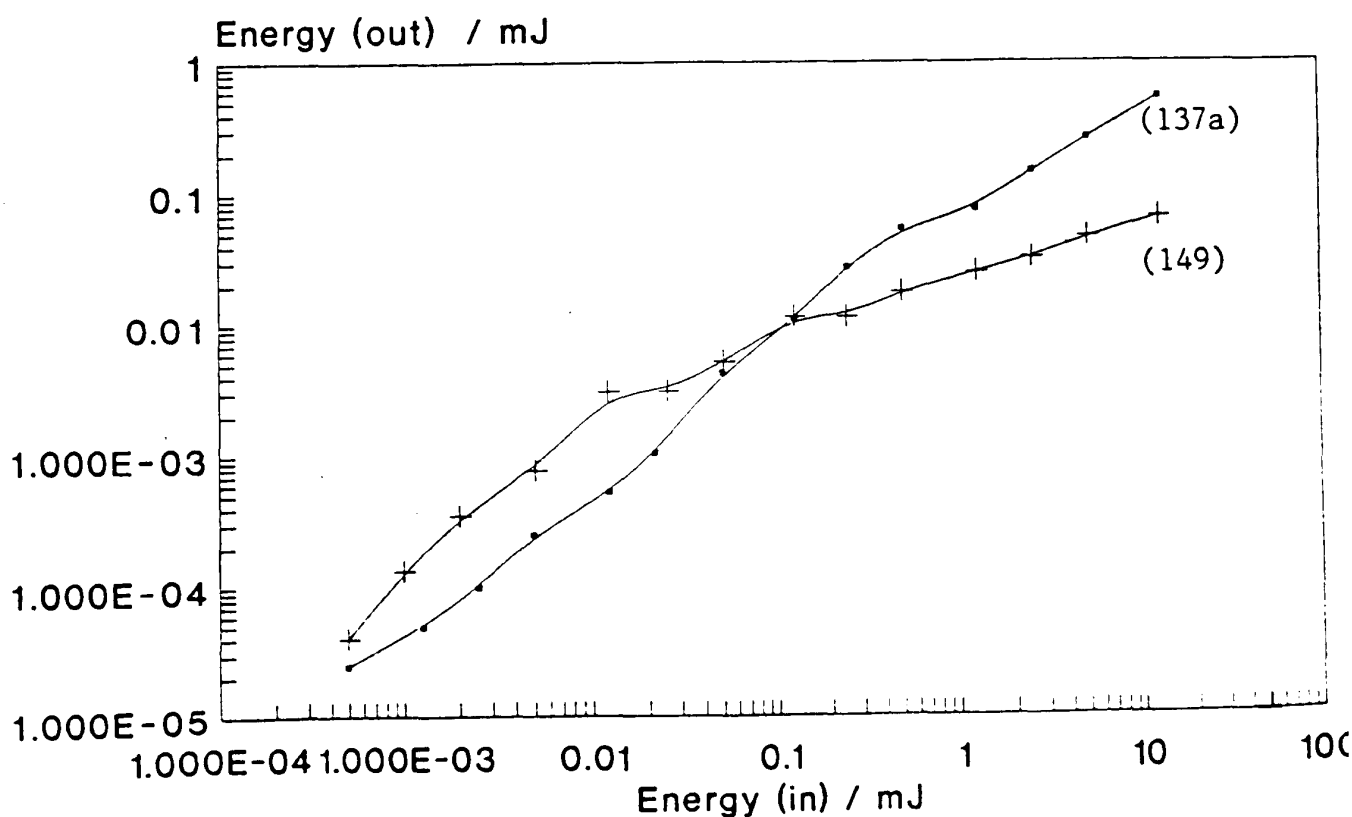
Figure 30.   Results from RSA testing in methanol (laser wavelength = 532nm) of dyes (137a) and (149)

Thus using 532nm radiation (at which wavelength neither dye shows any significant absorption), dye (137a) shows a linear relationship between input and transmitted laser energy, whereas with dye (149) the transmitted energy deviates from the linear relationship at high energy.

Other symmetrical dyes that were tested for RSA properties were the croconium dye (166), squarylium dye (160), cyanine dye (16) (HITCI), cyanine dye (149), holopolar dye (153) and (9) (IR140), and the results are summarised in Figures 31-34.

(166)
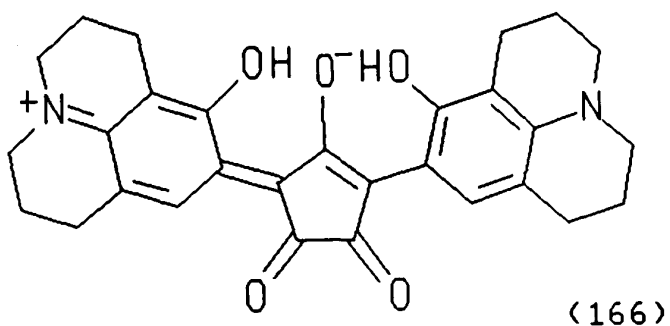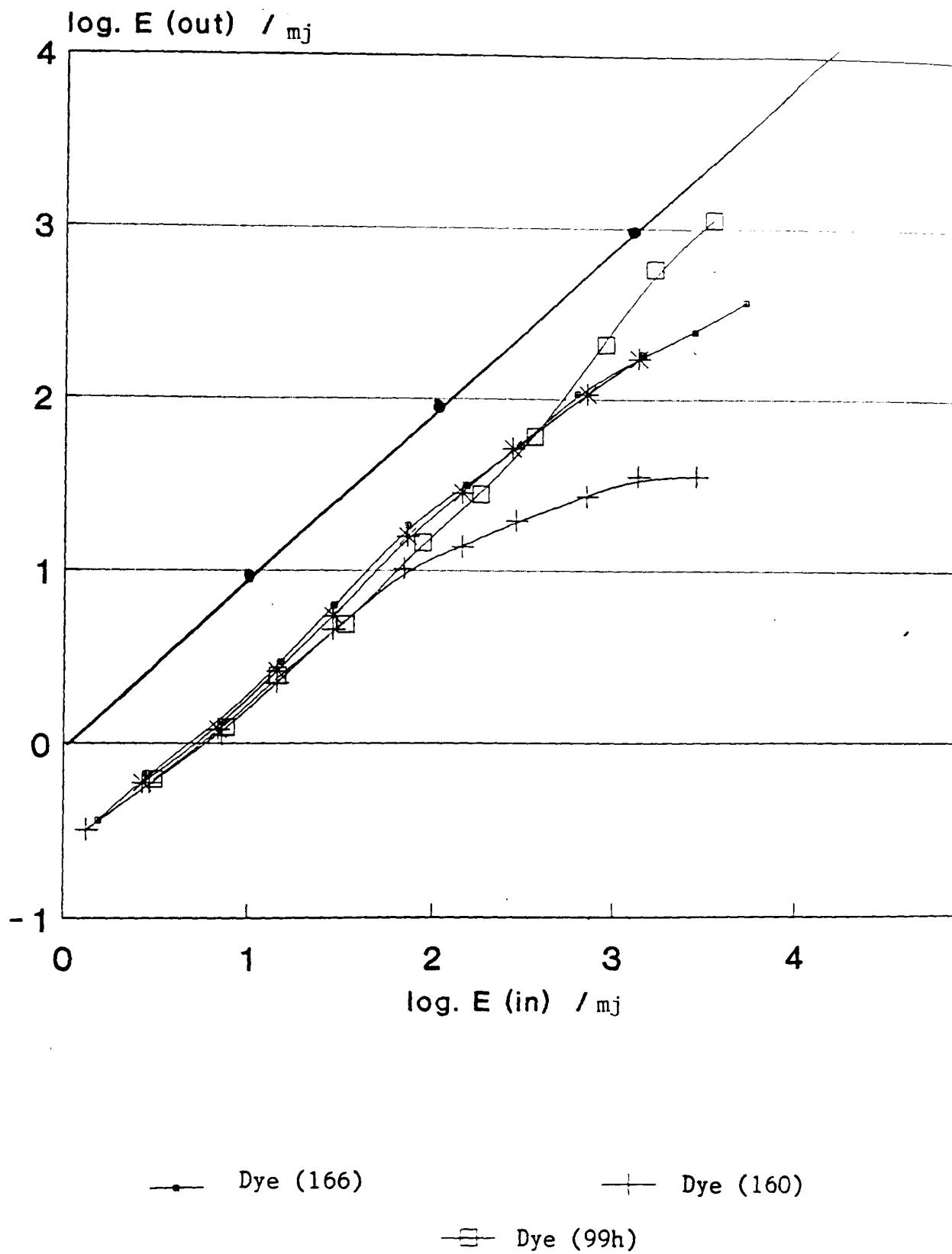
Figure 31. Results from RSA testing in methanol (laser wavelength = 532nm) of dyes (99h), (160) and (166)
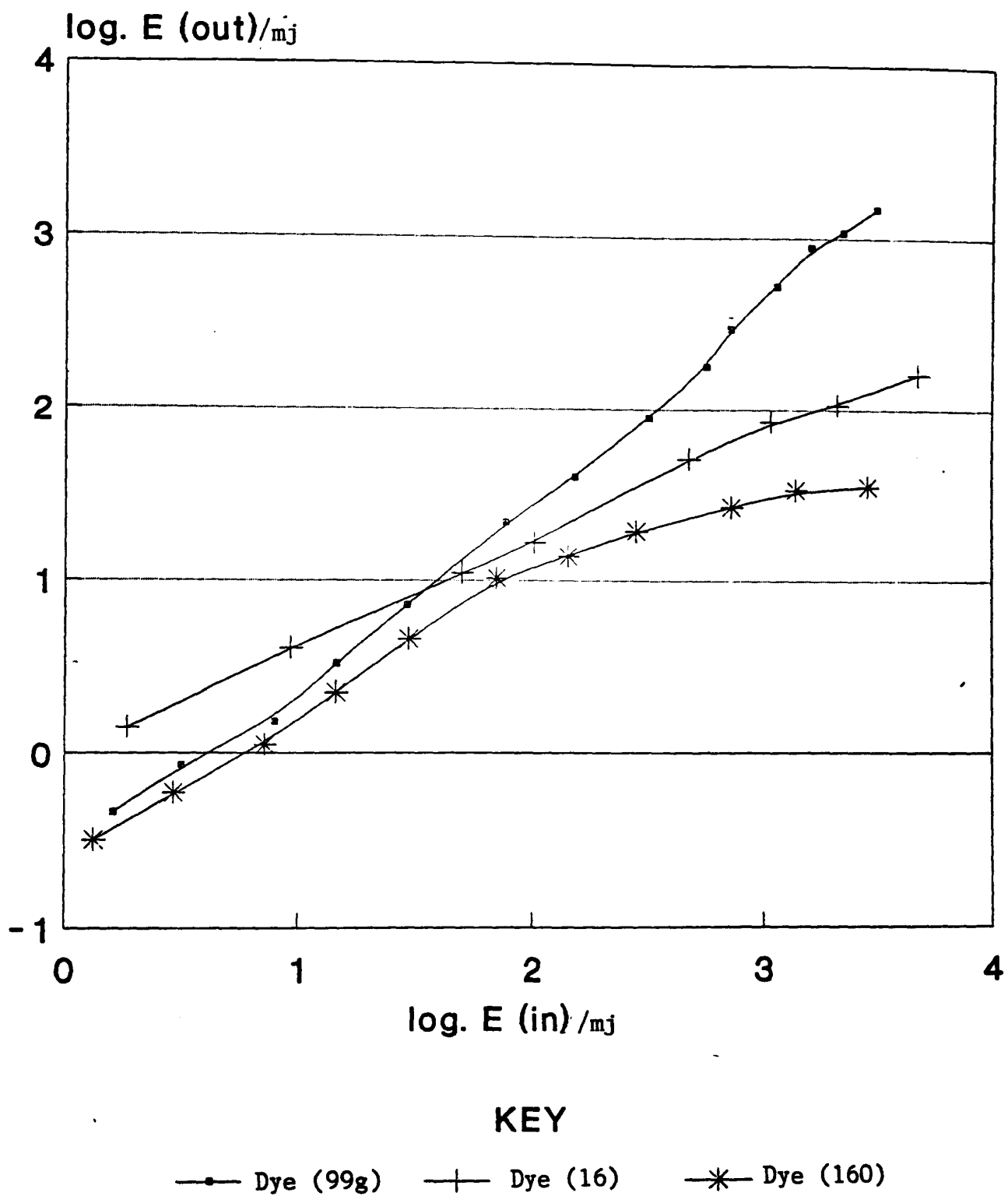
Figure 32. Results from RSA testing in methanol (laser wavelength = 532nm) of dyes (99g), (16) and (160)

Figure 33. Results from RSA testing in methanol (laser wavelength = 532nm) of dyes (160), (9) and (153)

RSA OF DYES IN METHANOL AT 532nm
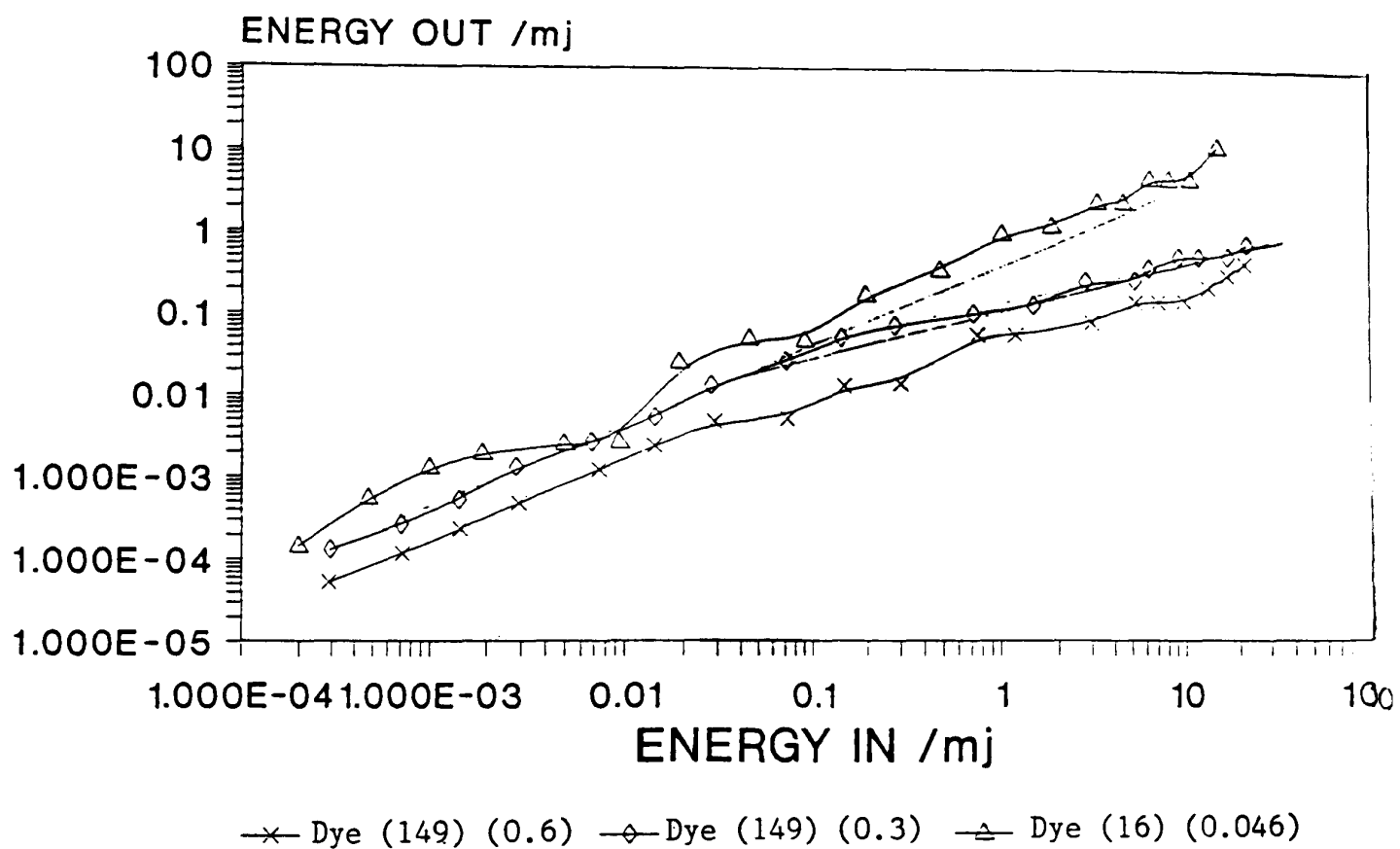
Figure 34. Results from RSA testing in methanol (laser wavelength = 532nm) of dyes (149) and (16)

As can be seen, some dyes show an RSA effect, and some show the reverse phenomenon of saturable absorption (SA). However in most cases, the dyes behave linearly and are inactive. To compare the relative effectiveness of dyes, some means of quantifying the response was required. Thus the following methods were adopted. Using the gradient plots, the point at which RSA/SA effect was first perceptible was noted, giving an approximate indication of the threshold energy required to cause the effect. In addition, the angle of divergence between the linear part of the curve and the average deviation was estimated. This gave an approximate measure of the degree of non-linearity shown by each dye. As examples, the squarylium dye (160) and the dye (99g) can be considered (Figure 35).
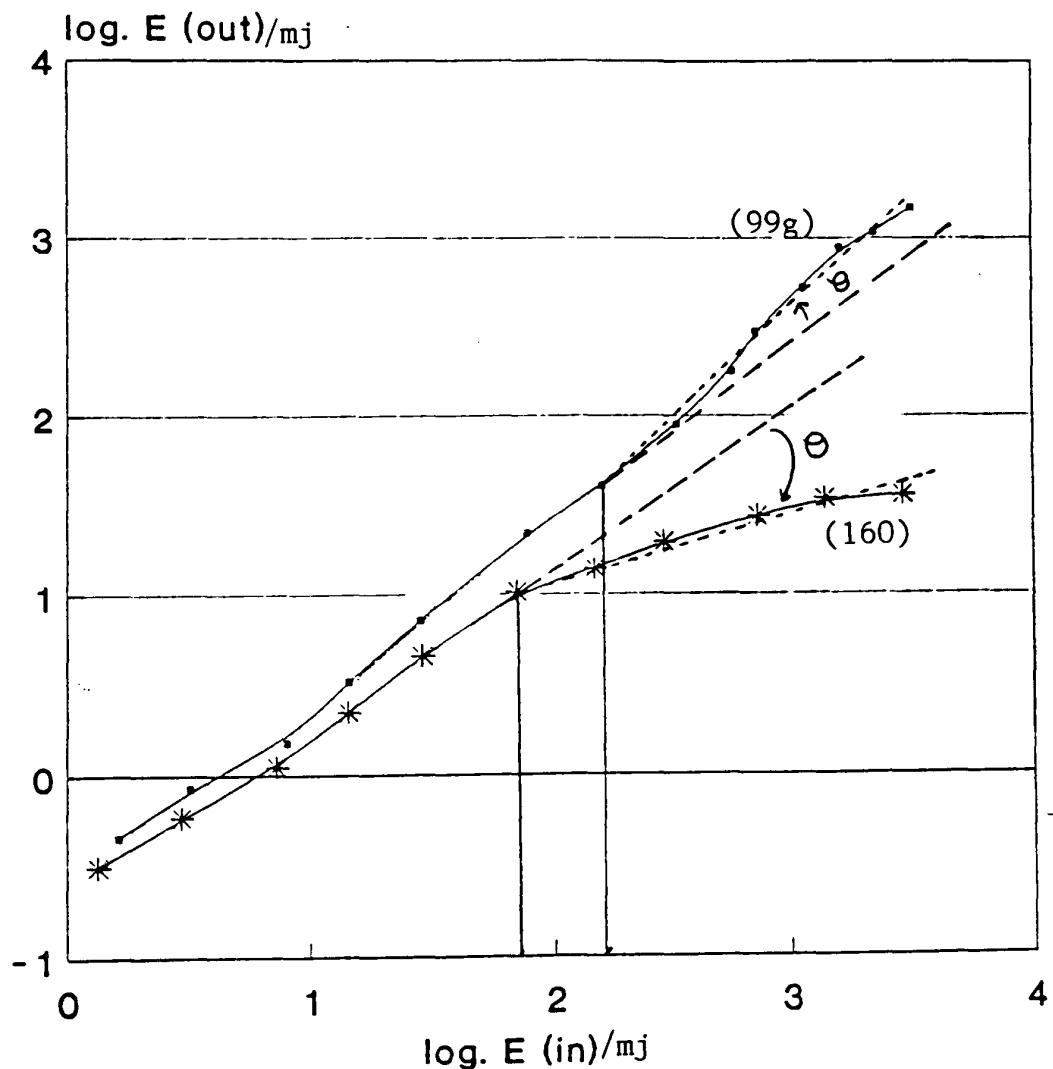
Figure 35. Absorption properties of dye (160) and (99g)

The point of divergence and angle of divergence estimated for these dyes were as follows:

Dye	Threshold for nonlinearity (log(energy))	Deviation angle σ
(160)	2.2	-17°
(99g)	1.89	+7°

Reverse saturable absorption shows a negative angle of deviation, and thus occurs with (160), whereas saturable absorption shows a positive angle of deviation, and is seen with dye (99g). Using this method of quantifying the nonlinear behaviour of a dye, the results for all those symmetrical dyes tested in methanol solution are summarised in Tables 30 (a) and (b).

Table 30. Results of RSA testing in methanol (laser wavelength 532nm).

(a) Dye	Figure	Threshold for non-linearity (energy input value) log(energy)	Deviation angle σ
160	31	1.68	-20°
166	31	2.86	-6°
99(h)	31	1.68	+9°
160	32	1.74	-17°
99(g)	32	1.20	+7°
16	32	slight RSA effect at end, gradient of slope different.	

(b) Dye	Figure	OD at 532nm	Threshold for non-linearity (energy.mJ)	Deviation angle θ
153	33	0.27	0.25mJ	-5°
153	33	0.8	0.03mJ	-6°
9	33	0.47	0.08mJ	-8°
160	33	0.37	0.25mJ	-14°
149	34	0.3	0.0029mJ	-9°
149	34	0.6	0.02mJ	-7°
16	34	0.046	no noticeable non-linearity	

Initial screening of the dyes (Figures 31 and 32), showed that the squarylium dye (160) exhibited the greatest degree of RSA so far observed. In contrast (166) and HITCI (16) had poor RSA properties.

It can be seen from θ values in Table 30 of dye (149) in solution that as the dye concentration (ie optical density) increases the RSA effect decreases. This observation was investigated in more detail with a study of the effect of dye concentration on the degree of RSA, using the dye chromophore HITCI (16). The results are shown in Figure 36. This again shows that at lower concentrations of dye the RSA effect is more pronounced. Another observation is that in general the RSA effect is greater in solution than in cellulose acetate films (Figure 37). This is particularly noticeable in the case of the squarylium dye. At an optical density of 0.37 in solution and film, θ in methanol is -14°, but in cellulose acetate is negligable. The squarylium dye was also tested in other polymer film systems, the results of which can be found in Appendix A. Structurally the squarylium dye is charge separated, and it was thought that this feature may contribute to the RSA effect. However this was not the case because (153) structurally a holopolar hybrid of HITCI (16) and (149) did not exhibit improved RSA properties, and if anything the degree of RSA was slightly reduced.

Figure 36.

RSA IN HITCI IN METHANOL AT 532nm

ENERGY OUT /mj

ENERGY IN /mj

— 10   + 20   △ 90   = 80
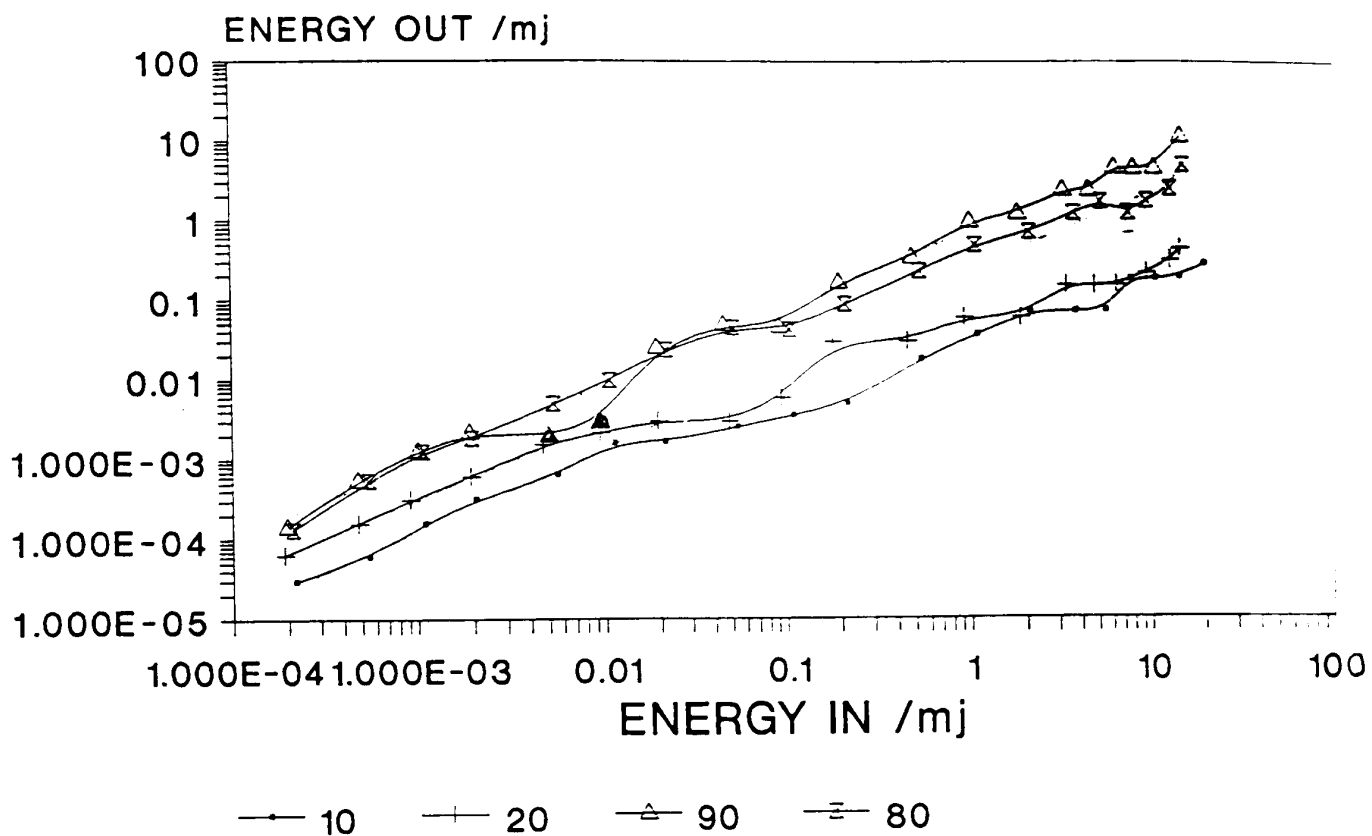
(% Transmission)

Figure 37.

RSA IN DYE FILMS AT 532nm

Output E/mj

Input E/mj

— Dye (153) (0.27)— Dye (153) (0.8)   — Dye (9) (0.47)

—□— Dye (160) (0.37)— Dye (149) (0.66)   — Dye (149) (0.3)
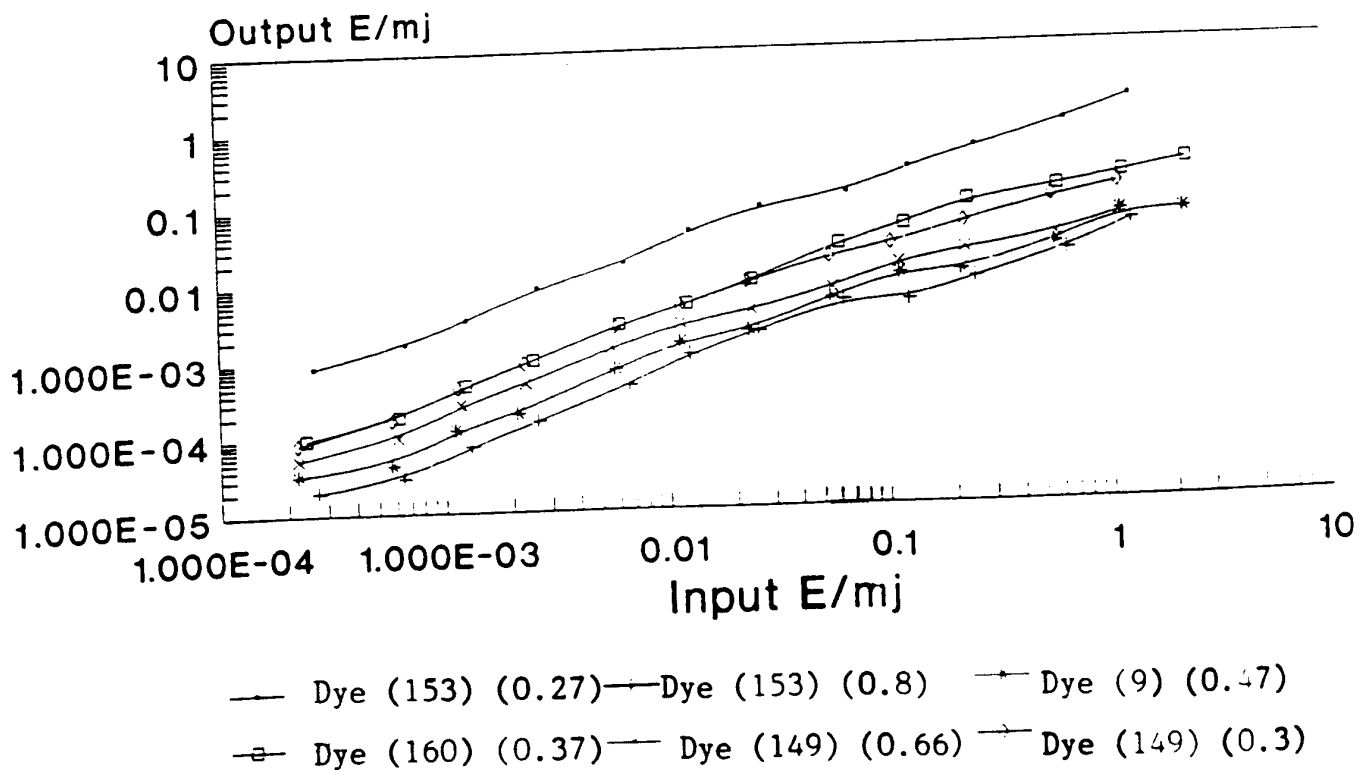
It had been hoped that by using a range of dye structural types, all closely or loosely related to the RSA-active IR140, an empirical relationship between structure and activity could be developed. However, no simple trends were seen, and thus a theoretical approach was sought, in order to explain, for example, why the squarylium dye (160) shows RSA, whereas others, such as the extended methines do not. Such an approach, if successful, might then be used for the design and development of new, more effective RSA dyes.

2.7.4   A possible approach to the theoretical qualitative prediction of reverse saturable properties of dye chromophores

2.7.4.1   Theory

The non-linear absorption effect in chromophores that leads to 'reverse saturable' behaviour may be handled theoretically by molecular orbital theory, at least in principle. It was part of this research programme to examine to what extent PPP-MO theory could be applied at least in a qualitative sense, to the prediction of reverse saturability.

Initial absorption of a photon of laser radiation causes excitation of an electron from the highest occupied molecular orbital (HOMO) to the lowest unoccupied orbital (LUMO), without reversal of electron spin, i.e. a singlet -> singlet allowed transition. Figure 38(a) -> 38(b).
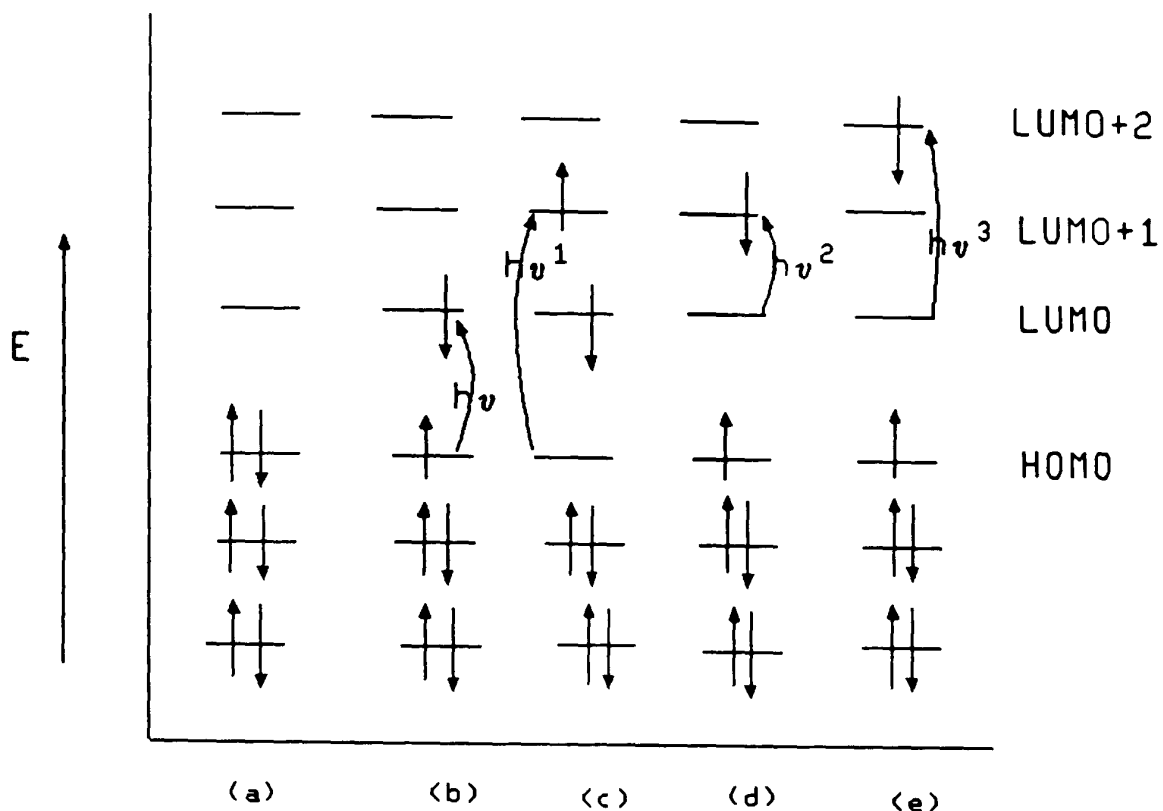
Figure 38. Light absorption processes

If the laser pulse is particularly intense, all molecules may arrive in the first singlet excited state, Figure 38(b), and if this state does not absorb at the laser wavelength, then the solution is effectively bleached, i.e. saturable absorption is observed.

However if the excited state Figure 38(b) has its own absorption spectrum which is particularly intense at the laser wavelength (preferably much more intense than even the ground state itself), then further intensified absorption of the laser radiation can occur, leading to 'reverse saturable absorption', i.e. the solution becomes even more opaque to the laser beam, (a "shutter" effect).

To predict by MO theory if excited state 38(b) has intense absorption bands at the laser wavelength would require an MO calculation specifically for the open shell system 38(b). Such calculations are not routinely available for complex dye molecules, and the PPP MO method cannot handle open-shell systems. Thus some approximation approach is required.

The PPP method applied to the ground state closed-shell dye molecule does give all the energies of the molecular orbitals shown in Figure 38(a) (the eigenvalues). If

interelectronic effects are ignored, eg. electron repulsion, electron correlation, then the light absorption of the excited state 38(b) can be approximated as the various electronic transitions shown in 38(c), 38(d), and 38(e), i.e. HOMO -> LUMO+1, LUMO -> LUMO+1, LUMO -> LUMO+2 respectively, and many higher energy transitions. Excitation energies calculated simply by taking the eigenvalue difference between the upper and lower orbitals in such transitions will be very inaccurate, although they will be qualitatively informative in a relative sense.

However, absorption intensities (transition moments) calculated from the MO coefficients of the upper and lower orbitals will be much more reliable and can be compared directly with the transition moment for the ground state. If a significant enhancement of the transition moment is found for one or more of the excited state transitions and if these match the input laser wavelength, then reverse saturable absorption is predicted. The reliability of the transition moment calculation (at least in a qualitative sense) stems from the insensitivity of the MO coefficients with respect to interelectronic effects (unlike transition energies, which are very sensitive to these). The main problem is how to establish which excited state transition matches the laser wavelength.

Calculation of Transition Moments.

The extinction coefficient (ε_{max}) is related to oscillator strength **f**. Oscillator strength **f** is related to transition moment **M** by the expression;

$$f = 4.703 \times 10^{29}. \ m.M^2$$

where m is the frequency of the absorption band,

   M is the quantity calculated by the PPP-MO method.

The calculation of **M** involves multiplying the eigenvectors (orbital coefficients) of the lower and upper orbitals involved in the transition, and introducing a distance factor for each atomic centre involved.

HOMO $\quad C_{A1}$ - - - - - - - - C_{B1} $\qquad \Psi_{HOMO} = C_{A1}\phi_A + C_{B1}\phi_B$

LUMO $\quad C_{A2}$ - - - - - - - - - - C_{B2} $\qquad \Psi_{LUMO} = C_{A2}\phi_A + C_{B2}\phi_B$
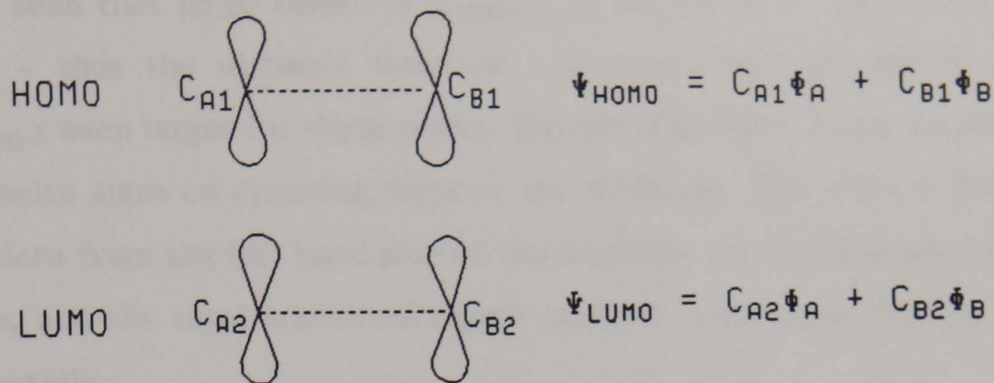
MULTIPLY MO
COEFFICIENTS $\qquad \left(C_{A1}C_{A2}\right) \xrightarrow{-r} \cdot \xrightarrow{+r} \left(C_{B1}C_{B2}\right)$
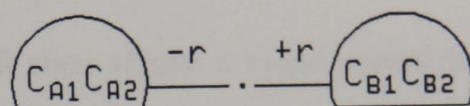
Transition moment $\underline{\mathbf{M} = \mathbf{C_{A1}} \cdot \mathbf{C_{A2}} \cdot \mathbf{-r} + \mathbf{C_{B1}} \cdot \mathbf{C_{B2}} \cdot \mathbf{r}}$

Here r is the distance of each atomic centre from the centre of charge. Here the algebraic signs of $C_{A1}.C_{A2}$ and $C_{B1}.C_{B2}$ must be opposite for large M.

The influence of the eigenvector products (+ or -) on transition moment can best be seen pictorially. For example, for the HOMO -> LUMO transition of the squarylium dye (10) the $C_{HOMO}.C_{LUMO}$ product functions are depicted by circles in Figure 39, a red circle representing a positive product, a black circle a negative product, the radius of the circles is proportional to the magnitude of $C_{HOMO}.C_{LUMO}$.
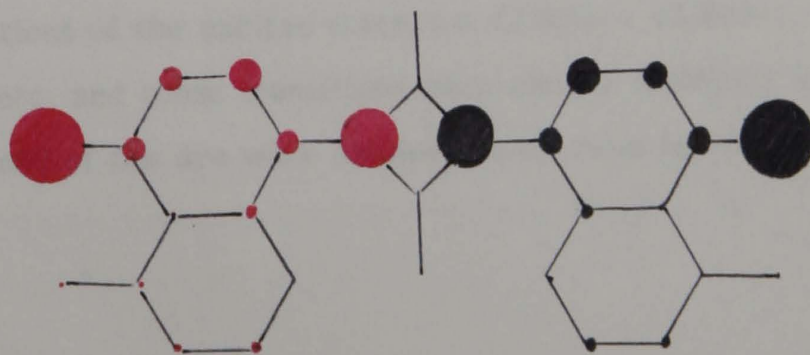
Figure 39. Transition dipole map for squarylium dye (160), HOMO->LUMO transition

It can be seen that large values of $C_{HOMO}.C_{LUMO}$ are found at the extremities of the molecule - thus the distance function r is large, and the dipole contribution $C_{HOMO}.C_{LUMO}.r$ even larger for these atoms. Equally important, these product functions have opposite signs on opposing sides of the molecule. This means that the dipole contributions from the left hand side of the molecule reinforce those from the right hand side, and the total transition dipole moment is extremely large, as observed experimentally.

Transition dipole maps as in Figure 39 thus afford a rapid visual inspection of the absorption band intensity for any transition, provided the molecule has a fairly self evident centre of charge.

2.7.4.2 Results

Transition dipole maps such as Figure 39 have been produced for the dyes (137b), squarylium (160), (142) and HITCI (16), which provide extreme examples of either good reverse saturable absorbers or minimal or zero reverse saturable absorbers. It was hoped therefore that some qualitative indication would be given as to why some dye chromophores show these properties and others do not. The maps were examined for secondary transitions of the excited state, i.e. LUMO -> LUMO+1, LUMO -> LUMO+2 etc. and those transitions most closely matching in energy the normal absorption band of the dye were assumed to be most relevant.

Transition Energies[*]

Transition	Transition ΔE/ev			
	Dye			
	(137b)	(160)	(142)	(16)
H-L	3.27	3.37	3.94	3.49
H-L+1	4.24	5.25	6.16	4.62
L-L+1	0.97	1.87	2.22	1.12
L-L+2	3.71	2.30	2.59	2.03
L-L+3		2.47	3.77	2.18
L-L+4		2.49	3.82	2.21
L-L+5		3.02	3.85	3.12
L-L+6		3.56	4.08	3.79

H = HOMO L = LUMO

[*]calculated as eigenvalue differences, neglecting electron repulsion.

Excited state transitions with similar ΔE values to the visible HOMO->LUMO transition

Dye (137b)	LUMO -> LUMO+2
Squarylium (160)	LUMO->LUMO+5, LUMO->LUMO+6
Dye (142)	LUMO->LUMO+5, LUMO->LUMO+6
HITCI (16)	LUMO->LUMO+5, LUMO->LUMO+6

These were considered to be the most important transitions, and transition dipole maps were drawn for them, a comparison between these excited state transitions and the visible, HOMO->LUMO transition was made.

Figure 40. Transition dipole maps of dye (137b)

TT MOLECULAR FRAMEWORK
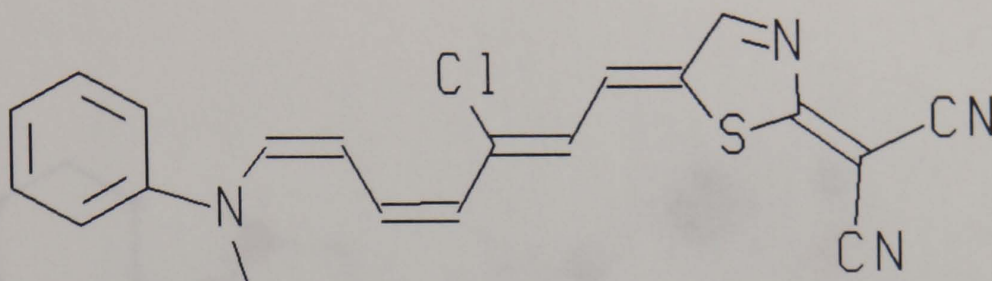
(a) HOMO – LUMO transition
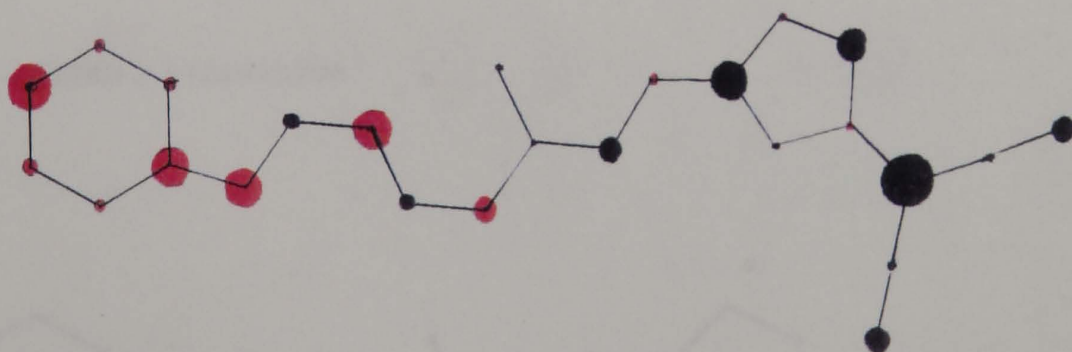
(b) LUMO – LUMO+1 transition

(c) LUMO — LUMO+2 transition

(d) LUMO — LUMO+3 transition

Figure 41. Transition dipole maps of squarylium dye (160)

TT MOLECULAR FRAMEWORK

(a) HOMO – LUMO transition

(b) LUMO – LUMO+1 transition

(c) LUMO – LUMO+5 transition

(d) LUMO – LUMO+6 transition

Figure 42. Transition dipole maps for dye (142)

π MOLECULAR FRAMEWORK
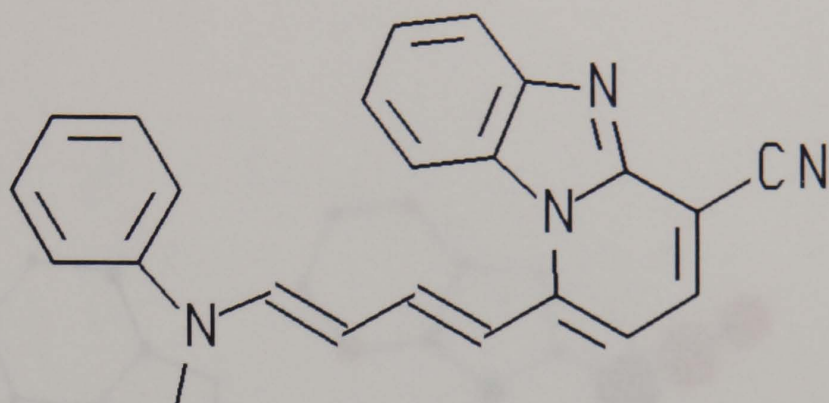
(a) HOMO – LUMO transition

(b) HOMO – LUMO+1 transition
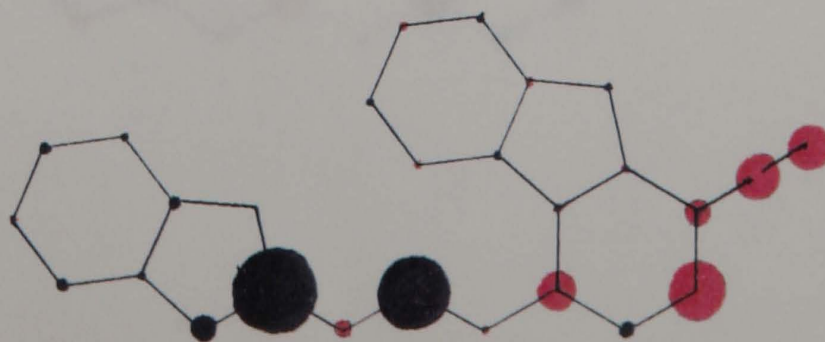
(c) LUMO — LUMO+5 transition

(d) LUMO — LUMO+6 transition

Figure 43. Transition dipole maps for cyanine dye (16)

TT MOLECULAR FRAMEWORK
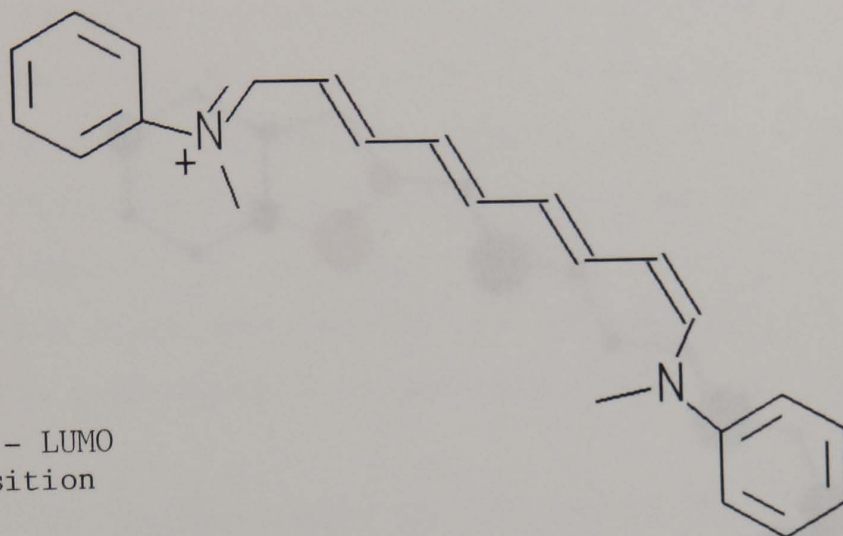
(a) HOMO – LUMO
    transition
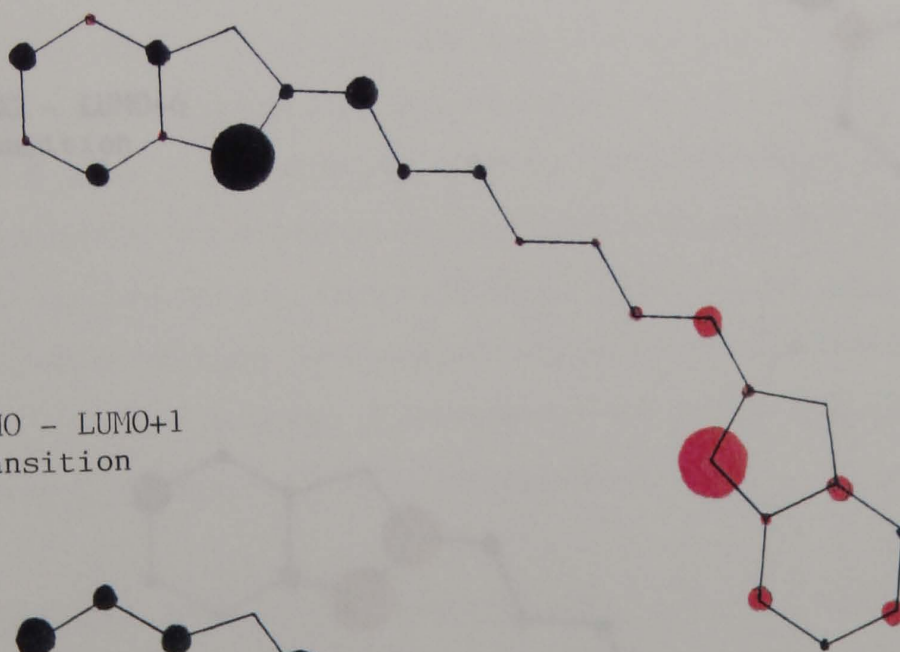
(b) LUMO – LUMO+1
    transition
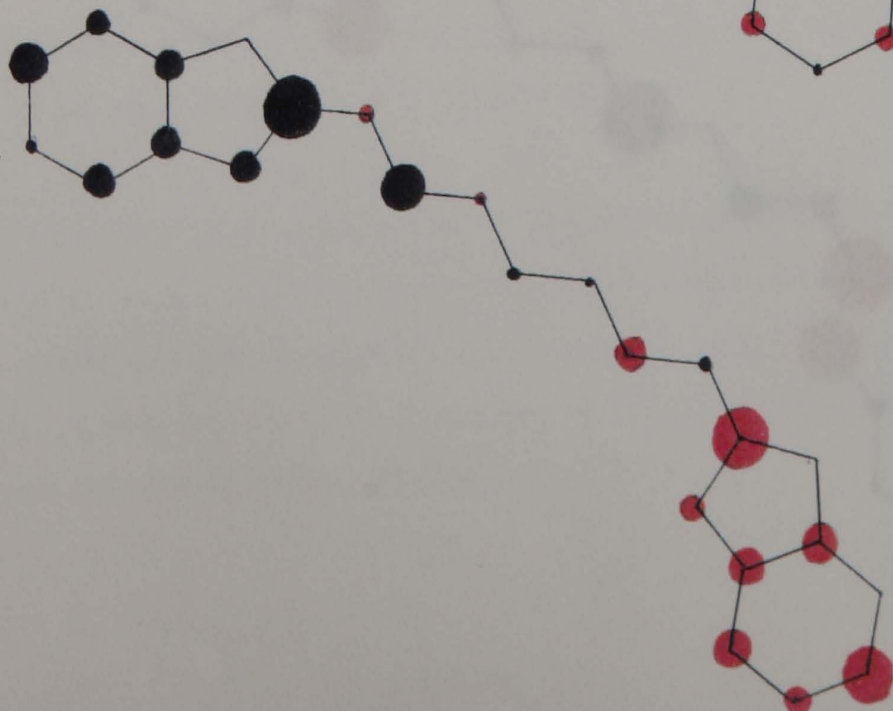
(c) LUMO – LUMO+5
    transition
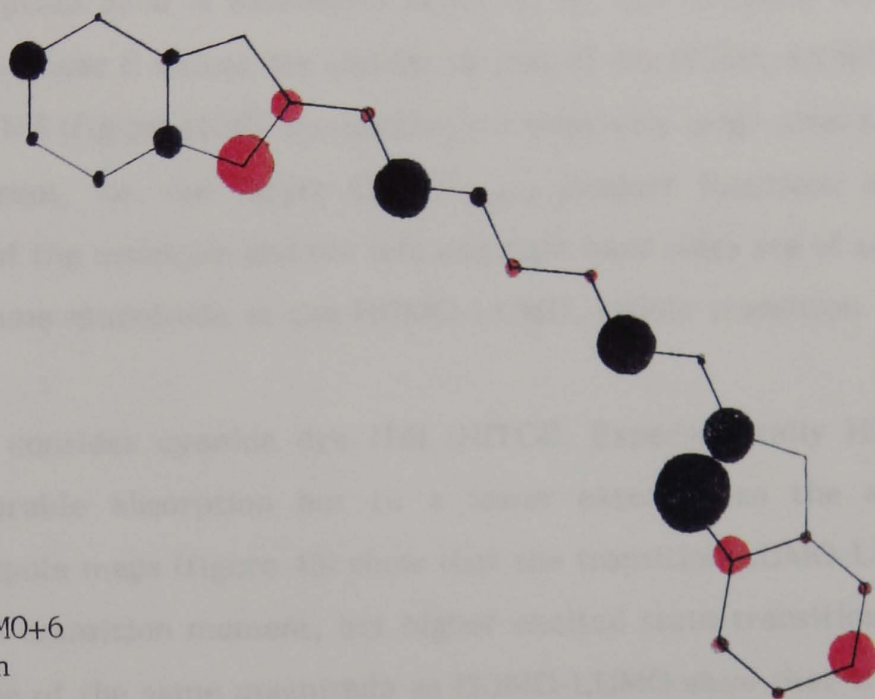
(d) LUMO – LUMO+6
    transition
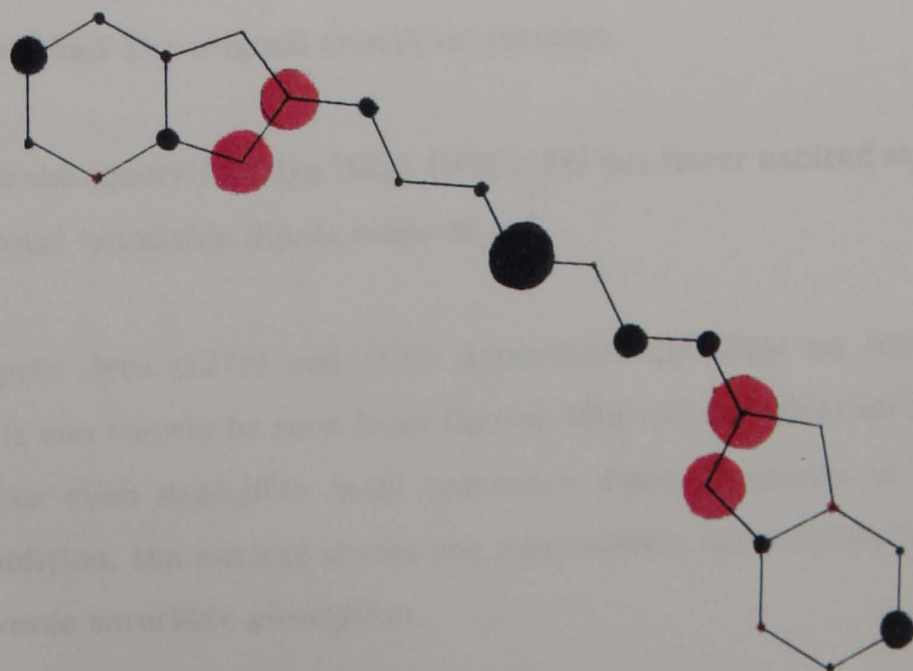
Experimentally the squarylium dye has shown the greatest degree of reverse saturable absorption. Inspection of the transition dipole map for the HOMO-LUMO transition (figure 41(a)) shows large values of $C_{HOMO}.C_{LUMO}$ at the extremities of the molecule separated by a large distance, r. Because the product functions at opposite ends of the molecule are of opposite sign the total transition dipole moment for the normal absorption band is extremely large. If we now consider transitions of the excited state whose E values are similar to that of the HOMO-LUMO transition i.e. LUMO-LUMO+6 (figure 41(d)), qualitatively a relatively large total transition dipole is still apparent, i.e. the larger $C_{LUMO}.C_{LUMO+6}$ product functions are still at the extremities of the molecule and the left and right hand sides are of apposite sign and r is of the same magnitude as the HOMO-LUMO, visible transition.

Let us now consider cyanine dye (16) (HITCI). Experimentally HITCI does show reverse saturable absorption but to a lower extent than the squarylium dye. Transition dipole maps (figure 43) show that the transition LUMO-LUMO+1 still has a large total transition moment, but higher excited state transitions corresponding to a ∆E value of the same magnitude as HOMO-LUMO show that transition LUMO-LUMO+5 still has a moderate total transition moment, but the LUMO-LUMO+6 transition does not i.e., figure (43(d)), although $C_{LUMO}.C_{LUMO+6}$ contributions are large on the left and right hand sides of the molecule the signs are both positive, this means that the transition dipole moment will be less than for the ground state, i.e. approximately half the original transition moment.

Compared to the squarylium dye (160), HITCI (16) has fewer excited state transitions with large total transition dipole moment.

Donor-acceptor dyes (137b) and (142) experimentally show no reverse saturable absorption. It can clearly be seen from figures 40(a)-(d) and 42(a)-(d) that these dyes have small or even negligible total transition dipole moments in higher excited states. In addition, the excited states are more widely spaced than in the dyes that do show reverse saturable absorption.

To test the MO approach further, the transition dipole maps for the excited state transitions of 7-diethylamino-4-methyl-coumarin (13), 4-methyl-umbelliforone (14), cresyl violet perchlorate (19) and phthalocyanine (20) were computed. These chromogens have been shown be various workers to exhibit reverse saturable absorption (cf introduction pg 14).

Results

Transition energies

Dye	H-L	L-L+1	L-L+2	L-L+3	L-L+4	L-L+5	L-L+6
(13)	5.98	1.27	2.02	3.40	4.74		
(14)	5.42	1.12	1.20	3.30	4.62		
(19)	3.87	0.83	2.87	3.08	3.39	4.14	4.51
(20)	4.22	0.02	1.04	1.54	1.66	1.68	1.77

Transition ΔE/eV

	L-L+7	L-L+8	L-L+9	L-L+10	L-L+11	L-L+12
(19)	6.04	6.61				
(20)	2.76	3.02	3.04	3.57	4.74	5.30

	L-L+13	L-L+14
(20)	5.35	5.74

L = LUMO, H = HOMO

Excited state transitions with similar ΔE value to the excitation laser

Dye	λmax/nm	Excitation laser/nm	Transitions
(13)	367	337	L-L+4
(14)	372	337	L-L+4
(19)	601	514.5	L-L+5 to L-L+8
(20)	695.5	694.3	L-L+11 to L-L+14

Transitions dipole maps are shown in Figures 44-47.

Figure 44. Transition dipole maps for 7-diethylamino-4-methylcoumarin (13)

ΤΤ MOLECULAR FRAMEWORK
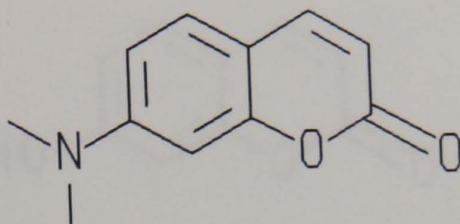
(a) HOMO – LUMO transition
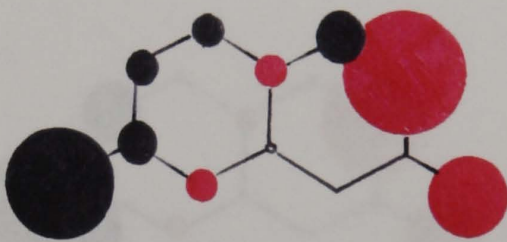
(b) LUMO – LUMO+1 transition
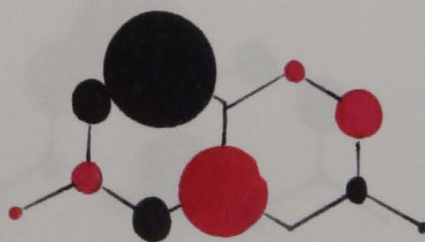
(c) LUMO – LUMO+2 transition
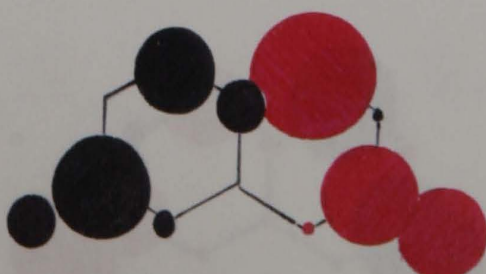
Figure 45. Transition dipole maps for 4-methyl-umbelliforone (14)

TT MOLECULAR FRAMEWORK
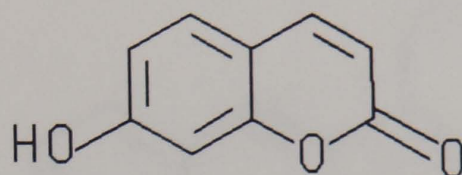
(a) HOMO – LUMO transition
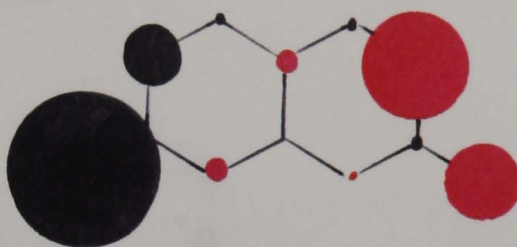
(b) LUMO – LUMO+1 transition
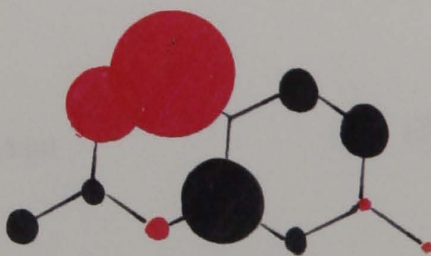
(c) LUMO – LUMO+2 transition
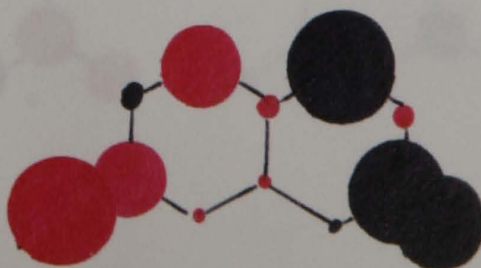
Figure 46. Transition dipole maps for cresyl violet perchlorate (19)
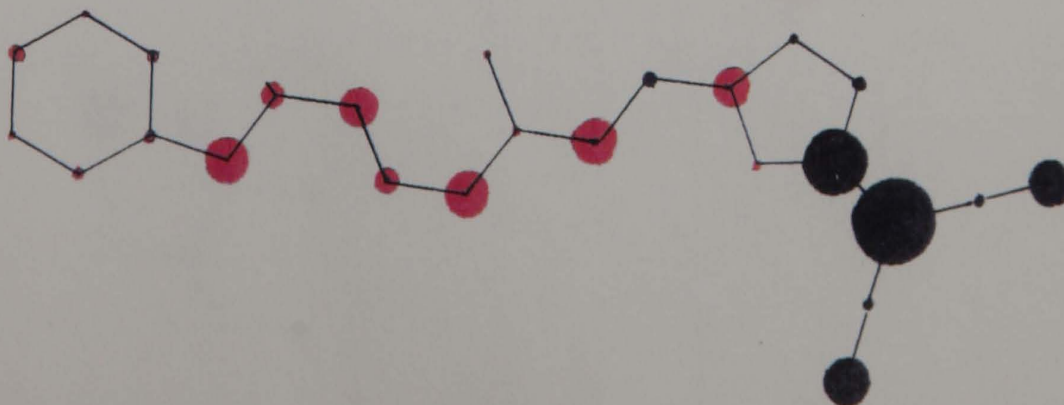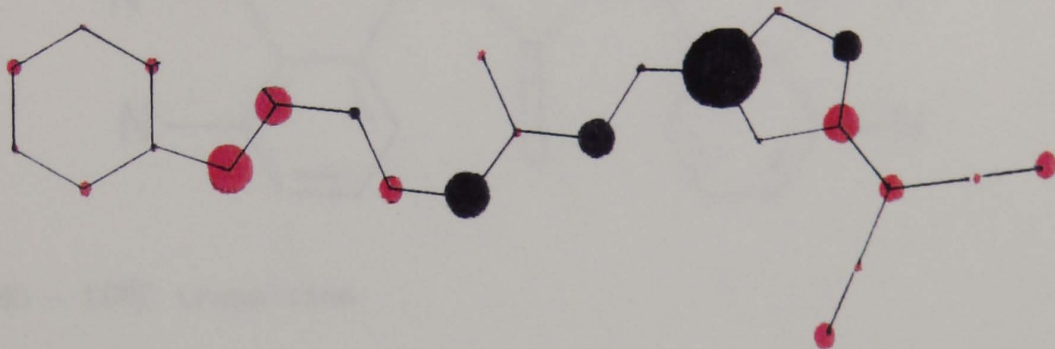
TT MOLECULAR FRAMEWORK
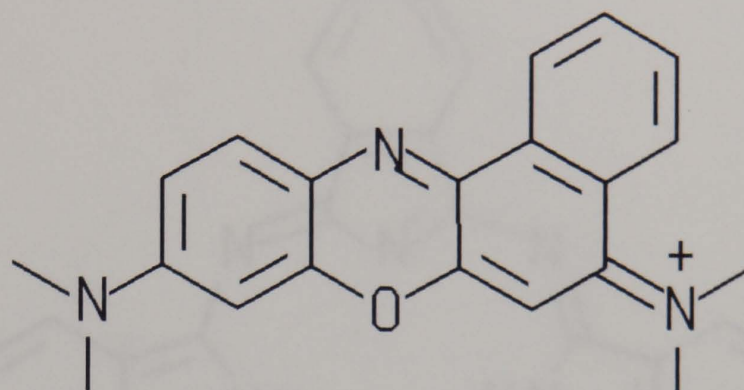
(a) HOMO – LUMO transition
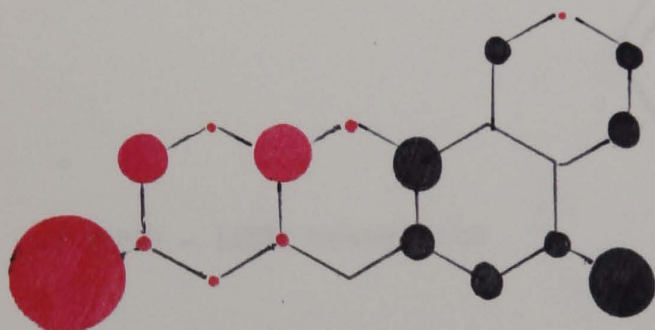
(b) LUMO – LUMO+1 transition
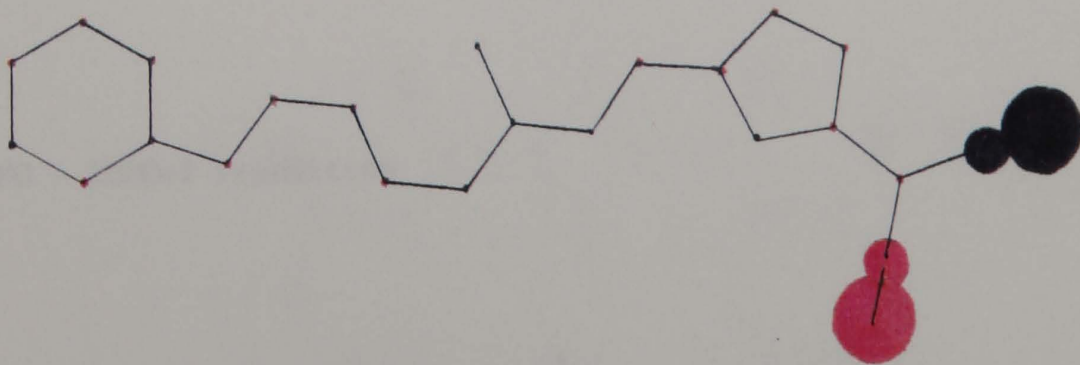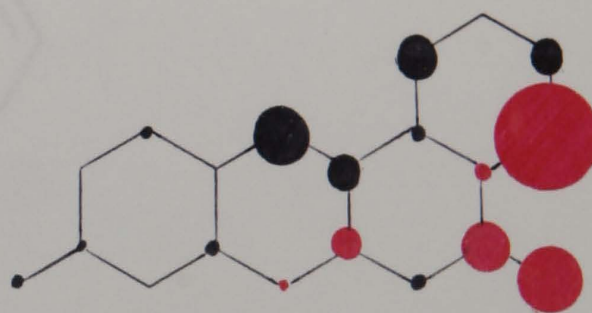
(c) LUMO – LUMO+4 transition
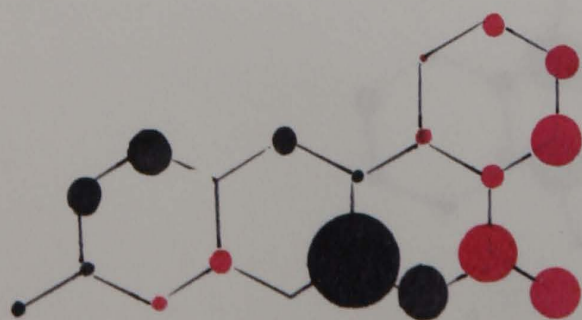
(d) LUMO – LUMO+4 transition
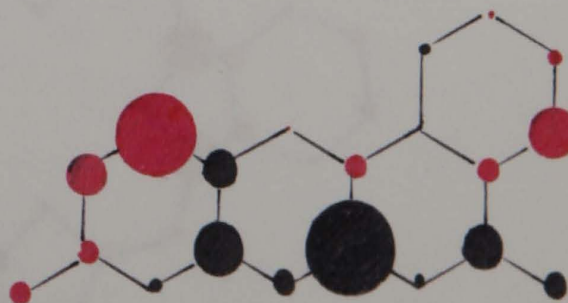
Figure 47. Transition dipole maps for metal free phthalocyanine (20)

TT MOLECULAR FRAMEWORK
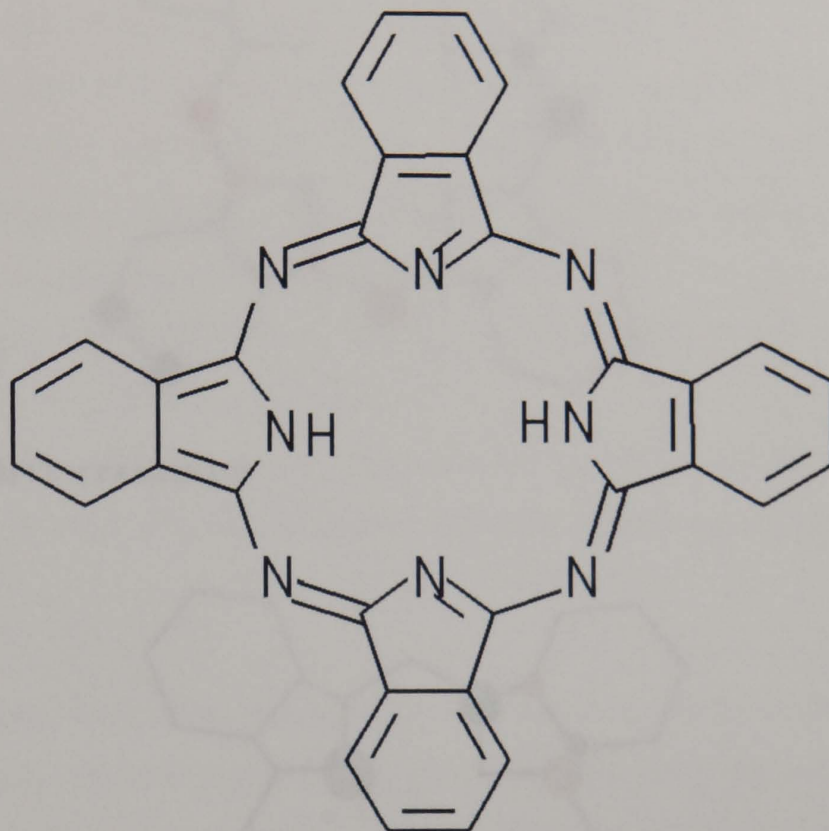
(a) HOMO – LUMO transition
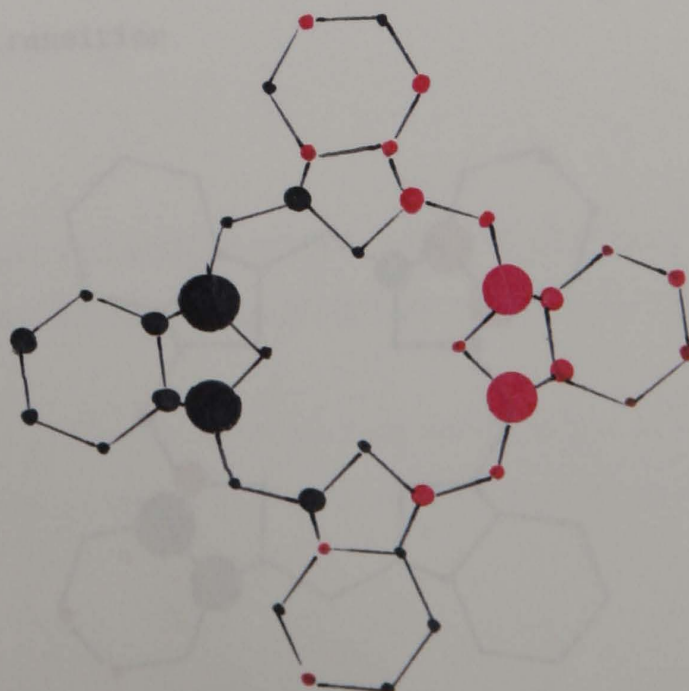
(b) LUMO – LUMO+10 transition
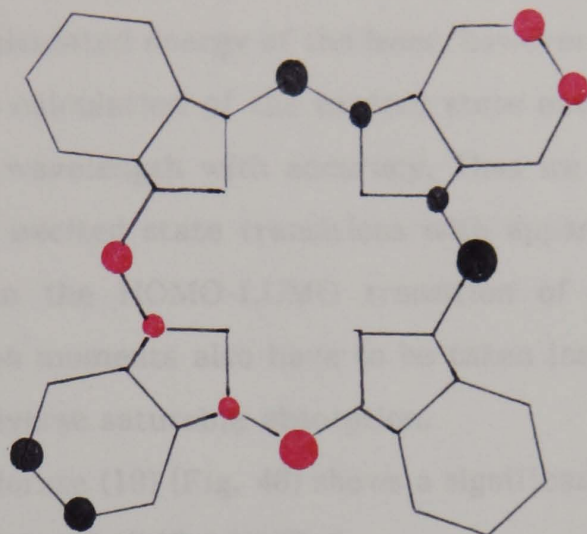
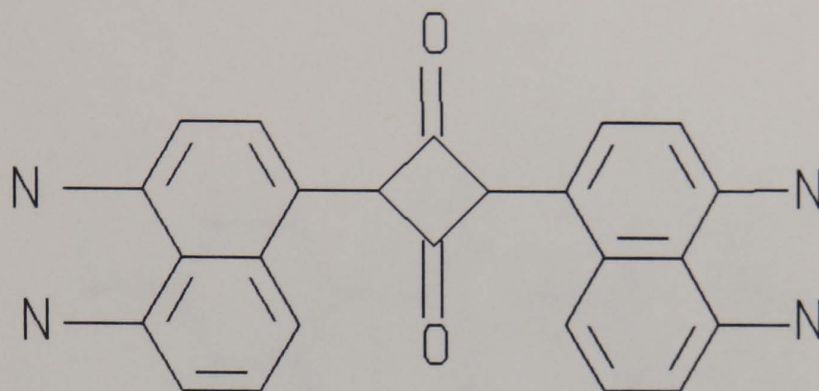(c) LUMO – LUMO+11 transition
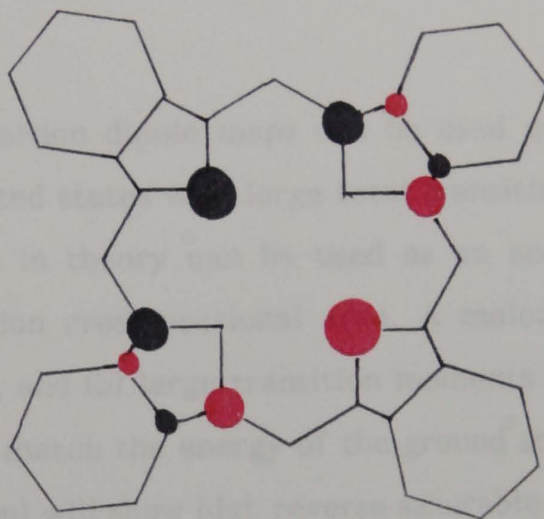
(d) LUMO – LUMO+14 transition
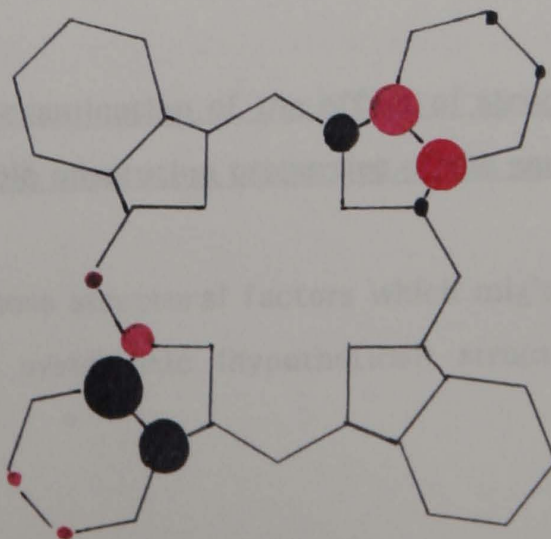
From the transition dipole maps it is evident that (13) (Fig. 44) and (14) (Fig. 45), have significant transition moments in the LUMO-LUMO+2 transition. This does not correspond to the calculated energy of the laser, however, but due to the large error associated with the calculation of the excited state energies, it is not possible to calculate the laser wavelength with accuracy. Thus we have to make the further approximation that excited state transitions with apparent energy values greater than or lower than the HOMO-LUMO transition of that chromophore having significant transition moments also have to be taken into account when predicting the possibility of reverse saturable absorption.

Cresyl violet perchlorate (19) (Fig. 46) shows a significant transition moment in the excited state transition, LUMO-LUMO+5.

Phthalocyanine (20) (Fig. 47) shows two possible states for excited singlet to singlet transitions, LUMO-LUMO+10 and LUMO-LUMO+14, both show significant transition moments.

PPP - generated transition dipole maps can be used qualitatively to predict the number of higher excited states with large total transition dipole moments of a dye molecule. This figure in theory can be used as an approximate measure of the excited state absorption cross sectional area. A molecule with (a) many closely spaced excited states, and (b) large transition moments for many of these states (especially those that match the energy of the ground state absorption band, or the incident laser radiation) will show high reverse saturable absorption properties. Thus it seems that the PPP-MO method provides a qualitative approach to predicting reverse saturable behaviour.

2.7.4.3 A theoretical examination of the effect of structural modification on the reverse saturable absorption properties of the squarylium dye (167)

In order to examine those structural factors which might affect reverse saturable absorption properties, systematic (hypothetical) structural modification of the

squarylium chromophore (167) was undertaken, and the effect of these modifications on excited state transition dipoles calculated. The following structural modifications were made to the squarylium structure (167);

1. An electron withdrawing group -Cl, was added to position 'X'.

2. An electron donating group, -NH$_2$, was added to position 'X'.

3. The conjugation was extended from position 'X', i.e. structure (168).

(167)

(168)
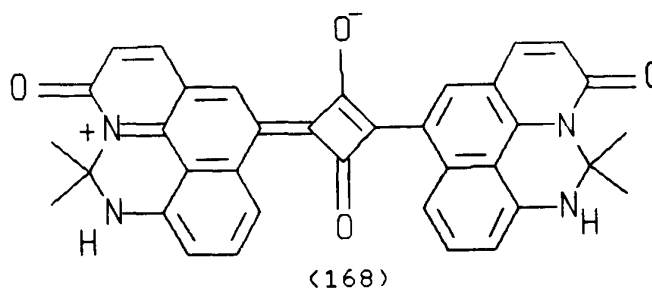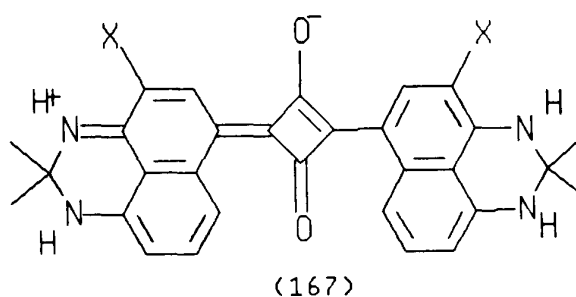
Wavelength maxima, eigenvalues and eigenvectors of the hypothetical chromophores were obtained from PPP-MO calculations. Transition dipole maps for the theoretical chromophores were produced as previously described.

Results

Transition energies

Transition	Transition ΔE/eV		
X =	NH$_2$	Cl	Cyclic ketone
H-L	3.01	3.33	3.20
L-L+1	1.92	1.90	2.03
L-L+2	2.38	2.42	2.14
L-L+3	2.65	2.50	2.29
L-L+4	2.69	2.52	2.75
L-L+5	3.09	2.56	3.33
L-L+6	3.62	3.57	3.56
L-L+7	4.07	3.98	3.61
L-L+8	4.67	4.54	4.02
L-L+9	4.87	4.78	4.66
L-L+10	6.19	6.13	5.12
L-L+11	6.63	6.56	5.94
L-L+12	7.52	7.43	5.96
L-L+13	-	-	6.73

Excited state transitions with ΔE values similar to, and greater than the HOMO-LUMO transition

X	λmax/nm (calc)	Transitions
NH$_2$	865	L-L+5 to L-L+9
Cl	815	L-L+6 to L-L+9
cyclic ketone	817	L-L+5 to L-L+10

Figure 48. Transition dipole maps for squarylium dye (167, X = NH$_2$)

(a) HOMO – LUMO transition
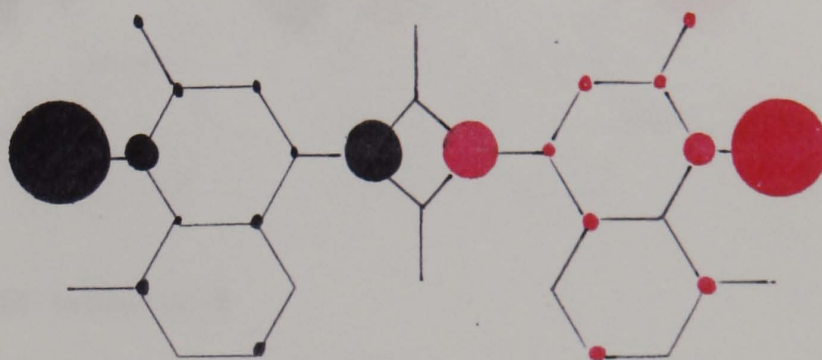
(b) LUMO – LUMO+7 transition
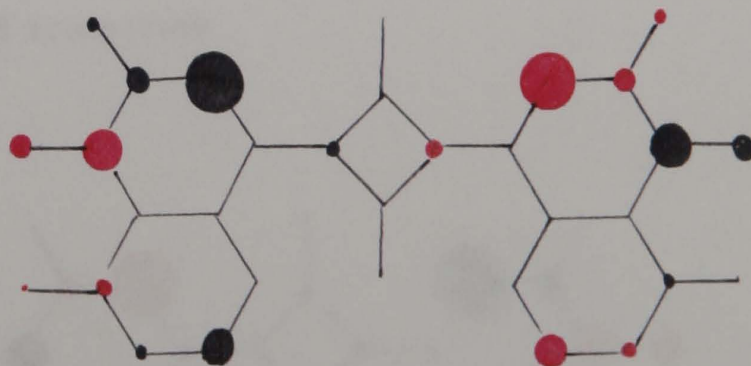
Figure 49. Transition dipole maps for squarylium dye (167, X = Cl)

(a) HOMO − LUMO transition
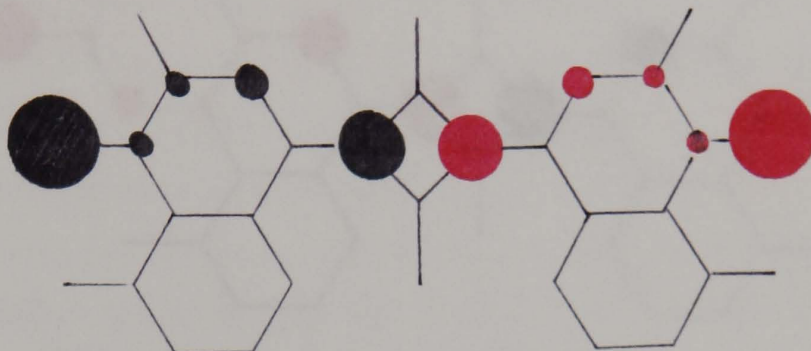
(b) LUMO − LUMO+6 transition
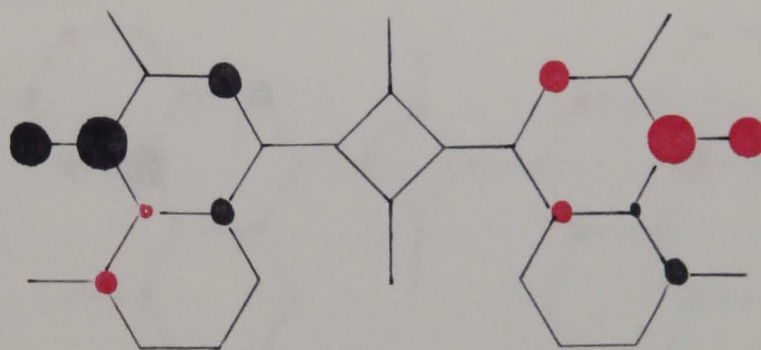
(c) LUMO − LUMO+8 transition
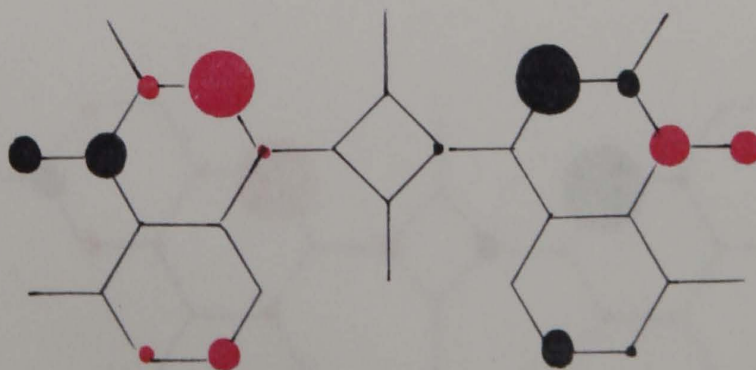
Figure 50. Transition dipole maps for squarylium dye (168)

(a) HOMO - LUMO transition
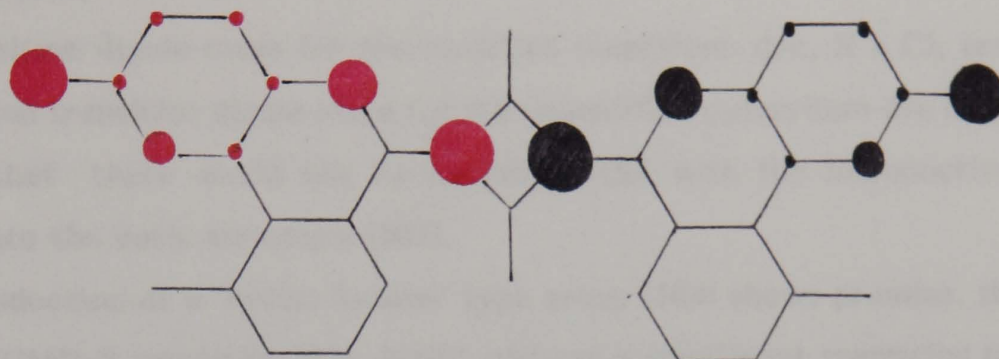
(b) LUMO - LUMO+8 transition
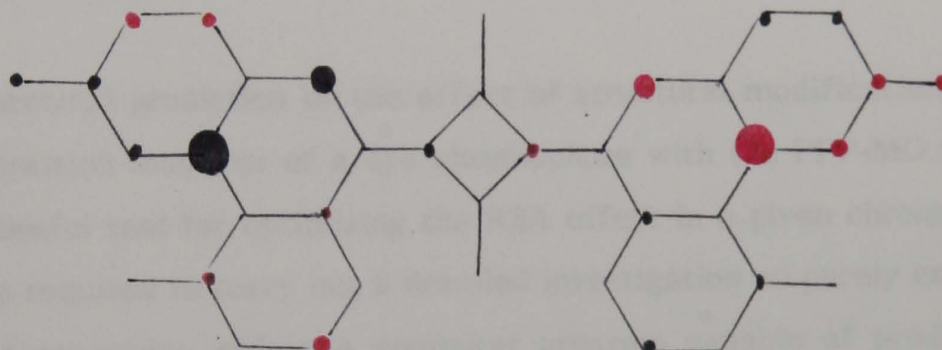
(c) LUMO - LUMO+10 transition
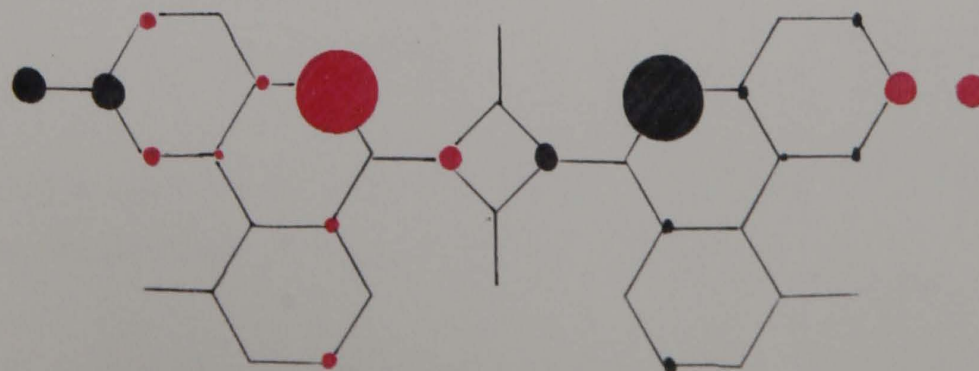
The modified squarylium dye, X = NH_2 (Figure 48), shows excited state transition dipole maps with no significant transition moments. The LUMO-LUMO+7 transition (Fig. 48(b)), does have a small transition moment. We predict that RSA is effectively reduced when amino groups are introduced at the positions indicated in the basic structure (167).

The transition dipole maps for the modified squarylium dye, X = Cl, are similar to the original transition dipole maps for the unmodified squarylium dye (Figure 49). We predict that there would not be improved RSA with the introduction of chloro groups into the basic structure (167).

The introduction of a 'cyclic ketone' type group (168) shows promise, the LUMO-LUMO+8 transition (Fig. 50(b)) still has a significant transition moment, the LUMO-LUMO+10 transition (Fig. 50(c)) also has a significant transition moment. We cannot quantitatively calculate the extent of the improvement to the RSA, however.

2.7.4.4 Conclusion

The theoretical prediction of the effect of structural modification on the excited state transition moments of a dye chromophore with the PPP-MO method appears to be a useful tool for optimising the RSA effect in a given chromophoric system. The time required to carry out a detailed investigation on purely empirical grounds would be excessive, and so a computer program capable of producing transition dipole maps for ground state and excited state transitions is a potentially useful tool for dye design.

3 EXPERIMENTAL

3.1 GENERAL DATA

<u>Melting points</u>

These were determined on an electrothermic melting point apparatus and are uncorrected. In some instances melting points were measured by differential scanning calorimetry, using Du Pont Instruments Thermal Analyser 2,000.

<u>Spectra</u>

Infrared spectra were recorded on a Perkin-Elmer 1720 series Infrared Fourier Transform Spectrometer.

Visible and Ultraviolet spectra were recorded on a Perkin-Elmer Lambda 15 uv/visible spectrophotometer. The instrument was set up according to the parameters cited in Table 31.

Table 31. Spectrophotometer settings used for recording uv - visible spectra

Ordinate mode	ABS
Slit	2nm
Scan speed	480nm/min
Response	0.5s
Lamp	UV/VIS
Cycles/time	1/0.05min
Peak threshold	0.02A
Recorder	ON
Ordinate min/max	0.000/1.500
Abscissa min/max	190.0/900.0nm

Fluorescence excitation and emission spectra were recorded on a Perkin-Elmer LS5 spectrofluorimeter. All spectra are uncorrected.

Chromatography

Thin layer chromatography was carried out on plastic sheets coated with Kiesel 60 (Merck) (without fluorescent indicator). Chromatography columns were prepared with Kieselgel 60 (70-230 mesh ASTM).

NMR spectra

Proton magnetic resonance spectra were recorded at the SERC N.M.R. center, University of Warwick using a WH400 n.m.r. instrument.

Mass spectra

The low resolution spectra were recorded on a VG 12-253 quadrupole spectrometer. The fast atom bombardment spectra were recorded on a VG ZAB-E spectrometer. Measurements were carried out at the SERC Mass Spectrmoetry Service Center, University of Swansea.

Elemental analyses (C,H,N)

These were carried out on a Technicon CHN Autoanalyser. Halogen analysis were carried out by conventional procedures.

3.2 EXPERIMENTAL PROCEDURES

Preparation of dye-containing cellulose acetate films

Cellulose diacetate films were prepared by the method described by Corns [59] Cellulose diacetate (1g) was added to a mixture of dichloromethane/methanol (10ml 9:1) containing the appropriate amount of dye in a beaker covered with a watch glass. The mixture was stirred at room temperature with a magnetic stirrer until a clear solution was obtained. The film was cast onto a glass plate with a t.l.c. spreader at a thickness of 0.5mm. Immediately after casting a similarly sized glass sheet was placed over the wet film a few mm from its surface, by using microscope slides as spacers. After drying over a hot air drier, the film was peeled off the glass plate and then stored in a vacuum dessicator. The film was cut into pieces which were then mounted in a slide frame. Such films were then sent to R.D.A. for testing for reverse saturable absorption properties and also

subjected to photostability testing.

Preparation of other polymeric film systems

Suitable polymer films were those which are optically transparent, compatible with the dye and can be cast from methylene chloride, tetrahydrofuran or ethyl acetate solvents. The following squarylium-dye containing polymer films were prepared. The corresponding cellulose acetate film was made by the procedure outlined above.

Poly(vinylchloride)

High molecular weight polyvinylchloride was dissolved in THF, to give a solution of high viscosity, the dye solution was then added to give a strong green colour. After casting the film was slowly dried to prevent misting.

Poly(methyl methacrylate)

PMMA granuals were dissolved in enough ethyl acetate to give a solution of high viscosity. The squarylium dye solution was then added. After casting the films were dried slowly to prevent misting.

Polycarbonate $[-C_6H_4-4-C(CH_3)_2C_6H_4-4-OCO_2-]_n$

Polycarbonate resin granules were dissolved in methylene chloride to give a solution of high viscosity. The squarylium dye solution was then added. After casting the films were slowly dried.

Polystyrene

Polystyrene was dissolved in ethyl acetate to give a solution of high viscosity. The squarylium dye solution was then added. After casting the films were slowly dried.

Synthesis of 7-diethylamino-3-formyl-coumarin (91)

4-Diethylaminosalicylaldehyde (17.92g, 0.093 mol), diethylmalonate (16.33g, 0.0102 mol) and piperidine (20ml) were stirred together at 40°C, for 12 hr. To this mixture hydrochloric acid (18%) (94ml) was then added. The reaction mixture

was stirred under reflux for 5 hours. During this time the yellow coloured solution decolourised. On cooling saturated sodium acetate solution (14ml) was added and the pH carefully adjusted to pH 4-5 with aqueous sodium hydroxide solution (45%). The resultant orange/brown precipitate was filtered off, washed with water (removing the orange colouration), and dried overnight in an oven at 50°C, to give crude 7-diethylaminocoumarin (17.2g: 77.7%).

Dimethylformamide (dry) (7.14g, 0.098 mol) was added dropwise to phosphorous oxychloride (16g, 0.104 mol) at 40°C. The mixture was then stirred at 50°C for 45 minutes with exclusion of moisture. To this was added a suspension of the 7-diethylaminocoumarin (15g, 0.07 mol) in dimethylformamide (18g). The reaction mixture was warmed to 60°C and stirred for 2 hours. The orange coloured reaction mixture was then poured into ice (150g) and stirred for a further 2 hours. The solid was filtered off, washed thoroughly with water and dried in an oven at 50°C overnight, giving (91) (9.6g: 56%) m.p. 151-156°C.

Synthesis of 4-methylthiazol-2-yl malononitrile

Sodium thiocyanate dihydrate (32.2g, 0.275 mol) and water (27ml) were stirred at room temperature and chloroacetone (20ml, 0.243 mol) added. With protection from light the mixture was stirred at room temperature overnight. Ether (100ml) was added to extract the mixture and the ether fraction was isolated and washed with 4x10ml water, and dried over sodium sulphate. Evaporation of the ether gave 26g of an orange coloured oil. To this was added malononitrile (14.7g, 0.223 mol) and methanol (44ml). With ice/water cooling, triethylamine (30.67ml, 0.303 mol) was slowly added, the reaction being extremely exothermic. The reaction mixture was stirred for 3 hours at room temperature and then diluted to 500ml with water. On addition of formic acid (40%) (13.32ml) a light brown solid precipitated. This was filtered off, washed with water, then methanol and dried, to give the product as a pale yellow solid (43g, m.p. 292.4°C).

General procedure for the synthesis of coumarin-based extended chromophores (99)

Equimolar quantities of 7-diethylamino-3-formylcoumarin and the appropriate active methylene was stirred together in a small volume of ethanol at reflux,

with piperidine/acetic acid catalyst (1:5). Isolated chromogens were purified by recrystallisation from ethanol or column chromatography (eluent methylene chloride). Synthesised dyes and their characterisation data are summarised in Table 32.

Table 32. Yields and characterisation data for coumarin dyes (99)

Structure	Yield %	Appearance of crystals and melting point/°C	Characterisation data
99(a)	89	Metallic green needles 224-225	$C_{23}H_{19}NO_4$ calc: C,73.99; H,5.13; N,3.75% found: C,74.20; H,5.25; N,3.55%
99(b)[#]	86	Hexagonal green 228-229	$C_{22}H_{19}NO_5S$ calc: C,64.53; H,4.69; N,3.42% found: C,64.50; H,4.60; N,3.30%
99(c)	69	Metalic green platelets 213-215	$C_{26}H_{19}N_3O_3$ calc: C,74.09; H,4.54; N,9.97% found: C,73.50; H,4.35; N,10.01%
99(d)	57	Metallic green platelets 205-206	$C_{25}H_{19}N_3O_4S$ calc: C,65.63; H,4.19; N,9.19% found: C,65.25; H,4.20; N,9.10%
99(e)[*##]	48	Dark blue powder 204-206	m/e = 470 (= m+1)
99(f)[##]	78	Purple needles 172-173	m/e = 458 (= m+1)
99(g)[#]	82	Purple powder 267-270	$C_{28}H_{18}N_3O_3Cl$ calc: C,65.63; H,4.55; N,9.99% found: C,65.60; H,4.35; N,10.0%

Table 32. Yields and characterisation data for coumarin dyes (99) continued

99(h)[#]	79	Pale yellow powder	$C_{38}H_{43}N_3O_2$ Calc: C,79.40; H,7.70; N,7.30% found: C,79.55; H,7.55; N,7.25% m/e = 573 (= m+1)
99(i)	76	Bronze powder 169-170	$C_{36}H_{44}N_2O_2$ m/e = 536
99(j)	85	Magenta crystals 227-228	$C_{31}H_{25}N_3O_2$ calc: C,79.13; H,5.14; N,8.93% found: C,78.70; H,5.15; N,8.80%
99(k)	79	Bronze crystals 249-251	$C_{26}H_{20}N_4O_2$ calc: C,74.26; H,4.80; N,13.33% found: C,74.25; H,4.75; N,13.45%
99(l)	82	Magenta/purple powder 253-254	$C_{23}H_{19}N_3O_2S$ calc: C,68.80; H,4.78; N,10.47% found; C,68.75; H,4.80; N,10.60%
99(m)[*##]	93	Orange crystals 264-265	$C_{23}H_{20}N_4O_2$ calc: C,71.80; H,5.20; N,14.48% found: C,71.80; H,5.00; N,14.56%
99(n)[*##]	89	Green powder 259-260	$C_{21}H_{20}N_3O_3Cl$ calc: C,63.39; H,5.03; N,10.37% found: C,63.00; H,5.15; N,10.55%
99(o)	87	Green powder 246-247	$C_{20}H_{17}N_5O_2$ calc: C,66.85; H,4.73; N,19.50% found: C,66.80; H,4.65; N,19.55%
99(q)[##]	88	Purple crystals 252-253	$C_{18}H_{17}N_3O_5$ calc: C,60.8; H,4.79; N,11.83% found: C,60.8; H,4.79; N,11.55%

Table 32. Yields and characterisation data for coumarin dyes (99) continued

99(r)[##]	94	Purple crystals 278-279	$C_{25}H_{20}N_2O_4$ calc: C,72.80; H,4.85; N,6.80% found: C,72.10; H,4.75; N,6.60%

* Reaction carried out in acetic anhydride at 100°C

Piperidine catalyst used

no catalyst required

Preparation of 7-diethylamino-4-chloro-3-formyl coumarin (112)

Malonic acid (5.2g, 0.05 mol), 2,4,6-trichlorophenol (19.8g, 0.10 mol) and phosphorous oxychloride (9.5ml) were stirred together for 90 minutes at 100°C, giving a white precipitate. Dilute sodium hydroxide solution was added and the resultant product bis (2,4,6-trichlorophenyl) malonate filtered off, washed with water and dried in an oven at 50°C, (22.9g, 99%).

The bis (2,4,6-trichlorophenyl) ester (18.4g, 0.04 mol) and m-diethylaminophenol (6.5g, 0.04 mol) were dissolved in dry toluene (40ml) and heated under reflux for 2 hours. The formation of a cream coloured solid was observed during the 2 hours and the reaction mixture turned dark brown in colour. The product was filtered off to give 7-diethylamino-4-hydroxycoumarin and washed with toluene and hot acetone. This was then stirred in DMF (11.7ml, 0.16 mol), and cooled to 0-5°C and POCl$_3$ (2.45g, 0.016 mol) was added dropwise with constant stirring. The reaction mixture was stirred at 25°C for 30 mins and then poured into ice with stirring. The resultant precipitate was filtered off, washed with 10% NaHCO$_3$ solution and dried giving (112) as an orange powder, (1.09g, 26%).

The aldehyde was purified by column chromatography (silica; CH$_2$Cl$_2$) and then recrystallised from ethyl acetate. The product had m.p. 140-141°C. (Found: C,60.30; H,5.00; N,5.1; Cl,12.55%, C$_{14}$H$_{14}$NO$_3$Cl requires C,60.1; H,5.05; Cl,12.7%).

A similar reaction procedure but using 8-hydroxyjulolidine in replace of m-diethylaminophenol gave intermediate (118).

Preparation of ring closed dye (117)

7-Diethylamino-4-chloro-3-formylcoumarin (0.09g, 0.3 mmol) and 2-cyanomethylbenzimidazole (0.06g, 0.4 mmole) were stirred together in acetic anhydride (3ml) at 100°C for 2 hours. On cooling the product cystallised out of solution as an orange solid, (0.12g, 86%).

The product was recystallised from ethyl acetate to give orange crystals, m.p. 278-279°C. (Found: C,72.40; H,4.70; N,14.75%, $C_{23}H_{18}N_4O_2$ requires C,72.23; H,4.75; N,14.65%).

A similar procedure but using the julolidine chloro-aldehyde (118) gave dye (119), (m/e = 407 (M+1)).

Synthesis of dye (121)

Equimolar quantities of 7-Diethylamino-4-chloro-3-formylcoumarin (112) and malononitrile dimer (120) were stirred together in ethanol under reflux for 2 hours. The product separated out on cooling, and was then recrystallised from ethanol, giving orange crystals. (Found C,59.70; H,3.75; Cl,8.80%, $C_{19}H_{16}N_5O_2Cl$ requires C,59.76; H,4.19; Cl,8.40%).

Synthesis of 3-dicyanomethylene-1,5,5-trimethylcyclohexene (124)

Isophorone (123) (14.5g, 0.105 mol) and malononitrile (6.7g, 0.1 mol) were dissolved in freshly distilled dimethylformamide (50ml). Piperidine (0.5g) and glacial acetic acid (0.3g) were added to the solution and the reaction mixture was stirred overnight at room temperature. Toluene (20ml) was then added and the mixture refluxed for 1 hour, the water formed during the condensation reaction being collected in a Dean and Stark trap. Toluene and DMF were removed successively by vacuum distillation at 95°C. The residue was poured into water (250ml) containing concentrated hydrochloric acid (1ml), giving a brown precipitate. After isolation of the solid and recrystallisation from

isopropanol/water (8:3 by volume) the product was obtained as a white solid (5.8g, 30%).

(FTIR, strong cyano peak at 2221cm^{-1}.)

General procedure for the synthesis of 3-dicyanomethylene-1,5,5-trimethylcyclohexene based dyes (128)

Equimolar quantities of 3-dicyanomethylene-1,5,5-trimethylcyclohexene (124) and the appropriate aldehyde were refluxed together in methanol with a trace amount of piperidine/acetic acid (1:5) catalyst for a minimum time of 7 hours. Products were purified by column chromatography and/or recrystallisation.

Yields of synthesised dyes and their characterisation data are summarised in Table 33.

Table 33. Characterisation data for dyes containing an isophorone-bridge (128)

Structure	Yield%	Appearance of crystals and melting points/°C	Characterisation data
128(a)[a]	70	Metallic magenta 223-224	$C_{21}H_{23}N_3$ calc: C,79.50; H,7.30; N,13.24% found: C,79.75; H,6.95; N,12.40%
128(b)[b]	49	Orange/brown powder 146-147	$C_{23}H_{26}N_3$ calc: C,80.40; H,7.35; N,12.24% found: C,80.85; H,7.30; N,12.10%
128(c)[b]	68	Magenta crystals 182-183	$C_{20}H_{22}N_4$ calc: C,75.43; H,6.98; N,17.60% found: C,75.75; H,7.10; N,17.40%
128(d)[b]	65	Dark purple powder 219-220	$C_{23}H_{27}N_3O$ calc: C,76.41; H,7.54; N,11.63% found: C,76.25; H,7.85; N,11.45%
128(e)[a]	60	Metallic green 204-205	$C_{26}H_{27}N_3O_2$ calc: C,75.51; H,6.59; N,10.16% found: C,75.45; H,6.60; N,10.20%

Table 33. Characterisation data for dyes containing an isophorone-bridge (128) continued

128(f)[c]	Dark blue powder 217-218	$C_{25}H_{27}N_3$ m/e = 369
128(g)[d]	Orange/red crystals 269-270	$C_{29}H_{22}N_2$ calc: C,87.44; H,5.53; N,7.04% found: C,85.80; H,5.90; N,6.45% m/e = 398

(a) - recrystallised from methanol
(b) - recrystallised from n-propanol/water 7:3
(c) - column chromatographed (eluent, toluene) then recystallised from ligoin 60/80
(d) - column chromatographed (eluent, toluene) then recrystallised from ethyl acetate

Synthesis of 2-chloro-1-formyl-3-hydroxymethylene-cyclohexene (133)

Dimethylformamide (40ml, 0.51 mol) mixed with dichloromethane (10ml) was added dropwise with stirring to a solution of phosphorous oxychloride (37ml, 0.4 mol) in dichloromethane (35ml), maintaining the temperature below 10°C. Cyclohexanone (10g, 0.10 mol) was then added dropwise and the temperature raised until boiling occurred. The reaction mixture was stirred under reflux for 3 hours, and after was poured onto ice and left to stand overnight. The pale yellow coloured product (133) was filtered off and dried at room temperature in vacuum.

Synthesis of dye (137a)

2-Chloro-1-formyl-3-hydroxymethylene-cyclohexene and one mol equivalent o: malononitrile were stirred together in a small quantity of methanol for 1!

minutes at room temperature. The colourless solution rapidly became yellow. To this was added a mol equivalent of Fischer's base, and the mixture was stirred for 30 minutes at room temperature, during which time the cyan coloured product crystallised out of solution. This was filtered off and recrystallised from ethanol to give dark blue crystals of (137a) (89%), m.p. 213-214°C. (Found C,73.10; H,5.90; N,10.95%, $C_{22}H_{22}N_3Cl$ requires: C,72.59; H,6.10; N,11.55%.)

Synthesis of 2-chloro-3-formyl-1-[[cyclohexene-2-yl]ethenyl]1,3,3-trimethyl-3H-indolin (136)

2-Chloro-1-formyl-3-hydroxymethylene-cyclohexene (133) (3g, 0.017 mol) and Fischer's base (3g, 0.017 mol) were stirred together in ethanol (10ml) for 1 hour at room temperature. The pale red coloured product crystallised out of solution and was filtered off and recrystallised from toluene, (4.7g, 82%), m.p. 211°C. (Found: C,73.35; H,6.8; N,4.2%, $C_{20}H_{22}NOCl$ requires C,73.3; H,6.8; N,4.3%).

General procedure for the syntheses of dyes (137) (142) and (143) derived from Fischer's base adduct (136)

Equimolar quantities of the Fischer's base adduct (136) and the appropriate active methylene were stirred together in acetic anhydride, at 100°C for 2 hours. On cooling the product precipitated out and was filtered off. Purification procedures and characterisation data are summarised in Table 34.

Table 34. Yields and characterisation data for dyes derived from Fischer's base adduct (136)

Structure	Yield	Appearance of crystals and melting point/°C	Characterisation data
137(b)	89	Bronze powder 217 decomp.	$C_{27}H_{26}N_4SCl$ calc: C,68.43; H,5.49; N,11.83; Cl,7.50% found: C;69.45; H,5.00; N,11.84; Cl,7.10%
137(c)	74	Green crystals 253 decomp.	$C_{29}H_{26}N_3OCl_2$ calc: C,69.18; H,5.10; N,8.30; Cl,14.1% found: C,68.90; H,4.85; N,8.05; Cl,13.9%
137(d)	78	Green crystals 210 decomp.	$C_{29}H_{27}N_4Cl$ calc: C,74.60; H,5.79; N,12.00; Cl,7.6% found: C,74.95; H,5.85; N,11.75; Cl,7.5%
137(e)	43	Green crystals 195 decomp.	$C_{26}H_{24}N_5Cl$ calc: C,70.67; H,5.44; N,15.86; Cl; 8.04% found: C,70.20; H,5.40; N,15.60; Cl,8.00%
142	98	Magenta powder 270	$C_{29}H_{26}N_4$ calc: C,80.93; H,6.05; N,13.2; Cl,0.00% found: C,80.10; H,6.20; N,12.6; Cl,0.60% m/e = 430
143(a)	72	Pale green powder 269 decomp.	$C_{24}H_{23}N_3O_3$ calc: C,71.82; H,5.74; N,10.47% found: C,71.10; H,5.70; N,10.25% m/e = 402 (m+1)

Table 34. Yields and characterisation data for dyes derived from Fischer's base adduct (136) continued

143(b)	69	Pale green powder 284 decomp.	$C_{24}H_{23}N_3O_2S$ calc: C,69.06; H,5.52; N,10.07% found: C,68.70; H,5.56: N,9.25% m/e = 417
143(c)	34	Dark blue powder	$C_{26}H_{28}N_3O_7Cl$ (perchlorate) calc: C,58.98; H,5.29; N,7.94% found: C,58.60; H,5.50; N,7.40%
143(d)	65	Pale green crystals 269 decomp.	$C_{27}H_{26}N_3O_2$ m/e = 424
143(e)	67	Metallic green crystals >500	$C_{27}H_{26}N_3O_5Cl$ calc: C,63.50; H,5.17; N,8.27% found: C,62.70; H,5.15; N,8.00%

Preparation of 2[2[2-chloro-3[2-(1,3-dihydro-1,3,-trimethyl-2H indol-2-ylidene)ethylidene-1-cyclohexen-1-yl)ethenyl]-1,3,3-trimethyl-3H indolium perchlorate (149)

Fischer's base (0.4g, 2.8 mmol) and 2-chloro-1-formyl-3-hydroxymethylene-cyclohexene (0.2g, 1.4 mmol) were stirred together in acetic anhydride (2ml) at 100°C for 5 hours. On cooling the reaction mixture was poured into water and the product precipitated by addition of perchloric acid. The pale green solid was recrystallised from ethanol, (0.57g:70%), m.p. 259°C.

Synthesis of 3,7a-diazaindan-2-one hydrochloride salt (150)

A mixture of chloroacetic acid (30.3g, 0.32 mol) and water (200ml) was stirred and sodium carbonate (17g, 0.16 mol) was slowly added. 2-Aminopyridine (30.3g, 0.32 mol) was then added and the mixture heated under reflux for 7 hours. The

mixture was then kept in the fridge overnight to precipitate the product. The cream coloured solid was filtered off, washed with isopropanol and dried, (19g, 28%).

To this was then added conc. hydrochloric acid (24ml) and the mixture heated under reflux for 15 minutes. The mixture was evaporated to a thick oil by heating under vacuum, and isopropanol was added to crystallise the product. The off-white crystals of (150) were filtered off, washed with isopropanol and dried, (14.3g, 93%), m.p. 256°C.

Synthesis of dye (152)

3,7a-Diazaindan-2-one hydrochloride salt (0.4g, 2.3 mmol) and 2-chloro-1-formyl-3-hydroxymethylene-cyclohexene (0.2g, 1.2 mmol) were stirred together in N-methylpyrrolidinone (1ml) at 100°C for 1 hour. On cooling the reaction mixture was diluted with distilled water and the product precipitated by the addition of perchloric acid. The solid was filtered off, washed with water and dried Recrystallisation from ethanol give (152) as a dark blue solid, (0.41g, 68%), m.p. 249°C. (Found: C,55.95; H,3.7; N,11.9%, $C_{22}H_{17}N_4O_6Cl$ requires: C,56.35; H,3.6; N,11.9%).

Preparation of cyclopentylidenel-N,N-dimethylbarbituric acid (155)

Dimethylbarbituric acid (7.7g, 0.05 mol), cyclopentanone (4.2g, 0.05 mol), ammonium acetate (1.2g), acetic acid (2ml), and toluene (30ml) were stirred under reflux for 6 hours. After cooling to room temperature, water (30ml) was added and the mixture stirred for 30 minutes. The toluene layer was separated, washed several times with water and evaporated under reduced pressure to give the crude product which was recrystallised from 95% ethanol as a pale yellow solid, (7.42g, 67%), m.p. 107-109°C. [Lit. m.p. 109°C [98]].

Preparation of bis-anil intermediate (156)

Cyclopentylidenel-N,N-dimethylbarbituric acid (7.42g, 0.032 mol), ethyl-N phenylformimidate (10g, 0.068 mol) and DMF (33ml) were stirred at 80°C for hour. The mixture was cooled to room temperature, methanol (30ml) was adde and the mixture cooled in ice. The precipitate was filtered off, slurried in watei

(156) as a purple solid, (11.93g, 84%), m.p. 199°C.

Synthesis of holopolar dye (153)

A solution of the bis-anil intermediate (156) (2g, 5 mmol), Fischer's base (1.64g, 0.01 mol) in DMF (20ml) containing triethylamine as catalyst was stirred at 100°C for 15 minutes. The solid which crystallised out on cooling was filtered off and dried in an oven at 50°C to give dye (153) as a dark green solid, (1.11g, 40%), m.p. 277°C, (m/e = 577 (m+1).

Synthesis of holopolar dye (154)

A solution of the bis-anil intermediate (156) (1.25g, 3 mmol), 3,7a-diazaindan-2-one hydrochloride salt (1g, 6 mmol) in DMF (10ml) containing TEA (0.17g) was stirred at 100°C for 20 minutes. The reaction was cooled in ice and 10ml acetone added. The solid was filtered off, slurried in methanol, filtered off and dried in an oven at 50°C to give (154) as lustrous green crystals, (1.07g, 76%), m.p. 211°C, (m/e = 508).

Preparation of 2,3-dihydro-2-(4-biphenylyl)-2-methylperimidine (159)

1,8-Diaminonaphthalene was purified by dissolving in ligroin (b.p. 100-120°C) at a temperature not higher than 55°C, filtering the hot solution and collecting the needle shaped, peach coloured crystals which formed on cooling, (50% recovery) m.p. 63-64°C.

The purified 1,8-diaminonaphthalene (6.32g, 0.04 mol), 4-acetylbiphenyl (8.4g, 0.042 mol), p-toluenesulphonic acid (0.07g) and ethanol (40ml) were stirred at 55°C for 4 hours. On cooling to room temperature a solid separated out. This was filtered off washed with water and dried in an oven at 50°C for 48 hours to give (159) as a beige coloured solid, (13g), m.p. 142-150°C [Lit m.p. 156-158°C [59]].

Preparation of squarylium dye (160)

A mixture of the dihydroperimidine (159) (9.82g, 0.029 mol), squaric acid (1.65g, 0.0145 mol), n-butanol (40ml) and toluene (20ml) were stirred under reflux for 1 hour, using a Dean and Stark trap to remove water from the reaction. The toluene was removed under reduced pressure and the mixture poured into ligroin. The resultant green precipitate of (160) was filtered off and dried, (7.9g, 68%), m.p. >300°C.

Preparation of dihydroperimidine (161)

Purified 1,8-diaminonaphthalene (2.35g, 0.015 mol), butyl levulinate (2.6g, 0.015 mol), p-toluenesulphonic acid (0.03g) and n-butanol (5ml) were stirred at 60°C for 6 hours. Water (20ml) was added and the mixture cooled in ice. A beige/pink solid deposited which was filtered off and washed with water until the washings were clear and acid free. The product was dried in an oven at 50°C and recrystallised from n-butanol to give (161), (4.8g, 98%), m.p. 87-89°C. (Found: C,73.2; H,7.85; N,9.1%. $C_{19}H_{24}N_2O_2$ requires: C,73.08; H,7.69; N,8.97%).

Preparation of squarylium dye (162)

Dihydroperimidine (161) (4.84g, 0.016 mol), squaric acid (0.89g, 0.008 mol), n-butanol (10ml), and a small quantity of molecular sieves (4A 8-12 mesh) were stirred together in a water bath at 100°C for 2 hours. A colour change from orange/brown to dark green was observed. The reaction mixture was filtered hot removing the molecular sieves and some beige coloured material. Extra butanol was added to wash out the flask and the butanol then removed by rotary evaporation, leaving a viscous green liquid. Ether (10ml) was added and the mixture stirred manually with ice cooling when a green solid formed on standing. The product was filtered off and washed with ether, removing a bright yellow coloured impurity and leaving the dye (162) a dark green coloured powder, (2.98g, 55%).

The electronic absorption spectrum of the product in acetone showed three absorption peaks in the range 700-800nm. TLC (eluent 25% acetone in ethyl acetate) showed the product to be very impure consisting of seven major bands.

References

1. J. Griffiths, "Colour and constitution of organic molecules", (London: Academic Press, 1976)

2. E. N. Abrahart, "Dyes and their intermediates, (London: Arnold, 2cnd ed. 1977)

3. W. M. Horspool, "Aspects of organic photochemistry", (London: Academic Press, 1976)

4. M. Maeda, "Laser dyes, properties of organic compounds for dye lasers", (London: Academic Press, 1984)

5. F. G. Zhang, F. P. Scafer, Appl. Phys., B26, 211, (1981)

6. K. Kato, Appl. Phys. Lett, 33, 509, (1978)

7. C. A. Parker, "Photoluminescence of solutions", (Elsevier, 1968)

8. J. Hecht, New Scientist, Inside Science, (17 June 1989)

9. Ed., J. D. Coyle, R. R. Hill, D. R. Roberts, "Light, chemical change and life : a source book in photochemistry", (Open University, 1982)

10. F. P. Schafer, "Principles of dye laser operation", In: Ed., F. P. Schafer, Topics in applied physics Vol 1."Dye lasers", (3rd Ed.) (Springer-Verlag, 1990)

11. K. H. Drexhage, "Structure and properties of laser dyes", In: Ed., F. P. Schafer, Topics in applied physics Vol 1."Dye lasers", (3rd Ed.) (Springer-Verlag, 1990)

12. P. P. Sorokin, J. R. Lankard, IBM J. Res. Dev., 10, 162, (1966)

13. Ed. J. Griffiths, "Developments in the chemistry and technology of organic dyes", (Blackwell, 1984)

14. Forster, Th: Fluoreszenz organischer verbindungen (Vandenhoeck and Ruprecht, Gottingen 1951)

15. K. H. Drexhage, Design of laser dyes, 7th Int. Quantum Electronics Conference (Montreal 1972)

16. K. H. Drexhage, Laser Focus, 9(3), 35 (1973)

17. I. Wieder, Appl. Phys. Lett., 21(7), 318 (Oct. 1983)

18. C. D. Decker, Appl. Phys. Lett., 27(11), 607, (Dec. 1975)

19. M. L. Shand, J. C. Walling, R. C. Morris, J. Appl. Phys., 52(2), (Feb. 1981)

20. D. J. Harter, M. L. Shand, Y. B. Band, J. Appl. Phys, 56(3), (Aug. 1984)

21. W. M. Fairbank Jr., G. K. Klauminzer, A. L. Schawlow, Phys. Rev, B11, 60 (1975)

22. J. Opt. Soc. Amer., 73, 1945, (1983)

23. P. R. Hammond, IEEE J. Quant. Elect., QE-16(11), 1157, (Nov 1980)

24. D. J. Harter, Y. B. Band, E. P. Ippen, IEEE J. Quant. Elect, QE-21(8), 1219, (Aug. 1985)

25. E. Sahar, I. Wieder, Chem. Phys. Lett., 23(4), 518, (1973)

26. C. R. Giuliano, L. D. Hess, IEEE, J. Quant. Elect., QE-3(8), 358, (Aug. 1967)

27. J. Shah, R.F. Lehery, Appl. Phys. Letts. 24(11), 562 (June 1974)

28. R.F. Lehery, J. Shah, IEEE J. Quant. Elect., QE-11(2), 70, (Feb 1975)

29. W.E.K. Gibbs, Appl. Phys. Letts. 11(4), 113 (Aug 1967)

30. M. Hercher, W. Chu, D.L. Stockman, IEEE J. Quant. Elect., QE-4(11) 954 (Nov 1968)

31. Y.B. Band, B. Scharf. Chem. Phys. Lett., 127(4), 381 (June 1986)

32. E. Sahar, I. Wieder, IEEE J. Quant. Elect., Correspondence, 612 (Aug 1974)

33. G. Dolan, C.R. Goldschmidt, Chem. Phys. Letts. 39(2), 320 (April 1976)

34. Y.B. Band, D.J. Haner, R. Bavli, Chem. Phys. Letts. 126(3) and (4). (May 1986)

35. Y.B. Band, J. Chem. Phys. 83(11), 5453 (Dec 1985)

36. Y.B. Band, Optical properties and applications of reverse saturable absorbers, in: Methods of laser spectroscopy, ed. Y. Prior (Plenum Press, New York 1986)

    Y.B. Band and R. Bavli, Extra cavity pulse compressor and intracavity mode - locking with saturable and reverse saturable absorbers, in: Methods of laser spectroscopy, ed. Y. Prior (Plenum Press, New York 1986)

37. D. M. Strumer, Synthesis and properties of cyanine and related dyes, In: The chemistry of heterocyclic compounds, Vol 30 (Ed. A. Weissberger, E. C. Taylor) N.Y., Int. Publ. 1977 441-587.

38. P.F. Gordon, P. Gregory, "Organic chemistry in colour" (Springer-Verlag Berlin Heidelberg New York 1983)

39. A.K. Bello, L. Cheng, J. Griffiths, J. Chem. Soc., Perkin Trans., 2, (1987), 815

40. C.G. Williams, Trans. Roy. Soc. Edinburgh 21 377 (1857)

41. L.G.S. Brooker, The search for longer conjugated chains in cyanine dyes, In: Recent progress in the chemistry of natural and synthetic colouring matters and related, Ed., T.S. Gore, B.S. Joshi, S.V.A Sunthankar, B.D. Tilak, Academic Press N.Y. and London 1962.

42. Z. Zheng-Hua "Studies of several novel polymethine dyes used in photography and lasers, In: 11th International colour symposium, manuscripts and abstracts, Montreux, Switzerland 23-26 Sept 1991

43. K. Venkataraman, in: The chemistry of synthetic dyes (K. Venkataraman, ed.) Vol II, p 1143, Vol IV, p 212, Academic press, London (1952)

44. N. Tyutyulkov, J. Fabian, A. Mehlhorn, F. Dietz, A. Tadjer, Polymethine dyes structure and properties, St Kliment Ohridski University Press, Sofia (1991)

45. Y. P. Kovtun, N. N. Romanov, Khim. Geterotsikl. Soed., 211, (1985)

46. N. N. Romanov, K. V. Fedotov, A. D. Kachkovskii, Dopov. Akad. Nauki., Ukr, RSR, ser. B, 51, (1984); CA, 102, 63 567, (1985)

47. P. Savarino, G. Viscardi, E. Barni, G. Di Modica, Heterocycl. Chem., 24, 1053 (1987)

48. M. A. El-Maghraby, A. K. Khallafallah, M. E. Hassan, H. A. Soleiman, J. Chem. Soc. (Taipei), 35, 53, (1988); CA, 110, 77479 (1989)

49. Ed. M. Matsuoka, <u>Topics in applied chemistry</u>, "Infrared absorbing dyes" (Plenum Press, New York 1990)

50. G.A. Reynold, K.H. Drexahage, <u>J. Org. Chem.</u> <u>42(6)</u>, 885, (1977)

51. D.F. O'Brien, T.M. Kelly, L.F. Costra, <u>Photogr. Sci. Eng.</u>, <u>18</u>, 76(1974)

52. G. Heilig, W. Lüttke, <u>Chem. Ber.</u>, <u>120</u>, 1863 (1987)

53. G. Heilig, W. Lüttke, <u>Chem. Ber.</u>, <u>119</u>, 3102 (1986)

54. L.G.S. Brooker, A. Skiar, H.W.J. Crossman, G. H. Keyes, L. A. Smith, R. H. Sprague, E. van Lare, G. van Zandt, F. L. White, W. W. Williams, <u>J. Am. Chem. Soc.</u>, <u>67</u>, 1875 (1945)

55. K. Takagi, M. Matsuoka, Y. Kubo, T. Kitao, <u>Dyes and Pigments</u>, <u>6</u>, 75, (1985)

56. L.G.S. Brooker, R. H. Sprague, C. P. Smyth, G. L. Lewis, <u>J. Am. Chem. Soc.</u> <u>62</u> 1116 (1940)

57. L.G.S. Brooker, G. H. Keyes, R. H. Sprague, R. H. van Dyke, E. van Lare, G. van Zandt, F. L. White, H. W. J. Cressman, S. G. Dent, <u>J. Am. Chem. Soc.</u> <u>73</u>, 5332 (1951)

58. J. Griffiths "Modern dye chemistry" in <u>Chem. in Britain</u> (Nov 1986)

59. S.N. Corns, Ph.D. Thesis, University of Leeds (1990)

60. S. Yasui, <u>Shikizai Kyokaishi</u>, <u>60</u>, 212 (1987)

61. S. H. Kim, M. Matsuoka, T. Kitao, <u>Chem. Lett.</u>, 1351, (1985)

62. K.Y. Chu, J. Griffiths, <u>J. Chem. Research</u>, (M)2319, (S)180, (1978)

63. K.A. Bello, J. Griffiths, <u>J.C.S. Chem. Commun.</u>, 1639 (1986)

64. F.A. Neugebaver, R. Bernhardt, H. Fischer, <u>Chem. Ber. 110</u>, 2254 (1977)

65. K. A. Bello, L. Cheng, J. Griffiths, <u>J. Chem. Soc. Perkin Trans. (II)</u>, 815, (1987)

66. M. Matsuoka, L. Han, T. Kitao, S. Mochizuki, K. Nakatsu, <u>Chem. Lett.</u>,905, (1988)

67. G.N. Schrauzer, V.P. Mayweg, <u>J. Am. Chem. Soc.</u>, <u>87</u>, 1483 (1965)

68. H. Shiozaki, H. Nakazumi, Y. Nakado, T. Kitao, <u>Chem. Lett.</u>, 2393 (1987)

69. S.H. Kim, M. Matsuoka, M. Yomoto, Y. Tsuchiya, T. Kitao, <u>Dyes and Pigments</u>, <u>8</u>, 381 (1987)

70. Y. Kubo, K. Sasaki, K. Yoshida, <u>Chem. Lett.</u>, 1563 (1987)

71. F.H. Moser, A.K. Thomas, <u>The phthalocynanines</u>, <u>Vols 1 and 2</u> CRC Press, Boca Raton, Florida (1983)

72. W.S. Chan, J.F. Marshall, R. Svenson, D. Phillips, I.R. Holt, <u>Photochem. and photobiol</u>, <u>45</u>, 757, (1987)

73. European Patent 313, 943 (1989)

74. Jpn. Patent 61 15,891 [CA 105, 42512 (1986)]

75. UK Patent 1 467 564

76. US Patent 4,384,973

77. N. R. Ayyangar, K. V. Srinivasan, T. Daniel, Dyes and Pigments, 13, 301-310, (1990)

78. UK Patent 1 464 706

79. W. Mach, D. Augart, H. Scheuermann (BASF AG), Ger Offen 2 253 538

80. V. U. Shenoy, S. Seshadri, Dyes and Pigments, 11, 137, (1989)

81. R. Rajagopal, V. U. Shenoy, S. Padmanabhan, S. Sequeira, S. Seshadri, Dyes and Pigments, 13, 167 (1990)

82. A. Knierzinger, O. S. Wolfbeis, J. Heterocyclic Chem., 17, 225 (1980)

83. Huadong, Huagong, Xueyuan, Xuebao, Cheng, J. East China Institute of Chemical Technology, 16(2), 176, (1990)

84. M. Weissenfels, A. Hantschmann, T. Steinfuhrer, E. Birker, Z. Chem., 29, 166 (1989)

85. O. T. Wolfbeis, Monatsch. Chem., 108(3), 499, (1977)

86. E. Ziegler, H. Maier, Mh. Chem., 89, 150, (1958)

87. S. R. Moorty, V. Sundaramurthy, N. V. Subba Rao, Indian Journal of Chemistry, 11, 884, (1973)

88. M. J. S. Dewar, J. Chem. Soc., 2329, (1950)

89. R. Lemke, Synthesis communications, 359, (May 1974)

90. Kodak Laboratory Chemicals Catalog No. 51 (1981)

91. T. G. Deligeorgiev, N. I. Gadjev, <u>Dyes and Pigments</u>, <u>12</u>, 157, (1990)

92. N. I. Gadjev, T. G. Deligeorgiev, <u>Dyes and Pigments</u>, <u>14</u>, 73, (1990)

93. L. Strekowski, M. Lipowska, G. Patanoy, <u>Synthetic communications</u>, <u>22(17)</u>, 2593, (1992)

94. L. Strekowski, M. Lipowska, G. Patonay, <u>J. Org. Chem.</u>, <u>57</u>, 4578, (1992)

95. J. Andrieux, J. P. Battioni, M. Giraud, D. Molho, <u>Bulletin de la Societe Chimique de France</u>, <u>6</u>, 2093, (1973)

96. A. L. M. Koraiem, M. M. Girgis, Z. H. Khalil, R.M. Abu El-Hamd, <u>Dyes and Pigments</u>, <u>15</u>, 89 (1991)

97. G. A. Reynolds, K. H. Drexhage, <u>J. Org. Chem.</u>, <u>42</u>, 885, (1977)

98. Private communication, Dr D. Fabricius, Du Pont Imaging Systems.

99. EP 0 335 236 A2

100. K. A. Bello, <u>PhD. Thesis</u>, University of Leeds 1986

APPENDIX

Polymer films containg Squarylium dye

Key to graphs

PVC = Polyvinyl chloride

PVC0 = Blank film

PVC1 = OD = 0.08 at 532nm

PVC2 = OD = 0.49 at 532nm

PM = Polymethylmethacrylate

PM0 = Blank film

PM1 = OD = 0.16 at 532nm

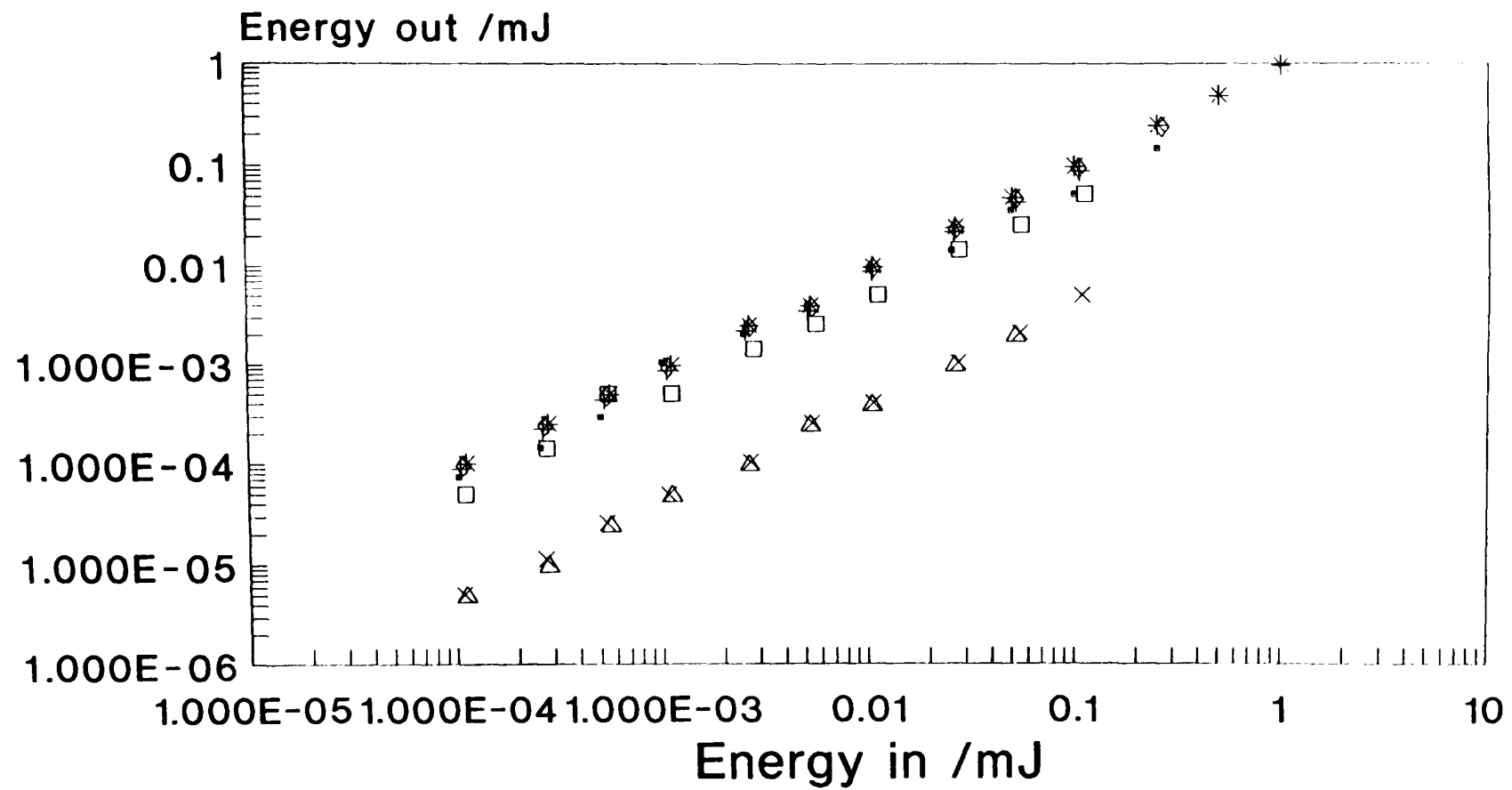PM2 = OD = 1.1 at 532nm

PC = Polycarbonate

PC0 = Blank film
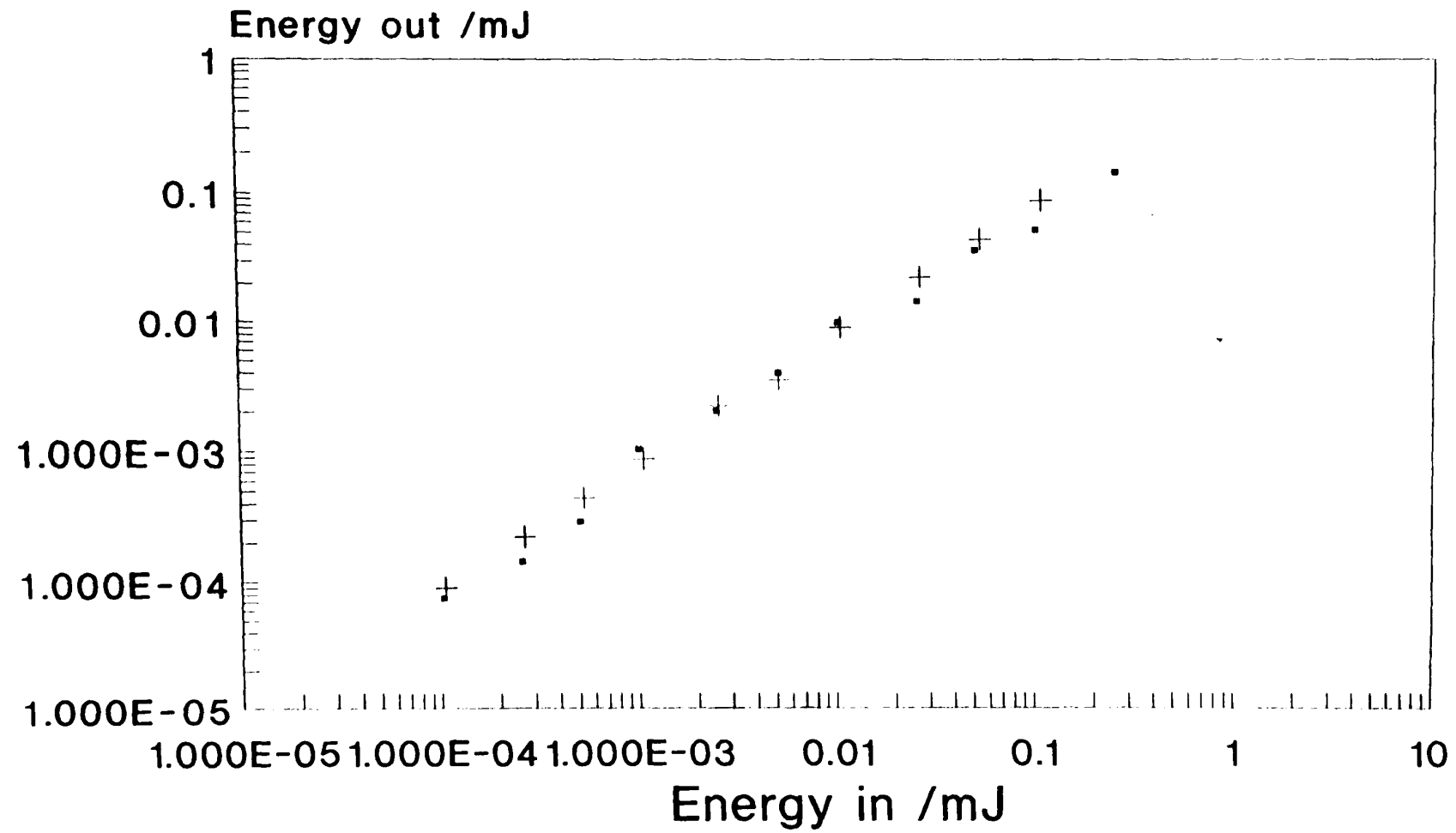
PC1 = OD = 1.21 at 532nm
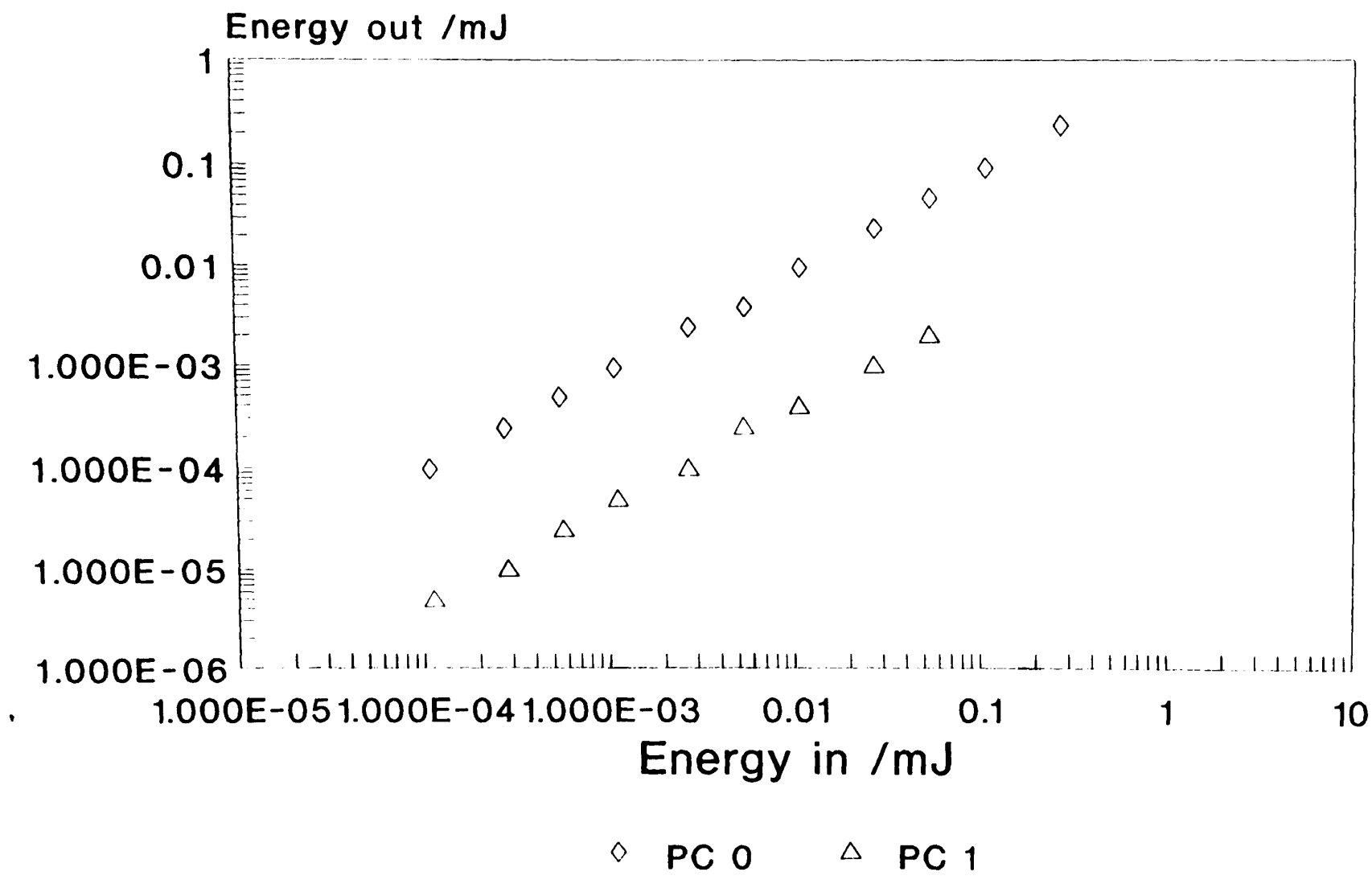

PS = Polystyrene

PS0 = Blank

PS1 = OD = 0.46 at 532nm

PS2 = OD = 0.77 at 532nm

Energy out /mJ

1.000E-05 1.000E-04 1.000E-03 0.01 0.1 1 10

Energy in /mJ
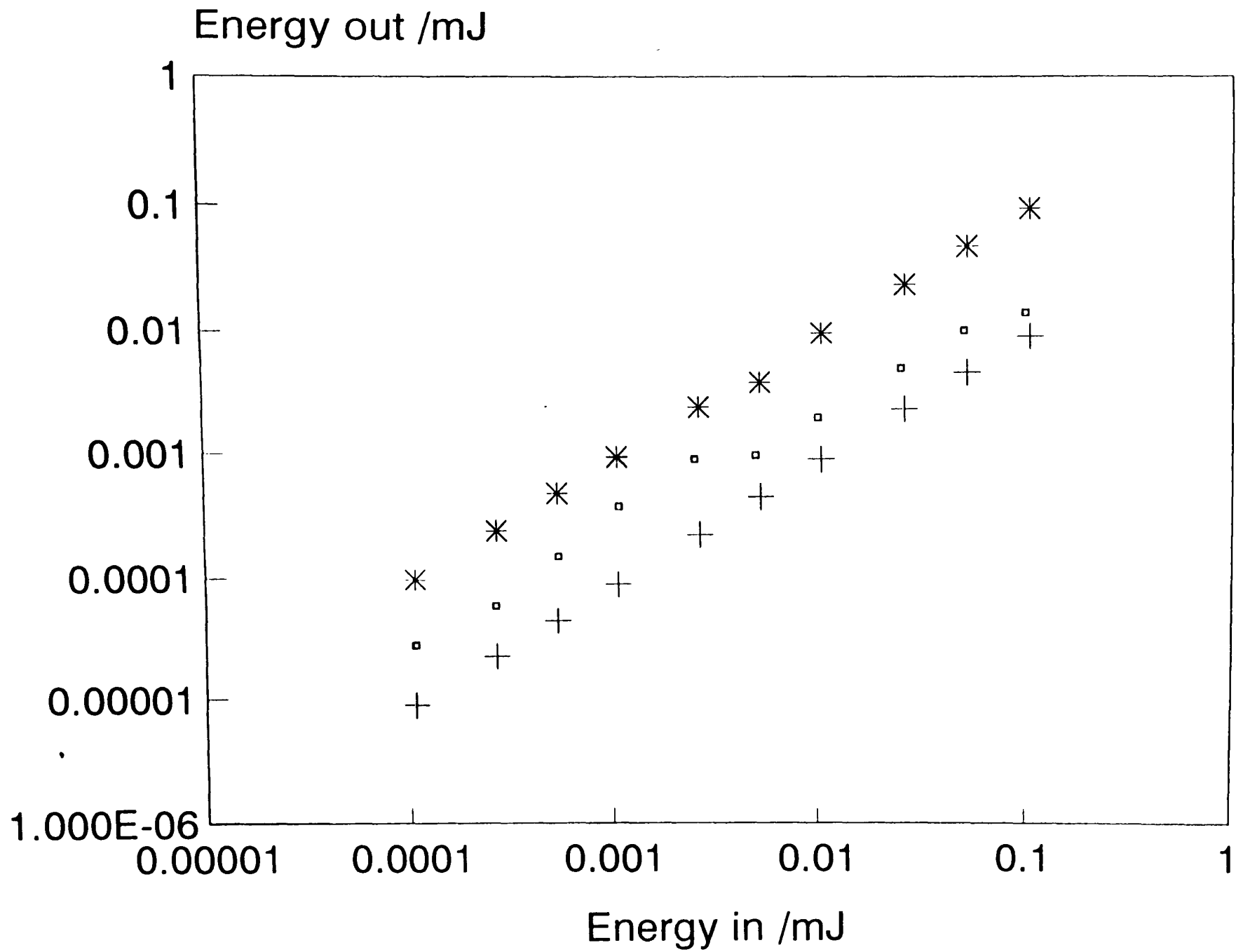
· PVC 1   + PVC 0   * PM 0 ·   □ PM 1 ·

× PM 2 ·   ◇ PC 0.   △ PC 1.